Title	Metric perturbations and their slow evolution for modelling extreme mass ratio inspirals via the gravitational self force approach
Authors(s)	Durkan, Leanne
Publication date	2022
Publication information	Durkan, Leanne. "Metric Perturbations and Their Slow Evolution for Modelling Extreme Mass Ratio Inspirals via the Gravitational Self Force Approach." University College Dublin. School of Mathematics and Statistics, 2022.
Publisher	University College Dublin. School of Mathematics and Statistics
Item record/more information	http://hdl.handle.net/10197/13302

Metric perturbations and their slow evolution
for modelling extreme mass ratio inspirals via the gravitational self force approach.

by

Leanne Durkan, BSc, MASt. (Cantab)

UCD Student Number: 12352491

August 2022

This thesis is submitted to University College Dublin in fulfilment of the requirements for the degree of Doctor of Philosophy in Mathematics.

UCD School of Mathematics and Statistics

Head of School: Dr Edward Cox

Primary Supervisor: Dr Niels Warburton

Secondary Supervisor: Professor Adrian Ottewill

Members of Research Studies Panel:

Dr Lennon Ó Náraigh

Professor Adrian Ottewill

Dr Barry Wardell

Contents

List of Figures

List of Tables

In 2015, gravitational waves (GWs) were observed by direct detection for the very first time, over one-hundred years since the publication of Einstein's theory of general relativity (GR). Since then, GWs produced by a variety of systems have been detected. The laser interferometer space antenna (LISA), due to be launched in 2037 by the European Space Agency, will be sensitive to a new frequency of the GW spectrum than we are currently capable of detecting with ground based interferometry. One of the most highly anticipated sources of GWs detectable to LISA, that we have so far been blind to, are extreme mass ratio inspirals (EMRIs). These are binary systems comprised of a black hole that is at least ten-thousand times more massive than its satellite. Provided our models are accurate enough, matched filtering between detected and theoretical GW signals can provide a measure of precisely how well GR describes our Universe. To achieve this scientific goal, we must calculate the phase of GWs sourced by EMRIs to post-adiabatic order, which in turn requires knowledge of the gravitational self-force (GSF) and metric perturbation through second-order in the small mass ratio. This thesis aims to further our understanding of the evolution of EMRI spacetimes, by determining the phase and amplitude of the GWs they emit.

Within the framework of GR, black hole perturbation theory (BHPT), GSF theory, and the two-timescale approximation, this work presents a number of novel calculations as tools for modelling EMRI waveforms. In particular, the MST package was developed for the Black Hole Perturbation Toolkit (BHPToolkit), which solves the Regge-Wheeler (RW) and Teukolsky equations via the Mano-Suzuki-Takasugi method. Another major result in this thesis is the Lorenz gauge calculation of the slowly-evolving first-order metric perturbation for quasicircular, equatorial orbits on a Schwarzschild background during inspiral. This provides a key ingredient to the source of the second-order metric perturbation, and is already being used to generate post adiabatic EMRI waveforms via the GSF approach. Post-adiabatic waveforms presented in this thesis are also found to describe intermediate mass ratio inspirals (IMRIs) to a high degree of accuracy. One IMRI, GW191219_163120 with a mass ratio of approximately 1:26 has already been detected by interferometers on the ground [7]. Thus work presented here is deemed applicable for GW science now and in the future. The transition to plunge is also examined in detail, and waveforms are computed during the transition regime to adiabatic order, again for quasicircular, equatorial orbits around a Schwarzschild black hole. Perturbations to a Kerr black hole will also be explored, and a final output of this work is a 'pure gauge' contribution to the first-order Lorenz gauge metric perturbation, generated by a gauge vector.

Statement of Original Authorship

I hereby certify that the submitted work is my own work, was completed while registered as a candidate for the degree stated on the title page, and I have not obtained a degree elsewhere on the basis of the research presented in this submitted work.

Collaborations

Chapter 3: This work was done in collaboration with Wardell, who implemented the recursion relations for the MST coefficients and asymptotic amplitudes for the MST package, in addition to scripting the package for use in the BHPToolkit [1]. Casals also provides some asymptotic expressions, with Ottewill acting as an additional advisor on this project. The Regge-Wheeler section of the MST package had already been implemented by Wardell, Kavanagh and others.

Chapters 4 and 5: The work in these chapters was done in collaboration with Niels Warburton and is based on the paper from Ref. [2]. The boundary conditions for the r_0 derivatives of the Regge-Wheeler fields in addition to the boundary conditions of M_{2af} and its r_0 derivative were derived by Warburton. Warburton proposed the splitting of $\partial_{r_0} M_{2af}$ into χ_1 and χ_2 as well as using the method of partial annihilators. The jump conditions were also derived independently by Warburton and I. The r_0 derivative of the energy flux was also calculated by Warburton. All other aspects of these chapters were derived and implemented by me, with the help of Warburton when needed.

Chapter 7: This work was done in collaboration with Lorenzo Küchler, Geoffrey Compère and Adam Pound. All derivations in this chapter were derived independently both by Küchler and I, with help from Compère and Pound.

Chapter 8: This work was done in collaboration with Lorenzo Küchler, Geoffrey Compère, Adam Pound, Niels Warburton, Barry Wardell, Jeremy Miller and Alexandre Le Tiec. The inspiral waveforms and the *Mathematica* notebooks that generate them were first implemented by Wardell, and were built on by Küchler and I for the transition regime. Le Tiec advised on the comparison with numerical simulations from the SXS catalogue and the inspiral results are based on the paper from Ref. [3]. Le Tiec also suggested using the binding energy and flux to compute the inspiral, rather than using the second-order self-force. The flux calculation is then based on the paper from Ref. [4]. Numerical solutions to $F_n^{\Delta\Omega}$ were obtained by Compère and are presented here. The metric perturbation, source and field equations were also derived independently by Küchler and I.

Chapter 9: This work was done in collaboration with Sam Dolan and Barry Wardell, and is based on the work of Ref. [5]. The results in this section were derived independently by Dolan and I. This work was supported by the STSM COST Action CA16104.

Dedication

For Mia.
(Dr. Anne Marie Ryan.)

Acknowledgements

Firstly I would like to thank all those on my defence committee for their time, to Dr James Herterich for kindly agreeing to chair the examination, to Dr Sarp Akcay for acting as the internal examiner and to Professor Bernard Whiting as the external examiner. I would also like to thank my research studies panel, Dr Lennon Ó Náraigh as chair, as well as Dr Barry Wardell and Professor Adrian Ottewill for their support and advice.

I would especially like to thank my supervisor Dr Niels Warburton. Niels has been the best supervisor a PhD student could ask for, and I have always been impressed by his unwavering understanding and diplomacy. Niels was always supportive when it came to exploring my own interests, public outreach opportunities, and taking much needed breaks. In particular I owe the success of the research presented here to Niels' guidance and vision. I must also thank my second supervisor, Professor Adrian Ottewill. Adrian's was the very first lecture I attended at university (it has something to do with how far you can get up a ladder propped against a wall before it slips). He is responsible for first introducing me to general relativity, and nurtured my interest in the subject by supervising my undergraduate dissertation on wormhole spacetimes. He also encouraged me to pursue Part III at Cambridge, and I owe a lot of where I am today to him. I also extend my thanks to Dr Barry Wardell, who at times acted as another supervisor to me, and always made time for my many questions on mathematical aspects of perturbation theory. I also extend my gratitude to my colleagues in the UCD Relativity Group for both their moral support and general tomfoolery. I had a lot of fun over the years with my PhD cohort on research visits, extended lunch breaks involving competitive Bananagrams, conference trips, and many office shenanigans along the way.

I would also like to thank the Mathematics and Statistics School office staff for keeping everything running, even during a pandemic, and for cultivating the sense of community over cups of tea and baked goods, which were so enjoyed by everyone in the school common room. A special thanks to Dr Nuria García Ordiales and Marian Woods for their help and hard work over the years.

I thank Dr Sam Dolan for kindly hosting my research visit to the University of Sheffield, and to COST Action for supporting this Short Term Scientific Mission. I extend many thanks to the CRAG group for making me feel so welcomed, and making my visit to Sheffield a memorable one. I would also like to thank Dr Adam Pound for his invitations to collaborate on research, during visits to the University of Southampton, and for his patience in answering all of my many questions

Chapter 1

Introduction

This aim of this chapter is to motivate the research presented in this work. An overview of the problems this thesis endeavours to solve will be outlined, with a brief description of the methodology required of the calculations involved. This will be followed by a summary of the structure of this work, including any conventions that may be used.

1.1 Motivation

Gravitational wave (GW) astronomy has seen huge progress since the first discovery by the Laser Interferometer Gravitational-Wave Observatory (LIGO)/ Virgo Collaboration in 2015 [6]. To date, GWs have been detected from numerous sources including compact binaries with mass ratios from 1:1 to $\sim$ 1:26, the latter of which being GW191219_163120. [7], binary neutron stars [8] and black hole-neutron star mergers [9]. The next generation of space-based GW detectors such as the Laser Interferometer Space Antenna (LISA) [10], with access to millihertz frequencies, will expand the current parameter space of compact binaries available to detection. This drives the need to develop GW models for millihertz sources: extreme-mass-ratio inspirals (EMRIs), one of the key anticipated sources detectable by LISA. EMRIs are binary systems of compact objects in which the larger body, which shall be referred to as the primary, has a mass M that is at least 10^4 times that of the smaller body, which shall be referred to as the secondary, with mass μ, giving rise to the quantity referred to as the small mass ratio, given by $\varepsilon = \mu/M \leq 10^{-4}$. Astrophysical observations establish the primary as a supermassive black hole (SMBH) with a mass of $\sim 10^4 - 10^7 M_\odot$ residing in galactic centres, and the secondary as a stellar-mass compact object, either a black hole (BH), neutron star, or some exotic compact object [11]. Most galaxies are expected to host a central SMBH with many smaller compact satellites, furnishing the hearts of galaxies as natural EMRI laboratories.

GWs produced by EMRIs are expected to have a frequency range between $\sim 10^{-3} - 10^{-2}$ Hz [10], placing them comfortably within the LISA band, detectable so long as their signal is sufficiently loud [12]. Astrophysical population studies estimate that LISA will observe between a few and a few thousand EMRIs over its lifetime [12]. Furthermore, owing to their extreme mass ratio, EMRIs inspiral slowly when sufficiently far from merger, giving rise to two different timescales: the orbital

timescale, t_{orb} and the radiation-reaction timescale, t_{rr}. The orbital timescale is the time taken to complete an orbit, which in the weak field is given by $t_{\mathrm{orb}} \sim M$ [13, 14]. The radiation-reaction timescale is then the time over which the orbit shrinks in size due to the back reaction from the emission of GWs, and is given by: $t_{\mathrm{rr}} \sim M/\varepsilon$ [13, 14]. By a simple scaling argument, taking the quotient of the two timescales, we can expect to see $\mathcal{O}(\varepsilon^{-1})$ [13, 14], or $\geq 10^4$ orbits over an EMRIs lifetime. Due to the large number of orbits and long radiation-reaction timescale, EMRI signals could last many years [10], making them detectable out to red-shifts of $z \sim 3 - 4$ [11, 10], though this number varies throughout the literature. These estimates provide substantial motivation to develop models of EMRIs with which to perform matched filtering of LISA's future data stream.

Searching for and parameterizing EMRI waveforms in the LISA data stream relies crucially on theoretical waveform templates. Therefore, we must compute the phase and amplitude of EMRI waveforms so that the error accumulated over the thousands of orbits during the EMRIs lifetime remains small. In fact, the total accumulated phase error, $\delta\Phi$, of the template with respect to the true signal must be $\ll 1$ radian [10, 13, 14]. While this level of precision may not be needed in order to detect EMRIs, an accuracy of $\delta\Phi \ll 1$ is required in order to perform precision tests of GR using parameter estimation [10]. Adiabatic templates are expected to enable an estimation of parameters such as the mass and angular momentum of the primary to within 10% accuracy [13, 14, 15]. While detecting EMRIs alone would be a phenomenal scientific achievement, accurate parameter estimation and precision tests of GR are two of LISAs main scientific goals [10], and will serve as the primary motivation of this thesis.

1.2 Overview

EMRIs detectable by LISA are estimated to have a mass ratio of 10^{-4} to 10^{-7} [11]. Modelling EMRIs is therefore a task for black hole perturbation theory (BHPT), where the primary dictates the background spacetime, usually described by either the Schwarzschild or Kerr metric, and the secondary introduces a perturbation to the background spacetime. The metric and physical quantities are perturbed about their background values and can be written in terms of an expansion in powers of the small mass ratio [16, 17, 14]. To leading order, the secondary can be modelled as a point-like particle [16]. In order to reach the accuracy of $\delta\Phi \ll 1$, required for precision tests of GR and parameter estimation, the metric perturbation must be calculated up to and including second-order in the small mass ratio expansion [13], corresponding to a calculation of the GW phase through to $\mathcal{O}(\varepsilon^0)$, such that $\delta\Phi \sim \mathcal{O}(\varepsilon)$. It is expected that the amplitude of a given GW, which is related to the amplitude of the metric perturbation, need only be determined to first-order in ε for detection by space-bourne interferometers. However, to calculate the phase to the degree of accuracy desired, the second-order piece of the metric perturbation is required as input. Therefore, the metric-perturbation will be calculated through to $\mathcal{O}(\varepsilon^2)$, to meet the phase accuracy goal.

Not only do we need to calculate the phase and amplitudes of EMRI produced GWs accurately enough, but also quickly enough, to cover the large parameter space that EMRIs encompass. Without

complete theoretical models, the LISA mission will fall short of its scientific goals. Our models must be able to generate GWs efficiently for every possible morphology, that is for every detectable mass ratio, orientation in space and spin configuration. The ultimate goal for EMRI science therefore, is to model GWs sourced by a Kerr primary, with a spinning secondary, following generic orbits. These are the systems expected to be found in nature and the most generic models will recover the most science from the many possible EMRI signals LISA may detect [10, 11, 18]. With LISA due to launch in 2037 (at the time of writing), our models must be able to generate a waveform template for a given set of parameters in milliseconds if we are to cover the parameter space by LISA's launch date. There are a number of ways to tackle waveform generation. Numerical relativity (NR) has had great success in modelling compact binary systems with mass ratios of 1:1 up to $\sim 1 : 10$ [19]. EMRIs cannot be modelled using NR however, as resolving the smaller secondary is extremely computationally expensive for the number of orbital cycles until merger that must be simulated, which scales as ε^{-1}. Post Newtonian (PN) theory has also been very successful for modelling GWs in the weak field [19]. Effective-one-body (EOB) theory goes further, covering the entire parameter space [19, 20, 21, 22], though relies on calibration with results from other approaches. The work in this thesis will model EMRIs following the gravitational self-force (GSF) approach, a branch of BHPT that has been over 25 years in the making, beginning with the MiSaTaQuWa equation in 1997 [23, 24]. The first waveforms to include post adiabatic corrections to the phase using the GSF approach were produced in late 2021, for quasicircular, equatorial orbits, on a Schwarzschild background [3]. These waveforms make use of work presented in Chapter 6 of this thesis. These results include the contribution of the second-order metric perturbation, which takes input from calculations in this thesis [3, 2]. This is the first step of many in developing a huge database of more generic waveforms. The GSF program has many moving parts. This thesis aims to summarise GSF theory, providing new tools for generating EMRI waveforms using the GSF approach. In particularly, this thesis will focus on calculating the first-order metric perturbation and related quantities that feed into the solution of the second-order metric perturbation, which are needed to determine the amplitude and phase of the GWs we are trying to model, and to ensure that $\delta\Phi \sim \mathcal{O}(\varepsilon)$.

The challenge of answering the question *'how does a gravitating body's trajectory evolve in space-time?'* has a long history, complicated by the fact that that same body is perturbing the background spacetime, hence influencing its own motion. When modelling EMRIs via the GSF approach, this is truly the question we must answer. Einstein's theory of GR dictates that a point-like particle, with no mass or size, necessarily follows a geodesic path [25, 26, 27]. It wasn't shown until the 1970s by Dixon that test-bodies (i.e. those that do not have their own gravitational field) of finite size introduce corrections beyond geodesic motion, due to coupling between the body's multipole moment with the curvature of the external spacetime in which it travels [28, 29, 30, 16]. Hartle and Thorne later progressed further [31, 32, 33], using perturbation theory to show that in the limit of small mass and size, neglecting finite size effects, such an object follows a geodesic path in the external spacetime, that is the full spacetime including the perturbing body. The external spacetime is of course influenced by the object itself, and was not fully determined at the time. Finally, as GW

detectors were becoming a reality, Mino, Saskai and Tanaka [23], in addition to Quinn and Wald [24], took a huge leap forward by deriving the so called MiSaTaQuWa equation of motion, which included the effect of the object's own gravitational field on its trajectory. It was then Detweiler and Whiting who realised the equivalence between the MiSaTaQuWa equation and the geodesic equation of a particular spacetime, that of a perturbed vacuum metric [34, 35], recovering the earlier results of Hartle and Thorne to first-order in the perturbation. Rather than paraphrasing the effect this self interaction has on a body's motion through a vacuum spacetime, a quote from Barack and Pound's 2018 review [16] could not have put it more succinctly:

"At leading order one has a pointlike particle moving in a geodesic orbit around the large black hole. At subsequent orders, interaction of the particle with its own gravitational perturbation gives rise to an effective "self-force", which drives the radiative evolution of the orbit, and whose effects can be accounted for order by order in the mass ratio." [16]

More recently, the problem of a gravitating body travelling through a vacuum spacetime, that is the problem of modelling EMRIs, is tackled using the GSF approach via the self-consistent and two-timescale approximations [16, 14, 17], which will be explained in more technical detail in the chapters that proceed. There is a preference for using the two-timescale approximation as calculations using the self-consistent approach alone must be done in the time domain for each point in time. This is much slower and more difficult to implement than the two-timescale approximation [14], and for these reasons the self-consistent approach has not been implemented even at first-order.

As explained by Barack and Pound [16], the self-force (SF) is what drives the secondary beyond geodesic motion, causing the compact objects in the binary to spiral in towards each-other, until they eventually collide and merge into a single body. The binary goes through a number of stages before this happens: between the time the binary forms and when the secondary nears the inner-most stable circular orbit (ISCO) is referred to as the inspiral. This is followed by a transition to plunge [36, 16], as the black holes begin to fall into one another. This is quickly followed by the plunge itself, just before the merger stage, after which the ring-down occurs [6, 16, 37, 38]. The resulting black hole will have a mass greater than M but less than $M + \mu$ by conservation arguments, and the area of its event horizon will not be less than the sum of the areas of the event horizons of the individual black holes, by the third law of black hole thermodynamics. Each of these different stages of the binary's lifecycle are reflected in the features of the GWs produced. Each stage has its own distinct dynamical behaviour and must be modelled separately. This thesis will focus on the treatment of both the inspiral and of the transition to plunge.

In the GSF approach, the secondary can be treated as a point-like particle at leading order in the perturbation [16]. The approximation of the secondary as a point-like particle simplifies certain calculations, as distributional sources are easier to deal with mathematically than those that are non-compact, as will be shown in Chapter 5 and Chapter 6. However, there is no such thing as a free lunch, and this treatment introduces singular behaviour requiring regularisation, analogous to

re-normalisation in quantum field theory. It was Detweiler and Whiting who first showed that the MiSaTaQuWa SF could be split into regular and singular contributions [35, 34]. Detweiler postulated that the same should be true of the second-order GSF, which was proven by Pound in 2017 [39]. The regularisation procedure of the metric perturbation will not be detailed here other than to say that it is best understood in the Lorenz gauge for a Schwarzschild background [16, 37, 17, 40]. It is worth noting that regularisation has been done to first-order in the radiation [41] and Regge-Wheeler (RW) gauges [42], with progress towards more regular second-order SF calculations using the Teukolsky formalism [43]. Regularisation parameters have also been calculated for a Kerr background in the Lorenz gauge to first-order, though we are currently lacking the metric perturbation to regularise [44, 45]. Furthermore, while the Teukolsky formalism requires solving for less fields than the 10 coupled fields of the Lorenz gauge, current algorithms have already been set up in the Lorenz gauge. The Teukolsky formalism will still require metric reconstruction. It is for these reasons that the majority of work in this thesis will be presented in the Lorenz gauge.

Returning to the problem at hand, the two-timescale approximation exploits the disparate timescales t_{orb} and t_{rr} introduced earlier, allowing us to define the quantity of 'slow-time', $\tilde{t}$, over which physical quantities such as the orbital radius, orbital frequency, orbital energy, angular momentum and metric perturbation evolve, while the phase evolves on a faster timescale over a single orbit. In the two timescale approximation, the slowly evolving first-order metric perturbation contributes to second-order source, and must be calculated if we wish to perform precision tests of GR or conduct parameter estimation from EMRI signals as discussed in Section 1.1. In this thesis, the first-order Lorenz gauge metric perturbation and its derivative with respect to $\tilde{t}$ will be calculated for quasicircular, equatorial orbits on a Schwarzschild background in the frequency domain during the inspiral. These calculations are based on the work from [2]. These Lorenz gauge quantities are calculated by making use of Berndtson's gauge transformation [46], which transforms RW gauge solutions into the Lorenz gauge. Rather than directly solving the 10 coupled linearised Einstein field equations in the Lorenz gauge to obtain the first-order metric perturbation, Berndtson allows us to construct the metric perturbation from 7 decoupled fields that obey very similar equations, simplifying the problem greatly. These are the RW and Zerilli (RWZ) master functions, in addition to two gauge fields. The slow-time derivative of the first-order metric perturbation in the Lorenz gauge can then be solved by taking the slow-time derivative of RW gauge quantities and the gauge transformation. This proves much simpler than directly solving for yet another coupled set of 10 partial differential equations which would be obtained by differentiating the Einstein field equations with respect to slow-time, as is shown in more detail later by Eq. (6.2). In Chapter 5 and Chapter 6, the slowly evolving RWZ fields, in addition to the gauge contributions are solved using the method of partial annihilators and variation of parameters. These novel results act as inputs to generating never before seen GSF waveforms, through second-order in the small mass ratio, in Ref. [3].

Another important quantity is the total energy flux, which is particularly important for EMRIs due to their long signal lengths, allowing us to take account of the accumulated orbital phase over tens or hundreds of thousands of orbits. The flux and the binding energy are used to determine

the evolution of the frequency of GWs, which dictates the motion of the secondary. While the energy flux radiated to infinity is something we can measure directly, the energy flux radiated through the horizon determines how the parameters of the primary evolve, such as its mass and angular momentum [47]. Results from this thesis have contributed the first calculation of the total energy flux via the GSF approach through second-order in the small mass ratio [4], a calculation which is presented again in Chapter 8. Both the second-order GSF (2GSF) inspiral waveforms and flux calculations have been found to agree very well with NR simulations for intermediate mass ratio inspirals (IMRIs), at least up until the secondary approaches the inner-most stable circular orbit (ISCO), where current inspiral models break down, which will be discussed at multiple stages throughout this thesis. Reasonably good agreement between GSF and NR results have even been found for near equal mass ratio inspirals, despite initially being intended for modelling EMRIs. These results are not completely surprising, as modelling IMRIs via the GSF approach is still expected to work well by virtue of the fact that $\varepsilon \sim 1/10$ can be considered numerically small, and $\delta\Phi = 0.1$ remains $\ll 1$ radian. Comparing with shorter NR GW signals also leaves less time for error to accumulate in the phase.

However, as mentioned earlier, the inspiral is not the full story. The radiation-reaction time hastens as the secondary begins its transition to plunge, and $\tilde{t}$ is no longer so slow. Physical quantities that evolve with respect to slow-time, such as the orbital radius, frequency, energy, angular momentum and GW amplitude will evolve more quickly [48]. The equations of motion, the field equations, and hence solutions to the metric perturbation and GW phase will evolve differently during the transitional period compared to the inspiral, and a new timescale must be chosen to correctly evolve GWs through the transition regime [48, 14]. The transition is more important for modelling IMRIs than EMRIs [49, 50], due to their shorter signal lengths, recalling earlier scaling arguments. Shorter signals rely on accurate waveform templates particularly during times surrounding the merger where the signal is loudest. On the other hand, detecting EMRIs relies much more on the accumulated signal-to-noise ratio (SNR) over long periods of time, as one tiny black hole falls quietly into another, much larger black hole. The LIGO, Virgo, KAGRA Collaboration recently detected a compact binary with a mass ratio of 26:1, comfortably labelling the binary in question as an IMRI [7]. Now that we are seeing IMRIs being detected by ground-based interferometry, models are needed with which to perform matched filtering for improved parameter estimation, as current EOB [51, 52, 53, 54] and Phenom [38] models, which have been calibrated to NR simulations, in addition to NR surrogate models [55, 56, 1], are not currently calibrated for higher IMRI mass ratios. Work from this thesis on the transition to plunge should therefore prove useful for both ground-based and space-based GW astronomy alike. It is rather encouraging to know that we may not have to wait until 2037 to see observational confirmation of the results presented here.

The transition to plunge will be treated in Chapter 7, which explores the structure of the phase and metric perturbation through to second-order during the transition regime. In collaboration with Kücheler, Compère and Pound, the phase and amplitude are calculated to adiabatic order in the transition for quasicircular, equatorial orbits on a Schwarzschild background. Adiabatic GSF

waveforms for the transition regime are then presented in Chapter 8, which include leading order dissipative SF effects. Research on the transition to plunge began in the year 2000 by Ori and Thorne (OT), who propose a scheme for generating GW templates in the transition regime for circular, equatorial orbits around a Kerr black hole [48]. A similar calculation was done independently at the same time by Buonanno and Damour [57]. The work by OT has since remained the basis of the vast majority of calculations in the transition regime. It was not until 2019 that the work of OT was extended to arbitrarily inclined orbits by Lim, Khana, Anuj and Hughes [58, 59]. Burke, Gair and Simón further extend the OT procedure for any spin, in particular for near extremal Kerr black holes [60]. They note one limitation of OT is the assumption that the energy and angular momentum evolve linearly in proper time, which is relaxed in Ref. [60]. Compère, Fansen and Jonas then include non-quasicircular effects [61]. Compère and Küchler then deviate from the OT prescription and present a self-consistent approach to the transition motion at leading order in the transition timescale, taking account of SF effects [62]. The key difference in the treatment of the transition regime in this thesis is that it easily allows for the extension to post-adiabatic corrections, which the OT prescription does not, and any restricting assumptions of the OT procedure are no longer required. Post-adiabatic contributions to the transition are left to be determined, in addition to attaching the plunge dynamics, which is currently undergoing research by collaborators.

While the majority of results in this thesis are specialised for a Schwarzschild background, perturbations to a Kerr black hole will be derived in Chapter 9. Introducing rotation deeply complicates perturbation calculations. To solve the perturbed Einstein field equations in Kerr, one employs the Newman-Penrose (NP) formalism to obtain the fully separable Teukolsky equation, whose solution is related to the perturbed Weyl scalars, which describe the perturbations to the curvature of the spacetime. The first metric perturbations to rotating black holes were constructed in the radiation gauge using a Hertz potential by Chrzanowski [63] in addition to Cohen and Kegeles [64, 65], which together will be referred to as the CCK reconstruction. It was Lousto and Whiting who later related the Hertz potential, from which the metric is constructed, to the perturbed Weyl scalars in the time-domain in the Schwarzschild limit [66]. The CCK method is applicable only in the absence of sources, but extensions of their work allow for sourced perturbations [67]. However, metric perturbations in the radiation gauge have an infinite string-like singularity [36] and are incomplete besides [68, 69]. By carrying out the CCK reconstruction in two different regions, either side of the secondary particle, a 'no-string' radiation gauge solution is obtained [70, 41, 71], though a singularity remains on the surface defined by the radial distance of the particle from the primary black hole. This is the most prominent approach to modelling EMRIs and performing GSF calculations in Kerr. In particular, work by Van de Meent has used the no-string reconstruction to implement the first-order SF calculation for a fully generic, inclined and eccentric bound orbits in the frequency domain [72]. There is ongoing work to implement metric reconstruction for GSF applications in the time domain [73, 74]. The singular surface at the particle however remains a large stumbling block for 2GSF calculations. There are a number of possible directions currently being explored to overcome this. For example, Green, Hollands and Zimmerman (GHZ) show how to construct the sourced metric

perturbation solution using a Hertz potential, a gauge transformation from the radiation gauge and a 'corrector tensor' [75]. The work of Toomani *et al.* [43] go further, combing the work of GHZ with the no-string radiation gauge, and a more regular Teukolsky puncture scheme is proposed.

As the regularisation of the SF is currently best understood in the Lorenz gauge, another desirable avenue therefore is to construct the Kerr metric perturbation in the Lorenz gauge. For example, Dolan calculates the first-order Lorenz gauge metric perturbation to a Kerr black hole in the time domain for circular, equatorial orbits. While this work remains unpublished, it is used in Refs. [76, 77, 78, 79]. More recent work by Osburn and Nishimura, who calculate the scalar SF in the Lorenz gauge on a Kerr background for circular orbits by using elliptical PDEs, thus circumventing numerical instabilities of hyperbolic PDEs [80], provide another promising method to obtain Lorenz gauge perturbations of rotating black holes. There has also been significant progress by Dolan, Kavanagh and Wardell, who have determined source-free perturbations in both the electromagnetic and gravitational case to a Kerr black hole in the Lorenz gauge [5, 81, 82], by construction from a Hertz potential and transforming from the radiation to the Lorenz gauge. This is the method we shall follow in Chapter 9.

The full metric perturbation is made up of a number of different contributions. Gravitational radiation is described fully by the perturbed Weyl scalars and is determined by spin-weight $s = 2$ perturbations [69]. Perturbations to the overall mass and angular momentum of the spacetime, i.e. perturbations to the mass and angular momentum of either a Schwarzschild or Kerr black hole, are then described by monopole and dipole contributions (for spherical l modes) to the metric perturbation respectively [69]. In some cases there exists contributions that are 'pure gauge', but they hold no physical information [69]. Detweiler and Poisson show that the low multipole modes, $l = 0$ and $l = 1$ of the metric perturbation have a significant contribution to the self-force [83]. The $s = 1$ contribution to the homogeneous, first-order metric perturbation of a Kerr black hole in the Lorenz gauge are not provided in [5], and will be derived in Chapter 9 for the first time, in collaboration with Dolan. While the gauge contributions to the metric are unphysical, they are required to determine a Lorenz gauge solution, for which the regularisation parameters for the SF have already been calculated [44, 45]. A pure gauge $s = 1$ metric perturbation is derived by construction from an $s = 1$ gauge vector, and the solution is written in terms of $s = 1$ Teukolsky fields. In the Schwarzschild limit, using the Chandrasekhar transformation, Berndtson's gauge transformation for the $s = \pm 1$ case can be recovered, where the Lorenz gauge metric perturbation is written in terms of $s = 1$ RW fields. However, there is currently no available analytic solution that relates the first-order Lorenz gauge metric perturbation of rotating black holes to the perturbed Weyl scalars in the presence of sources. As Berndtson's gauge transformation contains sources, research in Chapter 9 aims to provide insight as to how to introduce source terms to the Kerr case in the future, hence extending the work of Dolan *et al* [5].

A final tool derived in this thesis is the implementation of the Mano-Suzuki-Takasugi (MST) method [84, 85, 86], used for calculating semi-analytic solutions to the Teukolsky and RW equations in the low-frequency regime. MST solutions are written in terms of a convergent series of hypergeo-

metric and Coulomb functions, describing GWs radiated into the primary's horizon and to infinity, respectively [84, 85, 86, 87]. The coefficients of the MST series are written in terms of powers of small frequency $\epsilon = 2M\omega$, which corresponds directly to a post-Minkowskian (PM) expansion [85]. For bound orbits, the PM assumption that $\frac{GM}{c^2} \ll r$ coincides exactly to the PN assumption that $v^2 \ll c^2$ [85, 84]. For circular orbits, low frequencies correspond to large distances, and the MST method can be used to compute GWs radiated to infinity to arbitrarily high orders in a PN series [84, 87] as well as providing a means to write down PN series solutions of GWs absorbed into either a Schwarzschild or Kerr black hole, something that is difficult to do using other methods [84, 87]. In Chapter 3, the MST method was implemented for the Teukolsky case, while the RW case had already been implemented by Wardell *et al.* The MST package was implemented in *Mathematica* and published in the black hole perturbation toolkit (BHPToolkit) [1], an open source resource for computing useful quantities commonly needed to do BHPT. While the MST method was initially derived for low-frequencies, its implementation in the BHPToolkit allows for numerical valued solutions to be determined for any frequency, providing a useful tool for the scientific community. The MST method allows for extremely high precision calculations, though at the cost of speed. However, depending on one's goal, using the BHPToolkit one has the option to use either the MST method or standard numerical integration to solve the Teukolsky and RW equations. Given that the radiative piece of the metric perturbation is captured by the solutions to the Teukolsky equation [69], one could write the radiative contribution to the first-order metric perturbation in any gauge, entirely as a semi-analytic MST series for low frequencies, corresponding to a PN type solution. If one was able to determine a low-frequency expansion solution to the gauge contributions of Berndtson's gauge transformation, one could then obtain a PN series solution to the full Lorenz gauge metric perturbation to first-order in the small mass ratio for a Schwarzschild background. While there is currently no known semi-analytic solution to the gauge contributions of Berndtson's transformation, there is progress being made in recent research [88].

1.3   Structure

This thesis will be structured in the following way. A review of BHPT will first be provided in Chapter 2 to set up the machinery used throughout this work. Chapter 3 will then introduce the MST method for calculating semi-analytic solutions to the RW and Teukolsky equations in the low-frequency regime. This chapter will also discuss in detail the implementation of the MST package, which had been made available as part of the BHPToolkit [1], and is one of the main outputs of this thesis.

A review of GSF theory will then be provided in Chapter 4, which follows Ref. [14] and sets up in detail the motivation and methodology for the remaining chapters. Following Ref. [2], Chapter 5 will describe how to calculate the retarded first-order Lorenz gauge metric perturbation in the frequency domain for quasicircular, equatorial orbits on a Schwarzschild background. While this quantity has been calculated throughout the literature in both the frequency and time domain

[89, 90, 91, 46, 92, 83], this will serve as input to the algorithm in Chapter 6, which also follows Ref. [2]. Chapter 6 will detail the novel calculation of the retarded slowly evolving first-order Lorenz gauge metric perturbation, also in the frequency domain for quasicircular, equatorial orbits on a Schwarzschild background. Both Chapter 5 and Chapter 6 make use of Berndtson's gauge transformation, from RW gauge solutions to the Lorenz gauge. The calculation of the slowly evolving metric perturbation plays a vital role in the GSF program. The slowly evolving first-order metric perturbation contributes to the source of the second-order metric perturbation, which in turn goes into calculating the GW phase to post-adiabatic order, required to perform precision tests of GR and obtain accurate parameter estimations from EMRI signals. The data for the slowly evolving first-order Lorenz gauge metric perturbation is one of the major results produced in this thesis and has already been used to calculate waveforms and the energy flux via the GSF approach, and to compare them with NR simulations [4, 3]. These results have also been used to make comparisons with EOB theory [93, 94] and will be used in a number of forthcoming papers, for example, in the calculation of the second-order Teukolsky source, which is undergoing research by collaborators [43, 95].

The calculations from Chapter 5 and Chapter 6 are relevant only during the inspiral part of the waveform however, and break down as the secondary approaches the ISCO. The dynamics of the binary changes, and the orbital radius of the EMRI evolves on a faster timescale than during the inspiral as the binary begins its transition to plunge. Chapter 7 covers the transition to plunge regime in detail. The main results are the calculation of the adiabatic GW phase and amplitude during the transition, obtained in collaboration with Küchler, Compère and Pound. Results from previous chapters are then combined in Chapter 8, where the energy flux and waveforms generated by the GSF approach are presented, based on the work of Refs. [3, 4]. This chapter includes comparisons between the 2GSF calculations of the energy flux and waveforms with NR simulations during the inspiral, and for adiabatic waveforms during the transition regime. Results show that the GSF approach to second-order in the small mass ratio agrees extremely well with NR simulations for IMRIs and even reasonably well for equal mass ratios [3, 4].

For the majority of this thesis only a Schwarzschild background has been considered. The ultimate goal however is of course to solve for the GW phase and amplitudes, and hence the first and second-order metric perturbations for generic orbits on a Kerr background spacetime. Chapter 9 covers perturbations to rotating black holes, following the method of [5]. The primary outputs of this chapter are analytic solutions to gauge contributions of the homogeneous, first-order Lorenz gauge metric perturbation for a Kerr background, which are constructed for the first time using an $s = 1$ vector, in collaboration with Dolan. The results are shown to recover those of Berndtson [46] in the Schwarzschild limit. Finally, Chapter 10 concludes this work by summarising the main outputs and provides a discussion on future directions of this research. The conventions used in this thesis are outlined as follows. Geometric units will be used from the outset such that $G = c = 1$, with Lorentzian metric signature $(- + + +)$. A spacetime foliation of hypersurfaces defined by constant t is assumed and hereafter, orbits are specialised to quasicircular and equatorial inspirals.

Chapter 2

Black Hole Perturbation Theory

This chapter provides a review of BHPT, introducing tools required to obtain the results in later chapters.

2.1 The metric perturbation and linearised Einstein field equations

The Einstein field equations, relating curvature of the spacetime to matter present in the spacetime, are given by

$$G_{\mu\nu} = 8\pi T_{\mu\nu}, \tag{2.1}$$

where $T_{\mu\nu}$ is the stress-energy tensor (SET) and $G_{\mu\nu}$ is the Einstein tensor, defined by

$$G_{\mu\nu} = R_{\mu\nu} - \frac{1}{2}g_{\mu\nu}R, \tag{2.2}$$

where R and $R_{\mu\nu}$ are the Ricci scalar and tensor respectively, and are defined by

$$R_{\mu\nu} = g^{\alpha\beta}R_{\alpha\mu\beta\nu}, \tag{2.3}$$

$$R = g^{\mu\nu}R_{\mu\nu}, \tag{2.4}$$

and the Riemann tensor is defined as

$$R^{\mu}_{\nu\rho\sigma} = \nabla_{\rho}\Gamma^{\mu}_{\nu\sigma} - \nabla_{\sigma}\Gamma^{\mu}_{\nu\rho} + \Gamma^{\tau}_{\nu\sigma}\Gamma^{\mu}_{\tau\rho} - \Gamma^{\tau}_{\nu\rho}\Gamma^{\mu}_{\tau\sigma}, \tag{2.5}$$

with the Christoffel connection

$$\Gamma^{\mu}_{\sigma\rho} = \frac{1}{2}g^{\mu\nu}\left(g_{\sigma\rho,\nu} + g_{\nu\sigma,\rho} - g_{\nu\rho,\sigma}\right). \tag{2.6}$$

In the absence of sources, where $T_{\mu\nu} = 0$, the solution to the vacuum Einstein field equations describes either a black hole spacetime, or the most trivial solution, flat Minkowski space. By Birkhoff's theorem, in the static, spherically symmetric case, the solution to the vacuum Einstein field equations is that of the Schwarzschild metric, and in the stationary, axisymmetric case, the field

equations admit the Kerr solution. The line-element in the Schwarzschild spacetime is described by

$$ds^2 = -d\tau^2 = -f(r)dt^2 + \frac{1}{f(r)}dr^2 + r^2 d\theta^2 + r^2 \sin^2 \theta d\phi^2, \tag{2.7}$$

where

$$f(r) = 1 - \frac{2M}{r}, \tag{2.8}$$

and the Schwarzschild metric is given by

$$g_{\mu\nu} = \mathrm{diag}\left(-f(r), f(r)^{-1}, r^2, r^2 \sin^2 \theta\right). \tag{2.9}$$

The Kerr metric will be given later in Section 2.7. Adding a perturbation to the spacetime, $h_{\mu\nu}$ that describes some small compact object, the full spacetime is defined by the metric $\mathrm{g}_{\mu\nu}$, with coordinates x^μ, where

$$\mathrm{g}_{\mu\nu}(x^\alpha; z^\alpha) = g_{\mu\nu}(x^\alpha) + h_{\mu\nu}(x^\alpha; z^\alpha). \tag{2.10}$$

The background metric $g_{\mu\nu}$ depends on the background coordinates x^μ and the retarded perturbation $h_{\mu\nu}$ depends on both the background coordinates and the position on world-line of the object it describes, $z^\mu(\tau)$. In the case of EMRIs, the background metric $g_{\mu\nu}$ describes a supermassive black hole, which shall be referred to as the primary with mass M, and $h_{\mu\nu}$ describes the perturbation to the spacetime introduced by some small compact object, either a black hole, neutron star, or some other exotic compact object, and shall be referred to as the secondary with mass μ. BHPT is a natural choice for modelling EMRIs, where the small quantity in the perturbation is the small mass ratio ε, defined by

$$\varepsilon = \frac{\mu}{M} \ll 1. \tag{2.11}$$

The metric perturbation is then expanded in powers of ε [14]

$$h_{\mu\nu}(x^\alpha; z^\alpha) = \sum_{n=1}^{\infty} \varepsilon^n h_{\mu\nu}^n \left(x^\alpha; z^\alpha\right), \tag{2.12}$$

where $h_{\mu\nu}^n$ is the nth-order metric perturbation. This is what is referred to as the self-consistent approach. The Einstein field equations then become

$$\mathcal{G}_{\mu\nu} = 8\pi T_{\mu\nu} \tag{2.13}$$

where $\mathcal{G}_{\mu\nu}$ is the Einstein operator acting on the full spacetime and $T_{\mu\nu}$ is the SET of the full spacetime, which for a vacuum background is just the SET describing the source of the perturbation, which can also be expanded in powers of the small mass ratio

$$T_{\mu\nu}(x^\alpha; z^\alpha) = \sum_{n=1}^{\infty} \varepsilon^n T_{\mu\nu}^n(x^\alpha; z^\alpha). \tag{2.14}$$

By setting $g_{\mu\nu} \to g_{\mu\nu}$ in the definition of the Riemann tensor, in addition to the Ricci scalar and Ricci tensor, whose background quantities are zero in vacuum, the full Einstein tensor can be written as

$$\mathcal{G}_{\mu\nu} = G_{\mu\nu} + \sum_{n=1}^{\infty} \varepsilon^n \delta^n G_{\mu\nu}, \tag{2.15}$$

such that

$$G_{\mu\nu} = 0, \tag{2.16}$$
$$\delta^n G_{\mu\nu} = 8\pi T^n_{\mu\nu}, \tag{2.17}$$

where, at leading order in ε

$$\delta^1 G_{\mu\nu} = \frac{1}{2}\left(-\Box h_{\mu\nu} + 2R_{\alpha\nu\mu\beta}h^{\alpha\beta} + \nabla_\nu\nabla_\alpha h_\mu{}^\alpha + \nabla_\mu\nabla_\alpha h_\nu{}^\alpha - \nabla_\nu\nabla_\mu h - g_{\mu\nu}\nabla_\alpha\nabla_\beta h^{\alpha\beta} + g_{\mu\nu}\Box h\right), \tag{2.18}$$

and the trace h^n for a given order in the perturbation is defined as

$$h^n = \text{Tr}[h^n_{\mu\nu}] = g^{\mu\nu}h^n_{\mu\nu}. \tag{2.19}$$

The leading order linearised Einstein field equations can be expressed more simply as

$$\delta^1 G[h^1_{\mu\nu}] = 8\pi T^1_{\mu\nu}. \tag{2.20}$$

where $\delta^1 G$ is now the operator acting on $h^1_{\mu\nu}$ in $\delta^1 G_{\mu\nu}$. The remainder of this work will specialise to Boyer-Lindquist coordinates

$$x^\mu = \{t, r, \theta, \phi\} \tag{2.21}$$
$$z^\mu = \{t_{\text{p}}(\tau), r_{\text{p}}(\tau), \theta_{\text{p}}(\tau), \phi_{\text{p}}(\tau)\}, \tag{2.22}$$

where subscript p denotes quantities describing the position of the secondary particle. The spacetime will also be considered as a foliation of hyperbolic slices defined by constant t throughout this work, unless specified otherwise. Raising and lowering indices and differential operations are performed with respect to $g_{\mu\nu}$.

2.2   The tensor spherical harmonic basis

Solving the linearised Einstein field equations is often tackled using a tensor spherical harmonic basis, which exploits the spherical symmetry in Schwarzschild, or axis-symmetry in Kerr. Beginning with the explicit definitions of the tensor spherical harmonic basis from chapter 12 of Maggiore's textbook: "Gravitational Waves" [96], a tensor of type $(0,2)$ can be written as a mode-sum decomposition in

the following way

$$h_{\mu\nu}(x^\alpha) = \sum_i \sum_{l=0}^{\infty} \sum_{m=-l}^{l} h^i_{lm}(t,r)(\mathbf{t}^i_{lm})_{\mu\nu}(\theta,\phi), \tag{2.23}$$

where the explicit dependence on z^α has been dropped for now, and the tensor spherical harmonic basis elements, $\mathbf{t}^i$ are given explicitly by [96]

$$\mathbf{t}^{tt}_{lm} = \begin{pmatrix} 1 & 0 & 0 & 0 \\ 0 & 0 & 0 & 0 \\ 0 & 0 & 0 & 0 \\ 0 & 0 & 0 & 0 \end{pmatrix} Y_{lm}, \qquad \mathbf{t}^{Rt}_{lm} = \begin{pmatrix} 0 & 1 & 0 & 0 \\ 1 & 0 & 0 & 0 \\ 0 & 0 & 0 & 0 \\ 0 & 0 & 0 & 0 \end{pmatrix} Y_{lm}, \qquad \mathbf{t}^{L0}_{lm} = \begin{pmatrix} 0 & 0 & 0 & 0 \\ 0 & 1 & 0 & 0 \\ 0 & 0 & 0 & 0 \\ 0 & 0 & 0 & 0 \end{pmatrix} Y_{lm},$$

$$\mathbf{t}^{T0}_{lm} = \begin{pmatrix} 0 & 0 & 0 & 0 \\ 0 & 0 & 0 & 0 \\ 0 & 0 & 1 & 0 \\ 0 & 0 & 0 & \sin^2(\theta) \end{pmatrix} Y_{lm}, \quad \mathbf{t}^{Et}_{lm} = \begin{pmatrix} 0 & 0 & \partial_\theta & \partial_\phi \\ 0 & 0 & 0 & 0 \\ \star & 0 & 0 & 0 \\ \star & 0 & 0 & 0 \end{pmatrix} Y_{lm}, \quad \mathbf{t}^{E1}_{lm} = \begin{pmatrix} 0 & 0 & 0 & 0 \\ 0 & 0 & \partial_\theta & \partial_\phi \\ 0 & \star & 0 & 0 \\ 0 & \star & 0 & 0 \end{pmatrix} Y_{lm},$$

$$\mathbf{t}^{Bt}_{lm} = \begin{pmatrix} 0 & 0 & (1/\sin\theta)\partial_\phi & -\sin\theta\,\partial_\theta \\ 0 & 0 & 0 & 0 \\ \star & 0 & 0 & 0 \\ \star & 0 & 0 & 0 \end{pmatrix} Y_{lm}, \quad \mathbf{t}^{B1}_{lm} = \begin{pmatrix} 0 & 0 & 0 & 0 \\ 0 & 0 & (1/\sin\theta)\partial_\phi & -\sin\theta\,\partial_\theta \\ 0 & \star & 0 & 0 \\ 0 & \star & 0 & 0 \end{pmatrix} Y_{lm},$$

$$\mathbf{t}^{E2}_{lm} = \begin{pmatrix} 0 & 0 & 0 & 0 \\ 0 & 0 & 0 & 0 \\ 0 & 0 & W & X \\ 0 & 0 & \star & -\sin^2\theta\,W \end{pmatrix} Y_{lm}, \qquad \mathbf{t}^{B2}_{lm} = \begin{pmatrix} 0 & 0 & 0 & 0 \\ 0 & 0 & 0 & 0 \\ 0 & 0 & -(1/\sin\theta)X & \sin\theta\,W \\ 0 & 0 & \star & \sin\theta\,X \end{pmatrix} Y_{lm},$$

and Y_{lm} are the standard spherical harmonics, whose explicit dependence on θ and ϕ has been suppressed and will only be reintroduced where it is instructive to do so. In this work, the spherical harmonics are normalized such that

$$\int\int \mathrm{d}\theta\mathrm{d}\phi\, Y^*_{lm}(\theta,\phi)Y_{l'm'}(\theta,\phi) = \delta_{ll'}\delta_{mm'}, \tag{2.24}$$

where $*$ on the spherical harmonics denotes complex conjugation. The operators X and W are then given by [46, 96]

$$X = 2\partial_\theta\partial_\phi - 2\cot\theta\,\partial_\phi \tag{2.25}$$

$$W = \partial_\theta^2 - \cot\theta\,\partial_\theta - \frac{1}{\sin^2\theta}\,\partial_\phi^2. \tag{2.26}$$

The spherical harmonics transform under parity in the following way [97]

$$Y_{lm}(\pi - \theta, \phi + \pi) \rightarrow (-1)^l \, Y_{lm}(\theta, \phi), \tag{2.27}$$

so that [96]

$$\mathbf{t}^i \rightarrow \begin{cases} (-1)^l \mathbf{t}^i & \text{if} \quad i = \{L0, T0, E1, E2, tt, Rt, Et\}, \\ (-1)^{l+1}\mathbf{t}^i & \text{if} \quad i = \{B1, B2, Bt\}. \end{cases} \tag{2.28}$$

The basis elements $\mathbf{t}^i$ that pick up a factor of $(-1)^l$ under parity are said to have electric-like parity, or to be polar or even. Similarly, the basis elements $\mathbf{t}^i$ that pick up a factor of $(-1)^{l+1}$ under parity are said to have magnetic-like parity, or to be axial or odd. For this reason the metric perturbation, in the frequency domain, on constant t slices, is often written in terms of its even and odd sector basis elements as follows [96, 46]

$$h_{\mu\nu}(t, r, \theta, \phi) = \sum_{l=0}^{\infty} \sum_{m=-l}^{l} \int_{-\infty}^{\infty} e^{-i\omega t} \left(h_{\mu\nu}^{o,lm}(\omega, r, \theta, \phi) + h_{\mu\nu}^{e,lm}(\omega, r, \theta, \phi) \right) d\omega. \tag{2.29}$$

Following Berndtson's notation [46], the odd-sector metric perturbation contains 3 degrees of freedom given by $h_0^{lm}(r)$, $h_1^{lm}(r)$ and $h_2^{lm}(r)$. For convenience the explicit dependence on r of the odd-sector fields will be suppressed henceforth. The odd-sector metric perturbation in Berndtson's notation is then given by [46]

$$h_{\mu\nu}^{o,lm}(\omega, r, \theta, \phi) = \begin{pmatrix} 0 & 0 & h_0^{lm} \csc\theta \frac{\partial Y_{lm}}{\partial \phi} & -h_0^{lm} \sin\theta \frac{\partial Y_{lm}}{\partial \theta} \\ * & 0 & h_1^{lm} \csc\theta \frac{\partial Y_{lm}}{\partial \phi} & -h_1^{lm} \sin\theta \frac{\partial Y_{lm}}{\partial \theta} \\ * & * & -h_2^{lm} X_{lm} & h_2^{lm} \sin\theta W_{lm} \\ * & * & * & h_2^{lm} \sin^2\theta X_{lm}(\theta, \phi) \end{pmatrix}, \tag{2.30}$$

where X_{lm} and W_{lm} are defined by

$$W_{lm}(\theta, \phi) = \frac{\partial^2 Y_{lm}}{\partial \theta^2} - \cot\theta \frac{\partial Y_{lm}}{\partial \theta} - \frac{1}{\sin^2\theta} \frac{\partial^2 Y_{lm}}{\partial \phi^2}, \tag{2.31}$$

$$X_{lm}(\theta, \phi) = \frac{2}{\sin\theta} \frac{\partial}{\partial \phi} \left(\frac{\partial Y_{lm}}{\partial \theta} - \cot\theta Y_{lm} \right). \tag{2.32}$$

The operators X_{lm} and W_{lm} take on slightly different definitions in Berndtson thesis [46] compared to those in Maggiore's textbook [96]. The definitions from Eq. (2.31) and Eq. (2.32) shall be used for the remainder of this thesis, and the explicit dependence on θ and ϕ of X_{lm} and W_{lm} will be suppressed henceforth.

The even-sector metric perturbation then contains 7 degrees of freedom, given by $h_0^{lm}(r)$, $h_1^{lm}(r)$, $H_0^{lm}(r)$, $H_1^{lm}(r)$, $H_2^{lm}(r)$, $K^{lm}(r)$ and $G^{lm}(r)$, where $h_0^{lm}(r)$ and $h_1^{lm}(r)$ in the even-sector are distinct to those in the odd-sector. As in the odd-sector, the explicit dependence on r of these fields will be suppressed henceforth, and the full even-sector perturbation can be written as [46]

$$
h_{\mu\nu}^{e,lm}(\omega, r, \theta, \phi) =
$$
$$
\begin{pmatrix}
\left(1 - \frac{2M}{r}\right) H_0^{lm} Y_{lm} & H_1^{lm} Y_{lm} & h_0^{lm} \frac{\partial Y_{lm}}{\partial \theta} & h_0^{lm} \frac{\partial Y_{lm}}{\partial \phi} \\
* & \frac{H_2^m Y_{lm}}{\left(1 - \frac{2M}{r}\right)} & h_1^{lm} \frac{\partial Y_{lm}}{\partial \theta} & h_1^{lm} X_{lm} \\
* & * & \begin{aligned} r^2 \big(K^{lm} Y_{lm} \\ + G^{lm} W_{lm}\big) \end{aligned} & r^2 \sin\theta G^{lm} X_{lm} \\
* & * & * & \begin{aligned} r^2 \sin^2\theta \big(K^{lm} Y_{lm} \\ - G^{lm} W_{lm} \big) \end{aligned}
\end{pmatrix} .
\tag{2.33}
$$

Note that the radial fields h_0^{lm} and h_1^{lm} from the odd-sector should not be confused with those from the even-sector.

2.3   The stress-energy tensor

The source of the perturbation to the spacetime is described by the SET, $T_{\mu\nu}$. At leading order in ε, the secondary can be modelled as a point-like particle with mass μ at some position $z^\mu(\tau)$ in the spacetime [14, 98, 99, 40, 100]. This is also the reason why the SF is singular at the location of the source. For the remainder of this chapter only the leading order SET shall be discussed. As such, the superscript in $T_{\mu\nu}^1$ will be dropped. Assuming no internal structure, the leading order SET is therefore given by

$$
T^{\mu\nu} = \mu \int_{-\infty}^{\infty} \frac{\delta^4(x^\alpha - z^\alpha(\tau))}{\sqrt{-g}} \frac{dz^\mu}{d\tau} \frac{dz^\nu}{d\tau} d\tau,
\tag{2.34}
$$

where g is the determinant of $g_{\mu\nu}$. Similarly to the metric perturbation, the SET can be decomposed into a tensor spherical harmonic basis in the frequency domain, for constant t-slicing, in the following way [46]

$$
T_{\mu\nu}(t, r, \theta, \phi) = \mu \sum_{l=0}^{\infty} \sum_{m=-l}^{l} \int_{-\infty}^{\infty} e^{-i\omega t} \left(T_{\mu\nu}^{o,lm}(\omega, r, \theta, \phi) + T_{\mu\nu}^{e,lm}(\omega, r, \theta, \phi) \right) d\omega,
\tag{2.35}
$$

where the explicit dependence on z^α has been dropped for now. The odd- and even-sector SETs can then be written as

$$
T_{\mu\nu}^{o,lm} =
\begin{pmatrix}
0 & 0 & So_{02}^{lm}(r) \csc\theta \frac{\partial Y_{lm}}{\partial \phi} & -So_{02}^{lm}(r) \sin\theta \frac{\partial Y_{lm}}{\partial \theta} \\
* & 0 & So_{12}^{lm}(r) \csc\theta \frac{\partial Y_{lm}}{\partial \phi} & -So_{12}^{lm}(r) \sin\theta \frac{\partial Y_{lm}}{\partial \theta} \\
* & * & -So_{22}^{lm}(r) X_{lm} & So_{22}^{lm}(r) \sin\theta W_{lm} \\
* & * & * & So_{22}^{lm}(r) \sin^2\theta X_{lm}
\end{pmatrix}
\tag{2.36}
$$

and

$$T_{\mu\nu}^{e,lm} =$$

$$\begin{pmatrix} Se_{00}^{lm}(r)Y_{lm} & Se_{01}^{lm}(r)Y_{lm} & Se_{02}^{lm}(r)\frac{\partial Y_{lm}}{\partial \theta} & Se_{02}^{lm}(r)\frac{\partial Y_{lm}}{\partial \phi} \\ * & Se_{11}^{lm}(r)Y_{lm} & Se_{12}^{lm}(r)\frac{\partial Y_{lm}}{\partial \theta} & Se_{12}^{lm}(r)\frac{\partial Y_{lm}}{\partial \phi} \\ * & * & Ue_{22}^{lm}(r)Y_{lm} + Se_{22}^{lm}(r)W_{lm} & Se_{22}^{lm}(r)\sin\theta X_{lm} \\ * & * & * & \sin^2\theta\left(Ue_{22}^{lm}(r)Y_{lm} - Se_{22}^{lm}(r)W_{lm}\right) \end{pmatrix}.$$

$$(2.37)$$

The radial components can be derived in the following way. Defining the four-velocity u^μ

$$u^\mu = \frac{dz^\mu}{d\tau}, \tag{2.38}$$

the SET can be rewritten as

$$T^{\mu\nu} = \mu \int_{-\infty}^{\infty} \frac{\delta^4(x^\alpha - z^\alpha(\tau))}{\sqrt{-g}} u^\mu u^\nu d\tau, \tag{2.39}$$

$$= \mu \int_{-\infty}^{\infty} \frac{\delta^4(x^\alpha - z^\alpha(\tau))}{\sqrt{-g}} \frac{u^\mu u^\nu}{u^t} dt \tag{2.40}$$

$$= \mu \frac{1}{\sqrt{-g}} \frac{u^\mu u^\nu}{u^t} \delta^3\left(x^a - z^a(t)\right), \tag{2.41}$$

where

$$\delta^3(x^a - z^a(t)) = \delta(r - r_{\rm p}(t))\delta(\theta - \theta_{\rm p}(t))\delta(\phi - \phi_{\rm p}(t)). \tag{2.42}$$

For circular, equatorial orbits

$$r_p = r_0, \quad \theta_p = 0, \quad \frac{d\phi_{\rm p}}{dt} = \Omega, \tag{2.43}$$

where

$$\Omega = \sqrt{\frac{M}{r_0^3}}, \tag{2.44}$$

so that

$$u^\mu = \{u^t, 0, 0, \Omega u^t\}. \tag{2.45}$$

Assuming the secondary's world-line is time-like, the four-velocity obeys the normalisation condition

$$g_{\mu\nu}u^\mu u^\nu\big|_{x^\alpha = z^\alpha} = -1. \tag{2.46}$$

For a Schwarzschild background, the time-like normalisation condition amounts to

$$u^t = \frac{1}{\sqrt{-g_{tt} - g_{\phi\phi}\Omega^2}}\bigg|_{x^\alpha = z^\alpha} = \sqrt{\frac{r_0}{r_0 - 3M}}. \tag{2.47}$$

Therefore, components of the leading order SET for a particle travelling on circular, equatorial orbits are given in the frequency domain by [46]

$$So_{02}^{lm}(r) = \mu u^t \frac{f(r)\Omega}{l(l+1)}\delta(r-r_0)\partial_\theta Y_{lm}^*\left(\frac{\pi}{2},0\right), \tag{2.48a}$$

$$So_{12}^{lm}(r) = 0, \tag{2.48b}$$

$$So_{22}^{lm}(r) = -2im\mu u^t \frac{r^2\Omega^2}{2l(l+1)(l-1)(l+2)}\delta(r-r_0)\partial_\theta Y_{lm}^*\left(\frac{\pi}{2},0\right), \tag{2.48c}$$

$$Se_{00}^{lm}(r) = \mu u^t \frac{f(r)^2}{r^2}\delta(r-r_0)Y_{lm}^*\left(\frac{\pi}{2},0\right), \tag{2.48d}$$

$$Se_{01}^{lm}(r) = 0, \tag{2.48e}$$

$$Se_{11}^{lm}(r) = 0, \tag{2.48f}$$

$$Ue_{22}^{lm}(r) = \frac{1}{2}\mu u^t r^2\Omega^2\delta(r-r_0)Y_{lm}^*\left(\frac{\pi}{2},0\right), \tag{2.48g}$$

$$Se_{02}^{lm}(r) = im\mu u^t \frac{f(r)\Omega}{l(l+1)}\delta(r-r_0)Y_{lm}^*\left(\frac{\pi}{2},0\right), \tag{2.48h}$$

$$Se_{12}^{lm}(r) = 0, \tag{2.48i}$$

$$Se_{22}^{lm}(r) = \mu u^t \frac{r^2\Omega^2(l(l+1)-2m^2)}{2l(+1)(l-1)(l+2)}\delta(r-r_0)Y_{lm}^*\left(\frac{\pi}{2},0\right). \tag{2.48j}$$

All sources are compactly supported on the particle's world-line and are provided by reference [46]. For the remainder of this work, orbits will be specialised to circular and equatorial. The distinction to quasicircular orbits will be discussed later in Chapter 4.

2.4   The Regge-Wheeler gauge

The RW gauge is defined by setting the field h_2^{lm} from the odd-sector and the fields h_0^{lm}, h_1^{lm} and G^{lm} from the even-sector for all l and m to zero [46, 101, 96]. The RW and Zerilli (RWZ) equations for spin-weight $s=2$ are derived by applying the RW gauge to the odd and even-sectors of the generic first-order linearised Einstein field equations with a Schwarzschild background respectively. The odd- and even-sector solutions for the $s=0$, 1 RW equations are derived similarly from electromagnetic and scalar perturbations [96]. For generic spin-weight s and a given l, m mode, the RWZ master equations are given in the frequency domain on constant t slicing by [101, 96]

$$\mathcal{L}_s\psi_s(r) = S_s(r), \tag{2.49}$$

where

$$\mathcal{L}_s \equiv \left(\frac{d^2}{dr_*^2} - V(r) + \omega^2\right), \tag{2.50}$$

with

$$\omega = m\Omega, \tag{2.51}$$

having specialised to circular orbits. The tortoise coordinate r_* for a Schwarzschild background is defined such that

$$dr_*/dr = f(r)^{-1}. \tag{2.52}$$

Integrating this and choosing an integration constant yields

$$r_*(r) = r + 2\log[r/(2M) - 1]. \tag{2.53}$$

The RW equation for some spin weight s is obtained by setting the potential $V(r)$ to

$$V(r) = f(r)\left(\frac{l(l+1)}{r^2} + \frac{2M(1-s^2)}{r^3}\right). \tag{2.54}$$

Similarly, the Zerilli equation, defined only for $s = 2$, is obtained by setting the potential to

$$V(r) = \frac{f(r)}{r^2\Lambda^2}\left[2\lambda^2\left(\lambda + 1 + \frac{3M}{r}\right) + \frac{18M^2}{r^2}\left(\lambda + \frac{M}{r}\right)\right], \tag{2.55}$$

with

$$\Lambda = \lambda + 3M/r, \tag{2.56}$$

and

$$\lambda = (l+2)(l-1)/2. \tag{2.57}$$

The RWZ master functions, $\psi_s(r)$ are then sourced by $S_s(r)$, which are given explicitly in Appendix A. The inhomogeneous Regge-Wheeler gauge metric perturbation, $h_{\mu\nu}^{\mathrm{RW}}$ can then be reconstructed from the RWZ master functions as shown by Regge and Wheeler [101, 46]. Dropping the l, m labels for convenience, the leading order odd-sector metric perturbations components in the RW gauge, and in the absence of sources for a given l, m mode are [46]:

$$h_0^{\mathrm{RW}} = \frac{(2M - r)}{i\omega}\psi_2' - \left(1 - \frac{2M}{r}\right)\frac{\psi_2}{i\omega}, \tag{2.58}$$

$$h_1^{\mathrm{RW}} = \frac{r}{f}\psi_2, \tag{2.59}$$

where ψ_2 in this case obeys the RW equation, and in the even-sector, the leading order metric perturbation components for a given l, m mode in the absence of sources are [46]

$$\begin{aligned}
H_0^{\mathrm{RW}} = H_2^{\mathrm{RW}} &= \frac{\left(-3M^2 - 3\lambda Mr + \lambda r^2\right)\psi_2'}{r(3M + \lambda r)} - \frac{1}{(2M - r)r^2(3M + \lambda r)^2}\left[-18M^4 + 9(1 - 2\lambda)M^3r\right. \\
&+ \lambda^2 r^4\left(1 + \lambda + (i\omega)^2 r^2\right) + 3M^2r^2\left(3\lambda - 2\lambda^2 + 3(i\omega)^2 r^2\right) + \lambda Mr^3\left(\lambda - 2\lambda^2\right. \\
&\left.+ 6(i\omega)^2 r^2\right)\right]\psi_2,
\end{aligned} \tag{2.60}$$

$$H_1^{\text{RW}} = -i\omega r\psi_2' + \frac{i\omega\left(-3M^2 - 3\lambda Mr + \lambda r^2\right)\psi_2}{(2M-r)(3M+\lambda r)}, \tag{2.61}$$

$$K^{\text{RW}} = \left(1 - \frac{2M}{r}\right)\psi_2' + \frac{\left(6M^2 + 3\lambda Mr + \lambda(1+\lambda)r^2\right)\psi_2}{r^2(3M+\lambda r)}, \tag{2.62}$$

where ψ_2 now obeys the Zerilli potential. Returning to the RWZ equations, as a second-order ordinary differential equation (ODE), there are two independent solutions corresponding to ingoing and outgoing radiation respectively: ψ_s^{in} and ψ_s^{up}. These independent homogeneous solutions to Eq. (2.49) display the following asymptotic behaviour [86, 63]

$$\psi_s^{\text{in}}(r) \sim \begin{cases} \psi_s^{\text{in,tra}}e^{-i\omega r_*}, & r_* \to -\infty, \\ \psi_s^{\text{in,inc}}e^{-i\omega r_*} + \psi_s^{\text{in,ref}}e^{i\omega r_*}, & r_* \to +\infty, \end{cases} \tag{2.63}$$

and

$$\psi_s^{\text{up}}(r) \sim \begin{cases} \psi_s^{\text{up,inc}}e^{i\omega r_*} + \psi_s^{\text{up,ref}}e^{-i\omega r_*}, & r_* \to -\infty, \\ \psi_s^{\text{up,tra}}e^{i\omega r_*}, & r_* \to +\infty, \end{cases} \tag{2.64}$$

where $\psi_s^{\text{in/up,inc/ref/tra}}$ are the incidence/reflection/transmission coefficients respectively. In the BHPToolkit [1], the radial RWZ functions are normalised such that the transmission coefficient, $\psi_s^{\text{in,trans}} = 1$ by default.

2.5 The Lorenz gauge

The Lorenz gauge is a desirable choice for a number of reasons. In the Lorenz gauge, the Einstein field equations are manifestly hyperbolic and the solutions to the metric perturbation components are C^0 differentiable at leading order in the small mass ratio. The regularization of the SF is also best understood in the Lorenz gauge, as discussed earlier in the introduction. As such, most of the calculations relating to the SF, including those in this thesis, are done in the Lorenz gauge [36]. The calculation of $h_{\mu\nu}^{1\text{L}}$ can been found throughout the literature [89, 90, 91, 46, 92, 83]. The Lorenz gauge is defined by the gauge condition

$$\bar{h}_{\mu\nu}{}^{;\nu} = 0 \tag{2.65}$$

where the trace-reversed metric is defined for a given order n in the perturbation

$$\bar{h}_{\mu\nu}^n \equiv h_{\mu\nu}^n - \frac{1}{2}g_{\mu\nu}g^{\alpha\beta}h_{\alpha\beta}^n. \tag{2.66}$$

It shall be assumed that the trace-reversed metric refers to Lorenz gauge perturbations throughout. The first-order linearised Einstein field equations from 2.20 can then be written in the Lorenz gauge as

$$\Box\bar{h}_{\mu\nu}^1 + 2R^\alpha{}_\mu{}^\beta{}_\nu\bar{h}_{\alpha\beta}^1 = 16\pi T_{\mu\nu}^1, \tag{2.67}$$

where $\Box \equiv \nabla^\alpha\nabla_\alpha$. Then the Lorenz gauge metric perturbation $h_{\mu\nu}^{1\text{L}}$ can be determined either by solving Eq. (2.67) directly, as has been done numerically in both the time and frequency domains

[89, 90, 91, 46, 92, 83] or via a gauge transformation [46, 5, 102, 83, 2]. Similarly to Eq. (2.23), the first-order Lorenz gauge field equations can be tackled by using a mode-sum decomposition in the Barack-Sago-Lousto (BSL) basis [89, 90]

$$\bar{h}_{\mu\nu}(x^\alpha) = \sum_{l=0}^{\infty} \sum_{m=-l}^{l} \bar{h}_{\mu\nu}^{lm}(x^\alpha) = \sum_{l=0}^{\infty} \sum_{m=-l}^{l} \sum_{i=1}^{10} \frac{a_l^{(i)}}{r} \bar{h}_{lm}^{(i)}(r,t) Y_{\mu\nu}^{(i),lm}(r,\theta,\phi). \tag{2.68}$$

The explicit dependence on $z^\alpha(\tau)$ of the metric perturbation can be replaced by $z^\alpha(t)$ due to Eq. (2.41). The dependence on z^α of the metric perturbation can be written more simply as a dependence on the variable t, which will remain in place for the remainder of this section. The constant $\alpha_{(i)}$ are defined by [90, 89]

$$a_l^{(i)} = \frac{1}{\sqrt{2}} \times \begin{cases} 1 & \text{for } i = 1,2,3,6 \\ 1/\sqrt{l(l+1)} & \text{for } i = 4,5,8,9, \\ 1/\sqrt{(l+2)(l+1)l(l-1)} & \text{for } i = 7,10, \end{cases} \tag{2.69}$$

and the BSL tensor spherical harmonics are defined so that [90]

$$\int d\Omega \, \eta^{\alpha\mu} \eta^{\beta\nu} \left[Y_{\mu\nu}^{(i)lm} \right]^* Y_{\alpha\beta}^{(j)l'm'} = \delta_{ij} \delta_{ll'} \delta_{mm'}, \tag{2.70}$$

where $d\Omega$ is the solid angle and $\eta^{\mu\nu}$ is given by

$$\eta^{\mu\nu} \equiv \text{diag}\left(1, f(r), r^{-2}, r^{-2}\sin^{-2}\theta\right), \tag{2.71}$$

and the components $Y_{\mu\nu}^{(i)lm}$ are given explicitly in Ref. [90], though are not required for the results presented in this thesis and shall not be given here. The metric perturbation in the BSL basis takes on the following expansion

$$\bar{h}_{\mu\nu}^{lm}(x^\alpha) = \sum_{n=1}^{\infty} \varepsilon^n \bar{h}_{\mu\nu}^{n,lm}(x^\alpha), \tag{2.72}$$

$$\bar{h}_{lm}^{(i)}(t,r) = \sum_{n=1}^{\infty} \varepsilon^n \bar{h}_{lm}^{n,(i)}(t,r). \tag{2.73}$$

In the BSL basis, the SET becomes

$$T_{\mu\nu} = \mu \sum_{l=0}^{\infty} \sum_{m=-l}^{l} T_{\mu\nu}^{lm} = -\mu \sum_{l=0}^{\infty} \sum_{m=-l}^{l} \sum_{i=1}^{10} T_{lm}^{(i)}(t,r) Y_{\mu\nu}^{(i),lm}(r,\theta,\phi), \tag{2.74}$$

such that

$$T_{lm}^{(i)} = -\frac{1}{\mu\kappa_{(i)}} \int d\Omega \, \eta^{\alpha\mu} \eta^{\beta\nu} \, T_{\alpha\beta}^{lm} \left(Y_{\mu\nu}^{(i),lm}\right)^*, \tag{2.75}$$

where $\kappa_{(i)}$ is given by

$$\kappa_{(i)} := \begin{cases} f(r)^2 & \text{if } i = 3, \\ 1 & \text{otherwise.} \end{cases} \tag{2.76}$$

The sources $S_{lm}^{(i)}$ are defined such that

$$S_{lm}^{(i)} = \frac{\pi r f}{4 a_l^{(i)}} T_{lm}^{(i)}. \tag{2.77}$$

Both $S_{lm}^{(i)}$ and $T_{lm}^{(i)}$ take on the following expansions

$$T_{lm}^{(i)}(t,r) = \sum_{n=1}^{\infty} \varepsilon^n T_{lm}^{n,(i)}(t,r), \tag{2.78}$$

$$S_{lm}^{(i)}(t,r) = \sum_{n=1}^{\infty} \varepsilon^n S_{lm}^{n,(i)}(t,r) \tag{2.79}$$

The linearised Einstein field equations can then be written simply as [90, 89, 103, 14]

$$\Box_{(j)}^{(i)} \bar{h}_{lm}^{(j)} + \mathcal{M}_{l(j)}^{(i)} \bar{h}_{lm}^{(j)} = S_{lm}^{(i)}, \quad i \in \{1, \dots, 10\}, \tag{2.80}$$

where

$$\Box_{(j)}^{(i)} \equiv \delta_{(j)}^{(i)} \left(\frac{1}{4}(\partial_t^2 - \partial_{r_*}^2) + V_l(r) \right), \quad V_l(r) = \frac{f(r)}{4r^2} \left(l(l+1) + \frac{2M}{r} \right). \tag{2.81}$$

Defining the operator

$$\delta G_{(j)}^{(i)} := \Box_{(j)}^{(i)} + \mathcal{M}_{l(j)}^{(i)}, \tag{2.82}$$

with

$$\mathcal{M}_{l(j)}^{(i)} = \mathcal{M}_{\Omega,l(j)}^{(i)} \partial_t + \mathcal{M}_{r,l(j)}^{(i)}, \tag{2.83}$$

the field equations can be further simplified in the BSL basis as

$$\delta G_{(j)}^{(i)}[\bar{h}_{lm}^{(j)}] = S_{lm}^{(i)}. \tag{2.84}$$

The matrices $\mathcal{M}_{\Omega,l(j)}^{(i)}$ and $\mathcal{M}_{r,l(j)}^{(i)}$ are given in Appendix B explicitly for constant t slicing [90, 89, 104].

The radial Lorenz gauge metric perturbation components in the BSL basis can be written in terms of Berndtson's variables, introduced earlier for the even-sector as follows [2]

$$\bar{h}_{lm}^{(1)} = rf(H_0^{lm} + H_2^{lm}), \tag{2.85a}$$

$$\bar{h}_{lm}^{(2)} = 2rfH_1^{lm}, \tag{2.85b}$$

$$\bar{h}_{lm}^{(3)} = 2rK^{lm}, \tag{2.85c}$$

$$\bar{h}_{lm}^{(4)} = 2l(l+1)h_0^{lm}, \tag{2.85d}$$

$$\bar{h}_{lm}^{(5)} = 2l(l+1)fh_1^{lm}, \tag{2.85e}$$

$$\bar{h}_{lm}^{(6)} = r(H_0^{lm} - H_2^{lm}), \tag{2.85f}$$

$$\bar{h}_{lm}^{(7)} = 2r(l-1)l(l+1)(l+2)G^{lm}, \tag{2.85g}$$

and for the odd-sector

$$\bar{h}_{lm}^{(8)} = 2l(l+1)h_0^{lm}, \tag{2.85h}$$

$$\bar{h}_{lm}^{(9)} = 2l(l+1)fh_1^{lm}, \tag{2.85i}$$

$$\bar{h}_{lm}^{(10)} = -\frac{2(l-1)l(l+1)(l+2)}{r}h_2^{lm}. \tag{2.85j}$$

The above expressions are derived by comparing the components of $h_{\mu\nu}^{1L}$ in each of [46] and [89].

2.6 Transformation from the Regge-Wheeler to the Lorenz gauge

For a gauge vector $\xi^\mu \sim \mathcal{O}(\varepsilon)$, the infinitesimal coordinate transformation

$$x^\mu \to x'^\mu = x^\mu + \xi^\mu \tag{2.86}$$

allows the gauge transformation of the metric perturbation to be written as

$$h_{\mu\nu} \to h'_{\mu\nu} = h_{\mu\nu} + \pounds_\xi, \tag{2.87}$$

where $\pounds$ is the Lie derivative such that

$$\pounds_\xi, g_{\mu\nu} = -2\xi_{(\mu;\nu)}. \tag{2.88}$$

One can then transform to Lorenz gauge solutions from RW solutions in the following way

$$h_{\mu\nu}^L = h_{\mu\nu}^{RW} + \pounds_\xi g_{\mu\nu}, \tag{2.89}$$

where superscripts L and RW denote the Lorenz and RW gauges respectively.

To preserve the Lorenz gauge, the gauge vector must satisfy

$$\Box \xi^\mu = 0, \tag{2.90}$$

and can be written in terms of a mode-sum decomposition as

$$\xi_\mu(t, r, \theta, \phi) = \sum_{l=0}^{\infty} \sum_{m=-l}^{l} \left\{ \left[\int_{-\infty}^{\infty} e^{-i\omega t} \left(\xi_\mu^{o,lm}(\omega, r, \theta, \phi) \right. \right. \right. \tag{2.91}$$

$$\left. + \xi_\mu^{e,lm}(\omega, r, \theta, \phi) \right) d\omega \right] + \delta_{l0} \delta_{\mu t} C_0 \left(1 - \frac{2M}{r} \right) t Y_{00}(\theta, \phi) \tag{2.92}$$

$$+ \delta_{l1} C_1 t r^2 \left[\delta_{\mu\theta} \csc\theta \frac{\partial Y_{1m}(\theta, \phi)}{\partial \phi} - \delta_{\mu\phi} \sin\theta \frac{\partial Y_{1m}(\theta, \phi)}{\partial \theta} \right] \right\}, \tag{2.93}$$

where $\delta_{\alpha\beta}$ is the Kronecker delta and

$$\xi_\mu^{o,lm}(\omega, r, \theta, \phi) = \left(0, 0, Z^{lm}(\omega, r) \csc\theta \frac{\partial Y_{lm}}{\partial \phi}, -Z^{lm}(\omega, r) \sin\theta \frac{\partial Y_{lm}}{\partial \theta} \right) \tag{2.94}$$

$$\xi_\mu^{e,lm}(\omega, r, \theta, \phi) = \left(M_0^{lm}(\omega, r) Y_{lm}, M_1^{lm}(\omega, r) Y_{lm}, M_2^{lm}(\omega, r) \frac{\partial Y_{lm}}{\partial \theta}, M_2^{lm}(\omega, r) \frac{\partial Y_{lm}}{\partial \phi} \right). \tag{2.95}$$

The gauge transformation for a given l, m mode in the odd-sector then looks like

$$h_0^{\mathrm{L}} = h_0^{\mathrm{RW}} + i\omega Z, \tag{2.96}$$

$$h_1^{\mathrm{L}} = h_1^{\mathrm{RW}} + \frac{2}{r} Z - Z', \tag{2.97}$$

$$h_2^{\mathrm{L}} = h_2^{\mathrm{RW}} + Z, \tag{2.98}$$

where a prime on Z denotes differentiation with respect to r, and in the even-sector

$$H_0^{\mathrm{L}} = H_0^{\mathrm{RW}} + \frac{2i\omega}{\left(1 - \frac{2M}{r} \right)} M_0 + \frac{2M}{r^2} M_1, \tag{2.99}$$

$$H_1^{\mathrm{L}} = H_1^{\mathrm{RW}} - \frac{2M}{(2M - r)r} M_0 + i\omega M_1 - M_0', \tag{2.100}$$

$$H_2^{\mathrm{L}} = H_2^{\mathrm{RW}} - \frac{2M}{r^2} M_1 - 2 \left(1 - \frac{2M}{r} \right) M_1', \tag{2.101}$$

$$K^{\mathrm{L}} = K^{\mathrm{RW}} + \frac{2(2M - r)}{r^2} M_1 + \frac{2(1 + \lambda)}{r^2} M_2, \tag{2.102}$$

$$h_0^{\mathrm{L}} = h_0^{\mathrm{RW}} - M_0 + i\omega M_2, \tag{2.103}$$

$$h_1^{\mathrm{L}} = h_1^{\mathrm{RW}} - M_1 + \frac{2}{r} M_2 - M_2', \tag{2.104}$$

$$G^{\mathrm{L}} = G^{\mathrm{RW}} - \frac{M_2}{r^2}. \tag{2.105}$$

The definitions for the RW gauge quantities are given explicitly in Section 2.4 All previous calculations of $h_{\mu\nu}^{1\mathrm{L}}$ are numerical and done in either time or frequency domain [89, 90, 91, 46, 92, 83].

Using the decomposition of $h^1_{\mu\nu}$ in Eq. (2.30) and Eq. (2.33) and following Berndtson's prescription [46] where $h^{1L}_{\mu\nu}$ satisfies the gauge condition Eq. (2.65) to leading order, the homogeneous odd-sector components of $h^{1L}_{\mu\nu}$ for $\omega \neq 0$ and $l \geq 2$ are given by the radial fields [2]

$$h_0(r) = \frac{1}{i\omega}\left(\psi_1 + \frac{2\lambda}{3}\psi_2\right), \tag{2.106a}$$

$$h_1(r) = \frac{1}{(i\omega)^2}\left(-\frac{2\lambda}{3}\psi_2' + \frac{2}{r}\psi_1 - \frac{2\lambda}{3r}\psi_2 - \psi_1'\right), \tag{2.106b}$$

$$h_2(r) = \frac{1}{(i\omega)^2}\left(rf\,\psi_2' + \psi_1 + \frac{(3+2\lambda)r - 6M}{3r}\psi_2\right), \tag{2.106c}$$

where

$$\lambda = \frac{1}{2}(l-1)(l+2), \tag{2.107}$$

and the l, m labels on radial fields from Eq. (2.30) and Eq. (2.33) will be dropped henceforth for convenience. The fields ψ_1 and ψ_2 refer to solutions to Eq. (2.49), with a RW potential. Valid odd-sector solutions to h_0, h_1 and h_2 are constructed by solutions to ψ_1 and ψ_2 for which $l + m$ is an odd number. For $\omega \neq 0$ and $l \geq 2$, the even-sector components of $h^{1L}_{\mu\nu}$, given by the radial fields h_0, h_1, H_0, H_1, H_2, K and G can be written in terms of the fields ψ_2, ψ_1, ψ_0, ψ_{0b} and their radial derivatives, in addition to the gauge field M_{2af} and its radial derivative. Here ψ_1, ψ_0, ψ_{0b} refer to solutions of Eq. (2.49) with a RW potential. The fields ψ_0 and ψ_{0b} differ only by their sources, given in Appendix A. An explanation of the origin of ψ_{0b} can be found in Section (3.1.1) of Ref. [46]. The field ψ_2 is also a solution to Eq. (2.49) with a Zerilli potential. The additional gauge field M_{2af} will be discussed further in Chapters 5, 6 and 9. The explicit, source-free expressions are given below [46, 2]

$$
\begin{aligned}
H_0(r) = &-\frac{\lambda(1+\lambda)M(-3M + (3+\lambda)r)\psi_2'}{3(i\omega)^2 r^3(3M + \lambda r)} + \frac{(-M+r)\psi_0}{(2M-r)r} + \frac{4i\omega(1+\lambda)\psi_1}{2M-r} + \psi_0' \\
&-\frac{\lambda(1+\lambda)}{3(i\omega)^2(2M-r)r^4(3M+\lambda r)^2}\Big[18M^4 + 3(-3+4\lambda)M^3 r + (i\omega)^2\lambda^2 r^6 \\
&-3\lambda M r^3\left(1 + \lambda - 2(i\omega)^2 r^2\right) + M^2\left(6\lambda^2 r^2 + 9(i\omega)^2 r^4\right)\Big]\psi_2 + \frac{4(1+\lambda)M\psi_1'}{i\omega r^3} \\
&+\frac{2M\left(\psi_{0b}' + M_{2af}'\right)}{r^3} + \frac{2\left(-2M^2 + Mr + (i\omega)^2 r^4\right)(\psi_{0b} + M_{2af})}{(2M-r)r^4},
\end{aligned} \tag{2.108a}
$$

$$
\begin{aligned}
H_1(r) = &-\frac{\lambda(1+\lambda)\psi_2'}{3i\omega r} - \frac{\left(6M + 4\lambda M - 3r - 2\lambda r - 2(i\omega)^2 r^3\right)\psi_0}{4i\omega M r^2 - 2i\omega r^3} + \frac{(2+2\lambda)\psi_1}{2Mr - r^2} + \frac{\psi_0'}{2i\omega r} \\
&+\frac{2i\omega(-M+r)(\psi_{0b} + M_{2af})}{(2M-r)r^2} - \frac{\lambda(1+\lambda)\left(3M^2 + 3\lambda M r - \lambda r^2\right)\psi_2}{3i\omega(2M-r)r^2(3M + \lambda r)} \\
&+\frac{2i\omega(\psi_{0b}' + M_{2af}')}{r} + \frac{4(1+\lambda)\psi_1'}{r},
\end{aligned} \tag{2.108b}
$$

$$H_2(r) = \frac{\lambda(1+\lambda)\left(-9M^2 + (3-5\lambda)Mr + 2\lambda r^2\right)\psi_2'}{3(i\omega)^2 r^3(3M+\lambda r)} + \frac{(-3M+2r)\psi_0}{(2M-r)r} + \psi_0' \tag{2.108c}$$

$$- \frac{4(1+\lambda)(M-r)\psi_1'}{i\omega r^3} + \frac{2\left(6M^2 - (11+4\lambda)Mr + r^2\left(4+2\lambda+(i\omega)^2 r^2\right)\right)(\psi_{0b}+M_{2af})}{(2M-r)r^4}$$

$$+ \frac{(-6M+4r)(\psi_{0b}' + M_{2af}')}{r^3} + \frac{4(1+\lambda)\left(-4(1+\lambda)M + r\left(2+2\lambda+(i\omega)^2 r^2\right)\right)\psi_1}{i\omega(2M-r)r^3}$$

$$- \frac{\lambda(1+\lambda)}{3(i\omega)^2(2M-r)r^4(3M+\lambda r)^2}[-54M^4 + 3(9-16\lambda)M^3 r + \lambda^2 r^4(2+2\lambda+(i\omega)^2 r^2)$$

$$+ 9M^2 r^2(2\lambda - 2\lambda^2 + (i\omega)^2 r^2) + \lambda M r^3(3+5\lambda - 4\lambda^2 + 6(i\omega)^2 r^2)]\psi_2,$$

$$K(r) = \frac{\lambda(1+\lambda)(2M-r)\psi_2'}{3(i\omega)^2 r^3} + \frac{\psi_0}{r} + \frac{(-4M+2(2+\lambda)r)(\psi_{0b}+M_{2af})}{r^4} + \frac{4(1+\lambda)^2\psi_1}{i\omega r^3} \tag{2.108d}$$

$$+ \frac{2(1+\lambda)(2M-r)\psi_1'}{i\omega r^3} - \frac{\lambda(1+\lambda)\left(6M^2 + 3\lambda M r + \lambda(1+\lambda)r^2\right)\psi_2}{3(i\omega)^2 r^4(3M+\lambda r)} \tag{2.108e}$$

$$+ \frac{(4M-2r)(\psi_{0b}' + M_{2af}')}{r^3},$$

$$G(r) = -\frac{\lambda(3+2\lambda)(2M-r)\psi_2'}{6(i\omega)^2 r^2(3M+\lambda r)} - \frac{\psi_{0b}+M_{2af}}{r^3} - \frac{2(1+\lambda)\psi_1}{i\omega r^3} + \frac{(2M-r)\psi_1'}{i\omega r^3} \tag{2.108f}$$

$$+ \frac{1}{6(i\omega)^2 r^3(3M+\lambda r)^2}\left[4\lambda^3 r^2 + \lambda^4 r^2 + 27(i\omega)^2 M^2 r^2 + 9\lambda M\left(M + 2(i\omega)^2 r^3\right)\right. \tag{2.108g}$$

$$\left. + 3\lambda^2\left(M^2 + Mr + r^2 + (i\omega)^2 r^4\right)\right]\psi_2,$$

$$h_0(r) = \frac{\lambda(2M-r)\psi_2'}{3i\omega r} + \frac{(-2M+r)\psi_0}{2i\omega r^2} + \frac{2i\omega(\psi_{0b}+M_{2af})}{r} + \frac{4(1+\lambda)\psi_1}{r} + \left(1 - \frac{2M}{r}\right)\psi_1'$$

$$\tag{2.108h}$$

$$- \frac{(-2M+r)\psi_0'}{2i\omega r} - \frac{\lambda\left(6M^2 + 3\lambda M r + \lambda(1+\lambda)r^2\right)\psi_2}{3i\omega r^2(3M+\lambda r)},$$

$$h_1(r) = \frac{\lambda((3+\lambda)M + \lambda(2+\lambda)r)\psi_2'}{3(i\omega)^2 r(3M+\lambda r)} - \frac{r\psi_0}{4M-2r} + \frac{4\psi_{0b}+M_{2af}}{r^2} - \frac{2(\psi_{0b}'+M_{2af}')}{r} \tag{2.108i}$$

$$- \frac{\lambda}{3(i\omega)^2(2M-r)r^2(3M+\lambda r)^2}\left[9(i\omega)^2 M^2 r^3 + 2\lambda^3 r^2(-2M+r)\right.$$

$$\left. + \lambda^2 r\left(-12M^2 + 2Mr + 2r^2 + (i\omega)^2 r^4\right) + 3\lambda M\left(-4M^2 + r^2 + 2(i\omega)^2 r^4\right)\right]\psi_2$$

$$+ \frac{\left(8M + 8\lambda M - 4r - 4\lambda r + (i\omega)^2 r^3\right)\psi_1}{2i\omega M r^2 - i\omega r^3} - \frac{2(2M + r + 2\lambda r)\psi_1'}{i\omega r^2}.$$

Valid even-sector solutions are then constructed by solutions to ψ_0, ψ_{0b}, ψ_1, ψ_2 and M_{2af} for which $l + m$ is an even number. The even-sector fields h_0, h_1, ψ_1 and ψ_2 should not be confused with those from the odd-sector. The reader is referred to Ref. [46] for sourced expressions and for

expressions where $l = 0, 1$ and $\omega = 0$. Berndtson's gauge transformation from RW to Lorenz gauge metric perturbations is equivalent to that of Hopper and Evans [102], who provide the same gauge transformation for the $s = 2$ sector.

2.6.1 Differentiability of inhomogeneous expressions

For the sourced expressions of Berndtson's gauge transformation, the reader is referred to the appendices of Ref. [46]. The retarded ψ_2, ψ_1 and ψ_{0b} in both the odd- and even-sectors contain jump discontinuities, while ψ_0 and M_{2af} of the even-sector are continuous, and are C^0 differentiable. Any jump discontinuities exactly cancel when transforming to the Lorenz gauge expressions of Eq. (2.106) and Eq. (2.108). Additionally, the source for ψ_0, given in Eq. (A.5) contains Dirac-delta functions, but no derivatives, whereas all other RWZ sources, given in appendix A contain Dirac-delta functions and a radial derivative of a Dirac-delta function. This means that the radial derivative of the retarded fields $\psi_2, \psi_1, \psi_{0b}$ in either the odd- or even-sectors will contain a distributional term involving a Dirac-delta function. Without compensating, this distributional term introduced by radial derivatives of RWZ functions in transformation to the Lorenz gauge would spoil the C^0 differentiability. Berndtson's expressions for the inhomogeneous Lorenz gauge metric components therefore contain additional distributional terms, related to the components of the stress-energy tensor, which cancel any introduced by such radial derivatives of the fields [46, 102]. For a point-like particle on circular orbits, we may use the homogeneous expressions of Eq. (2.106) and Eq. (2.108) to obtain the retarded Lorenz gauge metric perturbation components everywhere except for at the particle, as any terms involving the Dirac-delta function will go to zero away from the particle. For this reason, in Chapter 5 and Chapter 6, only the homogeneous gauge transformation is considered.

2.6.2 Satisfying the Lorenz gauge condition and field equations

In the absence of sources, substituting the odd-sector fields h_0, h_1 and h_2 back into the odd-sector field equations Eq. (2.67) and Lorenz gauge condition in Eq. (2.65), and similarly substituting the even-sector fields h_0, h_1, H_0, H_1, H_2, K and G back into the even-sector field equations and Lorenz gauge conditions results in fourteen equations (ten from the linearised Einstein field equations and four from the Lorenz gauge conditions) which include combinations of the RW master equations, Zerilli equation, the equation for M_{2af} given by Eq. (5.17), and their radial derivatives. In the even-sector for example, the Lorenz gauge conditions and linearised Einstein field equations take the following form

$$A_{lm}(r)\mathcal{L}_0\psi_0 + B_{l\omega}(r)\mathcal{L}_1\psi_1 + C_{lm}(r)\mathcal{L}_2\psi_2 + D_{lm}(r)(\mathcal{L}_0 M_{2af} - f(r)\psi_0) + E_{lm}(r)\partial_r\left(\mathcal{L}_0\psi_0\right) \quad (2.109)$$
$$+ F_{l\omega}(r)\partial_r\left(\mathcal{L}_1\psi_1\right) + G_{lm}(r)\partial_r\left(\mathcal{L}_2\psi_2\right) + H_{l\omega}(r)\partial_r(\mathcal{L}_0 M_{2af} - f(r)\psi_0) = 0$$

The factors $A_{lm}(r)$, $B_{lm}(r), \dots$ are factors that depend on r, l and m, at least in the case of circular orbits. Note that in the homogeneous case, $\psi_{0b} = \psi_0$. It is easily seen that the individual contribution of each of the homogeneous RW master functions, homogeneous Zerilli master function

and M_{2af} to the Lorenz gauge condition and linearised Einstein field equations are identically zero. This suggests that any of the RWZ fields or M_{2af} can be 'turned off' (i.e. set to zero), while still preserving the Lorenz gauge condition and satisfying the first-order linearised Einstein field equations. Indeed this shows that the RWZ master functions, in addition to the gauge field M_{2af} form a basis of homogeneous solutions to the first-order linearised Einstein field equations in the Lorenz gauge, in the absence of sources.

2.7 Perturbations to rotating black holes

The metric describing a rotating, axisymmetric black holes with mass M and angular momentum a is given by the Kerr solution

$$ds^2 = -d\tau^2 \tag{2.110}$$

$$= -\left(1 - \frac{2Mr}{\Sigma}\right)dt^2 + \frac{\Sigma}{\Delta}dr^2 + \Sigma d\theta^2 + \left(r^2 + a^2 + \frac{2Mra^2}{\Sigma}\sin^2\theta\right)\sin^2\theta d\phi^2 \tag{2.111}$$

$$- \frac{4Mra\sin^2\theta}{\Sigma}dtd\phi,$$

where

$$\Sigma = r^2 + a^2\cos^2\theta, \tag{2.112}$$

$$\Delta = r^2 - 2Mr + a^2 \quad \text{or} \quad \Delta = (r - r_+)(r - r_-). \tag{2.113}$$

The radii $r_\pm$ are the radius of the outer and inner horizons of a Kerr black hole respectively. In the Schwarzschild limit, $r_- \to 0$ and $r_+ \to 2M$.

2.7.1 The Teukolsky formalism

There is no known separable solution to the linearised Einstein field in Kerr. However, in type D spacetimes such as Schwarzschild or Kerr [1], there exists a set of null tetrads, onto which equations describing perturbations to the curvature can be projected, and for which the resulting equations are separable [105, 68]. The separable equations in question are precisely the Teukolsky equations, whose solutions are related to the perturbed Weyl scalars. Often the Newman Penrose (NP) [106] or Geroch-Held-Penrose (GHP) [68, 37] formalisms are used to achieve this. The formalism used in this work follows that of Ref. [107] and is very similar to the NP and GHP formalisms, with some slight differences. Examples of tetrads that attain this separability are the Carter and Kinnersley tetrads, the latter of which shall be used throughout, for reasons discussed in Chapter 9. The Kinnersley

---

[1]While Schwarzschild and Kerr black holes are vacuum type D spacetimes, the statement applies to all type D spacetimes, including the Kerr-Newman metric [68].

tetrad is then defined as follows [107, 5, 68, 37, 107]

$$l^\mu = l^\mu_+, \tag{2.114a}$$

$$n^\mu = -\frac{\Delta}{2\Sigma}l^\mu_-, \tag{2.114b}$$

$$m^\mu = \frac{1}{\sqrt{2}\rho}m^\mu_+, \tag{2.114c}$$

$$\bar{m}^\mu = \frac{1}{\sqrt{2}\bar{\rho}}m^\mu_-, \tag{2.114d}$$

where [5],

$$l^\mu_\pm = \left\{ \pm\Delta^{-1}\left(r^2 + a^2\right), 1, 0, \pm\Delta^{-1}a \right\}, \tag{2.115a}$$

$$m^\mu_\pm = \left\{ \pm ia\sin\theta, 0, 1, \pm i\csc\theta \right\}, \tag{2.115b}$$

with

$$\rho \equiv \left(\nabla_\nu l_\mu\right)m^\mu\bar{m}^\nu = r + ia\cos\theta \tag{2.116}$$

$$\bar{\rho} \equiv \left(\nabla_\nu l_\mu\right)\bar{m}^\mu m^\nu = r - ia\cos\theta, \tag{2.117}$$

such that

$$\implies \rho\bar{\rho} = \Sigma. \tag{2.118}$$

The background metric can then be written as [46, 68, 37, 5]:

$$g^{\mu\nu} = -l^\mu n^\nu - n^\mu l^\nu + m^\mu\bar{m}^\nu + \bar{m}^\mu m^\nu. \tag{2.119}$$

The tetrad basis vectors have the normalisation conditions such that

$$g_{\mu\nu}m^\mu\bar{m}^\nu = 1, \tag{2.120}$$

$$g_{\mu\nu}l^\mu\bar{n}^\nu = -1, \tag{2.121}$$

$$g_{\mu\nu}l^\mu_+ l^\nu_- = \frac{2\Sigma}{\Delta}, \tag{2.122}$$

$$g_{\mu\nu}m^\mu_+ m^\nu_- = 2\Sigma, \tag{2.123}$$

with all other inner products equal to zero.

The directional derivatives along the tetrad $\{l_+^\mu, l_-^\mu, m_+^\mu, m_-^\mu\}$ are defined as follows [5]

$$\mathcal{D} \equiv l_+^\mu \partial_\mu = \partial_r - \frac{iK}{\Delta}, \tag{2.124a}$$

$$\mathcal{D}^\dagger \equiv l_-^\mu \partial_\mu = \partial_r + \frac{iK}{\Delta}, \tag{2.124b}$$

$$\mathcal{L}^\dagger \equiv m_+^\mu \partial_\mu = \partial_\theta - Q, \tag{2.124c}$$

$$\mathcal{L} \equiv m_-^\mu \partial_\mu = \partial_\theta + Q, \tag{2.124d}$$

where Q is given by [5]

$$Q = m \csc \theta - a\omega \sin \theta, \tag{2.125}$$

K is given by

$$K = \omega(r^2 + a^2) - am, \tag{2.126}$$

and m is the azimuthal mode number. The Weyl tensor, which is a measure of the curvature of the spacetime is then defined by

$$
\begin{aligned}
C_{\mu\nu\alpha\beta} = \ & R_{\mu\nu\alpha\beta} + \frac{1}{n-2} \left(R_{\mu\beta} g_{\nu\alpha} - R_{\mu\alpha} g_{\nu\beta} + R_{\nu\alpha} g_{\mu\beta} - R_{\nu\beta} g_{\mu\alpha} \right) \\
& + \frac{1}{(n-1)(n-2)} R \left(g_{\mu\alpha} g_{\nu\beta} - g_{\mu\beta} g_{\nu\alpha} \right),
\end{aligned}
\tag{2.127}
$$

where n is the number of dimensions of the spacetime. For the purposes of this work, $n = 4$. When projected onto the Kinnersley tetrad, the five independent complex components of the Weyl tensor are given by [68, 37]

$$\Psi_0 := C_{\alpha\beta\gamma\delta} l^\alpha m^\beta l^\gamma m^\delta, \tag{2.128a}$$

$$\Psi_1 := C_{\alpha\beta\gamma\delta} l^\alpha n^\beta l^\gamma m^\delta, \tag{2.128b}$$

$$\Psi_2 := C_{\alpha\beta\gamma\delta} l^\alpha m^\beta \bar{m}^\gamma n^\delta, \tag{2.128c}$$

$$\Psi_3 := C_{\alpha\beta\gamma\delta} l^\alpha n^\beta \bar{m}^\gamma n^\delta, \tag{2.128d}$$

$$\Psi_4 := C_{\alpha\beta\gamma\delta} n^\alpha \bar{m}^\beta n^\gamma \bar{m}^\delta. \tag{2.128e}$$

For vacuum background spacetimes, the Weyl curvature is entirely captured by the Riemann tensor, and the perturbed Weyl tensor is given by

$$\delta C_{\mu\nu\alpha\beta} = \delta\, R_{\mu\nu\alpha\beta}. \tag{2.129}$$

The perturbed Weyl scalars are then given by

$$\Psi_0^{\mathrm{P}} = \delta R_{\alpha\beta\gamma\delta} l^\alpha m^\beta l^\gamma m^\delta, \tag{2.130a}$$

$$\Psi_1^{\mathrm{P}} = \delta R_{\alpha\beta\gamma\delta} l^\alpha n^\beta l^\gamma m^\delta, \tag{2.130b}$$

$$\Psi_2^{\mathrm{P}} = \delta R_{\alpha\beta\gamma\delta} l^\alpha m^\beta \bar{m}^\gamma n^\delta, \tag{2.130c}$$

$$\Psi_3^{\mathrm{P}} = \delta R_{\alpha\beta\gamma\delta} l^\alpha n^\beta \bar{m}^\gamma n^\delta, \tag{2.130d}$$

$$\Psi_4^{\mathrm{P}} = \delta R_{\alpha\beta\gamma\delta} n^\alpha \bar{m}^\beta n^\gamma \bar{m}^\delta. \tag{2.130e}$$

In type D spacetimes, there exists four null directions. Choosing the tetrad legs such that they are parallel to these four null directions leaves only Ψ_0^{P} and Ψ_4^{P} non-zero of the perturbed and unperturbed Weyl scalars. It is this simplifications that allows for a separable solution of the metric perturbation to a Kerr background to be determined. The perturbed Weyl scalars can then be written in the separable form, using a mode-sum decomposition in the frequency domain

$$\Psi_0^{\mathrm{P}} = \sum_{l=0}^{\infty} \sum_{m=-l}^{l} R_2^{lm}(r) S_2^{lm}(\theta, \phi) e^{-im\phi_{\mathrm{p}}(t)}, \tag{2.131}$$

$$\Psi_4^{\mathrm{P}} = \sum_{l=0}^{\infty} \sum_{m=-l}^{l} \Delta R_{-2}^{lm}(r) S_{-2}^{lm}(\theta, \phi) e^{-im\phi_{\mathrm{p}}(t)}, \tag{2.132}$$

such that, for $s = 2$, the radial function $R_{\pm 2}$ satisfies

$$\Delta^{-s} \frac{d}{dr} \left(\Delta^{s+1} \frac{dR_s^{lm}}{dr} \right) + \left(\frac{K^2 - 2is(r-M)K}{\Delta} + 4is\omega r - \lambda \right) R_s^{lm}(r) = 0, \tag{2.133}$$

which is the homogeneous radial Teukolsky equation, for a Kerr black hole. Similarly to the RW equation, the spin-weights $s = \pm 1, 0$ correspond to electromagnetic and scalar perturbations respectively, and $s = \pm 2$ correspond to gravitational perturbations. The angular part of the perturbed Weyl scalars, S_s^{lm} are the standard spin-weighted spheroidal harmonics, which obey the equation [1]

$$\left[\frac{1}{\sin\theta} \frac{d}{d\theta} \left(\sin\theta \frac{d}{d\theta} \right) - a^2 \omega^2 \sin^2\theta - \frac{(m + s\cos\theta)^2}{\sin^2\theta} - 2a\omega s\cos\theta + s + 2ma\omega + \lambda_{slm} \right] S_s^{lm}(\theta, \phi) = 0, \tag{2.134}$$

and are normalised as

$$\int_0^\pi \left| S_s^{lm} \right|^2 \sin\theta \, d\theta = 1. \tag{2.135}$$

Any solution to Eq. (2.133) should recover the correct asymptotic behaviour, which for the radial Teukolsky function is given by [84] [86]

$$
R_{slm}^{\text{in}} \to \begin{cases} R_{slm}^{\text{in,trans}} \, \Delta^{-s} e^{-ikr^*} & \text{for } r \to r_+ \\ r^{1-2s} R_{slm}^{\text{in,ref}} \, e^{i\omega r^*} + r^{-1} R_{slm}^{\text{in,inc}} \, e^{-i\omega r^*} & \text{for } r \to +\infty \end{cases} \tag{2.136}
$$

$$
R_{slm}^{\text{up}} \to \begin{cases} R_{slm}^{\text{up,inc}} e^{ikr^*} + \Delta^{-s} R_{slm}^{\text{up,ref}} \, e^{-ikr^*} & \text{for } r \to r_+ \\ R_{slm}^{\text{up,trans}} \, r^{1-2s} e^{i\omega r^*} & \text{for } r \to +\infty, \end{cases} \tag{2.137}
$$

where R_{slm}^{in} and R_{slm}^{up} are two independent solutions and r^* is the well known tortoise coordinate given by

$$
r_* = r + \frac{2Mr_+}{r_+ - r_-} \ln \frac{r - r_+}{2M} - \frac{2Mr_-}{r_+ - r_-} \ln \frac{r - r_-}{2M}, \tag{2.138}
$$

and k is defined as

$$
k = \omega - \frac{ma}{2Mr_+}. \tag{2.139}
$$

How to use the perturbed Weyl scalars to construct the metric perturbation for a Kerr background will be discussed in the next subsection.

2.7.2 Metric reconstruction via a Hertz potential

In Ref. [108], Wald states and proves Theorem 1, which is true for any perturbation equations coming from solutions of decoupled equations

Theorem 1 *Suppose the identity $\mathcal{SE} = \mathcal{OT}$ holds for the linear partial differential operators $\mathcal{S}$, $\mathcal{E}$, $\mathcal{O}$ and $\mathcal{T}$. Suppose Ψ satisfies $\mathcal{O}^\dagger \Psi = 0$. Then $\mathcal{S}^\dagger \Psi$ satisfies $\mathcal{E}^\dagger \left(\mathcal{S}^\dagger \Psi \right) = 0$. Thus, in particular, if $\mathcal{E}$ is self-adjoint then $\mathcal{S}^\dagger \Psi$ is a solution of $\mathcal{E}(f) = 0$.*

Proof:

$$
\mathcal{SE} = \mathcal{OT}, \tag{2.140}
$$

$$
\mathcal{E}^\dagger \mathcal{S}^\dagger = \mathcal{T}^\dagger \mathcal{O}^\dagger, \tag{2.141}
$$

$$
\mathcal{E}^\dagger \mathcal{S}^\dagger \Psi = \mathcal{T}^\dagger \mathcal{O}^\dagger \Psi, \tag{2.142}
$$

$$
\mathcal{E}^\dagger \mathcal{S}^\dagger \Psi = 0, \tag{2.143}
$$

$$
\mathcal{E} \mathcal{S}^\dagger \Psi = 0, \tag{2.144}
$$

where the last equality is true only if $\mathcal{E}$ is self-adjoint [108].

Given that the first-order linearised Einstein field equations can be decoupled for both Schwarzschild and Kerr backgrounds, Theorem 1 can be applied to constructing the source-free metric perturbation in the following way. Let $\mathcal{E}$ be defined as the operator which acts on the metric perturbation to obtain the linearised Einstein field equations and is equivalent to $\delta^1 G$ in eq. (2.20). Let $\mathcal{T}$ be the operator which acts on the metric perturbation to obtain the perturbed Riemann tensor, which in

vacuum spacetimes are the perturbed Weyl scalars from Eq. (2.133). Let $\mathcal{O}$ be the operator that obtains the Teukolsky equation from the perturbed Weyl scalars, and let $\mathcal{S}$ be the operator that transforms the linearised Einstein field equations, if given in terms of the NP operators and scalars, into the Teukolsky equation. Then, Theorem 1 states that the source-free metric perturbation can be constructed from the Hertz potential Ψ in the following way[108, 68]

$$h_{\mu\nu} = \left(\mathcal{S}^\dagger \Psi \right)_{\mu\nu} \tag{2.145}$$

so long as Ψ is a solution to the homogeneous Teukolsky equation, $\mathcal{O}^\dagger \Psi = 0$. The operators $\mathcal{S}, \mathcal{E}, \mathcal{O}$ and $\mathcal{T}$ will not be given explicitly here as this would require introducing many spin-coefficients that are not used anywhere else in this thesis. Instead the reader is pointed to References [37] and [68] for the explicit definitions of these operators.

2.7.3 The radiation gauge

The metric reconstruction method that follows from Theorem 1 was first done in the radiation gauges by Cohen and Kegeles and Chrzanowski [64, 63]. For Petrov type II spacetimes, the ingoing radiation gauge (IRG) condition is defined by [68]

$$l^\mu h_{\mu\nu} = 0 \tag{2.146}$$
$$g^{\mu\nu} h_{\mu\nu} = 0, \tag{2.147}$$

such that the metric perturbation is trace free and has zero projection along the principal null direction of the tetrad leg l^μ. Similarly, the outgoing radiation gauge (ORG) condition is defined by [68]

$$n^\mu h_{\mu\nu} = 0 \tag{2.148}$$
$$g^{\mu\nu} h_{\mu\nu} = 0. \tag{2.149}$$

In type D spacetimes, the metric perturbation can also be written in the ORG similarly to Eq. (2.145) using the method of adjoints and a different choice of Hertz potential, but one that is related to Ψ^{IRG} [68]. All results that hold for the IRG also hold for the ORG [68] and the choice of radiation gauge will depend on the problem of interest at hand. The explicit form of Eq. (2.145) can be found in Chapter 3 of Ref. [68]. Neither the NP nor GHP formalisms shall be discussed in this report, as they are detailed extensively throughout the literature and aren't necessary for the main results of this chapter. For a comprehensive review the reader is pointed to references [68] and [37]. For either choice of radiation gauge, obtaining Ψ solves the source-free metric perturbation in that gauge, up to a caveat that will be discussed in Section 9.1, as it turns out that solving Ψ only solves for the *radiative* part of the metric perturbation in the corresponding radiation gauge. [69]

By Wald's result from [69], we can make the observation that the metric perturbation in Eq. (2.145), constructed using the Hertz potential Ψ is incomplete, missing perturbations to the

mass and angular momentum of the spacetime, in addition to any gauge contributions. The radiation gauges are also irregular for all orbits, as the metric perturbation due to a point-like particle diverges to form a one-dimensional sting-like singularity, such that any neighbourhood of the particle includes the singularity [36]. As mentioned in the introduction there are however 'no-string' gauge solutions [70, 41, 71, 72, 73, 74, 75, 43]. However, due to the fact that the SF is best understood in the Lorenz gauge, as discussed in Chapter 1, it is still desirable to obtain the Kerr metric perturbation in the Lorenz gauge by construction from a Hertz potential and transforming from the radiation gauge. These arguments provide the motivation for research presented in Chapter 9.

Chapter 3

Developing the MST Package for the BHPToolkit

The first section of this chapter will provide a review of the MST method, named after Mano, Suzuki and Takasugi. The remainder of the chapter will discuss the implementation of the MST package for the BHPToolkit, an open source repository for software and data related to BHPT [1]. The MST package was developed in collaboration with Wardell, Kavanagh, Casals and Ottewill.

3.1 The MST method

The MST method offers semi-analytic series solutions by means of a small frequency expansion to the radial Teukolsky and RW master equations given by Eq. (2.133) and Eq. (2.49) respectively. For circular orbits, a low-frequency expansion is equivalent to a solution that is valid in both the PM and PN regimes [85, 86, 84], recalling that PM expansions are written as a power series in G, the gravitational constant, corresponding to an expansion around Minkowski flat space, and the PN series is written in terms of powers of c^{-1}, corresponding to an expansion about Newtonian gravity [84, 85]. Using the MST series to study EMRIs is justified by the importance of matching strong and weak field regimes, in addition to the series' rapid convergence, allowing for many higher order terms to be calculated in the PN series. While the derivation in this section uses the underlying assumption that the frequency, ω, is small, higher frequencies can be used in numerical algorithms. [87] A brief derivation of the MST method will be detailed here for the radial Teukolsky equation, from which the MST series for the Regge-Wheeler master functions can be recovered using the Chandrasekhar transformation.

Throughout the literature, attempts to solve the radial Teukolsky equation begin by analysing the equation's properties. In its current form, Eq. (2.133) contains regular singularities at the horizons, $r = r_+$ and $r = r_-$, and an irregular singularity at $r = \infty$. Therefore, to solve Eq. (2.133) analytically, one might first try to eliminate the regular singularities by using a change of variables and rescaling the Teukolsky radial function, $R_s^{lm}(r)$. This was done by Teukolsky and Press in 1974 [109], by Leaver in 1986 [110] and by Mano, Suzuki and Takasugi in 1996 [85]. As Eq. (2.133) is

a second order ordinary differential equation, it will admit two independent solutions from which physically relevant solutions can be constructed, namely the ingoing and upgoing solution, R^{in} and R^{up} respectively. To obtain the ingoing and upgoing solutions, a sensible choice of rescaling and change of variables is required to recover the asymptotic behaviour of Eq. (2.136) and Eq. (2.137) respectively. The proposed change of variables for the ingoing solution and other relevant quantities defined in [85] are given by

$$x = \frac{z_+ - z}{\epsilon\kappa}, \qquad (3.1\text{a})$$

$$z_+ = \omega r_+, \qquad (3.1\text{b})$$

$$z_- = \omega r_-, \qquad (3.1\text{c})$$

$$\epsilon = 2M\omega, \qquad (3.1\text{d})$$

$$\kappa = \sqrt{1 - q^2}, \qquad (3.1\text{e})$$

$$z = \omega r, \qquad (3.1\text{f})$$

$$r_+ = M + \sqrt{M^2 - a^2}, \qquad (3.1\text{g})$$

$$r_- = M - \sqrt{M^2 - a^2}, \qquad (3.1\text{h})$$

$$q = a/M, \qquad (3.1\text{i})$$

$$\tau = (\epsilon - mq)/\kappa. \qquad (3.1\text{j})$$

The ingoing Teukolsky radial solution can be rescaled in such a way that eliminates the regular singularities of Eq. (2.133) and captures them in the solution. This rescaling is given by [85, 84]

$$R^{\text{in}}_{slm}(x) = e^{i\epsilon\kappa x}(-x)^{-s-i(\epsilon+\tau)/2}(1-x)^{i(\epsilon-\tau)/2}p_{\text{in}}(x), \qquad (3.2)$$

where $p_{\text{in}}(x)$ is to be determined, and depends on s, l and m. Rewriting Eq. (3.2) in terms of the tortoise coordinate r^* recovers the exact expression for the asymptotic behaviour of R^{in}_{slm} in Eq. (2.136) on the outer horizon and Appendix B of [85] gives a detailed derivation as to why the choice of rescaling in Eq. (3.2) removes, or rather captures, the singularity on the outer horizon [1]. Substituting Eq. (3.2) into Eq. (2.133), the radial Teukolsky equation becomes [84]

$$x(1-x)p''_{\text{in}} + [1 - s - i\epsilon - i\tau - (2 - 2i\tau)x]p'_{\text{in}} + [i\tau(1 - i\tau) + \lambda + s(s+1)]p_{\text{in}} =$$
$$2i\epsilon\kappa\left[-x(1-x)p'_{\text{in}} + (1 - s + i\epsilon - i\tau)xp_{\text{in}}\right] + \left[\epsilon^2 - i\epsilon\kappa(1 - 2s)\right]p_{\text{in}}. \qquad (3.3)$$

Having removed the poles of the radial Teukolsky equation, the resulting form is particularly interesting. The left hand side of Eq. (3.3) is in the form of the hypergeometric differential equation

$$x(1-x)\frac{\text{d}^2 w}{\text{d}x^2} + (c - (a+b+1)x)\frac{\text{d}w}{\text{d}x} - abw = 0, \qquad (3.4)$$

whose solutions are

$$w_1(x) = {}_2F_1(a, b; c; x), \qquad (3.5)$$

$$w_2(x) = x^{1-c}\,{}_2F_1(a - c + 1, b - c + 1; 2 - c; x), \qquad (3.6)$$

---

[1]The other poles at r_- and ∞ are removed but not captured by the solution Eq. (3.2).

for the case where there is a singularity at $x = 0$ [2]. This is equivalent to the case where there is a singularity at $r = r_+$, captured by Eq. (3.2). The solution to $p_{\text{in}}(x)$ should be chosen to correspond to w_1 in order to recover the desired asymptotic behaviour of R^{in}_{slm} on the outer horizon as w_1 contains no additional pre-factors that include the dependent variable. w_2 may produce a solution to the Teukolsky equation in some other basis, though it shall be disregarded here. The fact that the terms on the right hand side of Eq. (3.3) contain various powers of ϵ is suggestive of an expansion solution for $p_{\text{in}}(x)$, for which $\epsilon \ll 1$. It should be noted that the quantity, λ, the eigenvalue of the angular Teukolsky equation, which is equivalently the equation for the spin-weighted spheroidal harmonics, has the small frequency expansion [84]

$$\lambda = \lambda_0 + a\omega\lambda_1 + a^2\omega^2\lambda_2 + \mathcal{O}\left((a\omega)^3\right), \tag{3.7}$$

where $\lambda_0 = l(l+1) - s(s+1)$. The higher order terms can be determined by solving the equation for spin-weighted spheroidal harmonics perturbatively, and are given completely analytically to arbitrary order by the Spin Weighted Spheroidal Harmonics package in the BHPToolkit [1]. Therefore, the leading order solution to $p_{\text{in}}(x)$ in Eq. (3.3) for when $\epsilon \to 0$, is given by [84]

$$\lim_{\epsilon \to 0} p_{\text{in}}(x) = {}_2F_1(l + 1 - i\tau, -l - i\tau; 1 - s - i\tau; x). \tag{3.8}$$

To obtain the solution for $p_{\text{in}}(x)$ for the case where $\epsilon \neq 0$, the parameters in eq. (3.8) will change slightly. However, it is difficult to determine the parameters of the hypergeometric function for the case where $\epsilon \neq 0$ from Eq. (3.3) in its current form [3]. For this reason, the term $\lambda + s(s + 1)$ is moved to the right hand side of Eq. (3.3). This introduces an $\mathcal{O}(1)$ quantity to the right hand side of Eq. (3.3), which must be removed if the right hand side is to be treated as an $\mathcal{O}(\epsilon)$ perturbation. The renormalised angular momentum, $\nu = l + \mathcal{O}(\epsilon)$, is introduced and the term $\nu(\nu + 1)$ is added to both sides of Eq. (3.3). Without changing anything, Eq. (3.3) can be rewritten in the following form [84]

$$x(1-x)p''_{\text{in}} + [1 - s - i\epsilon - i\tau - (2 - 2i\tau)x]p'_{\text{in}} + [i\tau(1 - i\tau) + \nu(\nu + 1)]p_{\text{in}} =$$
$$2i\epsilon\kappa\left[-x(1-x)p'_{\text{in}} + (1 - s + i\epsilon - i\tau)xp_{\text{in}}\right] + \left[\nu(\nu + 1) - \lambda - s(s + 1) + \epsilon^2 - i\epsilon\kappa(1 - 2s)\right]p_{\text{in}}. \tag{3.9}$$

In this form, it is still easy to read what the hypergeometric parameters in $p_{\text{in}}(x)$ should be for

---

[2]There are additional solutions to Eq. (3.4) for which there are singularities at $x = 1$ and $x = \infty$. Each of these solutions have various alternate forms, which can be found in the Digital Library of Mathematical Functions (DLMF) [97]. For the ingoing radial Teukolsky solution, only the asymptotic amplitudes at $\mathcal{H}^+$, $\mathcal{I}^+$ and $\mathcal{I}^-$ are of interest, given by $R^{\text{in,tra}}_{slm}$, $R^{\text{in,ref}}_{slm}$ and $R^{\text{in,inc}}$ respectively. Therefore the solutions to the hypergeometric equation for which there is a singularity at $x = 1$ are not relevant to constructing the ingoing radial Teukolsky solution, as this occurs at $r = r_-$, on the inner horizon $\mathcal{H}^-$. The solution required to recover R^{in}_{slm} on $\mathcal{I}^+$ and $\mathcal{I}^-$ will be discussed later in this section.

[3]To determine the parameters a, b and c in ${}_2F_1(a, b, c, x)$ for the Teukolsky case requires solving a set of simultaneous equations, obtained by comparing the left hand side of Eq. (3.3) with Eq. (3.4). Solving $a + b + 1 = 2 - 2i\tau$ and $-ab = l(l+1) + i\tau(1 - i\tau)$ is much easier to solve than $a + b + 1 = 2 - 2i\tau$ and $-ab = \lambda + s(s + 1) + i\tau(1 - i\tau)$. For this reason, Eq. (3.3) is rearranged to the form in Eq. (3.9).

the case where $\epsilon \neq 0$, as well as ensuring that the right hand side of Eq. (3.9) is at least an $\mathcal{O}(\epsilon)$ perturbation, such that a solution to $p_{\text{in}}(x)$ that is an expansion in ϵ makes sense, where $\epsilon \ll 1$. For $\epsilon \neq 0$, $p_{\text{in}}(x)$ then becomes

$$p_{\text{in}} = \sum_{n=-\infty}^{\infty} f_n \, p_{n+\nu}(x), \tag{3.10}$$

$$p_{n+\nu}(x) = \, _2F_1(n + \nu + 1 - i\tau, -n - \nu - i\tau; 1 - s - i\epsilon - i\tau; x), \tag{3.11}$$

where f_n are the MST coefficients to be determined. If one was to try to solve Eq. (3.9) without introducing the renormalised angular momentum, one would eventually face an equivalent procedure in order for the series to converge to obtain a meaningful low-frequency expansion solution [84, 86]. As $\epsilon \to 0$, the quantities ν and λ should behave in such a way that $\nu \to l$ and $\lambda \to \lambda_0$. A derivation of the explicit form of ν can be found in References [84] or [86]. The solution in Eq. (3.11) is written as a sum over n to exploit the standard recurrence relation identities for the hypergeometric functions [86]

$$x \, _2F_1(a, b; c; x) = \frac{a(b - c)}{(a - b)(a - b + 1)} \, _2F_1(a + 1, b - 1; c; x) \tag{3.12}$$
$$+ \frac{c(a + b - 1) - 2ab}{(a - b - 1)(a - b + 1)} \, _2F_1(a, b; c; x)$$
$$+ \frac{b(a - c)}{(a - b - 1)(a - b)} \, _2F_1(a - 1, b + 1; c; x),$$

$$x(1 - x)\frac{\mathrm{d}}{\mathrm{d}x} \, _2F_1(a, b; c; x) = \frac{ab(c - b)}{(a - b)(a - b + 1)} \, _2F_1(a + 1, b - 1; c; x) \tag{3.13}$$
$$+ \frac{ab(2c - a - b - 1)}{(a - b + 1)(a - b - 1)} \, _2F_1(a, b; c; x)$$
$$+ \frac{ab(a - c)}{(a - b)(a - b - 1)} \, _2F_1(a - 1, b + 1; c; x).$$

Considering the right hand side of Eq. (3.9) as a perturbation, and applying the recurrence relations Eq. (3.12) and Eq. (3.13) to the equation

$$2i\epsilon\kappa \left[-x(1 - x)p'_{\text{in}} + (1 - s + i\epsilon - i\tau)xp_{\text{in}} \right] \tag{3.14}$$
$$+ \left[\nu(\nu + 1) - \lambda - s(s + 1) + \epsilon^2 - i\epsilon\kappa(1 - 2s) \right] p_{\text{in}} = 0,$$

a recurrence relation for the MST series coefficients f_n can be derived [86]

$$\alpha_n^\nu f_{n+1} + \beta_n^\nu f_n + \gamma_n^\nu f_{n-1} = 0, \tag{3.15}$$

where

$$\alpha_n^\nu = \frac{i\epsilon\kappa(n+\nu+1+s+i\epsilon)(n+\nu+1+s-i\epsilon)(n+\nu+1+i\tau)}{(n+\nu+1)(2n+2\nu+3)}, \tag{3.16}$$

$$\beta_n^\nu = -\lambda - s(s+1) + (n+\nu)(n+\nu+1) + \epsilon^2 + \epsilon(\epsilon-mq) + \frac{\epsilon(\epsilon-mq)\left(s^2+\epsilon^2\right)}{(n+\nu)(n+\nu+1)}, \tag{3.17}$$

$$\gamma_n^\nu = -\frac{i\epsilon\kappa(n+\nu-s+i\epsilon)(n+\nu-s-i\epsilon)(n+\nu-i\tau)}{(n+\nu)(2n+2\nu-1)}. \tag{3.18}$$

The renormalized angular momentum, ν is defined such that the MST series converges. As a small frequency expansion, ν is given by [84, 86]

$$\nu = l + \frac{1}{2l+1}\left(-2 - \frac{s^2}{l(l+1)} + \frac{((l+1)^2 - s^2)^2}{(2l+1)(2l+2)(2l+3)} - \frac{\left(l^2-s^2\right)^2}{(2l-1)2l(2l+1)}\right)\epsilon^2 + \mathcal{O}\left(\epsilon^3\right). \tag{3.19}$$

In the BHPToolkit, ν is calculated using monodromy in *Mathematica* [111] and by a root finding method for C++ [112]. Using Eqs. (3.15)-(3.18) and initialising the series with $f_0 = 1$, the coefficients f_n can be determined either numerically or semi-analytically, as a small frequency expansion [4]. Recall that f_n are derived from the underlying assumption that the right hand side of Eq. (3.3) is a perturbation, and hence analytic expressions for f_n are valid only for $\epsilon \ll 1$ and should be treated as such. A detailed analysis is given in [84] to ensure that the recurrence relation Eq. (3.15) converges, such that the MST series can indeed provide a meaningful low-frequency expansion for the radial Teukolsky solution. The ingoing radial Teukolsky solution in Eq. (3.2) then becomes

$$R^{\text{in}}(x) = e^{i\epsilon\kappa x}(-x)^{-s-i(\epsilon+\tau)/2}(1-x)^{i(\epsilon-\tau)/2}\sum_{n=-\infty}^{\infty} f_n \,_2F_1(n+\nu+1-i\tau, -n-\nu-i\tau; 1-s-i\epsilon-i\tau; x). \tag{3.20}$$

One of the key features of the MST series is that for larger values of $|n|$, the leading order terms of each coefficient f_n depend on higher powers of ϵ [86]. This means that for a given order in ϵ, only a relatively small number of terms in the MST series is required to obtain an accurate solution [86]. The solution in Eq. (3.20) is valid over the domain $-\infty < x \leq 0$ and recovers the desired asymptotic behaviour at $\mathcal{H}^+$, from which the asymptotic amplitude $R^{\text{in, trans}}$ can be calculated [84, 86, 85]. The solution in Eq. (3.20) is not valid at $|x| = \infty$ however and cannot therefore recover the asymptotic amplitudes $R_{slm}^{\text{in, inc}}$ and $R_{slm}^{\text{in, ref}}$, and an alternative solution must be found to complete R_{slm}^{in}. Recall that there are many alternate solutions to the hypergeometric equation, not all of them independent and each valid for a particular domain. For example, another solution for R_{slm}^{in} that is valid at large

---

[4]The choice of initialisation to solve for the MST series coefficients is arbitrary. A different choice for f_0 simply changes the overall normalisation of the series, rescaling the asymptotic amplitudes. It is worth noting that f_n has in fact two linearly independent solutions, however freedom within the choice of ν allows for a unique, consistent solution to be determined [84]. A number of examples for f_n are given in [86] for the Schwarzschild case, for different values of l and s. It is also worth keeping in mind that while all analytic MST expressions are derived under the assumption that ω is small, Eq. (3.3) and Eq. (3.15) can in principle be solved numerically for arbitrary frequencies.

x is given by

$$R_{slm}^{\mathrm{in}} = R_0^{\nu} + R_0^{-\nu-1}, \tag{3.21}$$

where

$$
\begin{aligned}
R_0^{\nu} =& e^{i\epsilon\kappa x}(-x)^{-s-(i/2)(\epsilon+\tau)}(1-x)^{(i/2)(\epsilon+\tau)+\nu} \\
&\times \sum_{n=-\infty}^{\infty} f_n^{\nu} \frac{\Gamma(1-s-i\epsilon-i\tau)\Gamma(2n+2\nu+1)}{\Gamma(n+\nu+1-i\tau)\Gamma(n+\nu+1-s-i\epsilon)} \\
&\times (1-x)^n \, {}_2F_1\left(-n-\nu-i\tau, -n-\nu-s-i\epsilon; -2n-2\nu; \frac{1}{1-x}\right),
\end{aligned}
\tag{3.22}
$$

and the *slm* label has been dropped for convenience. R_0^{ν} and $R_0^{-\nu-1}$ are linearly independent, and hence form a basis of solutions to the Teukolsky equation.

So far, only the ingoing solution to the Teukolsky equation Eq. (2.133) has been discussed. To determine the upgoing radial Teukolsky solution, a different rescaling to that of Eq. (3.2) is used, given by

$$R_{\mathrm{C}} = \hat{z}^{-1-n}\left(1 - \frac{\epsilon\kappa}{\hat{z}}\right)^{-s-i(\epsilon+\tau)/2} f(\hat{z}), \tag{3.23}$$

where

$$\hat{z} = z - z_- = \epsilon\kappa(1-x), \tag{3.24}$$

and $f(\hat{z})$ is to be determined, similarly to $p_{\mathrm{in}}(x)$ for the ingoing case. The *slm* label has also been dropped here. A derivation of the prefactor in Eq. (3.23) can be found in Appendix B of [85]. Unlike R_{slm}^{in} however, R_{C} does not correspond to the upgoing solution exactly, which will be given later in Eq. (3.32). Substituting Eq. (3.23) into Eq. (2.133) transforms the radial Teukolsky equation in to the form of a perturbed Coulomb equation (hence the suggestive subscript 'C') instead of a perturbed hypergeometric differential equation, as happened when substituting Eq. (3.2) into Eq. (2.133) [84]. The leading order Coulomb equation obtained has a regular singularity at $\hat{z} = 0$, corresponding to the inner horizon. The solutions to Coulomb's equation again have many alternate forms that can be found in the DLMF [97], such as the confluent hypergeometric function U [5], which is the usual choice for the upgoing MST series solution as its analytic properties allow for the solution of R_{C} to be simplified, as well as allowing for the asymptotic behaviour of R_{slm}^{up} to be recovered [84]. Similarly to $p_{\mathrm{in}}(x)$, a detailed derivation of $f(\hat{z})$ can be found in references [84] or [86] but will not

---

[5]It serves to list some of the many aliases of U that appear in the literature, in order to avoid confusion when visiting the references provided throughout this report. U is often written as Ψ, as is the case in Ref. [86], is referred to in the DLMF [97] as one of the confluent hypergeometric functions, namely a solution to Kummer's equation and is also occasionally referred to as Tricomi's function, which is also known as the confluent hypergeometric function of the second kind. The label U is chosen here to reflect the corresponding Mathematica function, `HypergeometricU[]` which will be used in Chapter 3.

be provided here for brevity. R_C is then given by [84, 86]

$$R_C = R_+^\nu + R_-^\nu, \tag{3.25}$$

where R_+^ν and R_-^ν are linearly independent for a given slm mode, and are given respectively by [84]

$$R_+^\nu = 2^\nu e^{-\pi\epsilon} e^{i\pi(\nu+1-s)} \frac{\Gamma(\nu+1-s+i\epsilon)}{\Gamma(\nu+1+s-i\epsilon)} e^{-i\hat{z}} \hat{z}^{\nu+i\epsilon} (\hat{z}-\epsilon\kappa)^{-s-i\epsilon_+} \tag{3.26}$$

$$\times \sum_{n=-\infty}^{\infty} i^n f_n^\nu (2\hat{z})^n U(n+\nu+1-s+i\epsilon, 2n+2\nu+2; 2iz), \tag{3.27}$$

$$R_-^\nu = 2^\nu e^{-\pi\epsilon} e^{-i\pi(\nu+1+s)} e^{i\hat{z}} \hat{z}^{\nu+i\epsilon_+} (\hat{z}-\epsilon\kappa)^{-s-i\epsilon_+} \tag{3.28}$$

$$\times \sum_{n=-\infty}^{\infty} i^n \frac{(\nu+1+s-i\epsilon)_n}{(\nu+1-s+i\epsilon)_n} f_n^\nu (2\hat{z})^n \tag{3.29}$$

$$\times U(n+\nu+1+s-i\epsilon, 2n+2\nu+2; -2iz), \tag{3.30}$$

with

$$\epsilon_+ = \frac{\epsilon+\tau}{2}, \qquad \epsilon_- = \frac{\epsilon-\tau}{2}. \tag{3.31}$$

Similarly to the ingoing solution, one solution to the Coulomb type Teukolsky equation is chosen such that the asymptotic behaviour of the upgoing radial function at $|x| = \infty$ in Eq. (2.137) is recovered, and is valid over the region $r_+ < r$. A suitable solution to R_{slm}^{up} that satisfies these conditions is found to be [84]

$$R_{slm}^{up}(\hat{z}) = R_-^\nu. \tag{3.32}$$

The solutions R_0^ν, $R_0^{-\nu-1}$, R_+^ν and R_-^ν cannot all be independent and must therefore satisfy some relation to each other. Each set of solutions can be thought of as an alternate basis to the Teukolsky equation, however not every solution will produce a result from which the physics of interest, in this case the asymptotic behaviour, is readily seen. While R_0^ν and $R_0^{-\nu-1}$ are valid in the region $r < \infty$, R_+^ν and R_-^ν are valid in the region $r_+ < r$, to compare these solutions they must match in the region $r_+ < r < \infty$. The only way this is possible is if the MST coefficients and the renormalized angular momentum ν work out to be the same for both sets of solutions. Thankfully this works out to be the case, and is the reason why both sets of MST coefficients can be referred to as f_n[6] . The relationship between R_C and R_0^ν is [84, 86]

$$R_0^\nu = K_\nu R_C, \tag{3.33}$$

where K_ν is given by Eq. (165) in [84] or Eq. (3.32) in [86].

---

[6]The fact that ν and f_n work out to be the same for both ingoing and upgoing solutions is often quoted in the literature as surprising. However, given that R_0^ν, $R_0^{-\nu-1}$, R_+^ν and R_-^ν cannot all be independent, perhaps it's no mystery as there is necessarily a way to relate the hypergeometric and confluent hypergeometric solutions. Relations between these functions can also be found in the DLMF [97] for special cases.

Therefore, R_{slm}^{in} can also be written as

$$R_{slm}^{\text{in}} = K_\nu R_{\text{C}}^\nu + K_{-\nu-1} R_{\text{C}}^{-\nu-1}, \tag{3.34}$$

which is valid in the region $r_+ < r$, including at $r = \infty$ [84]. Equation (3.34) can then be used to obtain the asymptotic amplitudes $R_{slm}^{\text{in, inc}}$ and $R_{slm}^{\text{in, ref}}$. Using the Chandrasekhar transformation, MST expressions can also be found for the ingoing and upgoing solutions to the Regge-Wheeler equation, Eq. (2.49) [86]. Respectively, these are given by [86]

$$\psi_s^{\text{in}}(x) = (1-x)^{s+1} e^{i\epsilon x}(-x)^{-i\epsilon} \sum_{n=-\infty}^{\infty} \frac{(-\nu+s-i\epsilon)_{-n}(\nu+s-i\epsilon+1)_n(\nu+i\epsilon+1)_n}{(\nu-i\epsilon+1)_n}(-1)^n f_n$$
$$\times\ {}_2F_1(n+\nu+1+s-i\epsilon, -n-\nu+s-i\epsilon; 1-2i\epsilon; x), \tag{3.35}$$

$$\psi_s^{\text{up}}(z) = 2^\nu e^{-\pi\epsilon} e^{-i\pi(\nu+1)} e^{iz} z^{\nu+1+i\epsilon}(z-\epsilon\kappa)^{-i\epsilon} \sum_{n=-\infty}^{\infty} \frac{(\nu+1+s-i\epsilon)_n}{(\nu+1-s+i\epsilon)_n} f_n (2iz)^n$$
$$\times\ U(n+\nu+1-i\epsilon, 2n+2\nu+2; -2iz). \tag{3.36}$$

The asymptotic behaviour of the Regge-Wheeler master functions is also satisfied by Eq. (3.35) and Eq. (3.36) as required [7] . Eq. (3.20), Eq. (3.32) Eq. (3.35) and Eq. (3.36) are all valid under the assumption that $\epsilon \ll 1$, and hence naturally lend themselves to a low-frequency expansion, which can easily be performed by using the Mathematica function, `Series[]`. As was the goal of the MST method, we now have semi-analytic solutions to the Teukolsky and Regge-Wheeler equations. While there are a number of alternate forms for R_{slm}^{in}, R_{slm}^{up}, ψ_s^{in} and ψ_s^{up}, which may be more suitable for analysis near the horizon or near infinity, the respective definitions in Eq. (3.20), Eq. (3.32) Eq. (3.35) and Eq. (3.36) shall be used whenever the MST series for the radial Teukolsky and Regge-Wheeler master functions are required throughout this report. These expressions are valid over almost the entire domain, and for the portions of the domain that they are not, the asymptotic definitions may be used.

3.2 The MST package

The goal of the MST package is to compute the MST series for the radial ingoing and radial upgoing Teukolsky and Regge-Wheeler master functions (and their derivatives) numerically, using Eq. (3.20), Eq. (3.32), Eq. (3.35) and Eq. (3.36). The MST package does this by defining

---

[7] Note that in [86], the functions ψ_s^{in} and ψ_s^{up} are referred to as X^{in} and X^{up} respectively. Note also that the MST coefficients f_n are denoted as a_n^T in [86]. In this report, the convention of [84] will be adopted and the MST coefficients will always be written in terms of f_n. The relationship between different definitions for the MST coefficients can be found in [86]. These relations explain the apparent differences between our ψ_s^{in} and ψ_s^{up} compared to X^{in} and X^{up} in [86]. These expressions however are in fact equivalent.

the functions `MSTRadialIn[s, l, m, q, ` ϵ `, ` ν `, ` λ `, norm]`, `MSTRadialUp[s, l, m, q, ` ϵ `, ` ν `, ` λ `, norm]` and their derivatives. The parameters s, l, m, q, ϵ, ν and λ have their usual meanings, defined earlier in this report. To compute these functions, the variable `$MasterFunction` must be set to either `Teukolsky` or `ReggeWheeler` according to the user's requirements. ν is calculated using the function `RenormalizedAngularMomentum[s, l, m, a, ` ω `, ` λ `]`, which is defined in another file of the MST package in the BHPToolkit [1]. The parameter 'norm' refers to the user's choice of normalisation. The MST package follows the conventions and therefore normalisation of [84], so a choice of 'norm' = 1 corresponds to the exact MST expressions from Eq. (3.20), Eq. (3.32), Eq. (3.35) and Eq. (3.36). The parameters in `MSTRadialIn[]` and `MSTRadialUp[]` will henceforth be dropped and for the remainder of this section parameters of Mathematica functions from the MST package will only be specified when initially introduced. It should be kept in mind that `MSTRadialIn[]` computes either R_{slm}^{in} or ψ_s^{in}, depending on the choice of `$MasterFunction`. Similarly, `MSTRadialUp[]` computes either R_{slm}^{up} or ψ_s^{up}. These functions also come with options for precision and accuracy that correspond to Mathematica's standard options. In this section, the MST coefficients will always be written in terms of f_n using the convention of [84].

In order to compute `MSTRadialIn[]` and `MSTRadialUp[]`, the MST package must also calculate f_n numerically, which it does by defining the function `fn[q, ` ϵ `, ` κ `, ` τ `, ` ν `, ` λ `, s, m, n]` and using a standard numerical algorithm to solve the recurrence relation in Eq. (3.15). The details of this algorithm can be found in the MST package [1]. For the remainder of this section, the inner workings of the MST package are described in detail, namely how `MSTRadialIn[]` and `MSTRadialUp[]` and their derivatives are programmed and computed, keeping efficiency, usability and readability of the package in mind. The MST package is valid for all values of s, l and m, though not all combinations will be physically relevant. Note also that $M = 1$ throughout the MST package.

3.3   Deriving recurrence relations for hypergeometric functions

Previously in Section 3.1 it was shown that the radial ingoing (and radial outgoing) Teukolsky and Regge-Wheeler master functions heavily depend on the (confluent) hypergeometric functions, $_2F_1$ (and U). Therefore, an understanding of such functions is required in order to sum the MST series efficiently. It is found in many cases that it is more efficient to calculate $_2F_1$ and U using recurrence relations than to compute them directly. As such, suitable recurrence relations for $_2F_1$ and U will be derived here for use in the MST package. The DLMF [97] provides an ample selection of relations for a given (confluent) hypergeometric function and its contiguous functions, a resource that shall be used throughout this section. The recurrence relations derived here should not be confused with those used in deriving the MST series coefficients f_n in Section 3.1 as they serve a different purpose.

3.3.1 Ingoing radial MST functions

Recall from Eq. (3.20) and Eq. (3.35) that a given term in the MST series for the radial ingoing Teukolsky [84] and RW [86] master functions are of the respective forms

$$R^{\text{in}} \sim {}_2F_1(n + \nu + 1 - i\tau, -n - \nu - i\tau; 1 - s - i\epsilon - i\tau; x), \tag{3.37}$$

$$\psi_s^{\text{in}} \sim {}_2F_1(n + \nu + s + 1 - i\epsilon, -n - \nu + s - i\epsilon; 1 - 2i\epsilon; x). \tag{3.38}$$

Instead of deriving recurrence relations for both the Teukolsky and RW cases separately, a more general recurrence relation can be derived for ${}_2F_1(a + n, b - n, c, x)$ where, for the Teukolsky case

$$
\begin{aligned}
a &= \nu + 1 - i\tau, \\
b &= -\nu - i\tau, \\
c &= 1 - s - i\epsilon - i\tau, \tag{3.39}
\end{aligned}
$$

and for the Regge Wheeler case

$$
\begin{aligned}
a &= \nu + s + 1 - i\epsilon \\
b &= -\nu + s - i\epsilon \\
c &= 1 - 2i\epsilon. \tag{3.40}
\end{aligned}
$$

Deriving a suitable recurrence relation for the general parameters a, b and c facilitates the implementation of further options beyond Teukolsky and Regge-Wheeler, should they ever be required in the future. Using a generic recurrence relation in the MST package also makes the derivation more transparent. A suitable recurrence relation should reflect the summation in the MST series. As n is the variable to be summed over, the relevant recurrence relation should take the following form

$$
\begin{aligned}
{}_2F_1(n + a, b - n, c, x) &= {}_2F_1(a + n - 1, b - (n - 1), c, x)A(a, b, c, x) \tag{3.41} \\
&\quad + {}_2F_1(a + n - 2, b - (n - 2), c, x)B(a, b, c, x), \\
&= {}_2F_1(a + n - 1, b - n + 1, c, x)A(a, b, c, x) \\
&\quad + {}_2F_1(a + n - 2, b - n + 2, c, x)B(a, b, c, x),
\end{aligned}
$$

where $A(a, b, c, x)$ and $B(a, b, c, x)$ are to be determined. To simplify notation, for a given n, the variables $\tilde{a}$ and $\tilde{b}$ are introduced

$$\tilde{a} = a + n, \tag{3.42}$$

$$\tilde{b} = b - n, \tag{3.43}$$

and the recurrence relation Eq. (3.41) becomes

$$_2F_1(\tilde{a}, \tilde{b}, c, x) = {}_2F_1(\tilde{a} - 1, \tilde{b} + 1, c, x)A(a, b, c, x) + {}_2F_1(\tilde{a} - 2, \tilde{b} + 2, c, x)B(a, b, c, x). \quad (3.44)$$

The tildes on $\tilde{a}$ and $\tilde{b}$ will henceforth be dropped for convenience, to be reinstated later on. To solve for $A(a, b, c, x)$ and $B(a, b, c, x)$, a good starting point is to determine a recurrence relation for $_2F_1(a, b, c, x)$ that is contiguous in the first parameter, a. Setting $a \to a - 1$ in DLMF(15.5.11) [97] gives

$$(a - 1)(x - 1)_2F_1(a, b, c, x) + [c - (a - 1)]_2F_1(a - 2, b, c, x)$$
$$+ [2(a - 1) - c + (b - (a - 1))x]_2F_1(a - 1, b, c, x) = 0. \quad (3.45)$$

The second and third terms of Eq. (3.45) need to be written in terms of $_2F_1(a, b, c, x)$, $_2F_1(a - 1, b + 1, c, x)$ and $_2F_1(a - 2, b + 2, c, x)$ in order to obtain a recurrence relation of the desired form, as in Eq. (3.44). This can be done by replacing the second and third term of Eq. (3.45) using DLMF(15.5.12) [97] and choosing $a \to a - 2$ and $a \to a - 1$ respectively, such that

$$_2F_1(a - 2, b, c, x) = \frac{(1 - (a - 1))_2F_1(a - 1, b, c, x) + b_2F_1(a - 2, b + 1, c, x)}{b - (a - 2)}, \quad (3.46)$$

$$_2F_1(a - 1, b, c, x) = \frac{(1 - a)_2F_1(a, b, c, x) + b_2F_1(a - 1, b + 1, c, x)}{b - (a - 2)}. \quad (3.47)$$

The first term on the right hand side of Eq. (3.46) can be replaced using Eq. (3.47). In this way, Eq. (3.45) can be written in terms of $_2F_1(a, b, c, x)$, $_2F_1(a - 1, b + 1, c, x)$ and $_2F_1(a - 2, b + 2, c, x)$, with an additional term including $_2F_1(a - 2, b + 1, c, x)$, which can be replaced by using DLMF(15.5.12) [97] and choosing $a \to a - 2$ and $b \to b + 1$ such that

$$_2F_1(a - 2, b + 1, c, x) = \frac{(2 - a)_2F_1(a - 1, b + 1, c, x) + (b + 1)_2F_1(a - 2, b + 2, c, x)}{b + 1 - (a - 2)}. \quad (3.48)$$

Using Eqs. (3.46) - (3.48) and Eq. (3.45) can be rewritten as

$$(a - 1)(x - 1)_2F_1(a, b, c, x) + [c - (a - 1)]\left\{\frac{1 - (a - 1)}{b - (a - 2)}\left(\frac{(a - 1)_2F_1(a, b, c, x) + b_2F_1(a - 1, b + 1, c, x)}{b - (a - 1)}\right)\right.$$

$$\left. + \frac{b}{b - (a - 2)}\left(\frac{(2 - a)_2F_1(a - 1, b + 1, c, x) + (b + 1)_2F_1(a - 2, b + 2, c, x)}{b + 1 - (a - 2)}\right)\right\}$$

$$+ \frac{[2(a - 1) - c + (b - (a - 1))x]}{b - (a - 1)}\{(1 - a)_2F_1(a, b, c, x) + b_2F_1(a - 1, b + 1, c, x)\} = 0. \quad (3.49)$$

As n is the variable to be summed over in the MST series, n must be reinstated into the recurrence relation. Reverting back to the original parameters by setting $a \to a + n$ and $b \to b - n$, and solving

Eq. (3.49) for $_2F_1(a, b, c, z)$, the simplified result is given by

$$
\begin{aligned}
_2F_1(a+n, b-n, c, x) = \Bigg(& \frac{(2-a-n)(1-a+c-n)}{(1+b-c-n)(-1+a+n)} - \frac{(2-a-n)(1-a+c-n)(1-a+b-2n)}{(3-a+b-2n)(1+b-c-n)(-1+a+n)} \\
& + \frac{(2-a+b-2n)(-c+2(-1+a+n)+(1-a+b-2n)x)}{(1+b-c-n)(-1+a+n)} \Bigg) \\
& \times\ _2F_1(a+n-1, b-n+1, c, x) \\
& + \frac{(1+b-n)(1-a+c-n)(1-a+b-2n)}{(3-a+b-2n)(1+b-c-n)(-1+a+n)}\,_2F_1(a+n-2, b-n+2, c, x).
\end{aligned}
$$

(3.50)

The recursion relation in Eq. (3.50) is now in the desired form as initially proposed in Eq. (3.44) and is almost ready to be implemented to the MST package. The functions $A(a, b, c, x)$ and $B(a, b, c, x)$ can be read directly from the coefficients of $_2F_1(a+n-1, b-n+1, c, x)$ and $_2F_1(a+n-2, b-n+2, c, x)$ in Eq. (3.50) respectively. There are however still a few more steps before the recurrence relation is 'package ready', which will be discussed in Section 3.4.

3.3.2   Upgoing radial MST functions

While the MST series for the radial ingoing Teukolsky and RW master functions required a recurrence relation for $_2F_1$, the radial upgoing solutions require a recurrence relation for U. The approach to deriving this recurrence relation is largely the same as that for its ingoing counterpart, with a few more intermediate steps. Recall from Section 3.1 that a given term in the MST series for the radial upgoing Teukolsky [84] and RW [86] solutions are of the respective forms

$$
R^{\mathrm{up}} \sim U(n+\nu+1+s-i\epsilon, 2n+2\nu+2; -2i\hat{z}),
$$

(3.51)

$$
\psi_s^{\mathrm{up}} \sim U(n+\nu+1-i\epsilon, 2n+2\nu+2; -2i\hat{z}).
$$

(3.52)

Similar to Eq. (3.41) in the ingoing case, a general recurrence relation for U that reflects the MST series for the upgoing case should be of the form

$$
U(n+a, 2n+b, c) = U(n-1+a, 2(n-1)+b, c)C(a, b, c) + U(n-2+a, 2(n-2)+b, c)D(a, b, c),
$$
$$
U(\tilde{a}, \tilde{b}, c) = U(\tilde{a}-1, \tilde{b}-2, c)C(a, b, c) + U(\tilde{a}-2, \tilde{b}-4, c)D(a, b, c),
$$

(3.53)

where $C(a, b, c)$ and $D(a, b, c)$ are to be determined, $\tilde{a} = a + n$ and $\tilde{b} = 2n + b$, with

$$
\begin{aligned}
a &= \nu + 1 + s - i\epsilon && \text{for the Teukolsky case,} \\
a &= \nu + 1 - i\epsilon && \text{for the RW case,} \\
b &= 2\nu + 2 && \text{for both the Teukolsky and RW cases,} \\
c &= -2i\hat{z} && \text{for both the Teukolsky and RW cases.}
\end{aligned}
$$

(3.54)

The tildes will again be dropped for convenience, to be reinstated later on. In order to determine $C(a,b,c)$ and $D(a,b,c)$, setting $a \to a-1$ in the relation given by DLMF(13.3.7), which is contiguous in the first parameter a, is again a good starting point

$$(a-1)(a-b)U(a,b,c) + (b-2(a-1)-c)U(a-1,b,c) + U(a-2,b,c) = 0. \qquad (3.55)$$

To obtain a recurrence relation of the form in Eq. (3.53), the second and third terms in Eq. (3.55) need to be written in terms of $U(a,b,c)$, $U(a-1,b-2,c)$ and $U(a-2,b-4,c)$. Treating the second term of Eq. (3.55) first, a shall be set to $a \to a-1$ in DLMF(13.3.9) and $a \to a-1, b \to b-1$ in DLMF(13.3.8), yielding the following equations respectively

$$U(a-1,b,c) - (a-1)U(a,b,c) - U(a-1,b-1,c) = 0, \quad (3.56)$$

$$(b-(a-1)-2)U(a-1,b-2,c) + (1-(b-1)-c)U(a-1,b-1,c) + cU(a-1,b,c) = 0. \quad (3.57)$$

Rearranging Eq. (3.57) for $U(a-1,b-1,c)$, substituting the result into Eq. (3.56) and then solving for $U(a-1,b,c)$ gives

$$U(a-1,b,c) = \frac{(a-1)U(a,b,c) - \dfrac{(b-(a-1)-2)}{(1-(b-1)-c)}U(a-1,b-2,c)}{\left(1 + \dfrac{c}{1-(b-1)-c}\right)}, \qquad (3.58)$$

which can be used to replace the second term in Eq. (3.55). Dealing now with the third term in Eq. (3.55), $U(a-2,b,c)$ can be rewritten by setting $a \to a-1$ in Eq. (3.58) to give

$$U(a-2,b,c) = \frac{(a-2)U(a-1,b,c) - \dfrac{(b-(a-2)-2)}{(1-(b-1)-c)}U(a-2,b-2,c)}{\left(1 + \dfrac{c}{1-(b-1)-c}\right)}. \qquad (3.59)$$

The first term in Eq. (3.59) is known from Eq. (3.58). All that remains to do is to determine $U(a-2,b-2,c)$ in terms of $U(a,b,c)$, $U(a-1,b-2,c)$ and $U(a-2,b-4,c)$, which can be done by using Eq. (3.58) and setting $a \to a-1$ and $b \to b-2$, recovering the relation

$$U(a-2,b-2,c) = \frac{(a-2)U(a-1,b-2,c) - \dfrac{((b-2)-(a-2)-2)}{(1-(b-3)-c)}U(a-2,b-4,c)}{\left(1 + \dfrac{c}{1-(b-3)-c}\right)}. \qquad (3.60)$$

Replacing $U(a-2,b-2,c)$ in Eq. (3.59) with the right hand side of Eq. (3.60) gives $U(a-2,b,c)$ completely in terms of $U(a,b,c)$, $U(a-1,b-2,c)$ and $U(a-2,b-4,c)$ as required. Replacing $U(a-1,b,c)$ in Eq. (3.55) with the right hand side of Eq. (3.58) and replacing $U(a-2,b,c)$ with the right hand side of Eq. (3.59), making the necessary substitutions for $U(a-1,b,c)$ and $U(a-2,b-2,c)$

using Eq. (3.59) and Eq. (3.60) respectively gives the following relation

$$
(a-1)(a-b)U(a,b,c) + (b-2(a-1)-2) \left\{ \frac{(a-1)U(a,b,c) - \left(\dfrac{b-(a-1)-2}{1-(b-1)-c} \right) U(a-1,b-2,c)}{\left(1 + \dfrac{c}{1-(b-1)-c} \right)} \right\}
$$

$$
+ \left\{ \frac{a-2}{1+\dfrac{c}{1-(b-1)-c}} \times \frac{(a-1)U(a,b,c) - \dfrac{b-(a-1)-2}{1-(b-1)-c}U(a-1,b-2,c)}{1+\dfrac{c}{1-(b-1)-c}} \right.
$$

$$
\left. - \frac{\dfrac{b-(a-2)-2}{1-(b-1)-c}}{1+\dfrac{c}{1-(b-1)-c}} \times \frac{(a-2)U(a-1,b-2,c) - \dfrac{(b-2)-(a-2)-2}{1-(b-3)-c}U(a-2,b-4,c)}{1+\dfrac{c}{1-(b-3)-c}} \right\}
$$

$$
= \ 0. \tag{3.61}
$$

Reinstating $a \to a+n$ and $b \to b+2n$ in Eq. (3.61), as was done for the ingoing case, rearranging for $U(a,b,c)$ and simplifying the result gives a recursion relation of the form Eq. (3.53), from which $C(a,b,c)$ and $D(a,b,c)$ can be read off directly

$$
\begin{aligned}
U(n+a, 2n+b, c) = &-\frac{(2+a-b-n)(-2+b+2n)}{(-1+a+n)(-4+b+2n)}U(n+a-2, 2n+b-4, c) \\
&+ \left(\frac{(-3+b+2n)(8+(b+2n)^2 + 2(a+n)c - (b+2n)(6+c))}{(-1+a+n)(-4+b+2n)c} \right) \\
&\times U(n+a-1, 2n+b-2, c).
\end{aligned} \tag{3.62}
$$

The recursion relation Eq. (3.62) is now almost ready to be implemented into the MST package. As for the ingoing case, there are still a few more steps required before the recurrence relation is 'package ready', which will be discussed in Section 3.4.

3.4 Implementing hypergeometric recurrence relations to the MST package

The recurrence relations Eq. (3.50) and Eq. (3.62) were derived in order to calculate the MST series efficiently. There are however a few subtleties that must be taken into account before these recurrence relations can be implemented into the MST package. Recall that the goal of the MST package is to compute solutions to Eqs. (3.20),(3.32), (3.35) and (3.36) via the functions `MSTRadialIn[]` and `MSTRadialUp[]`, for either the Teukolsky or Regge-Wheeler case, depending on the user's choice of

`$MasterFunction`. `MSTRadialIn[]` and `MSTRadialUp[]` will call on $_2F_1$ and U respectively, which will either be calculated by using the recurrence relations derived in Section 3.3.1 and Section 3.3.2 respectively, or by using Mathematica's inbuilt functions when necessary. For the latter case, the functions `H2F1Exact[n, s, `ν`, `τ`, `ϵ`, x]` and `HUExact[n, s, `ν`, `τ`, `ϵ`, zhat]` (where `zhat` represents $\hat{z}$) are defined using the inbuilt Mathematica functions, `Hypergeometric2F1[a,b,c,x]` and `HypergeometricU[a,b,c]` respectively, where a, b and c are replaced by the parameters from either Eq. (3.39), Eq. (3.40) or Eq. (3.54).

In the MST package, while `H2F1Exact[]` is defined exactly by `Hypergeometric2F1[]`, `HUExact[]` is defined by `HypergeometricU[]` with an additional overall factor of $(-2i\hat{z})^n$, or c^n, which serves to improve the convergence of the upgoing MST series and is divided out later on [1]. The recurrence relations for U should also include additional factors such that $U(n+a-1, 2n+b-2, c)$ picks up a factor of $(-2i\hat{z})$, $U(n+a-2, 2n+b-4, c)$ a factor of $(-2i\hat{z})^2$ and so on. These factors are accounted for throughout the code [1]. It is found that by not including this factor in the recurrence relations for U, the final function `MSTRadialUp[]` fails, albeit mysteriously, to converge. These factors should therefore be included in all final expressions involving U, that is they should be inserted into the expressions Eq. (3.62) and Eq. (3.64) etc. before being implemented into the MST package. All final expressions can be found in the BHPToolkit [1].

Recall from Section 3.3 it was mentioned that neither the recurrence relations in Eq. (3.50) or Eq. (3.62) were in the correct form to implement into the MST package. To implement the recurrence relations into the package, the following fact should be taken into account. As described in Section 3.1, the MST coefficient for $n = 0$, f_0, is set to 1. With this choice, the recurrence relations given by Eq. (3.50) and Eq. (3.62) suffice only for the terms in the series where $n > 0$, as they are written in such a way that any given term depends on the previous two terms. In other words, the MST terms are summed 'upwards'. By choosing to initialise the series at $n = 0$, if Eq. (3.50) and Eq. (3.62) were used in their current form, the $n < 0$ terms would depend on their previous two contiguous functions, which have not yet been calculated! To rectify this, another recurrence relation must be derived for the ingoing and upgoing case such that the terms in the MST series are summed 'downward'. The downward version of the recurrence relations can be readily obtained from their upward counterparts by rearranging Eq. (3.50) and Eq. (3.62) for $_2F_1(a+n-2, b-n+2, c, x)$ and $U(n+a-2, 2n+b-4, c)$ respectively, and setting $n \to n+2$, giving

$$
\begin{aligned}
_2F_1(a+n, b-n, c, x) = &\left(\frac{(2+a-b+2n)(-2-2a+2b+2ab+c-ac-bc-4n-2an+2bn-2n^2)}{(-1+b-n)(1+a-c+n)(3+a-b+2n)} \right. \\
&\left. + \frac{(2+a-b+2n)(1+a-b+2n)(3+a-b+2n)x}{(-1+b-n)(1+a-c+n)(3+a-b+2n)} \right) \\
&\times {}_2F_1(a+n+1, b-n-1, c, x) \\
&+ \frac{(1+a+n)(1-b+c+n)(1+a-b+2n)}{(-1+b-n)(1+a-c+n)(3+a-b+2n)} \\
&\times {}_2F_1(a+n+2, b-n-2, c, x),
\end{aligned}
\tag{3.63}
$$

49

and

$$U(n + a, 2n + b, c) = -\frac{(1 + b + 2n)(b^2 + 4n(1 + n) + b(2 + 4n - c) + 2ac)}{c(-a + b + n)(2 + b + 2n)}$$
$$\times U(n + a + 1, 2n + b + 2, c)$$
$$+ \frac{(1 + a + n)(b + 2n)}{(-a + b + n)(2 + b + 2n)} U(n + a + 2, 2n + b + 4, c). \qquad (3.64)$$

The recurrence relations Eq. (3.63) and Eq. (3.64) will be used to calculate terms in the MST series for which $n < 0$. So far, only the form of `H2F1Exact[]` and `HUExact[]` have been discussed. How the recurrence relations are implemented and used in the MST package will be detailed here. Four more functions will be defined in the package: `H2F1Up[]` `H2F1Down[]`, `HUUp[]` and `HUDown[]` [1], corresponding to the upwards and downwards sum for each of the hypergeometric and confluent hypergeometric functions, which will be used when it is more efficient to compute the (confluent) hypergeometric functions using a recurrence relation than by using inbuilt functions. A note of caution, the upwards sum should not be confused with the upgoing solutions from Section 3.1 . The functions `H2F1Up[]`, `H2F1Down[]`, `HUUp[]` and `HUDown[]` are then defined using Eq. (3.50) Eq. (3.63), Eq. (3.62) and Eq. (3.64), with the following replacements respectively

$$_2F_1(a + n, b - n, c, x) \to \texttt{H2F1Up[n,s,}\nu\texttt{,}\tau\texttt{,}\epsilon\texttt{,x]}, \qquad (3.65)$$
$$_2F_1(a + n - 1, b - (n-1), c, x) \to \texttt{H2F1[n-1]},$$
$$_2F_1(a + n - 2, b - (n-2), c, x) \to \texttt{H2F1[n-2]},$$

$$_2F_1(a + n, b - n, c, x) \to \texttt{H2F1Down[n,s,}\nu\texttt{,}\tau\texttt{,}\epsilon\texttt{,x]}, \qquad (3.66)$$
$$_2F_1(a + n + 1, b - (n+1), c, x) \to \texttt{H2F1[n+1]},$$
$$_2F_1(a + n + 2, b - (n+2), c, x) \to \texttt{H2F1[n+2]},$$

$$U(a + n, b + 2n, c) \to \texttt{HUUp[n,s,}\nu\texttt{,}\tau\texttt{,}\epsilon\texttt{,zhat]}, \qquad (3.67)$$
$$U(a + n - 1, b + 2(n-1), c) \to \texttt{HU[n-1]},$$
$$U(a + n - 2, b + 2(n-2), c) \to \texttt{HU[n-2]},$$

$$U(a + n, b + 2n, c) \to \texttt{HUDown[n,s,}\nu\texttt{,}\tau\texttt{,}\epsilon\texttt{,zhat]}, \qquad (3.68)$$
$$U(a + n - 1, b + 2(n+1), c) \to \texttt{HU[n+1]},$$
$$U(a + n - 2, b + 2(n+2), c) \to \texttt{HU[n+2]},$$

where it is understood that a, b and c for the hypergeometric functions are different to those for the confluent hypergeometric functions, as detailed in Section 3.3. The placeholders `H2F1[]` and `HU[]` are not explicitly defined functions, but are used to store values of the contiguous hypergeomet-

ric and confluent hypergeometric functions respectively. When the functions `MSTRadialIn[]` and `MSTRadialUp[]` are called, a check is performed for each term in the MST series as to whether it is more efficient to use Mathematica's inbuilt functions or the recurrence relations to calculate that term. In order to perform this check, the recurrence relations `H2F1Up[]`, `H2F1Down[]`, `HUUp[]` and `HUDown[]` should be written into a list format. Once written in this form, the recurrence relations are ready to be implemented into the package For the final definitions of `H2F1Up[]`, `H2F1Down[]`, `HUUp[]` and `HUDown[]` in their listed format, the reader should refer to the MST package in the BHPToolkit [1].

The MST series for a given set of parameters is then calculated as follows. Take the ingoing case for example. For the $n = 0$ and $n = 1$ terms, Mathematica's inbuilt function is used via `H2F1Exact[]` to initialise the series. The efficiency check is then performed for all other terms in the series. If the efficiency check for the nth term determines that it is preferable to use Mathematica's inbuilt function, `H2F1[n]` is calculated using the function `H2F1Exact[]`, and its value is stored. However, if the check determines that it is preferable to use the recurrence relations, the function `H2F1Up[]` is called when $n > 0$, and `H2F1Down[]` when $n < 0$. These functions in turn call on the previously stored values of their contiguous terms that have been calculated either by using Mathematica's inbuilt functions, or by the recurrence relations. An identical procedure is followed for the upgoing case. Once the MST series has been calculated, the stored values of `H2F1[n]` and `HU[n]` are cleared to free up memory.

All terms and factors within `MSTRadialIn[]` and `MSTRadialUp[]` that depend on n are summed over using a while loop, which is terminated when the result of the summation differs by machine precision, or by some user specified precision. The asymptotic amplitudes of the MST series are also defined, the expressions for which can be found in the MST package [1], and can be used to renormalise the result as the user requires.

3.5   Derivatives of recurrence relations and MST radial functions

The derivatives of the MST series for the radial Teukolsky and Regge-Wheeler master functions may also need to be calculated, particularly to check that the solution satisfies either the Teukolsky or Regge-Wheeler equation to sufficient accuracy. In order to calculate the derivatives of the MST radial functions, `MSTRadialIn[]` and `MSTRadialUp[]`, the first derivatives of $_2F_1$, U and the derivatives of their recurrence relations need to be determined. The derivatives of `H2F1Exact[]` and `HUExact[]`, defined in the MST package as `dH2F1Exact[]` and `dHUExact[]`, employ the identities given by DLMF(15.5.1) and DLMF(13.3.22) respectively. Care should be taken when deriving the derivatives of the recurrence relations however. For the upgoing case, recall that $c = -2i\hat{z}$, and the chain rule should be applied appropriately. By applying the appropriate Leibniz rules, the derivatives of `H2F1Up[]`, `H2F1Down[]`, `HUUp[]` and `HUDown[]` are defined in the package as `dH2F1Up[]`, `dH2F1Down[]` and `dHUUp[]` and `dHUDown[]` respectively in terms of `dH2F1[]` and `dHU[]`, again in a listed format. The reader is referred to the MST package for the final form of these expressions [1].

Second (and higher) derivatives of the radial Teukolsky and Regge-Wheeler master functions may also need to be calculated, again to check that they are solutions to their respective equations. Rather than defining a new recurrence relation for each higher derivative of $_2F_1$ and U, the higher derivatives of `MSTRadialIn[]` and `MSTRadialUp[]` can be calculated by using the Teukolsky and Regge-Wheeler equations recursively. It is much quicker to calculate the first derivative of the MST series once, as described in Section 3.5, and then to calculate its second derivative in terms of the original function and its first derivative by rearranging either Eq. (2.133) or Eq. (2.49) than it is to calculate all of the MST coefficients and derivatives of (confluent) hypergeometric functions each time the user needs a higher derivative of the MST radial functions. This recursive procedure works for all higher derivatives of the radial Teukolsky and Regge-Wheeler master functions. Further details on how the second and higher derivatives of the radial Teukolsky and Regge-Wheeler master functions are calculated can be found in the MST package [1]. One can then show using the MST package that the RW and Teukolsky equations are satisfied by the MST solutions.

Chapter 4

Gravitational Self-Force Theory

To meet the accuracy requirements for performing precision tests of GR by matching theoretical templates to experimental signals, the GSF approach appears to be the most viable method for modelling EMRIs [16, 17, 43]. This chapter shall serve as a review of GSF theory. As discussed in the introduction, the self-interaction between the secondary and the spacetime it perturbs gives rise to the GSF. Energy conservation demands the binary orbit shrinks due to the radiation-reaction by emission of GWs and it is the SF that drives the binary to inspiral beyond geodesic motion. To generate EMRI waveforms we need two things: the phase and the amplitude. Within GSF theory, we shall approach modelling EMRIs using the two-timescale approximation in conjunction with the self-consistent framework of BHPT from Chapter 2. The two-timescale approximation will be used for the purposes of this chapter, in addition to Chapters 5 - 8. For a review of various other methods for modelling EMRIs the reader is directed to Ref. [14] and the references therein. Using the two-timescale approach, a simple scaling argument, which is detailed below [13], shows us that we must calculate the phase to first post-adiabatic (1PA) order, which in turn requires the determination of the metric perturbation through second-order in the small mass ratio [14]. While this level of accuracy may not be required for the detection of EMRIs by space-bourne detectors, it is certainly required if we wish to extract the parameters such as the mass and spin of the compact bodies, or perform precision tests of GR using EMRI signals. In this chapter we will summarise the procedure for calculating the GW phase using three different approaches, introducing any necessary quantities such as the GSF, GW energy fluxes and the binding energy. We shall also introduce the field equations for the second-order metric perturbation, which we must solve to obtain the full 1PA phase correction. The second-order field equations also provide the motivation for one of the main calculations in this work, given in Chapter 6, on the slow evolution of the first-order metric perturbation. For the purposes of this work, all calculations will be done on constant t-slicing. Results for hyperboloidal slicing can be found in Ref. [14].

4.1 The two-timescale approximation

When modelling EMRIs we can consider two different timescales. During the inspiral, these two timescales are the orbital timescale, t_{orb}, and the radiation-reaction timescale, t_{rr}. The orbital timescale is the time taken to complete an orbit, which in the weak field is $t_{\text{orb}} \sim M$ [13, 14]. The radiation-reaction timescale is then the time over which the radius of the orbit shrinks in size due to the radiation reaction from the emission of GWs, and is given by: $t_{\text{rr}} \sim M/\varepsilon$ [13, 14]. These timescales change as the EMRI begins its plunge into merger. We will leave the discussion of the transition to plunge to Chapter 7, and consider only the inspiral and hence inspiral timescales during this chapter. By the scaling arguments above, we find that the number of orbits we can expect to see during an EMRIs lifetime is given by the ratio of the two timescales: $t_{\text{rr}}/t_{\text{orb}} \sim 1/\varepsilon \geq 10^4$ [13, 14]. Due to the large number of orbits and long radiation-reaction timescale, EMRI signals could last many years [10]. Therefore, we must compute the phase and amplitude of EMRI produced GWs accurately enough so that the error accumulated over the thousands of orbits during the EMRIs lifetime remains small.

Due to the disparate timescales, the radius of the orbit, r_{p} evolves much more slowly than the orbital phase. Any other physical orbital parameters that depend on the orbital radius, such as the frequency and amplitude of the GWs, in addition to the orbital energy and angular momentum, will also be slowly evolving. Therefore, GWs produced by EMRIs will be comprised of a slowly evolving amplitude and a quickly evolving phase. We shall introduce the quantity slow-time, defined on constant t-slicing by

$$\tilde{t} = \varepsilon t \tag{4.1}$$

, over which the above listed 'slow' parameters evolve. In the two-timescale approximation we can then expand the orbital frequency Ω and radius r_{p} in powers of ε such that [14]

$$\Omega\left(\tilde{t}\right) = \sum_{n=0}^{\infty} \varepsilon^n \Omega_n\left(\tilde{t}\right), \tag{4.2}$$

$$r_{\text{p}}\left(\tilde{t}\right) = \sum_{n=0}^{\infty} \varepsilon^n r_n\left(\tilde{t}\right). \tag{4.3}$$

Specialising to quasicircular, equatorial orbits, the quickly evolving GW phase, Φ is defined as the time integral over the orbital frequency

$$\Phi = \int^t m\Omega\left(t'\right) dt'. \tag{4.4}$$

Using Eq. (4.2), the orbital phase ϕ_{p} then becomes [1] [14]

$$\phi_{\mathrm{p}}(t) = \frac{1}{\varepsilon} \int^t \left(\Omega_0 \left(\tilde{t} \right) + \varepsilon \Omega_1 \left(\tilde{t} \right) + \mathcal{O} \left(\varepsilon^2 \right) \right) d\tilde{t} \tag{4.5}$$

$$= \frac{1}{\varepsilon} \left(\phi_0(t) + \varepsilon \phi_1(t) + \mathcal{O} \left(\varepsilon^2 \right) \right). \tag{4.6}$$

Here we see that we must calculate both ϕ_0, referred to as the adiabatic or 0PA correction to the phase, and ϕ_1, referred to as the first post-adiabatic or 1PA correction, to ensure that the accumulated error in the phase remains small, or $\mathcal{O}(\varepsilon)$, over the EMRIs lifetime. Fields such as the metric perturbation must be treated with more attention in the two-timescale approximation than the orbital parameters. In the self-consistent approximation the metric perturbation is written in the following way [14]

$$h_{\alpha\beta}(x^\mu; z^\nu) \rightarrow h_{\alpha\beta}(t, x^a, \varepsilon) = \sum_{n=1}^\infty \varepsilon^n h_{\alpha\beta}^n(t, x^a), \tag{4.7}$$

where $x^a = \{r, \theta, \phi\}$. We can write Eq. (4.7) this way because any dependence on z^α or functions of z^α depend on t. Now we must also consider the dependence on $\tilde{t}$. In the two-timescale approximation, we assume that the self-consistent fields can be written as [14]

$$h_{\alpha\beta}(t, x^a, \varepsilon) \rightarrow h_{\alpha\beta}(\tilde{t}, \phi_{\mathrm{p}}(t, \varepsilon), x^a, \varepsilon), \tag{4.8}$$

where we are splitting up the dependence on fast and slow time, and $\phi_{\mathrm{p}}(t, \varepsilon)$ is given by Eq. (4.6). We can do this because the only quantity that evolves on the fast timescale t is ϕ_{p}, with all other quantities evolving slowly with respect to $\tilde{t}$. The explicit dependence on ε is also more complicated now in the two-timescale approximation, as the metric perturbation's dependence on functions of z^α, such as r_{p}, are also now written as expansions in ε, as in Eq. (4.3). The metric perturbation can then be written as a regular asymptotic expansion with fixed $\tilde{t}$, x^a and ϕ_{p} in the following way

$$h_{\alpha\beta}(\tilde{t}, \phi_{\mathrm{p}}(t, \varepsilon), x^a, \varepsilon) = \sum_{n=1}^\infty \varepsilon^n h_{\alpha\beta}^n(\tilde{t}, \phi_{\mathrm{p}}, x^a, \varepsilon), \tag{4.9}$$

$$= \sum_{n=1}^\infty \varepsilon^n \left[h_{\alpha\beta}^n(\tilde{t}, \phi_{\mathrm{p}}, x^a, 0) + \varepsilon \partial_\varepsilon h_{\alpha\beta}^n(\tilde{t}, \phi_{\mathrm{p}}, x^a, 0) + \mathcal{O}(\varepsilon^2) \right].$$

We then choose

$$\tilde{h}_{\alpha\beta}(\tilde{t}, \phi_{\mathrm{p}}(t, \varepsilon), x^a, \varepsilon) = \sum_{n=1}^\infty \varepsilon^n \tilde{h}_{\alpha\beta}^n(\tilde{t}, \phi_{\mathrm{p}}, x^a), \tag{4.10}$$

with

$$\tilde{h}_{\alpha\beta}^1 = h_{\alpha\beta}^1(\tilde{t}, \phi_{\mathrm{p}}, x^a, 0), \tag{4.11}$$

---

[1] Terms involving $\varepsilon^{1/2}$ may appear if resonances are included. However, these only appear when the primary is a Kerr black hole and the secondary follows some generic orbit, but not for quasicircular orbits [113].

and

$$\tilde{h}^n_{\alpha\beta} = h^n_{\alpha\beta}(\tilde{t}, \phi_\mathrm{p}, x^a, 0) + \partial_\varepsilon h^{n-1}_{\alpha\beta}(\tilde{t}, \phi_\mathrm{p}, x^a, 0), \quad \text{for} \quad n > 1. \tag{4.12}$$

Similarly to $\bar{h}_{\alpha\beta}$ in Eq. (2.68), the trace reversal of $\tilde{h}_{\alpha\beta}$ can be written in terms of a mode-sum decomposition with the separable form

$$\tilde{\bar{h}}_{\mu\nu}(x^\alpha; z^\alpha) = \sum_{l=0}^{\infty} \sum_{m=-l}^{l} \tilde{\bar{h}}_{\mu\nu}^{lm}(x^\alpha; \alpha) = \sum_{l=0}^{\infty} \sum_{m=-l}^{l} \sum_{i=1}^{10} \frac{a_l^{(i)}}{r} \tilde{\bar{h}}_{lm}^{(i)}(\tilde{t}, \phi_\mathrm{p}, r) Y_{\mu\nu}^{(i),lm}(x^a), \tag{4.13}$$

and $\tilde{\bar{h}}_{lm}^{(i)}$ takes the expansion

$$\tilde{\bar{h}}_{lm}^{(i)} = \sum_{n=1}^{\infty} \varepsilon^n \tilde{\bar{h}}_{lm}^{n,(i)}. \tag{4.14}$$

We will use tildes to denote fields such as the metric perturbation and the SF in the two-timescale approximation in this chapter. However, in later chapters the tilde notation will be dropped.

4.2   Modelling waveforms

In practice, GWs are observed at null asymptotic infinity with respect to the primary black hole, with cross-plus plane polarization. The amplitude of GWs need only be calculated to first-order in the small mass ratio, as will be shown in Section 4.4, though the phase must be calculated through 1PA order, as shown by Eq. (4.6), which in turn requires knowledge of the metric perturbation through second-order. Therefore, we will use the following expression to extract the GW amplitude and phase that we will actually measure, to the level of accuracy required

$$h^\infty(x^\alpha; z^\alpha) = h_+(x^\alpha; z^\alpha) - i h_\times(x^\alpha; z^\alpha) \tag{4.15}$$

$$= \lim_{r \to \infty} \frac{r}{M + \mu} h^1_{\bar{m}\bar{m}} + \mathcal{O}(\varepsilon), \tag{4.16}$$

where $h^1_{\bar{m}\bar{m}} = \bar{h}^1_{\alpha\beta} \bar{m}^\alpha \bar{m}^\beta$, and $\bar{m}$ is given in Eq. (2.114d) for a Schwarzschild background, and the tetrad decomposition is discussed earlier in Section 2.7.1. Choosing an l, m mode decomposition, the part of the metric perturbation from which GWs can be observed in the two-timescale approximation becomes

$$h^\infty(x^\alpha; z^\alpha) = \frac{1}{r} \sum_{lm} h_{lm}^\infty(\tilde{t}, \phi_\mathrm{p}(t, \varepsilon), r, \varepsilon)_{-2}Y_{lm}(\theta, \phi). \tag{4.17}$$

Converting from the tetrad basis to the BSL basis, we obtain

$$h^1_{\bar{m}\bar{m}} = \frac{a_l}{r} \left(\tilde{\bar{h}}_{lm}^{1,(7)}(\tilde{t}, \phi_\mathrm{p}(t, \varepsilon), r, \varepsilon) + i \tilde{\bar{h}}_{lm}^{1,(10)}(\tilde{t}, \phi_\mathrm{p}(t, \varepsilon), r, \varepsilon) \right)_{-2}Y_{lm}(\theta, \phi) \Big|_{\varepsilon=0}, \tag{4.18}$$

where $a_l = a_l^{(7)} = a_l^{(10)}$, defined in Eq. (2.69).

The observable GW for a given l and m mode can therefore be written in the BSL basis that will be used throughout this thesis in the following way

$$\tilde{h}_{lm}^{\infty}(\tilde{t}, \phi_{\mathrm{p}}(t,\varepsilon), r, \varepsilon) = \lim_{r \to \infty} a_l \left(\tilde{\tilde{h}}_{lm}^{(7)} + i\tilde{\tilde{h}}_{lm}^{(10)} \right) e^{-im\phi_{\mathrm{p}}(t,\varepsilon)} \tag{4.19}$$

$$= \tilde{A}_{lm}^{\infty}(\tilde{t}, r, \varepsilon) e^{i\Phi_{lm}(t,\varepsilon)}, \tag{4.20}$$

where

$$\tilde{A}_{lm}^{\infty} = \sum_{n=1}^{\infty} \varepsilon^n \tilde{A}_{lm}^{n,\infty}. \tag{4.21}$$

In the following sections we will introduce the necessary ingredients to calculate the phase to 1PA order in three different ways; one which makes use of the equations of motion in the two-timescale approximation while holding $\tilde{t}$ fixed for the purposes of differentiation, the second similar to the first except with fixed Ω instead of $\tilde{t}$, and a third which makes use of the GW energy fluxes and binding energy.

4.3 Equations of motion

The equation of motion describing the trajectory of the secondary is given by [14]

$$\frac{D^2 z^\mu}{d\tau^2} = f^\mu, \tag{4.22}$$

where

$$\frac{D}{d\tau} \equiv \frac{dz^\alpha}{d\tau} \nabla_\alpha \tag{4.23}$$

is a differential operator with respect to the background metric $g_{\alpha\beta}$ and f^μ is the GSF due to radiation-reaction. Writing out the differential operator explicitly, Eq. (4.22) becomes [14]

$$\frac{d^2 z^\mu}{dt^2} + \frac{1}{u^t} \frac{du^t}{dt} \frac{dz^\mu}{dt} + \Gamma_{\beta\gamma}^\mu \frac{dz^\beta}{dt} \frac{dz^\gamma}{dt} = \frac{1}{(u^t)^2} f^\mu, \tag{4.24}$$

where

$$u^\alpha = \frac{dz^\alpha}{d\tau}. \tag{4.25}$$

In the two-timescale approximation, we write the GSF as

$$f^\mu(t,\varepsilon) = \varepsilon \tilde{f}_1^\mu(\varepsilon t) + \varepsilon^2 \tilde{f}_2^\mu(\varepsilon t) + \mathcal{O}\left(\varepsilon^3\right), \tag{4.26}$$

and derivatives with respect to time at fixed r become [14]

$$
\begin{aligned}
\left(\frac{\partial}{\partial t}\right)_r &= \frac{\partial \phi_{\mathrm{p}}}{\partial t}\frac{\partial}{\partial \phi_{\mathrm{p}}} + \frac{\partial \tilde{t}}{\partial t}\frac{\partial}{\partial \tilde{t}} \\
&= \Omega\frac{\partial}{\partial \phi_{\mathrm{p}}} + \varepsilon\frac{\partial}{\partial \tilde{t}} \\
&= \Omega_0\partial_{\phi_{\mathrm{p}}} + \varepsilon\left(\partial_{\tilde{t}} + \Omega_1\partial_{\phi_{\mathrm{p}}}\right) + \mathcal{O}\left(\varepsilon^2\right).
\end{aligned}
\tag{4.27}
$$

For quasicircular equatorial orbits, the normalization condition $g_{\alpha\beta}u^\alpha u^\beta = -1$ determines the Detweiler redshift to be

$$
u^t\left(\tilde{t}\right) = \frac{1}{\sqrt{1 - \frac{3M}{r_{\mathrm{p}}(\tilde{t})}}}.
\tag{4.28}
$$

Defining the two-timescale expansion of u^t and u^r as

$$
u^t = \sum_{n=0}^{\infty}\varepsilon^n U_n,
\tag{4.29}
$$

$$
u^r = \sum_{n=0}^{\infty}\varepsilon^n u_n^r,
\tag{4.30}
$$

then at leading order we have

$$
U_0\left(\tilde{t}\right) = \frac{1}{\sqrt{1 - \frac{3M}{r_0(\tilde{t})}}},
\tag{4.31}
$$

and

$$
u_0^r\left(\tilde{t}\right) = \frac{dr_0}{dt} = \frac{d\tilde{t}}{dt}\frac{dr_0}{d\tilde{t}} = \varepsilon\frac{dr_0}{d\tilde{t}}.
\tag{4.32}
$$

Replacing u^t, u^r, r_{p}, Ω and f^μ with their corresponding two-timescale expansions, the leading and next to leading order of the r component of the equations of motion Eq. (4.24) yield [14]

$$
\Omega_0(\tilde{t}) = \sqrt{\frac{M}{r_0^3}},
\tag{4.33}
$$

$$
\Omega_1(\tilde{t}) = -\frac{1}{2f_0 r_0\Omega_0}\left(U_0^{-2}\tilde{f}_1^r + \frac{3Mr_1 f_0}{r_0^3}\right),
\tag{4.34}
$$

where

$$
f_0 = f(r_0) = 1 - \frac{2M}{r_0}.
\tag{4.35}
$$

Similarly, the leading and next to leading order of the t component of Eq. (4.24) give [14]

$$\frac{dr_0}{d\tilde{t}} = \frac{2\left(r_0 - 3M\right)^2 \left(r_0 - 2M\right)}{M\left(r_0 - 6M\right)} \tilde{f}_1^t, \tag{4.36}$$

$$\frac{dr_1}{d\tilde{t}} = \frac{2r_0 f_0 \left(r_0 - 3M\right)^2}{M\left(r_0 - 6M\right)} \tilde{f}_2^t + \frac{r_0^3 \left(r_0 - 3M\right)}{M\left(r_0 - 6M\right)} \frac{d\tilde{f}_1^r}{d\tilde{t}} + \frac{2r_0^2 \left(r_0 - 3M\right)^2 \left(r_0^2 - 6Mr_0 + 6M^2\right)}{M^2 \left(r_0 - 6M\right)^2} \tilde{f}_1^r \tilde{f}_1^t \tag{4.37}$$
$$+ \frac{4\left(r_0 - 3M\right)\left(r_0^2 - 10Mr_0 + 18M^2\right)}{M\left(r_0 - 6M\right)^2} r_1 \tilde{f}_1^t.$$

Notice how both Eq. (4.36) and Eq. (4.37) blow up at the inner-most stable circular orbit (ISCO), which occurs at $r = 6M$ in Schwarzschild spacetime. We will shortly describe in Section 4.8 how to use the quantities derived in this section to calculate the phase to 1PA order. Namely we solve for r_0 and r_1 as input to Ω_0 and Ω_1. Firstly however, we must calculate the first and 2GSF in the two-timescale approximation.

4.4 Calculating the Gravitational self-force

From Eq. (4.36) we see that calculating the phase to 0PA order requires knowledge of the t component of the first-order SF. Equation (4.37) then shows that the 1PA correction to the phase also requires the calculation of $\tilde{f}_1^t$, in addition to $\tilde{f}_1^r$ (and its slow-time derivative, by Eq. (4.37)) and $\tilde{f}_2^t$. Using a slightly different form of the equations of motion we have [14, 17, 98]

$$\frac{D^2 z^\mu}{d\tau^2} = -\frac{1}{2} P^{\mu\nu} \left(\delta_\nu^\rho - h_\nu^{\mathcal{R}\rho}\right) \left(2h_{\beta\rho;\alpha}^{\mathcal{R}} - h_{\alpha\beta;\rho}^{\mathcal{R}}\right) u^\alpha u^\beta + \mathcal{O}\left(\varepsilon^3\right), \tag{4.38}$$

where

$$P^{\mu\nu} = g^{\mu\nu} + u^\mu u^\nu, \tag{4.39}$$

and $h_{\alpha\beta}^{\mathcal{R}}$ is the residual piece of the metric perturbation, which in the self-consistent approximation has the expansion [14]

$$h_{\alpha\beta}^{\mathcal{R}} = \varepsilon h_{\alpha\beta}^{1\mathcal{R}} + \varepsilon^2 h_{\alpha\beta}^{2\mathcal{R}}. \tag{4.40}$$

Rather than solving for the retarded field $h_{\alpha\beta}$, we solve for the residual field $h_{\alpha\beta}^{\mathcal{R}}$, defined by [14]

$$h_{\alpha\beta}^{\mathcal{R}} = h_{\alpha\beta} - h_{\alpha\beta}^{\mathcal{P}}, \tag{4.41}$$

where $h_{\alpha\beta}^{\mathcal{P}}$ is the puncture field. The puncture contains all of the singular behaviour of $h_{\alpha\beta}$, which can be subtracted mode-by-mode from the physical field using the decomposition in Eq. (2.68). For a Schwarzschild background, this regularisation process is best understood in the Lorenz gauge [17, 40, 16, 37], as discussed in the introduction. It is not possible to perform the subtraction in Eq. (4.41) in a mode-sum decomposition when not in the Lorenz gauge. Therefore, the Lorenz gauge shall be used throughout this thesis. We did not make the distinction between the retarded and residual field in Section 2.5 when discussing the first-order metric perturbation, as we can solve

Eq. (2.20) in the Lorenz gauge directly for the retarded field. It was shown by Warburton and Wardell in 2013 how to puncture the first-order order scalar field [114], who later went on to show how to puncture the first-order metric perturbation [115]. However, it is not necessary to subtract the regularisation parameters mode-by-mode in the frequency domain for first-order calculations, though in the time domain the m modes become divergent and a puncture scheme is required. A puncture scheme is also necessary for solving the second-order metric perturbation in the Lorenz gauge [14] [2].

Applying the two-timescale approximation to the right-hand side of Eq. (4.38) evaluating at the particle, and matching order-by-order to the right-hand side of Eq. (4.26) gives a direct relation between the SF and the metric perturbation components [14]

$$\tilde{f}_1^\alpha\left(\tilde{t}\right) = \frac{1}{2}g^{\alpha\beta}\tilde{h}_{u_0u_0,\beta}^{1\mathcal{R}}, \tag{4.42}$$

$$\tilde{f}_2^\alpha\left(\tilde{t}\right) = \frac{1}{2}g^{\alpha\beta}\tilde{h}_{u_0u_0,\beta}^{2\mathcal{R}} + \frac{1}{2}\left[r_1\left(\partial_r g^{\alpha\beta}\tilde{h}_{u_0u_0,\beta}^{1\mathcal{R}} + g^{\alpha\beta}\tilde{h}_{u_0u_0,r\beta}^{1\mathcal{R}}\right)\right. \tag{4.43}$$

$$\left. + 2g^{\alpha\beta}\tilde{h}_{u_0u_1,\beta}^{1\mathcal{R}} + P_0^{\alpha\beta}\left(2\Gamma^\gamma\tilde{h}_{\beta\gamma}^{1\mathcal{R}} - 2U_0u_0^\gamma\partial_t\tilde{h}_{\beta\gamma}^{1\mathcal{R}} - \tilde{h}_\beta^{1\mathcal{R}\gamma}\tilde{h}_{u_0u_0,\gamma}^{1\mathcal{R}}\right)\right],$$

where the quantities $\tilde{h}_{u_0u_0,\beta}^{n\mathcal{R}}$ are all evaluated on the world-line at leading order and are defined as [14]

$$\tilde{h}_{u_0u_0,\beta}^{n\mathcal{R}} = \tilde{h}_{\mu\nu,\beta}^{n\mathcal{R}}\Big|_{z_0^\alpha}u_0^\mu u_0^\nu, \tag{4.44}$$

where a comma denotes differentiation with respect to fixed slow time. The quantity P_0 in Eq. (4.43) is given by [14]

$$P_0^{\alpha\beta} = g^{\alpha\beta} + u_0^\alpha u_0^\beta, \tag{4.45}$$

and

$$\Gamma^\alpha = U_0^2\left(2\Gamma_{\dot{z}_0\dot{z}_1}^\alpha - 3\Omega_0^2 f_0 r_1\delta_r^\alpha\right), \tag{4.46}$$

is the leading order term of $\Gamma_{\beta\gamma}^\alpha(z^\mu)u^\beta u^\gamma$ in the two-timescale approximation, where $\Gamma_{\dot{z}_0\dot{z}_1}^\alpha$ is given by

$$\Gamma_{\dot{z}_0\dot{z}_1}^\alpha = \Gamma_{\beta\gamma}^\alpha(z^\mu)\dot{z}_0^\beta\dot{z}_1^\gamma. \tag{4.47}$$

Finally, we also use the following definitions in the equations above

$$z_0^\alpha = (t, r_0, \pi/2, \phi_p), \tag{4.48}$$

$$z_1^\alpha = (0, r_1, 0, 0), \tag{4.49}$$

$$\dot{z}_0^\alpha = (1, 0, 0, \Omega_0), \tag{4.50}$$

$$\dot{z}_1^\alpha = \left(0, dr_0/d\tilde{t}, 0, \Omega_1\right), \tag{4.51}$$

$$u_0^\alpha = U_0 \dot{z}_0^\alpha, \tag{4.52}$$

$$u_1^\alpha = U_1 \dot{z}_0^\alpha + U_0 \dot{z}_1^\alpha. \tag{4.53}$$

The t component of the first-order SF in the two-timescale expansion is then given by [14]

$$\tilde{f}_1^t = -\frac{1}{2}\frac{\Omega_0}{f_0}\tilde{h}_{u_0 u_0, \phi_p}^{1\mathcal{R}} \tag{4.54}$$

$$= \frac{1}{2r_0 f_0}\sum_{ilm} a_l^{(i)} i\omega(\tilde{t})\tilde{h}_{lm}^{1\mathcal{R},(i)}\left(\tilde{t}, r_0\right) Y_{\alpha\beta}^{(i),lm}\left(r_0, \pi/2, 0\right) u_0^\alpha u_0^\beta, \tag{4.55}$$

where $\tilde{h}_{lm}^{1\mathcal{R},(i)}$ is the residual piece of the trace reversed version of $\tilde{\bar{h}}_{lm}^{1,(i)}$ from Eq. (4.14). The r component of $\tilde{f}_1^\mu$ is then given by [14]

$$\tilde{f}_1^r = \frac{1}{2}f_0\tilde{h}_{u_0 u_0, r}^{1\mathcal{R}} \tag{4.56}$$

$$= \frac{1}{2}f_0 \sum_{i\ell m} a_l^{(i)}\partial_{r_0}\left[\tilde{h}_{lm}^{1\mathcal{R},(i)}\left(\tilde{t}, r_0\right) Y_{\alpha\beta}^{(i),lm}\left(r_0, \pi/2, 0\right)\right] u_0^\alpha u_0^\beta. \tag{4.57}$$

The t component of the second-order SF can then be evaluated similarly, and is given by[14]

$$\tilde{f}_2^t(\tilde{t}) = -\frac{1}{2}f_0^{-1}\Omega_0\tilde{h}_{u_0 u_0, \phi_p}^{2\mathcal{R}} - f_0^{-1}\Omega_0\tilde{h}_{u_0 u_1, \phi_p}^{1\mathcal{R}} + \frac{1}{2}f_0^{-2}\Omega_0 r_1\left(f_0'\tilde{h}_{u_0 u_0, \phi_p}^{1\mathcal{R}} - f_0\tilde{h}_{u_0 u_0, r\phi_p}^{1\mathcal{R}}\right) \tag{4.58}$$

$$+ \frac{1}{2}\left(-f_0^{-1}\delta_t^\beta + U_0 u_0^\beta\right)\left(2\Gamma^\gamma\tilde{h}_{\beta\gamma}^{1\mathcal{R}} - 2U_0 u_0^\gamma\partial_{\tilde{t}}\tilde{h}_{\beta\gamma}^{1\mathcal{R}} + f_0^{-1}\Omega_0\tilde{h}_{\beta t}^{1\mathcal{R}}\tilde{h}_{u_0 u_0, \phi_p}^{1\mathcal{R}} - f_0\tilde{h}_{\beta r}^{1\mathcal{R}}\tilde{h}_{u_0 u_0, r}^{1\mathcal{R}}\right.$$

$$\left. + r_0^{-2}\tilde{h}_{\beta\phi}^{1\mathcal{R}}\tilde{h}_{u_0 u_0, \phi_p}^{1\mathcal{R}}\right),$$

where a prime on f denotes a derivative with respect to r. Note the appearance of the quantity $\partial_{\tilde{t}}\tilde{h}_{\mu\nu}^{1\mathcal{R}}$. To calculate the second-order SF we must calculate the slow-time derivative of the first-order metric perturbation. This will be done in Chapter 6. It is also worth noting the distinction between the dissipative and conservative contributions to the GSF, which are given simply in the quasicircular case by [14]

$$\tilde{f}_{n,\text{diss}}^\mu = \left(\tilde{f}_n^t, 0, 0, \tilde{f}_n^\phi\right), \tag{4.59}$$

$$\tilde{f}_{n,\text{cons}}^\mu = \left(0, \tilde{f}_n^r, 0, 0\right), \tag{4.60}$$

where the former is antisymmetric under the time reversal operation $(t, \phi) \rightarrow (-t, -\phi)$, and the latter is symmetric.

4.5 The second-order metric perturbation

We have applied the two-timescale approximation to the equations of motion. We must now apply the two-timescale approximation to the linearised Einstein field equations as well, so that we can solve for the metric perturbation in the two-timescale approach. We have already seen the self-consistent equations for the first-order metric perturbation earlier in Eq. (2.20) from Chapter 2. We will discuss how to solve the first-order field equations, at leading order in the two-timescale approximation for quasicircular orbits in the Lorenz gauge, later in Chapter 5. This is equivalent to solving for $\tilde{h}^1_{\alpha\beta}(\tilde{t}, \phi_\mathrm{p}, x^a, 0)$ from Eq. (4.11), where the metric perturbation has been evaluated at the leading order contribution to the slowly evolving parameters it depends on, for example $r_\mathrm{p} \to r_0$. We know from Sections (4.3)-(4.4) that we must also calculate the metric perturbation to second-order in the small mass ratio in order to meet the accuracy requirements for the calculation of the phase. In this section we will present the field equations that must be solved in order to calculate $h^2_{\alpha\beta}$.

Recall that the linearised Einstein field equations, in no particular gauge, and in the self-consistent approximation are given by

$$\left(\delta^1 G + \delta^2 G + \cdots\right)\left(\varepsilon h^1_{\mu\nu} + \varepsilon^2 h^2_{\mu\nu} + \cdots\right) = 8\pi\left(\varepsilon T^1_{\mu\nu} + \varepsilon^2 T^2_{\mu\nu} + \cdots\right), \tag{4.61}$$

where $\delta^1 G$ acts linearly on the metric perturbation, $\delta^2 G$ quadratically, $\delta^3 G$ cubicle etc. The operators $\delta^n G$ have l, m dependence, but this will not be written explicitly and is assumed throughout. At first-order in the small mass ratio, in the self-consistent approximation, the linearised Einstein field equations are

$$\delta^1 G\left[h^1_{\mu\nu}\right] = 8\pi T^1_{\mu\nu}, \tag{4.62}$$

where square brackets denote an operator acting on the metric perturbation. In the Lorenz gauge and using the BSL basis, Eq. (4.61) becomes

$$\delta^1 G^{(i)}_{(j)}\left(\varepsilon\bar{h}^{1,(j)}_{lm} + \varepsilon^2\bar{h}^{2,(j)}_{lm} + \cdots\right) + \delta^2 G^{(i)}_{(j)(k)}\left(\varepsilon\bar{h}^{1,(j)}_{lm} + \varepsilon^2\bar{h}^{2,(j)}_{lm} + \cdots\right)\left(\varepsilon\bar{h}^{1,(k)}_{lm} + \varepsilon^2\bar{h}^{2,(k)}_{lm} + \cdots\right)$$
$$= 8\pi\left(\varepsilon S^{1,(i)}_{lm} + \varepsilon^2 S^{2,(i)}_{lm} + \cdots\right). \tag{4.63}$$

In the Lorenz gauge, using the BSL basis, Eq. (4.62) becomes

$$\delta^1 G^{(i)}_{(j)}\left[\bar{h}^{1,(j)}_{lm}\right] = S^{1,(i)}_{lm}. \tag{4.64}$$

In the two-timescale approximation, time derivatives in the Einstein operator can be written in the two-timescale expansion using Eq. (4.27), so that

$$\delta^1 G^{(i)}_{(j)} = \sum_{n=0}^{\infty}\varepsilon^n \delta^1 G^{n,(i)}_{(j)}, \quad \delta^2 G^{(i)}_{(j)(k)} = \sum_{n=0}^{\infty}\varepsilon^n \delta^2 G^{n,(i)}_{(j)(k)}, \quad \text{etc.,} \tag{4.65}$$

where $\delta^1 G^{n,(i)}_{(j)}$ are given explicitly in Eq. (7.95), and in the two-timescale approximation, the Lorenz gauge field equations become

$$
\begin{aligned}
&\left(\delta^1 G^{0,(i)}_{(j)} + \varepsilon\delta^1 G^{1,(i)}_{(j)} + \cdots\right)\left(\varepsilon\tilde{\bar{h}}^{1,(j)}_{lm} + \varepsilon^2\tilde{\bar{h}}^{2,(j)}_{lm} + \cdots\right) \\
&+ \left(\delta^2 G^{0,(i)}_{(j)(k)} + \varepsilon\delta^2 G^{1,(i)}_{(j)(k)} + \cdots\right)\left(\varepsilon\tilde{\bar{h}}^{1,(j)}_{lm} + \varepsilon^2\tilde{\bar{h}}^{2,(j)}_{lm} + \cdots\right)\left(\varepsilon\tilde{\bar{h}}^{1,(k)}_{lm} + \varepsilon^2\tilde{\bar{h}}^{2,(k)}_{lm} + \cdots\right) + \cdots \\
&= 8\pi\left(\varepsilon\tilde{S}^{1,(i)}_{lm} + \varepsilon^2\tilde{S}^{2,(i)}_{lm} + \cdots\right).
\end{aligned}
\tag{4.66}
$$

Therefore in the two-timescale approximation, the first-order field equations are

$$
\delta^1 G^{0,(i)}_{(j)}\left[\tilde{\bar{h}}^{1,(j)}_{lm}\right] = \tilde{S}^{1,(i)}_{lm}.
\tag{4.67}
$$

At second-order in the small mass ratio, in the Lorenz gauge, and in the two-timescale expansion we have

$$
\delta^1 G^{0,(i)}_{(j)}\left[\tilde{\bar{h}}^{2,(j)}_{lm}\right] = \tilde{S}^{2,(i)}_{lm} - 2\delta^2 G^{0,(i)}_{(j)(k)}\left[\tilde{\bar{h}}^{1,(j)}_{lm}, \tilde{\bar{h}}^{1,(k)}_{lm}\right] - \delta^1 G^{1,(i)}_{(j)}\left[\tilde{\bar{h}}^{1,(j)}_{lm}\right],
\tag{4.68}
$$

where the second-order source in the two-timescale approximation is given explicitly by Eq. (7.78). Note how the term $\partial_{\tilde{t}}\tilde{\bar{h}}^{1,(i)}_{lm}$ will appear in the third term of Eq. (4.68) and hence contributes to the inhomogeneous solutions of $\tilde{\bar{h}}^2$. Therefore, a piece of the second-order metric perturbation in the two-timescale approximation is sourced in part by the slowly evolving first-order metric perturbation. In order to solve for the full second-order metric perturbation, we must solve for the slowly evolving first-order metric perturbation, which we will do in Chapter 6. Furthermore, using the fact that we can write

$$
\partial_{\tilde{t}} = \frac{dr_0}{d\tilde{t}}\partial_{r_0},
\tag{4.69}
$$

during the inspiral, we see from Eq. (4.36) that the two-timescale approximation breaks down as the secondary approaches the ISCO, and the compact objects in the binary approach their transition to plunge. This issue will be treated in Chapter 7.

4.6 Gravitational energy flux

An additional quantity we may wish to calculate is the GW energy flux, which will be referred to as the flux henceforth. Flux calculations are extremely important for modelling EMRIs, as they determine the dominant contribution of the accumulated phase at first-order, with 2GSF corrections determining the last few radians [4]. The flux radiated to infinity is given by [117]

$$
\dot{E}^{\infty}_{lm} = \frac{1}{16\pi}\left|\dot{\tilde{h}}^{\infty}_{lm}\right|^2,
\tag{4.70}
$$

where an overdot denotes a derivative with respect to t.

Substituting $\dot{\tilde{h}}_{lm}^{\infty}$ from Eq. (4.20) in Eq. (6.38) yields [4]

$$\dot{E}_{lm}^{\infty} = \frac{1}{16\pi} |\dot{\tilde{A}}_{lm}^{\infty} + \tilde{A}_{lm}^{\infty} i\dot{\Phi}_{lm}|^2 \tag{4.71}$$

$$= \lim_{r\to\infty} \frac{|\dot{\tilde{\tilde{h}}}_{lm}^{(7)} - i\dot{\tilde{\tilde{h}}}_{lm}^{(10)} + \left(\tilde{\tilde{h}}_{lm}^{(7)} - i\tilde{\tilde{h}}_{lm}^{(10)}\right) i\dot{\Phi}_{lm}|^2}{64\pi(l+2)(l+1)l(l-1)}. \tag{4.72}$$

Recall from Eq. (4.4) and Eq. (4.5) that $\dot{\Phi}_{lm}$ can be written as

$$\dot{\Phi}_{lm} = -m\left(\Omega_0(\tilde{t}) + \varepsilon\Omega_1(\tilde{t}) + \cdots\right) \tag{4.73}$$

and recalling the expansion in Eq. (4.14) so that

$$\dot{\tilde{\tilde{h}}}_{lm}^{(i)} = \sum_{n=1}^{\infty} \varepsilon^{n+1} \partial_{\tilde{t}} \tilde{\tilde{h}}_{lm}^{n,(i)}, \tag{4.74}$$

the flux can then also be expanded as

$$\dot{E}_{lm}^{\infty} = \sum_{n=1}^{\infty} \varepsilon^{n+1} \dot{E}_{lm}^{n,\infty} \tag{4.75}$$

At leading order, that is $\mathcal{O}(\varepsilon^2)$, the flux radiated to infinity is then given by [117]

$$\dot{E}_{lm}^{1,\infty} = \lim_{r\to\infty} \frac{m^2\Omega_0^2}{64\pi(l+2)(l+1)l(l-1)} \left|\tilde{\tilde{h}}_{lm}^{1,(7)} - i\tilde{\tilde{h}}_{lm}^{1,(10)}\right|^2. \tag{4.76}$$

The total energy fluxes radiated to infinity (which is directly observable) and into the horizon of the primary are given respectively by

$$\mathcal{F}^{\infty} = \sum_{l=0}^{\infty} \sum_{m=-l}^{l} \dot{E}_{lm}^{\infty}, \tag{4.77}$$

$$\mathcal{F}^{\mathcal{H}} = \sum_{l=0}^{\infty} \sum_{m=-l}^{l} \dot{E}_{lm}^{\mathcal{H}}, \tag{4.78}$$

and the total energy flux by

$$\mathcal{F} = \mathcal{F}^{\mathcal{H}} + \mathcal{F}^{\infty}. \tag{4.79}$$

Similarly to the energy flux radiated to infinity, the horizon energy flux is defined as

$$\dot{E}_{lm}^{\mathcal{H}} = \frac{1}{16\pi} \left|\dot{\tilde{h}}_{lm}^{\mathcal{H}}\right|^2, \tag{4.80}$$

where

$$\tilde{h}_{lm}^{\mathcal{H}}(\tilde{t}, \phi_{\mathrm{p}}(t,\varepsilon), r, \varepsilon) = \lim_{r\to 2M} a_l \left(\tilde{\tilde{h}}_{lm}^{(7)} + i\tilde{\tilde{h}}_{lm}^{(10)}\right) e^{-im\phi_{\mathrm{p}}(t,\varepsilon)}. \tag{4.81}$$

The horizon energy flux admits a similar expansion to that of $\dot{E}_{lm}^{\infty}$ to infinity, given by

$$\dot{E}_{lm}^{\mathcal{H}} = \sum_{n=1}^{\infty} \varepsilon^{n+1} \dot{E}_{lm}^{n,\mathcal{H}}, \tag{4.82}$$

such that

$$\mathcal{F}^{\mathcal{H}} = \sum_{n=1}^{\infty} \varepsilon^{n+1} \mathcal{F}^{n,\mathcal{H}}, \tag{4.83}$$

$$\mathcal{F}^{\infty} = \sum_{n=1}^{\infty} \varepsilon^{n+1} \mathcal{F}^{n,\infty}, \tag{4.84}$$

$$\mathcal{F} = \sum_{n=1}^{\infty} \varepsilon^{n+1} \mathcal{F}^{n}. \tag{4.85}$$

4.7   Binding energy

The binding energy of the EMRI is yet another quantity that we need in order to calculate the phase via one of the methods detailed in Section 4.8. The binding energy is given by [118]

$$E_{\text{bind}} = M_{\text{B}} - M_{\text{BH}} - \mu, \tag{4.86}$$

where M_{B} is the Bondi mass and M_{BH} is the full perturbed mass of the primary black hole, taken to be the irreducible mass of the black hole, defined by its surface area [118]. These quantities are given respectively by [118]

$$M_{\text{B}} = M + \varepsilon(\mathcal{E}_0 + \delta M) + \varepsilon^2 M_{\text{B}}^{(2)} + \mathcal{O}\left(\varepsilon^3\right), \tag{4.87}$$

$$M_{\text{BH}} = M + \varepsilon(\delta M) + \varepsilon^2 M_{\text{BH}}^{(2)} + \mathcal{O}\left(\varepsilon^3\right), \tag{4.88}$$

where δM is the perturbation to the mass M of the primary, the use of round brackets in the superscripts are to distinguish from squared quantities, and for a point-like particle on a circular orbit, the orbital energy at leading-order is given by [118, 4]

$$\mathcal{E}_0 = \frac{f_0}{U_0} = \left(1 - \frac{2M}{r_0}\right) \Big/ \sqrt{1 - \frac{3M}{r_0}}, \tag{4.89}$$

and $M_{\text{B}}^{(2)}$ and $M_{\text{BH}}^{(2)}$ are calculated from the second-order metric perturbation at infinity and on the horizon [118], though they shall not be detailed in this thesis. Substituting the expressions for M_{B} and M_{BH} into Eq. (4.86) then yields

$$E_{\text{bind}} = \varepsilon \mathcal{E}_0 + \varepsilon^2 \left(M_{\text{B}}^{(2)} - M_{\text{BH}}^{(2)}\right) - \mu. \tag{4.90}$$

4.8 Calculating the phase

With all of the relevant quantities defined in the previous sections of this chapter, we can now begin to construct the phase to 1PA order. Following the work of Ref. [14], there are three possible approaches that use the two-timescale approximation within the self-consistent approach.

Method 1

Firstly, the metric perturbation is computed to second-order in the small mass ratio in the Lorenz gauge. Specifically the pieces $\tilde{h}_{lm}^{1\mathcal{R},(i)}(\tilde{t}, r_0)$ and $\tilde{h}_{lm}^{2\mathcal{R},(i)}(\tilde{t}, r_0)$. These are computed using Eq. (4.67) and Eq. (4.68). The latter also requires input of $\partial_{\tilde{t}}\tilde{h}_{lm}^{1\mathcal{R},(i)}(\tilde{t}, r_0)$, which shall be calculated in Chapter 6. The metric-perturbation is then substituted into the equations for the first- and second-order GSF, $\tilde{f}_1^t$, $\tilde{f}_1^r$ and $\tilde{f}_2^t$, which are given by Eq. (4.54), Eq. (4.56) and Eq. (4.58) respectively. Note that $\tilde{f}_1^r$ and $\tilde{f}_2^t$ also require input of $\partial_{r_0}\tilde{h}_{lm}^{1\mathcal{R},(i)}(\tilde{t}, r_0)$ and $\partial_{\tilde{t}}\tilde{h}_{lm}^{1\mathcal{R},(i)}(\tilde{t}, r_0)$ respectively. The solutions to the GSF are then substituted into the expressions for $\frac{dr_0}{dt}$ and $\frac{dr_1}{dt}$ from Eq. (4.36) and Eq. (4.37) respectively, which are then integrated to solve for r_0 and r_1. In turn, the slowly evolving radius and SF are substituted into expressions for Ω_0 and Ω_1 from Eq. (4.33) and Eq. (4.34) respectively, which are subsequently integrated to obtain the phase at 1PA order in the small mass ratio in the two-timescale approximation. The flowchart below summarises the procedure for calculating the phase using method 1

$$h_{\mu\nu} = \varepsilon\tilde{h}_{\mu\nu}^{1,\mathcal{R}} + \varepsilon^2\tilde{h}_{\mu\nu}^{2,\mathcal{R}} + \cdots$$

$$f^\mu(t,\varepsilon) = \varepsilon\tilde{f}_1^\mu\left(\tilde{t}\right) + \varepsilon^2\tilde{f}_2^\mu\left(\tilde{t}\right) + \cdots$$

$$\Omega\left(\tilde{t}\right) = \Omega_0\left(\tilde{t}\right) + \varepsilon\Omega_1\left(\tilde{t}\right) + \cdots$$

$$\phi_{\mathrm{p}}(t) = \frac{1}{\varepsilon}\int^t \Omega\left(\tilde{t}\right) d\tilde{t}, \quad \Phi_{lm} = -m\phi_{\mathrm{p}}$$

(boxes: Metric Perturbation → Self Force → Frequency → Phase)
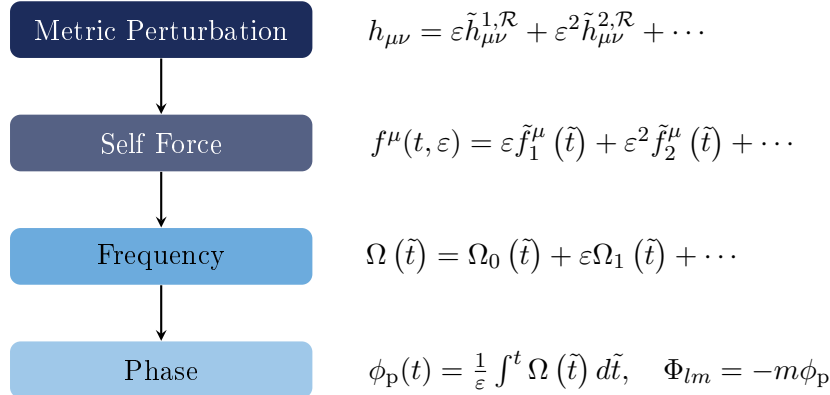
Method 2

In this second method, rather than calculating Ω order-by-order directly, we calculate the evolution of Ω, that is $d\Omega/dt$ order-by-order and integrate this twice to obtain the phase through 1PA order. We have the freedom to choose $\Omega = \Omega_0$ and $\Omega_n = 0 \ \forall \ n$ for some initial time t, with $\Omega_1 = 0 \ \forall \ t$ [?], and then solve for the evolution of the frequency. Integrating the resulting expression gives us a solution to each order of Ω. Therefore, the phase can also be calculated by integrating over time

twice the following expression [3]

$$\frac{d\Omega}{dt} = -\left(\frac{\partial E_{\mathrm{bind}}}{\partial \Omega}\right)^{-1}\mathcal{F}, \tag{4.91}$$

We shall rewrite the flux and binding energy from Eq. (4.79) and Eq. (4.90) respectively in terms of the variable $x = [(\mu + M)\,\Omega]^{2/3}$ and symmetric mass ratio ν, where

$$\nu = \frac{\mu M}{(\mu + M)^2} = \frac{\varepsilon}{(1 + \varepsilon)^2}, \tag{4.92}$$

so that

$$\varepsilon = \frac{1 - \sqrt{1 - 4\nu}}{1 + \sqrt{1 - 4\nu}}, \tag{4.93}$$

$$= \nu + 2\nu^2 + 5\nu^3 + \mathcal{O}\left(\nu^4\right). \tag{4.94}$$

The variable x is used in order to make comparisons with NR and expansions in ε are re-summed in terms of ν to restore the inherent symmetry of the full perturbed solution, which also yields the most accurate waveforms when comparing with NR [3]. Using the two-timescale approximation, both the binding energy and the flux can be written in the following way: [3, 4, 118]

$$\mathcal{F}(x) = \nu^2 \mathcal{F}_\nu^1(x) + \nu^3 \mathcal{F}_\nu^2(x) + \mathcal{O}(\nu^4), \tag{4.95}$$

$$E_{\mathrm{bind}}(x) = \nu(\mu + M)\left[\hat{\mathcal{E}}_0(x) - 1 + \nu\hat{E}_{\mathrm{SF}}(x) + \mathcal{O}\left(\nu^2\right)\right], \tag{4.96}$$

where [3]

$$\mathcal{F}_\nu^1(x) = \sum_{l=0}^{\infty}\sum_{m=-l}^{l}\left(\dot{E}_{\nu,lm}^{1,\infty} + \dot{E}_{\nu,lm}^{1,\mathcal{H}}\right), \tag{4.97}$$

and

$$\mathcal{F}_\nu^2 = \sum_{l=0}^{\infty}\sum_{m=-l}^{l}\dot{E}_{\nu,lm}^{2,\infty}, \tag{4.98}$$

and a subscript ν denotes re-summation with respect to ν. The second-order flux, which appears at $\mathcal{O}(\nu^3)$ does not include the second-order horizon flux as there is currently no data for $\dot{E}_{lm}^{2,\mathcal{H}}$, but this quantity is expected to be negligible [93, 94]. The quantity $\hat{\mathcal{E}}_0$ is then defined as

$$\hat{\mathcal{E}}_0 = \mathcal{E}_0/(M + \mu). \tag{4.99}$$

Substituting the expression for Ω_0 from Eq. (4.33) into x and expressing $\mathcal{E}_0$ in terms of x then gives [119, 3]

$$\hat{\mathcal{E}}_0(x) = \frac{1 - 2x}{\sqrt{1 - 3x}}, \tag{4.100}$$

and $\hat{E}_{\mathrm{SF}}$ is the contribution to the flux from the second-order SF [119, 3].

To calculate the phase to 1PA order, we will need $\dot{\Omega}$ to next-to-leading order in ε. This will require calculating the metric perturbation through second-order in the small mass ratio as input to the flux. Additionally, there will be self-force contributions to the next-to-leading order terms in the binding energy and the flux, particularly as the leading-order binding energy is $\mathcal{O}(\varepsilon^2)$ [14, 119, 4, 3]. To solve for Ω from its evolution we can write Eq. (4.91) as [3]

$$\frac{d\Omega}{dt} = \frac{\nu}{(\mu + M)^2} \left(F_0 + \nu F_1 \right), \tag{4.101}$$

where [3]

$$F_0(x) = - \left(\partial_\Omega \hat{\mathcal{E}}_0 \right)^{-1} \mathcal{F}_\nu^1, \tag{4.102}$$

and

$$F_1(x) = - \left(\partial_\Omega \hat{\mathcal{E}}_0 \right)^{-1} \mathcal{F}_\nu^2 - \left(\partial_\Omega \hat{\mathcal{E}}_0 \right)^{-2} \mathcal{F}_\nu^1 \partial_\Omega \hat{E}_{\mathrm{SF}}. \tag{4.103}$$

In summary, the GW phase can be calculated using the following procedure
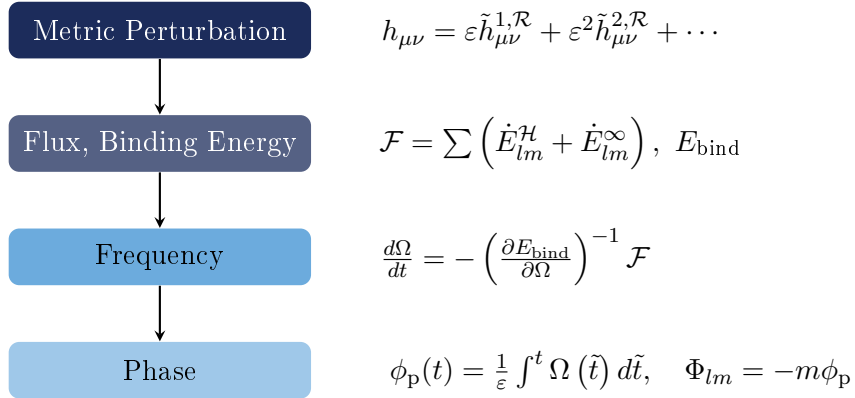
The implementation of method 2 will be presented in Chapter 8, where the flux and waveform during the inspiral, calculated using the two-timescale approximation within the GSF approach will be compared to results from NR simulations. The results of this comparison are based on Refs. [4] and [3]. The reason method 2 has been implemented and not method 1 or 3 is due to legacy and convenience. It just so happened that data for the binding energy [119] and flux [3] had already been calculated, whereas the second-order SF had not. We'll see in Chapter 8 that we actually use a different formula for the binding energy than presented in this chapter, that is the first-law binding energy, again as a matter of convenience. The binding energy is slicing dependent and the correct choice has yet to be determined. One way to determine the correct binding energy is to compare results for the frequency evolution with those of method 3, after computing the second-order SF, which has not yet been done. Reference [119] demonstrates using the first-law binding energy is a reasonable starting point at least to begin generating 2GSF waveforms.

Method 3

Alternatively, once again choosing $\Omega = \Omega_0$ and $\Omega_n = 0 \; \forall \; n$ for some initial time t, with $\Omega_1 = 0 \; \forall t$ [14], we could write the slow evolution of Ω instead as

$$\frac{d\Omega}{d\tilde{t}} = \varepsilon F_0^\Omega(\Omega) + \varepsilon^2 F_1^\Omega(\Omega). \tag{4.104}$$

Returning to the equations of motion and solving for $\frac{d\Omega}{d\tilde{t}}$ similarly to method 2, we find that the first- and second-order pieces of the t component of Eq. (4.24) yield[3] [14, 3]

$$F_0^\Omega = -\frac{3 f_0 \Omega \tilde{f}_1^t}{(M\Omega)^{2/3} U_0^4 \left[1 - 6(M\Omega)^{2/3}\right]}, \tag{4.105}$$

$$F_1^\Omega = -\frac{3 f_0 \Omega \tilde{f}_2^t}{(M\Omega)^{2/3} U_0^4 \left[1 - 6(M\Omega)^{2/3}\right]} - \frac{2 \dot{F}_0^\Omega \partial_\Omega \tilde{f}_1^r}{M U_0^4 \left[(M\Omega)^{1/3} - 8M\Omega + 12(M\Omega)^{5/3}\right]} \tag{4.106}$$

$$- \frac{4 \left[1 - 6(M\Omega)^{2/3} + 12(M\Omega)^{4/3}\right] \tilde{f}_1^r \tilde{f}_1^t}{M\Omega U_0^6 f_0 \left[1 - 6(M\Omega)^{2/3}\right]^2}, \tag{4.107}$$

For the purposes of this thesis however, any evolution of the spin or mass of either the primary or secondary shall be ignored, motivated by arguments in Refs. [3, 93]. The quantities F_0^Ω and F_1^Ω are related to F_0 and F_1 from method 2 via $F_0^\Omega = \frac{F_0}{M+\mu}$ and $F_1^\Omega = \frac{F_1}{M+\mu}$. The metric perturbation should be calculated through second-order in the small mass ratio in the two-timescale approximation and then substituted into expressions for the SF. In turn, the 0PA and 1PA corrections to the slow evolution of the frequency are calculated using input from the SF. The slowly evolving frequency can then be integrated over time twice to yield the orbital and hence GW phase for quasicircular orbits. The procedure for calculating the phase using method 3 is summarised in the diagram below

Metric Perturbation $\qquad h_{\mu\nu} = \varepsilon \tilde{h}_{\mu\nu}^{1,\mathcal{R}} + \varepsilon^2 \tilde{h}_{\mu\nu}^{2,\mathcal{R}} + \cdots$

Self Force $\qquad f^\mu(t, \varepsilon) = \varepsilon \tilde{f}_1^\mu\left(\tilde{t}\right) + \varepsilon^2 \tilde{f}_2^\mu\left(\tilde{t}\right) + \cdots$

Frequency $\qquad \frac{d\Omega}{d\tilde{t}} = F_0^\Omega + \varepsilon F_1^\Omega + \cdots$

Phase $\qquad \phi_{\mathrm{p}}(t) = \frac{1}{\varepsilon} \int^t \Omega\left(\tilde{t}\right) d\tilde{t}, \quad \Phi_{lm} = -m\phi_{\mathrm{p}}$
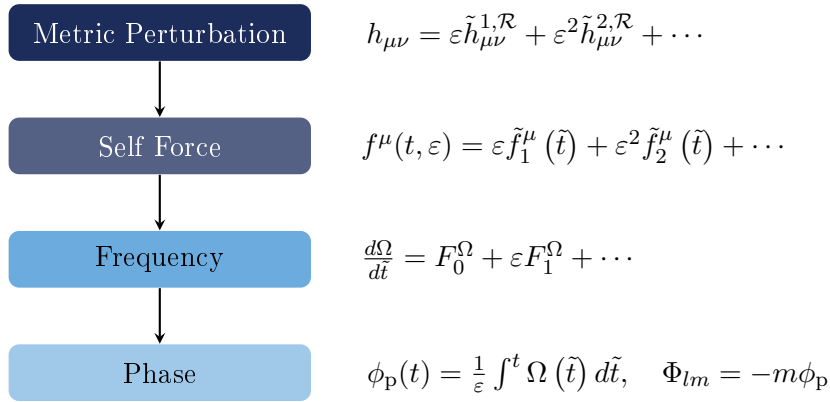
The implementation of method 3 will also be seen in Chapter 8 when generating waveforms during the transition to plunge, where a new timescale of orbital evolution must be introduced and quantities in the two-timescale approximation in this section are re-expanded near the ISCO.

---

[3]This statement is true when excluding perturbations to the mass and spin of the primary.

Chapter 5

Perturbations to Schwarzschild Spacetime

One of the main goals and outputs of this thesis is to calculate the slowly evolving first-order metric perturbation, the algorithm for which is presented in the next chapter. The slowly evolving metric perturbation however depends on solutions to the first-order metric perturbation. As such, in this Chpter an algorithm for calculating the Lorenz gauge metric perturbation to first-order in the small mass ratio will be presented, in addition to numerical results. The calculation will be performed in the frequency domain[1] using the two-timescale approximation, on a Schwarzschild background with a secondary following quasicircular equatorial orbits, with a spacetime foliation of hypersurfaces defined by constant t. While the first-order Lorenz gauge metric perturbation has been calculated throughout the literature [89, 90, 91, 46, 92, 83], an in-house solver is implemented, on which to build the slowly evolving metric perturbation calculation in the next chapter. To implement an algorithm which calculates the first-order metric perturbation in the Lorenz gauge, we follow Berndtson's prescription [46], which relies on the gauge transformation from RW to Lorenz gauge quantities, as outlined in Section 2.6. In this section, solutions to the RWZ master functions, in addition to the gauge field M_{2af} will be presented, from which the first-order Lorenz gauge, and indeed the RW gauge metric perturbation can be constructed. To solve for M_{2af} we employ the method of partial annihilators in conjunction with the method of variation of parameters, the latter of which will be used to solve for the RWZ fields. All of the research presented in this chapter was done in collaboration with Warburton.

---

[1]Recall the frequency domain expression of the metric perturbation from Eq. (2.29). Replacing ω with $m\phi_{\mathrm{p}}(t)$ we obtain a solution that is not strictly in the frequency domain, and is in fact the solution we use for the two-timescale expansion discussed in later chapters. At leading order, for quasicircular equatorial orbits, these approaches are equivalent. As such, we shall continue to use frequency domain solutions in this chapter and the proceeding chapter.

5.1 Solving the Regge-Wheeler and Zerilli master functions

For a given l, m mode, the radial RWZ master equations, given by Eq. (2.49), can be solved using the standard method of variation of parameters. With this approach the inhomogeneous solution can be written as

$$\psi_s(r) = C_s^+(r)\psi_s^+(r) + C_s^-(r)\psi_s^-(r),\tag{5.1}$$

where $\psi_s^\pm$ are the two linearly independent homogenous solutions that represent ingoing and outgoing radiation, to asymptotic null infinity, $\mathcal{I}^+$ and the future event Horizon $\mathcal{H}^+$ respectively. These homogeneous solutions are determined by the BHPToolkit [1]. Their asymptotic boundary conditions are

$$\psi_s^+ \propto e^{i\omega r_*}, \quad \text{as} \quad r_* \to \infty,\tag{5.2}$$

$$\psi_s^- \propto e^{-i\omega r_*}, \quad \text{as} \quad r_* \to -\infty.\tag{5.3}$$

The weighting functions $C_s^\pm$ are given by

$$C_s^+(r_*) = \int_{-\infty}^{r_*} \frac{\psi_s^-(r_*')\, S_s(r_*')}{W_s(r_*')}\mathrm{d}r_*',\tag{5.4}$$

$$C_s^-(r_*) = \int_{r_*}^{\infty} \frac{\psi_s^+(r_*')\, S_s(r_*')}{W_s(r_*')}\mathrm{d}r_*',\tag{5.5}$$

and the Wronskian, W_s is defined in the usual way

$$W_s(r_*) \equiv \frac{d\psi_s^+(r_*)}{dr_*}\psi_s^-(r_*) - \frac{d\psi_s^-(r_*)}{dr_*}\psi_s^+(r_*).\tag{5.6}$$

As there are no first derivatives with respect to r_* in Eq. (2.49), W_s is a constant by Abel's theorem. Accordingly, we drop the dependence on r_* of W_s. As the secondary can be treated as a point-like particle to first-order in ε [14, 16], the sources of the RWZ master functions take the form

$$S_s(r) = p_s(r, r_\mathrm{p})\delta(r - r_\mathrm{p}) + q_s(r, r_\mathrm{p})\delta'(r - r_\mathrm{p}),\tag{5.7}$$

where a prime denotes differentiation with respect to r. In the case of quasicircular equatorial orbits, at leading order we have

$$S_s(r) = p_s(r, r_0)\delta(r - r_0) + q_s(r, r_0)\delta'(r - r_0),\tag{5.8}$$

where the factors $p_s(r, r_0)$ and $q_s(r, r_0)$ can be determined from Eqs. (A.1)-(A.6) and Eqs. (2.48a)-(2.48j). For example, the leading order source for the spin-weight $s = 2$ RW master function in the odd-sector is [46]

$$S_2^{lm}(r) = \frac{4im\pi f(r)(2\delta(r - r_0) + rf(r)\delta'(r - r_0))}{\lambda(\lambda + 1)rr_0^3}\sqrt{\frac{r_0}{r_0 - 3}}\,\partial_\theta Y_{lm}^*\left(\frac{\pi}{2}, 0\right).\tag{5.9}$$

We can immediately read off $p_s(r, r_0)$ and $q_s(r, r_0)$ as

$$p_2(r, r_0) = \frac{8im\pi f(r)}{\lambda(\lambda + 1)rr_0^3} \sqrt{\frac{r_0}{r_0 - 3}} \, \partial_\theta Y_{lm}^* \left(\frac{\pi}{2}, 0\right), \tag{5.10}$$

$$q_2(r, r_0) = \frac{4im\pi f(r)^2}{\lambda(\lambda + 1)r_0^3} \sqrt{\frac{r_0}{r_0 - 3}} \, \partial_\theta Y_{lm}^* \left(\frac{\pi}{2}, 0\right). \tag{5.11}$$

Due to the distributional form of S_s in Eq. (5.8), Eq. (5.4) and Eq. (5.5) become

$$C_s^+(r) = c_s^+ \Theta(r - r_0), \tag{5.12}$$

$$C_s^-(r) = c_s^- \Theta(r_0 - r), \tag{5.13}$$

where integration by parts has been used to evaluate terms in Eq. (5.4) and Eq. (5.5) involving δ', and Θ is the Heaviside step function, defined so that $\Theta(x) = 1$ for $x > 0$ and $\Theta(x) = 0$ for $x \leq 0$. The constants $c_s^\pm$ are the weighting coefficients

$$c_s^\pm = \left. \frac{1}{W_s} \left\{ \frac{\psi_s^\mp(r_0) \, p_s(r, r_0)}{f(r_0)} - \frac{\partial}{\partial r} \left(\frac{\psi_s^\mp(r) \, q_s(r, r_0)}{f(r)} \right) \right\} \right|_{r=r_0}, \tag{5.14}$$

and the radial derivatives of ψ_s can be determined by taking the radial derivative of Eq. (5.1). Our numerical integrator returns the ψ_s and its first, second, and third radial derivatives.

5.1.1 Numerical boundary conditions and implementation

When solving for perturbations on hypersurfaces of constant t we cannot place numerical boundary conditions at future null infinity, $\mathcal{I}^+$, and the future event Horizon $\mathcal{H}^+$. Instead we will find series expansions of the solutions at finite radii. For the homogeneous solutions to the RWZ equations we expand the asymptotic boundary conditions in Eqs. (5.2) and (5.3) as

$$\psi_s^+(r) = e^{i\omega r_*} \sum_{i=0}^{n_{\max}} \frac{A_i^+}{(r\omega)^i} \Bigg|_{r=r_{\text{out}}}, \tag{5.15}$$

$$\psi_s^-(r) = e^{-i\omega r_*} \sum_{i=0}^{n_{\max}} A_i^- f(r)^i \Big|_{r=r_{\text{in}}}, \tag{5.16}$$

where the coefficients $A_i^\pm$ depend on the parameters s, l, m, r_0. In order for the expansion in Eq. (5.15) to converge, r_{out} must be in the wave zone such that $r\omega \gg 1$ [120]. In practice we find that $r_{\text{out}} = 10^4 M$ is sufficient for the parameters we consider in this work. Similarly we find that $r_{\text{in}} = (2 + 10^{-5})M$ ensures rapid convergence of the expansion in Eq. (5.16). We shall use these values of $r_{\text{in/out}}$ though out this work. We also find a value of $n_{\max} = 50$ is sufficient to ensure the series expansions satisfy the homogeneous field equation to beyond machine precision. We find this value of $n_{\max}$ is sufficient for all later boundary condition expansions as well. By substituting the above expansions into the homogeneous field equation, Eq. (2.49), recurrence relations can be derived for

the coefficients $A_i^{\pm}$ in terms of the leading $i = 0$ coefficient. In our code we use the `ReggeWheeler` package of the BHPToolkit [1] to compute $\psi_s^{\pm}$, which includes the boundary conditions for the RWZ fields. The numerical integration option in this package implements the above boundary condition expansions and then numerically integrates to r_0 to find the homogeneous solutions at any radius. We note here that the `ReggeWheeler` package uses the MST method, introduced in Chapter 3, by default. This method allows for very high precision numerical results to be obtained but has the downside that it often requires extended precision arithmetic and typically is slower to compute the homogeneous solution at a given radius for strong-field orbits. As the goal of this work is to provide $h_{\mu\nu,r_0}^{1\mathrm{L}}$ on a dense grid of r values for use in constructing the source to second-order perturbations, we instead opt to use the faster numerical integration method.

5.1.2 Numerical results

As an example, in Fig. (5.1) we plot the results of the spin-weight $s = 2$ RW master function for the $(l, m) = (2, 1)$ mode at $r_0 = 10M$ out to large r.
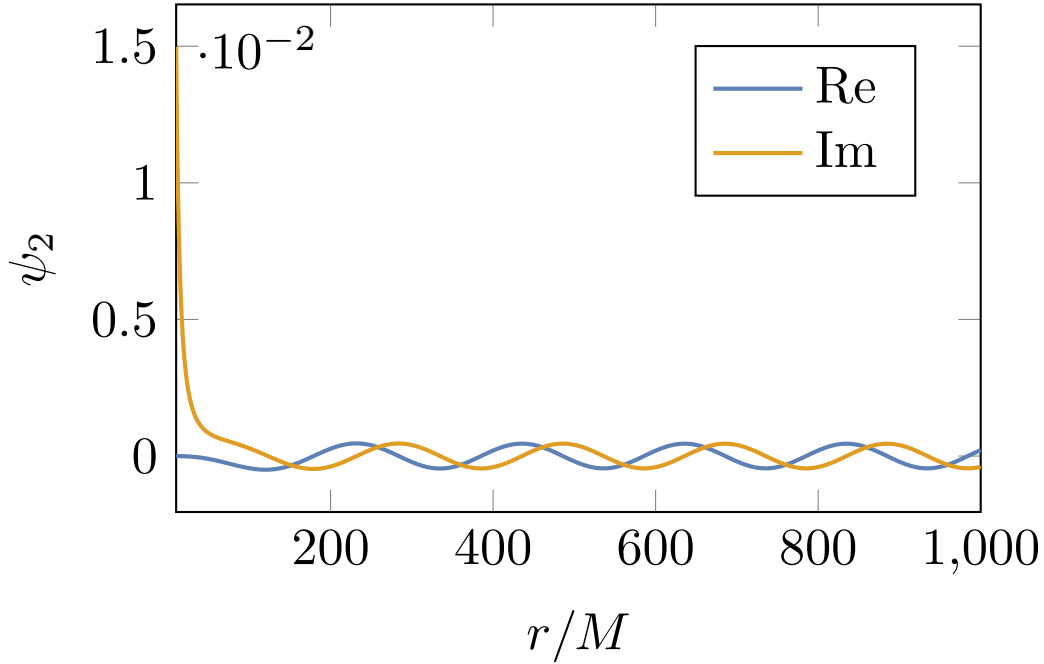
Figure 5.1: Real and imaginary parts of ψ_2 for the $(l, m) = (2, 1)$ mode with $r_0 = 10M$ [2].

5.2 Solving for the gauge field M_{2af}

The equation governing M_{2af} is given by [46]

$$\mathcal{L}_0 M_{2af}(r) = f(r)\, \psi_0(r), \tag{5.17}$$

where $\mathcal{L}_0$ is the operator from Eq. (2.50) with a RW potential and spin-weight $s = 0$. Equation (5.17) is exactly the RW equation, with a source that now contains ψ_0 and is thus unbounded, where previously we had distributional sources containing Dirac delta functions. The form of Eq. (5.17) means that we can tackle it with the method of partial annihilators [102], which allows us to replace the unbounded source with a compact one, at the expense of introducing a higher-order operator on the left hand side of the field equations. Applying an additional $\mathcal{L}_0$ operator to Eq. (5.17) yields [2]

$$\mathcal{L}_0 \left(\frac{1}{f} \mathcal{L}_0 M_{2af} \right) = S_0, \tag{5.18}$$

where we have made use of the fact that $\mathcal{L}_0 \psi_0 = S_0$, with the source S_0 provided in Eq. (A.5). As an inhomogeneous, fourth-order ODE, Eq. (5.18) will have four independent homogeneous solutions. Two of these solutions will be $\psi_0^\pm$ from Section 5.1. Our numerical integrator returns the M_{2af} and its first, second, and third radial derivatives.

5.2.1 Numerical boundary conditions and implementation

As the fourth-order Eq. (5.18) does not have a known MST-type solution, the other two homogeneous solutions must be obtained by numerical integration starting with appropriate boundary conditions at finite radii. Series expansions of the homogeneous solutions near infinity and the horizon are given by [2]

$$M_{2af}^{h4,+}(r) = re^{i\omega r_*} \sum_{i=0}^{n_{\max}} \left. \frac{A_i^{h4,+}}{(r\omega)^i} \right|_{r=r_{\mathrm{out}}}, \tag{5.19}$$

$$M_{2af}^{h4,-}(r) = f(r)e^{-i\omega r_*} \sum_{i=-1}^{n_{\max}} f(r)^i A_i^{h4,-} \Bigg|_{r=r_{\mathrm{in}}}. \tag{5.20}$$

The coefficients $A_i^{h4,\pm}$, not to be confused with those from Section 5.1.1, are derived by substituting the above ansätze into Eq. (5.18) and matching the coefficients of r and $f(r)$. For brevity we have suppressed some indices and functional dependence of the coefficients in the series expansion which depend on the parameters l, m and r_0. The coefficients $A_i^{h4,\pm}$ obey recursion relations provided in the supplementary material of Ref. [2]. For Eq. (5.19) if we set $A_0^{h4,+} = 1$ and $A_1^{h4,+} = 0$ we find the series expansion satisfies Eq. (5.18) in the homogeneous case, but not $\mathcal{L}_0 M_{2af}^{h4,+} = 0$ and thus we know we have found another linearly independent homogeneous solution. If we set $A_0^{h4,+} = 0$ and $A_1^{h4,+} = 1$ we recover the boundary conditions for ψ_0^+ given in Eq. (5.15). Similarly for Eq. (5.20) if we set $A_{-1}^{h4,-} = 1$ and $A_0^{h4,-} = 0$ we find a solution that satisfies Eq. (5.18) in the homogeneous case, but not $\mathcal{L}_0 M_{2af}^{h4,-} = 0$. If we set $A_{-1}^{h4,-} = 0$ and $A_0^{h4,-} = 1$ we recover the boundary conditions for ψ_0^- given in Eq. (5.16).

Following the same procedure as in Section 5.1 when deriving ψ_s, the inhomogeneous solution to Eq. (5.17) can be written as

$$M_{2af}(r) = \left(c^{h2,-}\psi_0^-(r) + c^{h4,-}M_{2af}^{h4,-}(r)\right)\Theta(r_0 - r) + \left(c^{h2,+}\psi_0^+(r) + c^{h4,+}M_{2af}^{h4,+}(r)\right)\Theta(r - r_0). \tag{5.21}$$

Substituting Eq. (5.21) into Eq. (5.18) and using the identity in Eq. (6.15), we match the coefficients of the Dirac delta functions and their radial derivatives with those in S_0 and solve the linear system of equation for $c^{h2/4,\pm}$. We can write this system of linear equations in the following form

$$\mathbf{C} = \mathbf{\Phi}^{-1} \cdot \mathbf{J}, \tag{5.22}$$

where $\mathbf{C} = (c^{h2,-}, c^{h4,-}, c^{h2,+}, c^{h4,+})$ and

$$\mathbf{\Phi} = \begin{pmatrix} -\psi_0^- & -M_{2af}^{h4,-} & \psi_0^+ & M_{2af}^{h4,+} \\ -\partial_r\psi_0^- & -\partial_r M_{2af}^{h4,-} & \partial_r\psi_0^+ & \partial_r M_{2af}^{h4,+} \\ -\partial_r^2\psi_0^- & -\partial_r^2 M_{2af}^{h4,-} & \partial_r^2\psi_0^+ & \partial_r^2 M_{2af}^{h4,+} \\ -\partial_r^3\psi_0^- & -\partial_r^3 M_{2af}^{h4,-} & \partial_r^3\psi_0^+ & \partial_r^3 M_{2af}^{h4,+} \end{pmatrix}_{r=r_0}. \tag{5.23}$$

As the source S_0 contains only Dirac delta functions with no radial derivatives, the vector $\mathbf{J}$ has only one non-zero component such that $\mathbf{J} = (0, 0, 0, J_3)$, where

$$J_3 = \frac{-16\pi\sqrt{r_0(r_0 - 3M)}}{(r_0 - 2M)^2}Y_{lm}^*(\pi/2, 0). \tag{5.24}$$

5.2.2 Numerical results

In this section we present our numerical results for M_{2af} and a check to provide confidence in our results. We begin by showing results for M_{2af} in Fig. 5.2.
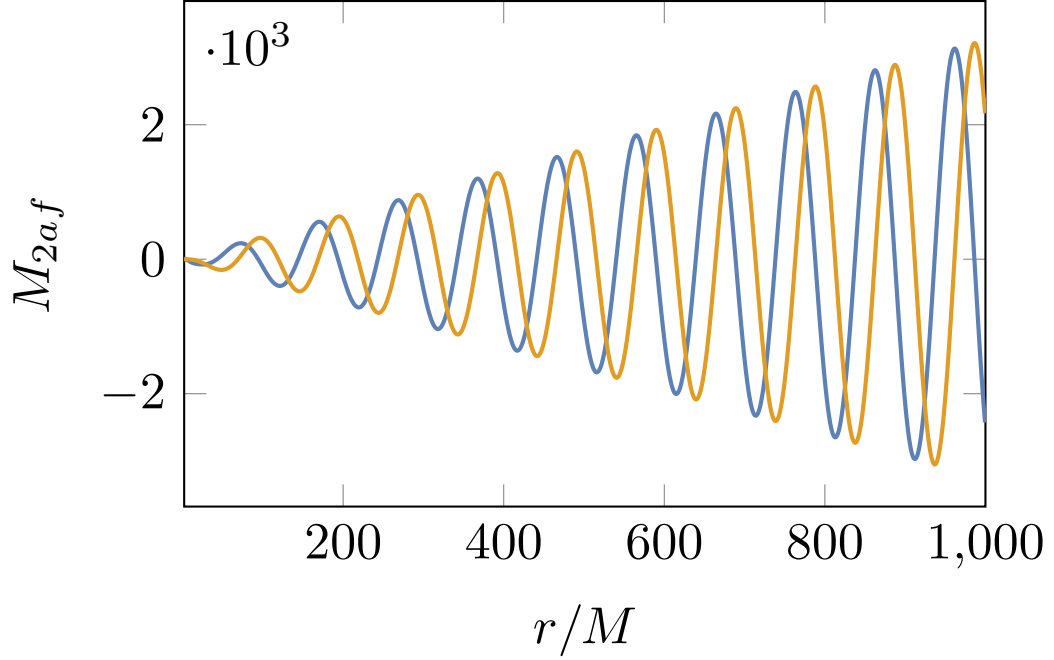
Figure 5.2: Real and imaginary parts of M_{2af} for the $(l,m) = (2,2)$ mode with $r_0 = 10M$. The amplitudes of the field grows proportional to r for large r, as determined by the asymptotic boundary conditions, Eq. (5.19). Similar results are obtained for other even-sector multiple modes and different values of r_0.

As a check on the implementation of our partial annihilator scheme for M_{2af} we verify that our solution to the fourth-order equation with a distributional source, Eq. (5.18), satisfies the original second-order equation Eq. (5.17) with an unbounded source. Figure 5.3 then shows that the relevant second-order equation is satisfied to near machine precision.
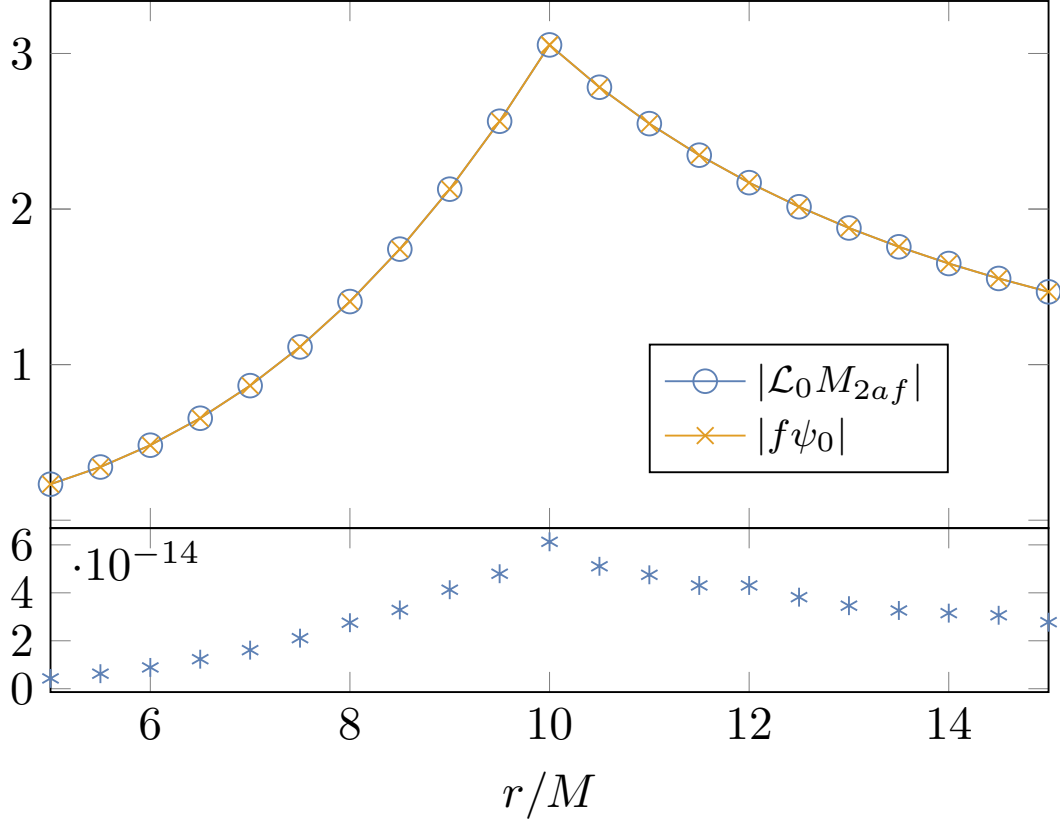
Figure 5.3: The top panel shows the absolute values of the left- and right-hand sides of Eq. (5.17), given the solution for M_{2af} computed using the fourth-order equation, Eq. (5.18). The data shown is for $r_0 = 10M$ and $(l, m) = (2, 1)$. The lower panel shows that the absolute value of the difference between the data sets for the left- and right-hand side of Eq. (5.17) is near machine precision. The lines joining data points are for visualisation purposes only.

5.3 Numerical results for the Lorenz gauge metric perturbation

We now have all ingredients we need to completely reconstruct Berndtson's or the BSL fields. With confidence in our solution for M_{2af} we can compute $h_{\mu\nu}^{1\mathrm{L}}$. An example of the level of agreement with previously published results from Ref. [91] is demonstrated in Fig. (5.4).
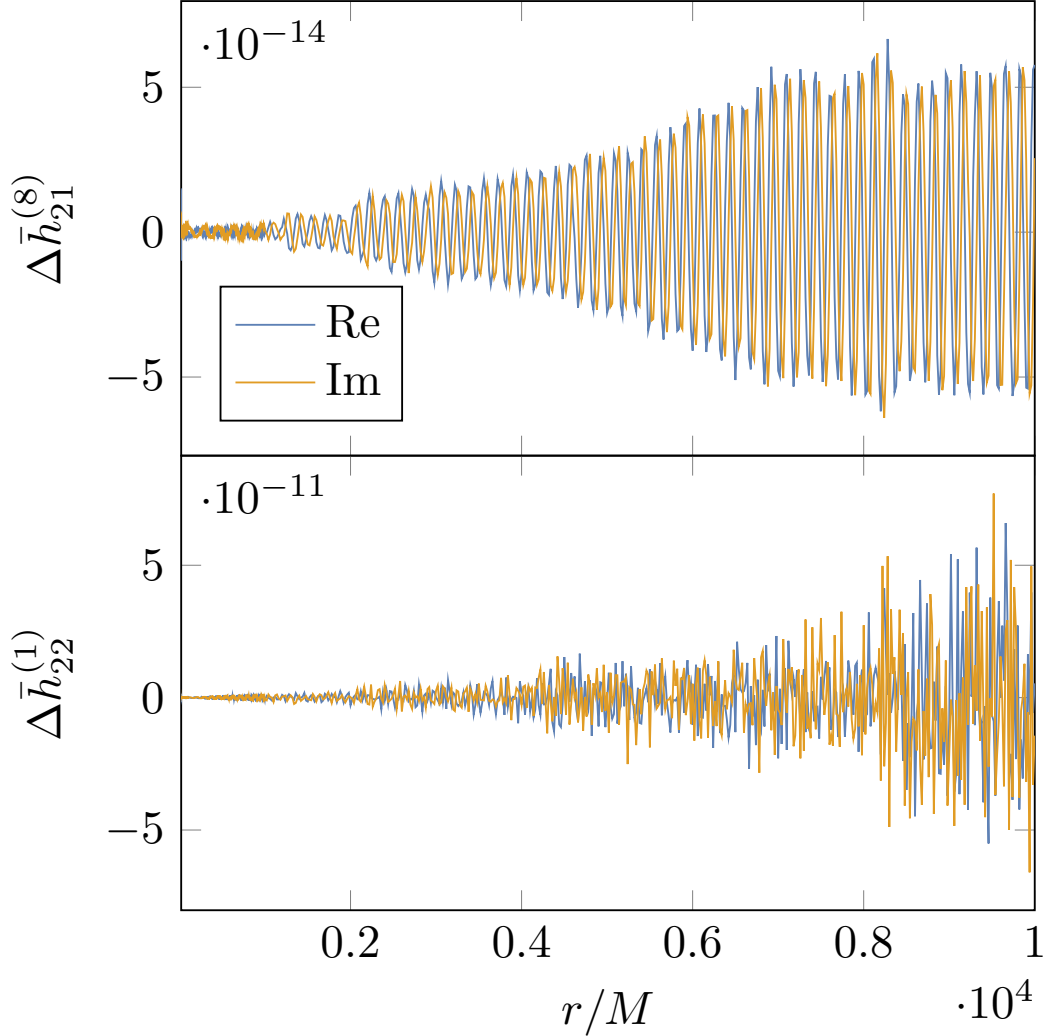
Figure 5.4: Real and imaginary parts of the difference between the calculation of the metric perturbation components as computed using methods outlined in this work compared to results from Ref. [91]. The top panel shows results for the $i = 8$ odd-sector component in the BSL basis for the $(l, m) = (2, 1)$ mode. The bottom panel then shows results for the $i = 1$ even-sector component in the BSL basis for the $(l, m) = (2, 2)$ mode. The orbital radius was chosen to be $r_0 = 9M$ and results were plotted from $20M$ to $10000M$ for visualisation purposes. The difference can be as small as machine precision nearer the horizon. The error is found to be smaller nearer the horizon due to the choice of precision of the radial coordinate r, which was chosen to have 5 significant figures.

We can also ensure that our solutions to $h_{\mu\nu}^{1\mathrm{L}}$ are behaving as expected by checking that they are C^0 differentiable, as required in the Lorenz gauge, as shown in Fig. (5.5), though it is important to note that this is a sanity check rather than a check on the validity of the results.
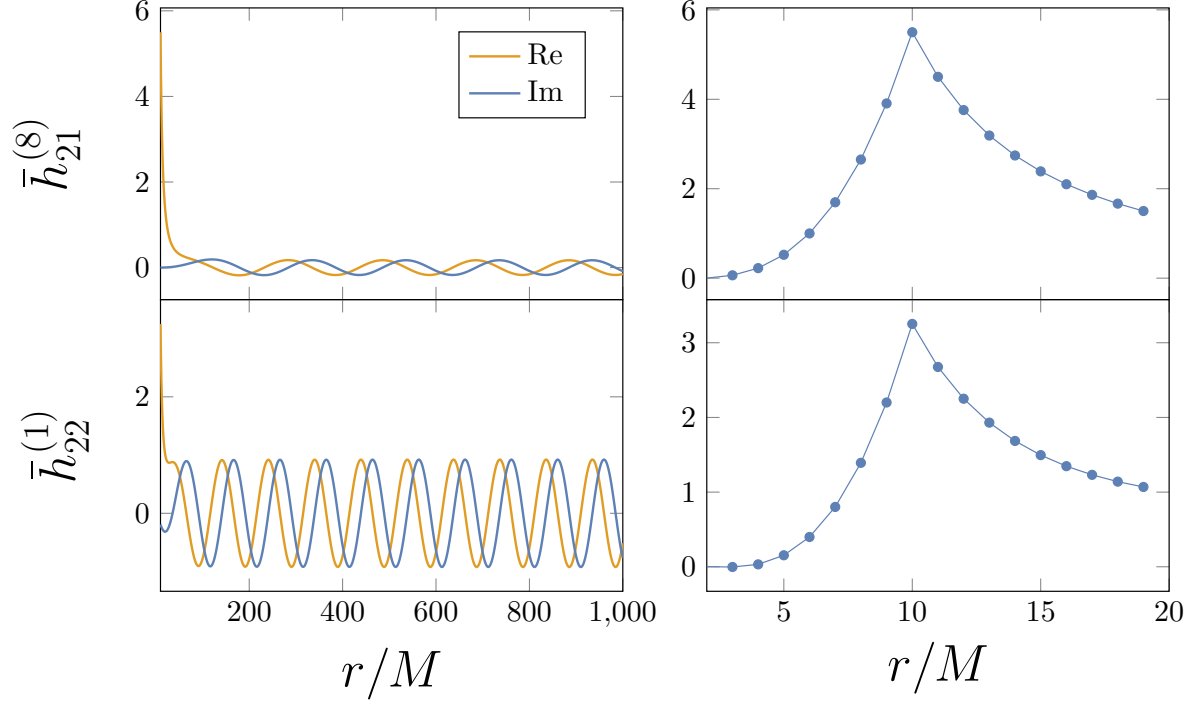
Figure 5.5: Numerical results for $h_{\mu\nu}^{1\mathrm{L}}$, with the particle at $r_0 = 10M$. The top and bottom left panels show the real and imaginary parts of $\bar{h}_{21}^{(8)}$ and $\bar{h}_{22}^{(1)}$ respectively, as r goes to infinity. The top and bottom right panels show the behaviour of the imaginary parts of $\bar{h}_{21}^{(8)}$ and $\bar{h}_{22}^{(1)}$ near the particle respectively. We find similar results for all other remaining Lorenz gauge fields, for different choices of modes, and different values of r_0. The lines joining data points in the right panels are for visualisation purposes only.

Chapter 6

The Slow Evolution of Perturbations to Schwarzschild Spacetime

In this chapter, a novel algorithm for calculating the slow-time derivative of the first-order Lorenz gauge metric perturbation will be described in detail, in addition to numerical results. We will focus on radiative modes as the static modes are known analytically [92] and thus it is straightforward to take the r_0 derivative of them. Recall from Chapter 4 the motivation for this calculation. We saw in Chapter 4 that the slow-time derivative of the metric perturbation contributes to the source of the second-order metric perturbation, which goes into calculating the GW phase to post-adiabatic order, required to perform precision tests of GR and obtain accurate parameter estimates from EMRI signals. Due to the fact that the orbital radius of an EMRI evolves slowly, for quasicircular orbits and using the two-timescale approximation, the slow-time derivative of the metric perturbation can be written as

$$\frac{dh_{\mu\nu}^{1L}}{d\tilde{t}} = \frac{dr_0}{d\tilde{t}} \frac{dh_{\mu\nu}^{1L}}{dr_0} + \mathcal{O}(\varepsilon), \tag{6.1}$$

so that the slow-time derivative becomes a derivative with respect to r_0. The terms slow-time derivative and r_0 derivative will be used interchangeably throughout this chapter, with a simple transformation between the two given above. Taking an r_0-derivative of the radial linearised Einstein field equations from Eq. (2.84) we get

$$\Box_{(j)}^{(i)} \bar{h}_{lm,r_0}^{(j)} - \mathcal{M}_{l(j)}^{(i)} \bar{h}_{lm,r_0}^{(j)} = S_{lm,r_0}^{(i)} - \Box_{(j),r_0}^{(i)} \bar{h}_{lm}^{(i)}. \tag{6.2}$$

This equation is challenging to solve for two main reasons: (i) the source on the right-hand side is unbounded, and (ii) the coupling between the tensor harmonic i-modes via the $\mathcal{M}_{l(j)}^{(i)}$ matrix increases the complexity and computational burden of the calculation. The non-compact source is particularly challenging for the standard variation of parameters approach for constructing inhomogeneous solutions to ordinary differential equations (ODEs), as this approach relies on having the homogeneous solutions computed for all radii inside the source. Nonetheless a numerical code using the variations of parameters method to find solutions to Eq. (6.2) was implemented in Ref. [121].

We present in this chapter a novel approach to calculating $\partial_{\tilde{t}} h^1_{\alpha\beta}$ by (i) making use of the gauge transformation from Regge-Wheeler (RW) to Lorenz gauge solutions [46, 102] and (ii) using the method of partial annihilators [102]. The combination of these two techniques means we only have to numerically solve homogeneous equations for a handful of uncoupled scalar fields that describe the RW master variables and their r_0 derivatives. We can then construct the inhomogeneous solutions entirely from data obtained on the world-line. We find this approach more efficient and easier to implement than the variation of parameters method with an unbounded source, such as that of Ref. [121].

Taking the r_0 derivative of Berndtson's gauge transformation [46] from Section 2.6, the slowly evolving Lorenz gauge metric perturbation can be written in terms of RWZ fields and their slow-time derivatives, in addition to the gauge field M_{2af} and its slow-time derivative, and the radial derivatives of all of the listed fields. The r_0 derivative of the first of Berndtson's gauge transformations from Eq. (2.106a) is given by

$$h_{0,r_0}(r) = \frac{1}{i\omega}\left(\psi_{1,r_0} + \frac{2\lambda}{3}\psi_{2,r_0}\right) - \frac{h_0}{\omega}\omega_{,r_0}. \tag{6.3}$$

The r_0 derivative of all of Berndtson's gauge transformations are trivial to derive from Eq. (2.106) and Eq. (2.108), and won't be detailed here for brevity. All of the results in this chapter can be found in Ref. [2] and play a vital role in the GSF program. The data for $h^{1L}_{\mu\nu,r_0}$ has already been used to calculate waveforms and the energy flux via the GSF approach and compare them with NR simulations [4, 3] in addition to comparisons with EOB theory [93, 94] and will be used in a number of forthcoming papers, for example, in the calculation of the second-order Teukolsky source, which is ongoing research by collaborators [43, 95]. In this chapter, the r_0 derivatives of the RWZ master functions and the gauge field M_{2af} will be determined, and their numerical results presented, in addition to the r_0 derivative of the first-order Lorenz gauge metric perturbation. The slowly-evolving energy flux will also be calculated to demonstrate further applications of this work. All of the results presented in this chapter were obtained in collaboration with Warburton.

6.1   Slowly evolving Regge-Wheeler and Zerilli master functions

The slowly evolving RWZ master functions, $\partial_{r_0}\psi_s$, described by the following equation, are obtained by taking the r_0 derivative of Eq. (2.49) which yields

$$\mathcal{L}_s\phi_s = S_{s,r_0} - 2\omega\omega_{,r_0}\psi_s, \tag{6.4}$$

where we have defined

$$\phi_s \equiv \psi_{s,r_0}, \tag{6.5}$$

and a comma followed by r_0 denotes a derivative with respect to r_0. Unlike S_s, the source in Eq. (6.4) is no longer compact, as ψ_s is defined over the entire domain. There are a variety of numerical techniques for finding solutions to equations of the form of Eq. (6.4) e.g., [46, 121, 95], but none of them are as efficient or easy to implement as solving an equation with a distributional

source. We can find an equation for ϕ_s with a distributional source by noticing that applying the operator $\mathcal{L}_s$ to the second term on the right hand side of Eq. (6.4), then making use of Eq. (2.49), compactifies that term. Applying the operator $\mathcal{L}_s$ to Eq. (6.4) therefore 'partially annihilates' the non-compact term on the right hand side [102, 122], yielding a fourth-order differential equation with a compact, distributional source

$$\mathcal{L}_s^2 \phi_s = \mathcal{L}_s S_{s,r_0} - 2\omega\omega_{,r_0} S_s. \tag{6.6}$$

Thus we obtain a family of fourth-order ODEs with compact sources, which we shall solve using the method of variation of parameters. As a fourth-order differential equation, there are four independent homogeneous solutions. Two of these are the homogeneous solutions to Eq. (2.49) as $\mathcal{L}(\mathcal{L}(\psi_s^\pm)) = \mathcal{L}(0) = 0$. The remaining two we denote by $\phi_s^{h4,\pm}$. These are homogeneous solutions to the fourth-order equation Eq. (6.6) but not the second-order equation, Eq. (2.49), and have the asymptotic boundary conditions

$$\phi_s^{h4,+} \propto r e^{i\omega r_*}, \quad \text{as} \quad r_* \to \infty, \tag{6.7}$$

$$\phi_s^{h4,-} \propto \log(f(r)) e^{-i\omega r_*}, \quad \text{as} \quad r_* \to -\infty. \tag{6.8}$$

Similarly to Eq. (5.1), and due to the distributional source, we can write the inhomogeneous solution as

$$\phi_s(r) = \left[c_s^{h2,+} \psi_s^+(r) + c_s^{h4,+} \phi_s^{h4,+}(r) \right] \Theta(r - r_0) + \left[c_s^{h2,-} \psi_s^-(r) + c_s^{h4,-} \phi_s^{h4,-}(r) \right] \Theta(r_0 - r) \tag{6.9}$$
$$+ c_s^\delta \phi_s^\delta(r) \delta(r - r_0),$$

where the constant coefficients (for a given s, l, m, r_0) are given by

$$c_s^{i,+} \Theta(r - r_0) = \int_{-\infty}^{r_*} \frac{\mathcal{W}_s^{i,+}(r'_*) \, \mathcal{S}_s(r'_*)}{\mathcal{W}_s} \mathrm{d}r'_*, \tag{6.10}$$

$$c_s^{i,-} \Theta(r_0 - r) = \int_{r_*}^{\infty} \frac{\mathcal{W}_s^{i,-}(r'_*) \, \mathcal{S}_s(r'_*)}{\mathcal{W}_s} \mathrm{d}r'_*, \tag{6.11}$$

where $i \in \{h2, h4\}$ and $\mathcal{S}_s$ is defined as

$$\mathcal{S}_s \equiv \mathcal{L}_s S_{s,r_0} - 2\omega\omega_{,r_0} S_s. \tag{6.12}$$

The fourth-order Wronskian $\mathcal{W}_s$ is also constant by Abel's Theorem and has the standard definition

$$\mathcal{W}_s = \det \begin{pmatrix} \psi_s^- & \phi_s^{h4,-} & \psi_s^+ & \phi_s^{h4,+} \\ \partial_{r_*} \psi_s^- & \partial_{r_*} \phi_s^{h4,-} & \partial_{r_*} \psi_s^+ & \partial_{r_*} \phi_s^{h4,+} \\ \partial_{r_*}^2 \psi_s^- & \partial_{r_*}^2 \phi_s^{h4,-} & \partial_{r_*}^2 \psi_s^+ & \partial_{r_*}^2 \phi_s^{h4,+} \\ \partial_{r_*}^3 \psi_s^- & \partial_{r_*}^3 \phi_s^{h4,-} & \partial_{r_*}^3 \psi_s^+ & \partial_{r_*}^3 \phi_s^{h4,+} \end{pmatrix}, \tag{6.13}$$

and $\mathcal{W}_s^{h2/4,\pm}$ are given by the determinant of the matrices obtained from deleting the final row and the column containing the corresponding field, $\phi_s^{h2/4,\pm}$ and its derivatives from the matrix in Eq. (6.13) [123, 102], where we have defined $\phi_s^{h2,\pm} \equiv \psi_s^{\pm}$. The field $\phi_s^{\delta}(r)$ in Eq. (6.9) is required to balance the forth derivative of the delta function that appears in the source in Eq. (6.6).

Owing to the distributional source, the integrals in Eqs. (6.10) and (6.11) can be carried out analytically by repeated application of integration by parts. An equivalent approach is to match the coefficients of the delta function and its derivatives from the left- and right-hand side of Eq. (6.6). Following from Eq. (5.8) and Eq. (6.12), $\mathcal{S}_s$ takes the form

$$\mathcal{S}_s = a_0(r,r_0)\delta(r-r_0) + a_1(r,r_0)\delta'(r-r_0) + a_2(r,r_0)\delta''(r-r_0) + a_3(r,r_0)\delta'''(r-r_0) \qquad (6.14)$$
$$+ a_4(r,r_0)\delta^{(4)}(r-r_0),$$

where the functions $a_0(r,r_0),\ldots,a_1(r,r_0)$ can be identified with combinations of $p(r,r_0)$, $q(r,r_0)$ and their derivatives with respect to r and r_0 by replacing the $\mathcal{S}_s$ in Eq. (6.12) with the right-hand side of Eq. (5.8). Making use of the following identity

$$f(r)\delta(r-r_0) = f(r_0)\delta(r-r_0), \qquad (6.15)$$

and other identities derived from radial derivatives of Eq. (6.15), given in Appendix C, the source $\mathcal{S}_s$ can be written in terms of Dirac delta functions and their radial derivatives with constant coefficients

$$\mathcal{S}_s = b_0(r_0)\delta(r-r_0) + b_1(r_0)\delta'(r-r_0) + b_2(r_0)\delta''(r-r_0) + b_3(r_0)\delta'''(r-r_0) \qquad (6.16)$$
$$+ b_4(r_0)\delta^{(4)}(r-r_0),$$

where the constants $b_0(r_0),\ldots,b_4(r_0)$ can be identified with combinations of $a_0(r_0,r_0),\ldots,a_4(r_0,r_0)$ and their radial derivatives, evaluated at $r = r_0$ such that they are now functions of r_0 only. As an example, the coefficients of the Dirac delta functions and their derivatives are given explicitly for the odd-sector source for spin-weight $s = 2$ in Appendix D. Substituting Eq. (6.9) into Eq. (6.6), and making use of Eq. (6.15) and other identities from Appendix C, we obtain

$$\mathcal{L}_s^2 \phi_s = \beta_1(r)\Theta(r-r_0) + \beta_2(r)\Theta(r_0-r) + c_0(r_0)\delta(r-r_0) + c_1(r_0)\delta'(r-r_0) \qquad (6.17)$$
$$+ c_2(r_0)\delta''(r-r_0) + c_3(r_0)\delta'''(r-r_0) + c_4(r_0)\delta^{(4)}(r-r_0),$$

where $c_0(r_0),\ldots,c_4(r_0)$ can be identified with combinations of $c_s^{h2/4,\pm}$ and c_s^{δ}. Immediately we find $\beta_1(r) = \beta_2(r) = 0$ as these coefficients satisfy the homogeneous field equation, and there are no Heaviside terms on the right-hand side of Eq. (6.6). Equating the constant coefficients of the Dirac delta functions and their radial derivatives from Eq. (6.17) with those in Eq. (6.16), we obtain a linear system which we can solve for $c_s^{h2/4,\pm}$ and c_s^{δ} in terms of $p(r_0,r_0)$, $q(r_0,r_0)$ and their derivatives, evaluated at $r = r_0$.

We can write this linear system of equations in the following form

$$\mathbf{C}_s = \mathbf{\Phi}_s^{-1} \cdot \mathbf{J}_s, \tag{6.18}$$

where $\mathbf{C}_s = (c_s^{h2,-}, c_s^{h4,-}, c_s^{h2,+}, c_s^{h4,+})$ and

$$\mathbf{\Phi}_s = \begin{pmatrix} -\psi_s^- & -\phi_s^{h4,-} & \psi_s^+ & \phi_s^{h4,+} \\ -\partial_r\psi_s^- & -\partial_r\phi_s^{h4,-} & \partial_r\psi_s^+ & \partial_r\phi_s^{h4,+} \\ -\partial_r^2\psi_s^- & -\partial_r^2\phi_s^{h4,-} & \partial_r^2\psi_s^+ & \partial_r^2\phi_s^{h4,+} \\ -\partial_r^3\psi_s^- & -\partial_r^3\phi_s^{h4,-} & \partial_r^3\psi_s^+ & \partial_r^3\phi_s^{h4,+} \end{pmatrix}_{r=r_0} . \tag{6.19}$$

The vector $\mathbf{J}_s$ is given by $\mathbf{J} = (J_0, J_1, J_2, J_3)$ where J_n is the jump in the nth derivative of ϕ_s on the world-line. We give the explicit form of $\phi_s^\delta(r_0)$ and these jumps for the $s = 2$ RW field in odd-sector in Appendix E. The jump conditions for the Zerilli master function are too long to write here but are included in the supplemental material of Ref. [2].

6.1.1   Numerical boundary conditions and implementation

The asymptotic boundary conditions for $\phi_s^{h4,\pm}$, given in Eqs. (6.7) and (6.8), can be expanded as

$$\phi_s^{h4,+}(r) = re^{i\omega r_*} \sum_{i=0}^{n_{\max}} \frac{[A_i^{h4,+} + B_i^{h4,+} \log(r)]}{(r\omega)^i}\bigg|_{r=r_{\text{out}}}, \tag{6.20}$$

$$\phi_s^{h4,-}(r) = e^{-i\omega r_*} \sum_{i=0}^{n_{\max}} [A_i^{h4,-} + B_i^{h4,-} \log(f(r))]f(r)^i\big|_{r=r_{\text{in}}}. \tag{6.21}$$

As before, the coefficients $A_i^{h4,\pm}$ and $B_i^{h4,\pm}$ depend on the parameters s, l, m, r_0 and are derived by substituting the above ansätze into the fourth-order equations Eq. (6.6), and should not be confused with the coefficients from Section 5.2.1 which are labelled similarly. The recurrence relations for these coefficients is provided in the supplementary material of Ref. [2], and depend on the choice of potential, either RW or Zerilli. The series approximation to the homogeneous solutions near the boundaries are then given in terms of one of the leading coefficients. For the expansion at large radius for both the RW and Zerilli cases we find $A_0^{h4,+} = B_1^{h4,+}/2$ and $B_0^{h4,+} = 0$. For the series approximation that satisfies the homogeneous fourth-order equation, but not the homogeneous second-order equation, we find we can set, e.g., $B_1^{h4,+} = 1$ and $A_1^{h4,+} = 0$. Note if we set $B_1^{h4,+} = 0$ and $A_1^{h4,+} = 1$ we recover the boundary condition expansion in Eq. (5.15) above for the homogeneous second-order equation. For the expansion near the horizon we find that setting $A_0^{h4,-} = 0$ and $B_0^{h4,-} = 1$ provides an approximate solution to the fourth-order equation (but not the second-order equation). Setting $A_0^{h4,-} = 1$ and $B_0^{h4,-} = 0$ we similarly recover the boundary condition in Eq. (5.16). Once the value of the leading terms is set, all other coefficients are then determined by the recurrence relations. These homogeneous solutions are not calculated by any package in the BHPToolkit so we solve the recurrence relations with the above conditions. This provides the

boundary conditions at r_{out} and r_{in} and we use the `NDSolve` function of *Mathematica* to numerically integrate the solutions to r_0. As mentioned in Chapter 5, we once again find that a value of $n_{\text{max}} = 50$ is sufficient to ensure the series expansions satisfy the homogeneous field equation to beyond machine precision.

6.1.2   Numerical results

Using the homogeneous solutions computed numerically as described in Section 5.1.1 and the jump conditions from Eq. (6.18), Appendix E and the supplementary material of Ref. ([2]), we obtained numerical results for the r_0 derivatives of all of the RWZ master functions. As an example, in Fig. (6.1) we plot the results of the spin-weight $s = 2$ RW master function for the $(l, m) = (2, 1)$ mode at $r_0 = 10M$ out to large r.
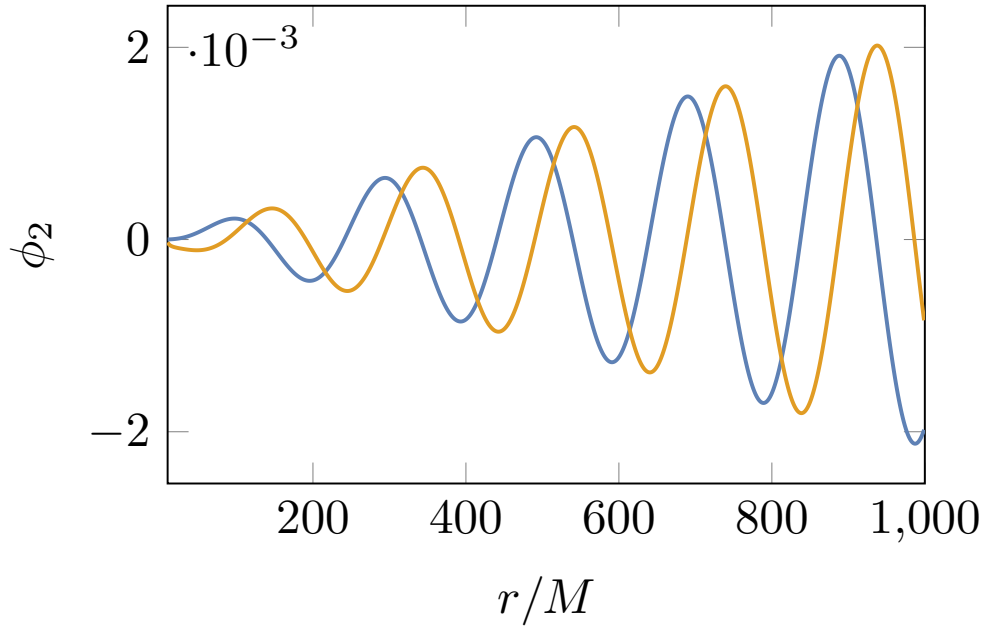
Figure 6.1:   Real and imaginary parts of $\phi_2 = \psi_{2,r_0}$ for the $(l, m) = (2, 1)$ mode with $r_0 = 10M$. The amplitude of the wave grows proportional to r for large r, as determined by the asymptotic boundary condition in Eq. (6.20).

To test the results of our partial annihilator method, we check that ϕ_2 satisfies the original second-order equation with a non-compact source, Eq. (6.4). Our numerical integrator returns the ϕ_2 and its first, second, and third radial derivatives which we use to compute the left-hand side of Eq. (6.4). We compute the right-hand side of Eq. (6.4) using the inhomogeneous solution to ψ_2 calculated in Chapter 5 and find this matches the left-hand side to near machine precision. We give an example of this for the $(l, m) = (2, 1)$ mode in Figure 6.2.
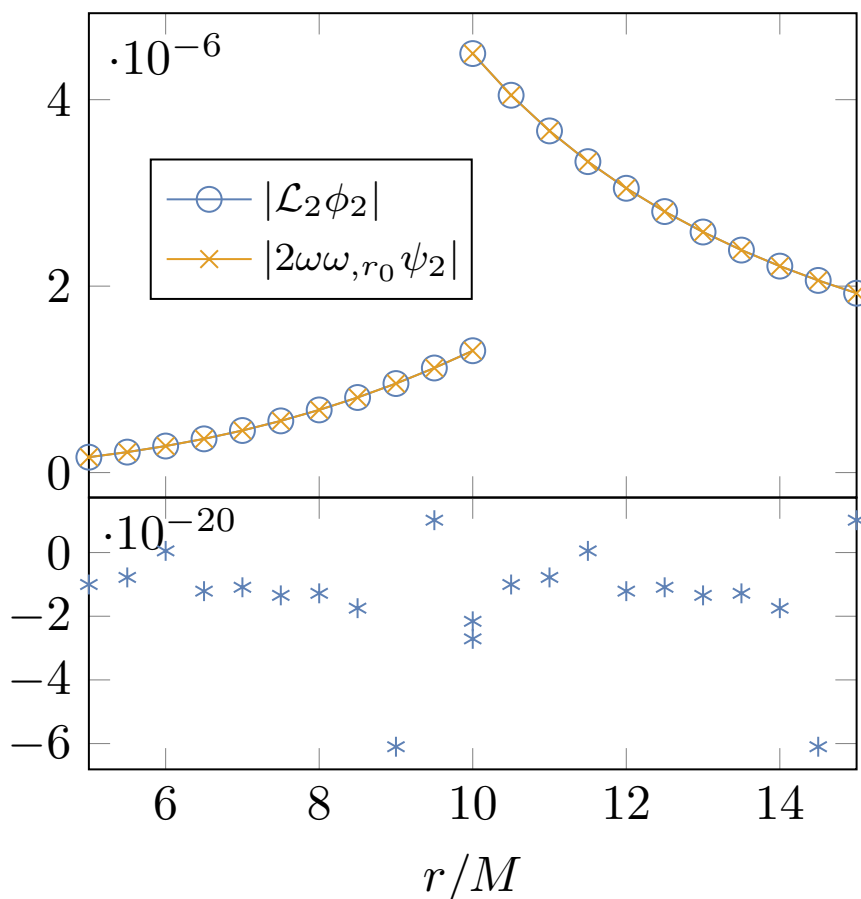
Figure 6.2: Absolute values of the left and right hand sides of Eq. (6.4). The top panel demonstrates that our calculation of ϕ_2, where $\phi_2 = \psi_{2,r_0}$, for $r_0 = 10M$ and $(l, m) = (2, 1)$ solves Eq. (6.4), ignoring terms involving the Dirac delta functions and its derivatives. The lower panel shows the absolute value of the difference between the data sets for the left- and right-hand side of Eq. (6.4). This error is dominated by the interpolation of the numerical homogeneous solutions and their radial derivatives. When performing the numerical integration, the default method for interpolation of *Mathematica* was used, with the options set are `WorkingPrecision` $\rightarrow 40$, `MaxSteps` $\rightarrow 10^6$, `InterpolationOrder` $\rightarrow$ `All`. A numerical choice for the interpolation order such as 10 would decrease the accuracy but increase the speed of the code. The lines joining data points are for visualisation purposes only.

6.2 Slowly evolving gauge field M_{2af}

To compute the slow-time derivative of the Lorenz gauge metric perturbation we must also compute M_{2af,r_0}. By taking an r_0 derivative of Eq. (5.17) we obtain

$$\mathcal{L}_0 M_{2af,r_0} = f\phi_0 - 2\omega\omega_{,r_0} M_{2af}, \tag{6.22}$$

which also has a unbounded source. In fact both terms on the right hand side of Eq. (6.22) are unbounded as they are defined everywhere from the horizon to infinity. We can choose to write M_{2af,r_0} as a linear combination of two fields such that

$$M_{2af,r_0}(r) = \chi_1(r) + \chi_2(r), \tag{6.23}$$

with

$$\mathcal{L}_0 \chi_1 = f\phi_0, \tag{6.24}$$

$$\mathcal{L}_0 \chi_2 = -2\omega\omega_{,r_0} M_{2af}. \tag{6.25}$$

As both of these equations have unbounded sources, we turn once again to the method of partial annihilators. By making use of Eq. (2.49) for $s = 0$, Eq. (6.4) and Eq. (5.17), we obtain two sixth-order ODEs with distributional sources

$$\mathcal{L}_0^2 \left(\frac{1}{f} \mathcal{L}_0 \chi_1 \right) = \mathcal{L}_0 S_{0,r_0} - 2\omega\omega_{,r_0} S_0, \tag{6.26}$$

$$\mathcal{L}_0 \left(\frac{1}{f} \mathcal{L}_0^2 \chi_2 \right) = -2\omega\omega_{,r_0} S_0, \tag{6.27}$$

which we shall also solve via the method of variation of parameters. Both Eq. (6.26) and Eq. (6.27) have six independent homogeneous solutions. For Eq. (6.26), four of these are given by $\psi_0^\pm$ and $M_{2af}^{h4,\pm}$. The final pair we will denote by $\chi_1^{h6,\pm}$ which satisfy the homogeneous sixth-order equation but neither the homogenous second-order equation $\left(\mathcal{L}_0 \chi_1^{h6,\pm} \neq 0 \right)$ nor the homogenous fourth-order equation $\left(\mathcal{L}_0 (1/f\mathcal{L}_0) \chi_1^{h6,\pm} \neq 0 \right)$. For Eq. (6.27), four of the homogeneous solutions are given by $\psi_0^\pm$ and $\phi_0^\pm$. Similarly we will denote the final pair by $\chi_2^{h6,\pm}$.

6.2.1 Numerical boundary conditions and implementation

For our numerical scheme we use the following series expansion of the $\chi_k^{h6,\pm}$ fields at finite radii as boundary conditions

$$\chi_k^{h6,+}(r_{\text{out}}) = r^2 e^{i\omega r_*} \sum_{i=0}^{n_{\max}} \frac{A_{k,i}^{h6,+} + B_{k,i}^{h6,+} \log(r)}{(r\omega)^i} \Bigg|_{r=r_{\text{out}},} \tag{6.28}$$

and

$$\chi_k^{h6,-}(r_{\text{in}}) = e^{-i\omega r_*}\sum_{i=0}^{n_{\max}}[A_{k,i}^{h6,-} + B_{k,i}^{h6,-}\log(f(r))]f(r)^i\big|_{r=r_{\text{in}},} \tag{6.29}$$

where $k \in \{1,2\}$. The recursion relations for $A_{k,i}^{h6,\pm}$ and $B_{k,i}^{h6,\pm}$ are derived by substituting the above ansätze into Eq. (6.26) and Eq. (6.27). Similarly to those for M_{2af}, the recursion relations depend on the parameters l, m and r_0. These recurrence relations are provided in the supplementary material of Ref. [2]. For $\chi_1^{h6,+}$ the three undetermined coefficients are $A_{1,1}^{h6,+}, A_{1,2}^{h6,+}$ and $B_{1,1}^{h6,+}$. The field equations Eq. (6.26) and Eq. (6.27) also enforce that $B_{0,0}^{h6,+} = 0$, $A_{1,0}^{h6,+} = B_{1,1}^{h6,+}/4$ and $B_{1,2}^{h6,+} = i(l(l+1)+1+4i\omega)B_{1,1}^{h6,+}/2\omega$. Setting $A_{1,1}^{h6,+} = B_{1,1}^{h6,+} = 0$ and $A_{1,2}^{h6,+} = 1$ we find the series in Eq. (6.28) approximates a solution that satisfies Eq. (6.26) in the homogenous case, but not the homogenous ODEs with operators $\mathcal{L}_0$ or $\mathcal{L}_0(1/f\mathcal{L}_0)$. Thus $\chi_1^{h6,+}$ is a linearly independent of the other two bases $\{\psi_0^+, M_{2af}^{h4,+}\}$. For $\chi_1^{h6,-}$ the three undetermined coefficients are $A_{1,0}^{h6,-}, A_{1,1}^{h6,-}$ and $B_{1,1}^{h6,-}$. The field equation also sets $B_{1,0}^{h6,-} = 0$. Setting $A_{1,0}^{h6,-} = A_{1,1}^{h6,-} = 0$ and $B_{1,1}^{h6,-} = 1$ we find the series in Eq. (6.29) approximates a solution that satisfies Eq. (6.26) in the homogenous case, but neither the second- nor fourth-order ODEs. This demonstrates that we have found another linearly independent homogeneous solution.

For $\chi_2^{h6,+}$, the three undetermined coefficients are $A_{2,0}^{h6,+}, A_{2,1}^{h6,+}$ and $A_{1,1}^{h6,+}$. The field equations Eq. (6.26) and Eq. (6.27) also enforce that $B_{2,0}^{h6,-} = B_{2,1}^{h6,-} = 0$ and $B_{2,1}^{h6,-} = -i(4+l+l^2)A_{2,0}^{h6,+}/\omega + 2_{2,1}^{h6,+}$. Setting $A_{2,0}^{h6,+} = 1$ and $A_{2,1}^{h6,+} = A_{2,2}^{h6,+} = 0$ we find the series in Eq. (6.28) approximates a solution that satisfies Eq. (6.27) in the homogenous case, but not the homogeneous ODEs with operators $\mathcal{L}_0$ or $\mathcal{L}_0^2$. Thus $\chi_2^{h6,+}$ is linearly independent from the other two bases $\{\psi_0^+, \phi^{h4,+}\}$. For $\chi_2^{h6,-}$ the three undetermined coefficients are $A_{2,0}^{h6,-}, A_{2,1}^{h6,-}$ and $B_{2,0}^{h6,-}$. The field equation also enforces that $B_{2,1}^{h6,-} = i(1+l+l^2)B_{2,0}^{h6,-}/(i+4\omega)$. Setting $A_{2,0}^{h6,-} = A_{2,1}^{h6,-} = 0$ and $B_{2,0}^{h6,-} = 1$ we find the series in Eq. (6.29) approximates a solution that satisfies Eq. (6.27) but not the second- or fourth-order ODEs. This demonstrates that we have found the final linearly independent homogeneous solution. We can then write the retarded solutions to Eq. (6.26) and Eq. (6.27) in the form

$$\chi_1(r) = \chi_1^-(r)\Theta(r_0 - r) + \chi_1^+(r)\Theta(r - r_0), \tag{6.30}$$

$$\chi_2(r) = \chi_2^-(r)\Theta(r_0 - r) + \chi_2^+(r)\Theta(r - r_0), \tag{6.31}$$

where

$$\chi_1^\pm(r) = \left(c^{h2,\pm}\psi_0^\pm(r) + c^{h4,\pm}M_{2af}^{h4,\pm}(r) + c^{h6,\pm}\chi_1^{h6,\pm}(r)\right), \tag{6.32}$$

$$\chi_2^\pm(r) = \left(c^{h2,\pm}\psi_0^\pm(r) + c^{h4,\pm}\phi_0^{h4,\pm}(r) + c^{h6,\pm}\chi_2^{h6,\pm}(r)\right). \tag{6.33}$$

The coefficients in the above equations can be found by substituting Eqs. (6.30) and (6.31) into Eqs. (6.26) and Eqs. (6.27), respectively, and matching the coefficients of the delta functions and their derivatives on the left- and right-hand sides of the resulting equations. For χ_1 we can once

again write the resulting system of equations in the now familiar form

$$\mathbf{C} = \mathbf{\Phi}^{-1} \cdot \mathbf{J}, \tag{6.34}$$

where $\mathbf{C} = (c^{h2,-}, c^{h4,-}, c^{h6,-}, c^{h2,+}, c^{h4,+}, c^{h6,+})$ and

$$\mathbf{\Phi} = \begin{pmatrix} -\psi_0^- & -M_{2af}^{h4,-} & -\chi_1^{h6,-} & \psi_0^+ & M_{2af}^{h4,+} & \chi_1^{h6,+} \\ -\partial_r\psi_0^- & -\partial_r M_{2af}^{h4,-} & -\partial_r^2\chi_1^{h6,-} & \partial_r\psi_0^+ & \partial_r M_{2af}^{h4,+} & \partial_r\chi_1^{h6,+} \\ -\partial_r^2\psi_0^- & -\partial_r^2 M_{2af}^{h4,-} & -\partial_r^3\chi_1^{h6,-} & \partial_r^2\psi_0^+ & \partial_r^2 M_{2af}^{h4,+} & \partial_r^2\chi_1^{h6,+} \\ -\partial_r^3\psi_0^- & -\partial_r^3 M_{2af}^{h4,-} & -\partial_r^4\chi_1^{h6,-} & \partial_r^3\psi_0^+ & \partial_r^3 M_{2af}^{h4,+} & \partial_r^3\chi_1^{h6,+} \\ -\partial_r^4\psi_0^- & -\partial_r^4 M_{2af}^{h4,-} & -\partial_r^4\chi_1^{h6,-} & \partial_r^4\psi_0^+ & \partial_r^4 M_{2af}^{h4,+} & \partial_r^4\chi_1^{h6,+} \\ -\partial_r^5\psi_0^- & -\partial_r^5 M_{2af}^{h4,-} & -\partial_r^5\chi_1^{h6,-} & \partial_r^5\psi_0^+ & \partial_r^5 M_{2af}^{h4,+} & \partial_r^5\chi_1^{h6,+} \end{pmatrix}_{r=r_0}. \tag{6.35}$$

For χ_1, the four non-zero components of the vector $\mathbf{J}$ are given in Appendix E.0.2. For χ_2, the matrix $\mathbf{\Phi}$ is the same in Eq. (6.35) except $M_{2af}^{h4,\pm}$ is replaced by $\phi_0^{h4,\pm}$ and $\chi_1^{h6,\pm}$ is replaced by $\chi_2^{h6,\pm}$. As the source for χ_2 contains only Dirac delta functions with no radial derivatives, the vector $\mathbf{J}$ has only one non-zero component and we find that $\mathbf{J} = (0, 0, 0, 0, 0, J_5)$ where

$$J_5 = -\frac{48\pi m^2 M \sqrt{r_0 - 3M}}{r_0^{3/2}(r_0 - 2M)^4} Y_{lm}^*(\pi/2, 0). \tag{6.36}$$

6.2.2   Numerical results

We check that our solution for M_{2af,r_0}, computed as the sum of the solutions of two inhomogeneous sixth-order equations, Eq. (6.26) and Eq. (6.27), satisfies the original second-order equation, Eq. (6.22), with an unbounded source.
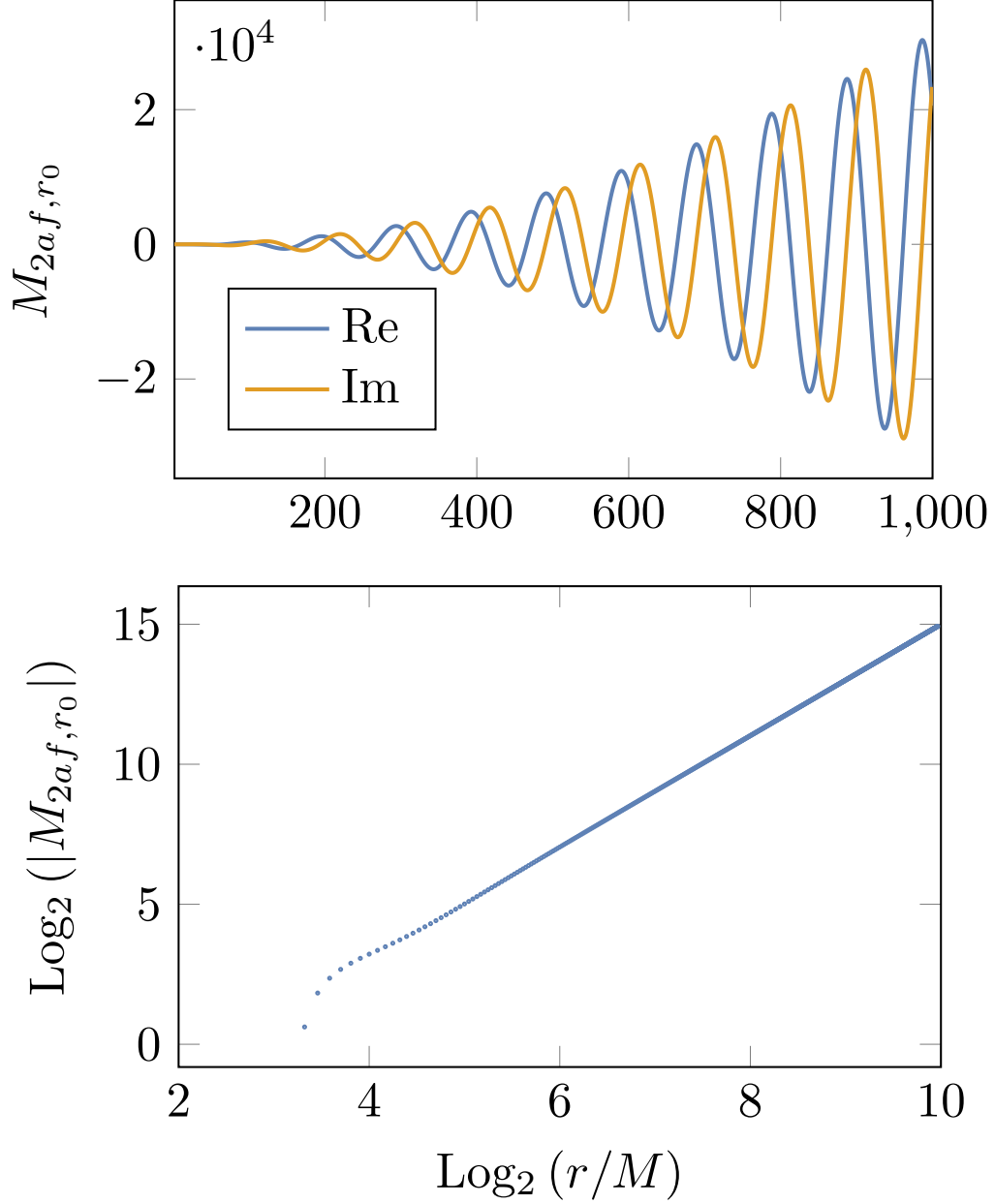
Figure 6.3: Top panel: Real and imaginary parts of M_{2af,r_0} for the $(l,m) = (2,2)$ mode with $r_0 = 10M$. The amplitudes of the fields grow as r^2 at large r, as determined by the asymptotic boundary condition Eq. (6.28). Similar results are obtained for other even-sector multiple modes and different values of r_0. Bottom panel: demonstrates r^2 behaviour at large r.

Figure 6.4 then shows that the relevant second-order equations are satisfied to near machine precision.
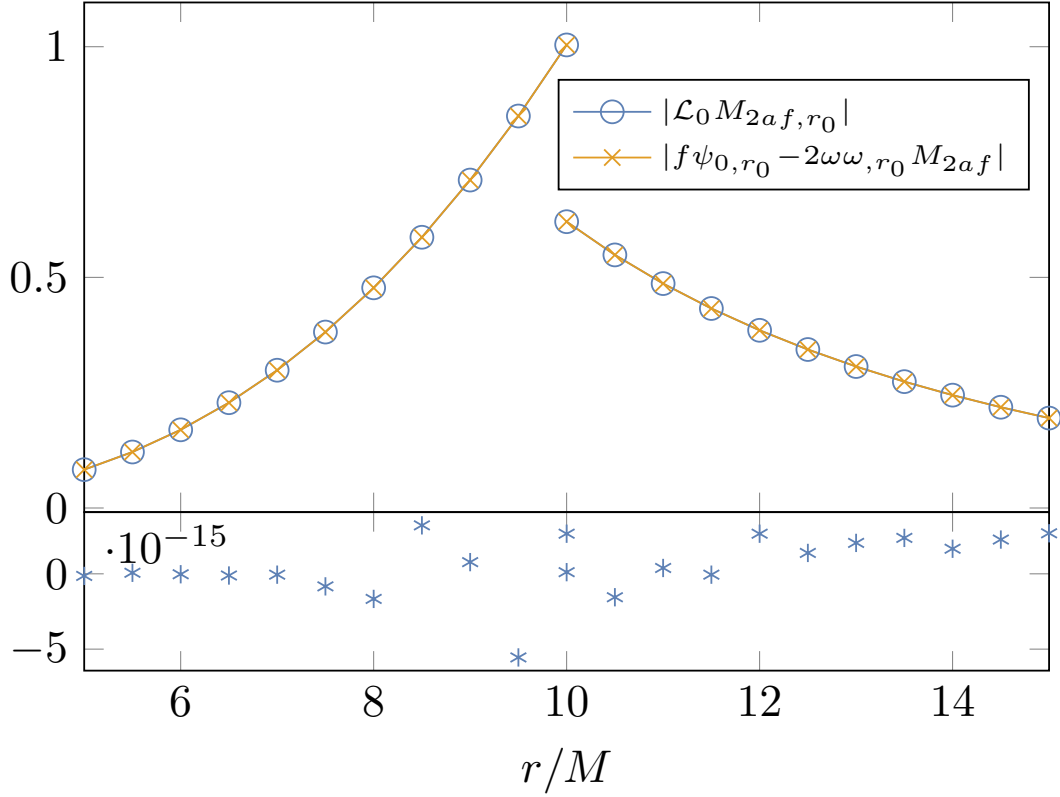
Figure 6.4: The top panel shows the absolute values of the left- and right-hand sides of Eq. (6.22), for M_{2af,r_0} given the solution computed using Eq. (6.23) and the two sixth-order equations, Eq. (6.26) and Eq. (6.27). The data shown is for $r_0 = 10M$ and $(l, m) = (2, 2)$. The lower panel shows the absolute value of the difference between the data sets for the left- and right-hand side of Eq. (6.22) is near machine precision. The lines joining data points are for visualisation purposes only.

6.3 Numerical results for the slowly evolving Lorenz gauge metric perturbation

Sample results of $h^{1L}_{\mu\nu,r_0}$ are presented below in Fig. (6.5).
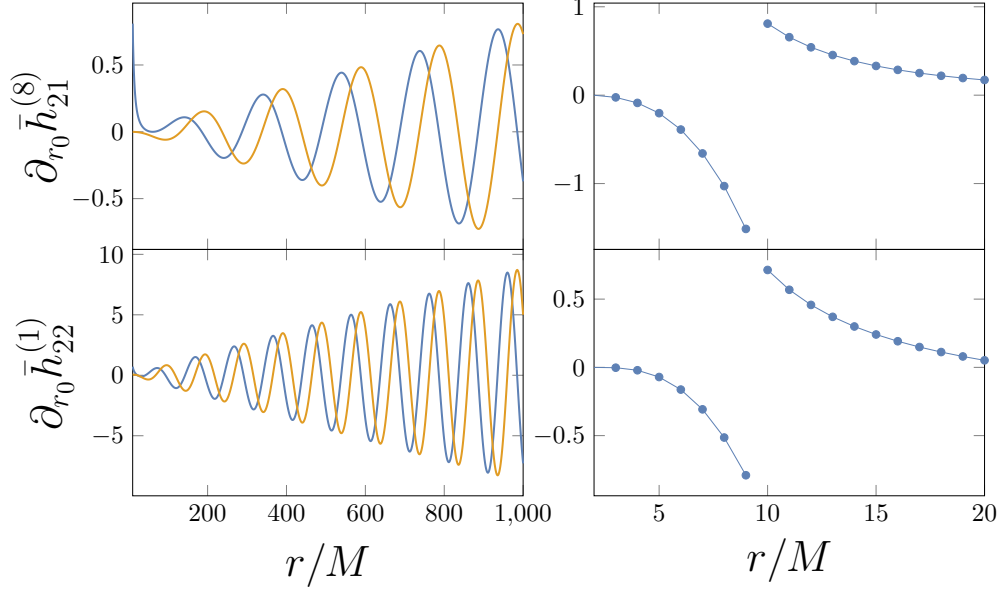
Figure 6.5: Numerical results for $h^{1L}_{\mu\nu,r_0}$, with the particle at $r_0 = 10M$. The top and bottom left panels show the real and imaginary parts of $\partial_{r_0}\bar{h}^{(8)}_{21}$ and $\partial_{r_0}\bar{h}^{(1)}_{22}$ respectively, as r tends towards infinity. The top and bottom right panels show the behaviour of the imaginary parts of $\partial_{r_0}\bar{h}^{(8)}_{21}$ and $\partial_{r_0}\bar{h}^{(1)}_{22}$ near the particle respectively. We find similar results for all other remaining Lorenz gauge fields, for different choices of modes, and different values of r_0. The lines joining data points in the right panels are for visualisation purposes only.

As a check on our results for $\partial_{r_0}\bar{h}^{(i)}_{lm}$ we compare them with a numerically computed r_0 derivative of $\bar{h}^{(i)}_{lm}$. In our check we computed data from our partial annihilator method at $r = 50M$ with r_0 ranging from $6.4M$ to $7.3M$ in steps of $0.1M$. The numerical derivatives are obtained by interpolating data for the metric perturbation for different values of r_0, keeping the field point r constant. For the numerical derivatives data was computed at $r = 50M$ for r_0 ranging from $6.5M$ to $7.5M$ in steps of $0.1M$. The end points of the interpolation were then discarded to mitigate error. We present the result of the comparison in Fig. 6.6 where we find near machine precision agreement between our results for $\partial_{r_0}\bar{h}^{(8)}_{21}$ and $\partial_{r_0}\bar{h}^{(1)}_{22}$ and the numerical r_0 derivatives of $\bar{h}^{(8)}_{21}$ and $\bar{h}^{(1)}_{22}$ respectively. In general, using numerical derivatives is less accurate and much less efficient as data for each field point r needs to be calculated for a number of values of r_0 to interpolate and differentiate. As such, our method of calculating $h^{1L}_{\mu\nu,r_0}$ is favourable.
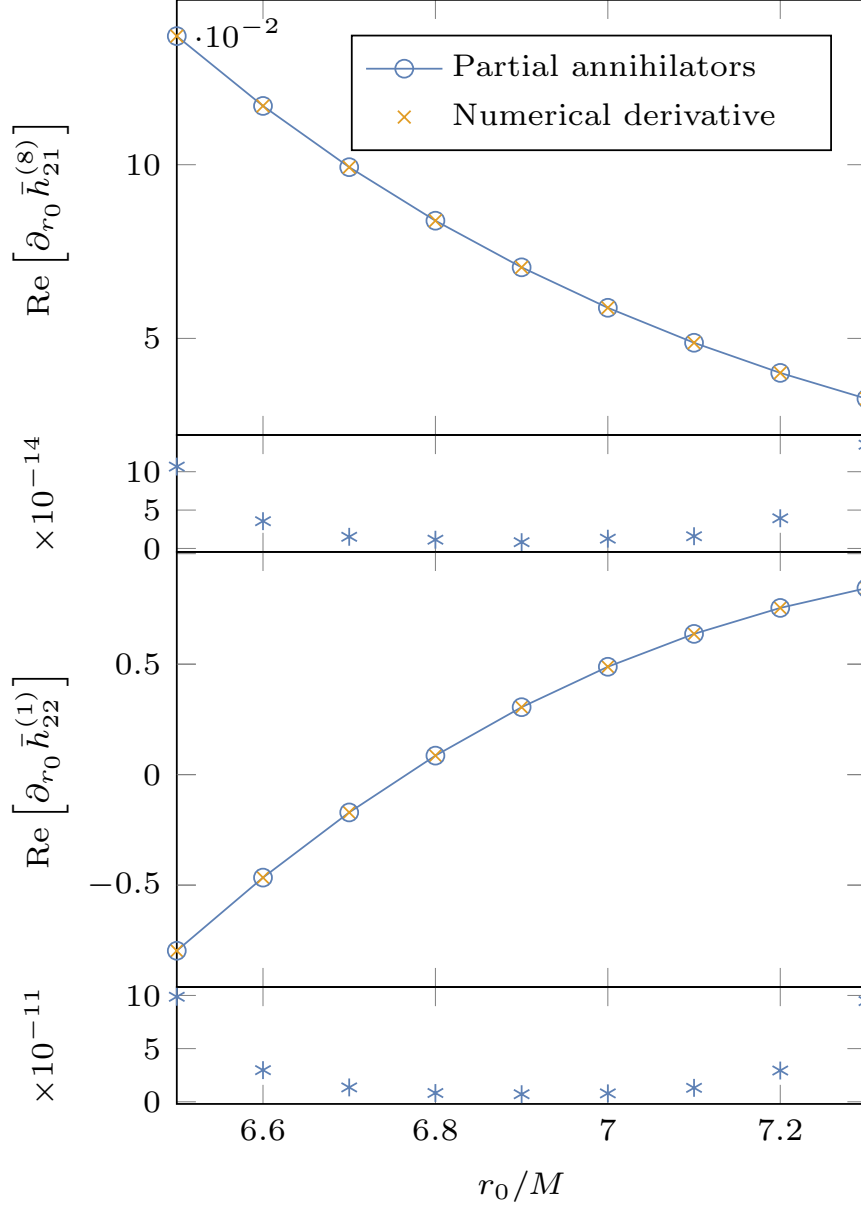
Figure 6.6: Comparison of numerical results for $h^{1L}_{\mu\nu,r_0}$ computed using the partial annihilator method and by taking a numerical derivative of $h^{1L}_{\mu\nu}$. The top panel shows the real part of $\partial_{r_0}\bar{h}^{(8)}_{21}$ and the third panel shows the real part of $\partial_{r_0}\bar{h}^{(1)}_{22}$ at a fixed field point $r = 50$ as a function of r_0. The second and forth panels show that the absolute value of the difference between numerically computing the r_0 derivative and computing the r_0 derivative using our partial annihilators method is near machine precision. The error is larger near the end points on the plot due to the fact that the error from interpolating data is larger at the end points. The error is also greater in the even-sector due to the larger number of fields involved in calculating the metric perturbation. We find similar results for all other remaining Lorenz gauge fields, their radial derivatives as well as for a different choice of modes, fixed field point and set of radii r_0. The lines joining data points are for visualisation purposes only.

It is instructive to consider the efficiency of the partial annihilator approach versus taking the numerical derivative for computing the slowly evolving metric perturbation. One significant new calculation introduced in the gauge transformation in the even sector is the calculation of M_{2af,r_0}. Using the partial annihilator method we must solve the left-hand side of Eq. (6.26) 6 times and Eq. (6.27) 4 times (two less as two of the bases are the same as for Eq. (6.26)), giving a total of 10 ODE evaluations. Computing M_{2af} requires solving the left-hand side of Eq. (5.18) 4 times and to numerically calculate its r_0 derivative to a relative precision of $\sim 10^{-15}$ at, e.g., $r_0 = 7.5M$ we find we must evaluate M_{2af} 8 times at equally spaced radii between $r_0 = 7.5 \pm 0.1M$ and fit to an eighth-order polynomial. This gives a total of $4 \times 8 = 32$ ODE evaluations. This means our approach is $32/10 = 3.2$ times faster than numerically computing the derivative of M_{2af,r_0}. In practice, when computing $h_{\mu\nu,r_0}^{1L}$ the speed up is about twice this as four of the homogeneous solutions for Eqs. (6.26) and (6.26), namely $\psi_0^{\pm}$ and $\phi_0^{\pm}$, will already be computed in other parts of the calculation.

6.4   Slowly evolving energy flux

In order to calculate the GW energy flux radiated to null infinity we consider perturbations with constant retarded time, $u = t - r_*$. These perturbations can be related to the perturbations on constant t slices via

$$\psi_2^{lm,[u]} = \psi_2^{lm} e^{-i\omega r_*}, \tag{6.37}$$

where ψ_2^{lm} denotes evaluation on t slicing and $\psi_2^{lm,[u]}$ on u slicing, and we have reintroduced the labels l and m. The GW energy flux radiated to infinity can then be calculated via [103, 124]

$$\dot{E}_{lm}^{\infty} = \frac{\lambda l(l+1)}{8\pi} g(r_0) |\psi_2^{lm,[u]}|_{r \to \infty}^2, \tag{6.38}$$

$$= \frac{\lambda l(l+1)}{8\pi} g(r_0) |c_{2,lm}^+|^2, \tag{6.39}$$

where $g(r_0) = 1$ for the RW case in the odd-sector, $g(r_0) = (\omega/2)^2$ for the Zerilli case in the even-sector, and the limit to infinity is taken with respect to fixed retarded time. Taking an r_0 derivative of Eq. (6.38) we obtain

$$\partial_{r_0} \dot{E}_{lm}^{\infty} = \frac{\lambda l(l+1)}{8\pi} \left\{ 2g(r_0) \text{Re} \left[\phi_2^{lm,[u]} \psi_2^{lm,[u]*} \right] + g'(r_0) |\psi_2^{lm,[u]}|^2 \right\}_{r \to \infty}. \tag{6.40}$$

To evaluate this formula we start by taking the r_0 derivative of Eq. (6.37) to obtain

$$\phi_2^{lm,[u]} = e^{-i\omega r_*} \left(\phi_2^{lm} - i r_* \omega_{,r_0} \psi_2^{lm} \right). \tag{6.41}$$

Now using Eqs. (5.1), (6.9) and the following leading terms in the boundary condition expansions Eqs. (5.15) and (6.20), given by

$$\psi_2^{lm} e^{-i\omega r_*} \sim c_2^+ \left[1 + \frac{il(l+1)r_0^{3/2}}{2mr} \right], \tag{6.42}$$

$$\phi_2^{lm} e^{-i\omega r_*} \sim c_2^{h2,+} + c_2^{h4,+} \left[\frac{r}{2} + \log(r) \right], \tag{6.43}$$

we get

$$\phi_2^{lm,[u]} \sim \left(c_2^{h4,+} + \frac{3ic_2^+ m}{r_0^{5/2}} \right) \left[\frac{r}{2} + \log(r) \right] + c_2^{h2,+} - c_2^+ \left[\frac{3l(l+1)}{4r_0} + \frac{3im\log(2)}{r_0^{5/2}} \right]. \tag{6.44}$$

Note that the expansions given in Eqs. (6.42) and (6.43) are valid for both the RW and Zerilli potentials. In order for this result to be finite, when we take the limit to infinity we must have

$$c_2^{h4,+} = -\frac{3ic_2^+ m}{r_0^{5/2}}. \tag{6.45}$$

Combining the above results, the GW flux to infinity in the odd-sector is given by

$$\partial_{r_0} \dot{E}_{lm}^{\infty,\mathrm{RW}} = \frac{\lambda l(l+1)}{4\pi} \left[\mathrm{Re} \left(c_2^{h2,+} c_2^{+*} \right) - |c_2^+|^2 \left(\frac{3l(l+1)}{4r_0} \right) \right], \tag{6.46}$$

and in the even-sector by

$$\partial_{r_0} \dot{E}_{lm}^{\infty,\mathrm{Z}} = \frac{m^2}{4r_0^3} \left(\partial_{r_0} \dot{E}_{lm}^{\infty,\mathrm{RW}} - \frac{6|c_2^+|^2}{4r_0} \right). \tag{6.47}$$

As a further check that our results are working correctly, we compute $\partial_{r_0}\dot{E}_{lm}^{\infty}$ using Eq. (6.46) and Eq. (6.47) and compare these results to the r_0 derivative of the flux when computed numerically. To compute the latter we compute the flux on a dense grid of r_0 values using the `ReggeWheeler` package [1]. Using the standard least-squares algorithm we fit this data to an eighth-order polynomial centred on the r_0 value where we wish to compute the r_0 derivative of the flux. The linear coefficient in this fit is the numerical approximation to the r_0 derivative of flux. We find excellent agreement between these two methods and present some sample numerical results in Table 6.1. We also numerically check that the relation in Eq. (6.45) between $c_2^{h4,+}$ and c_2^+ holds to machine precision.

To assess the efficiency of our partial annihilator method while avoiding issues regarding the level of code optimisation between our code and the BHPToolkit we can count the number of times our approach must solve an ODE versus the number of times required when computing the r_0 derivative numerically. Numerically computing the homogeneous basis of solutions is by far the largest computational cost as all the other steps, such as matching to get the inhomogeneous solutions or calculating the flux, are quick algebraic operations. Computing ϕ_2 using the partial annihilator method requires solving the left-hand side of Eq. (6.6) four times. To numerically compute the r_0 derivative of the flux at, e.g., $r_0 = 8M$, to a relative precision of $\sim 10^{-12}$ we find we must compute

r_0/M	$\frac{M^3}{\mu^2}\partial_{r_0}\mathcal{F}^\infty$	rel. err.
6	$-8.859960015046 \times 10^{-4}$	4.1×10^{-11}
8	$-1.291224908187 \times 10^{-4}$	1.2×10^{-12}
10	$-3.155702796251 \times 10^{-5}$	1.2×10^{-13}

Table 6.1: Numerical results for the r_0 derivative of the first-order GW energy flux radiated to null infinity, with modes summed up to $l_{\max} = 15$, where $\mathcal{F}]^\infty$ is given by Eq. (4.77). The first column gives the orbital radius, the second column shows the r_0 derivative of the flux radiated to infinity as computed from our partial annihilator calculation. The third column shows the relative error compared to a result computed by caclculating the flux at many orbital radii and taking a numerical derivative as described in the main text.

the flux at 11 equally spaced radii between in the range $r_0 \pm 0.2M$, and fit to an eighth-order polynomial. This requires solving the left-hand side of Eq. (2.49) 22 times. Thus our method is $22/4 = 5.5$ faster to compute $\partial_{r_0}\dot{E}^{lm}_\infty$ than the numerical derivative approach. In practice, when performing the Regge-Wheeler to Lorenz transformation the speed up is closer to a factor of 10 as two of the homogeneous solutions to Eq. (6.6) are $\psi^\pm_2$ which will already be computed for other parts of the transformation. We also note that in order to reach a relative precision beyond $\sim 10^{-9}$ in the numerical r_0 derivative computed using the `ReggeWheeler` BHPToolkit package, we had to use extended precision arithmetic.

6.5   Differentiability of second-order source

In this section we examine the differentiability of the slowly evolving terms that contribute to the source of the second-order metric perturbation. Recall from Eq. (4.68) that (dropping the tildes from the original equation and assuming a two-timescale expansion)

$$\delta^1 G^{0,(i)}_{(j)}\left[\bar{h}^{2,(j)}_{lm}\right] = \tilde{S}^{2,(i)}_{lm} - 2\delta^2 G^{0,(i)}_{(j)(k)}\left[\bar{h}^{1,(j)}_{lm}, \bar{h}^{1,(k)}_{lm}\right] - \delta^1 G^{1,(i)}_{(j)}\left[\bar{h}^{1,(j)}_{lm}\right], \tag{6.48}$$

and let

$$\bar{h}^{2,(j)}_{lm} = \bar{h}^{2,(j)}_{\mathcal{P}} + \bar{h}^{2,(j)}_{\mathcal{R}}, \tag{6.49}$$

such that

$$\delta^1 G^{0,(i)}_{(j)}\left[\bar{h}^{2,(j)}_{\mathcal{R}}\right] = S^{2,(i)}_{lm} - \delta^1 G^{0,(i)}_{(j)}\left[\bar{h}^{2,(j)}_{\mathcal{P}}\right] - 2\delta^2 G^{0,(i)}_{(j)(k)}\left[\bar{h}^{1,(j)}_{lm}, \bar{h}^{1,(k)}_{lm}\right] - \delta^1 G^{1,(i)}_{(j)}\left[\bar{h}^{1,(j)}_{lm}\right]. \tag{6.50}$$

Due to the order of the puncture, the contribution

$$\delta^1 G^{0,(i)}_{(j)}\left[\bar{h}^{2,(j)}_{\mathcal{P},\mathrm{ms}}\right] + \delta^1 G^{1,(i)}_{(j)}\left[\bar{h}^{1,(j)}_{lm}\right], \tag{6.51}$$

is expected to be C^0 differentiable, where $\bar{h}^{2,(j)}_{\mathcal{P},\mathrm{ms}}$ is defined to be the piece of the puncture that is proportional to $\dot{r}_0$ and is referred to as the multi-scale piece. Figure 6.7 shows how any jumps appearing in the individual terms from Eq. (6.51) cancel so that their sum is C^0 differentiable, providing an additional useful check on our calculation of $h^{1\mathrm{L}}_{\mu\nu,r_0}$. The position of the particle was chosen to be at $r_0 = 8.4M$, with the even-sector components shown for the $(l, m) = (2, 2)$ mode below.
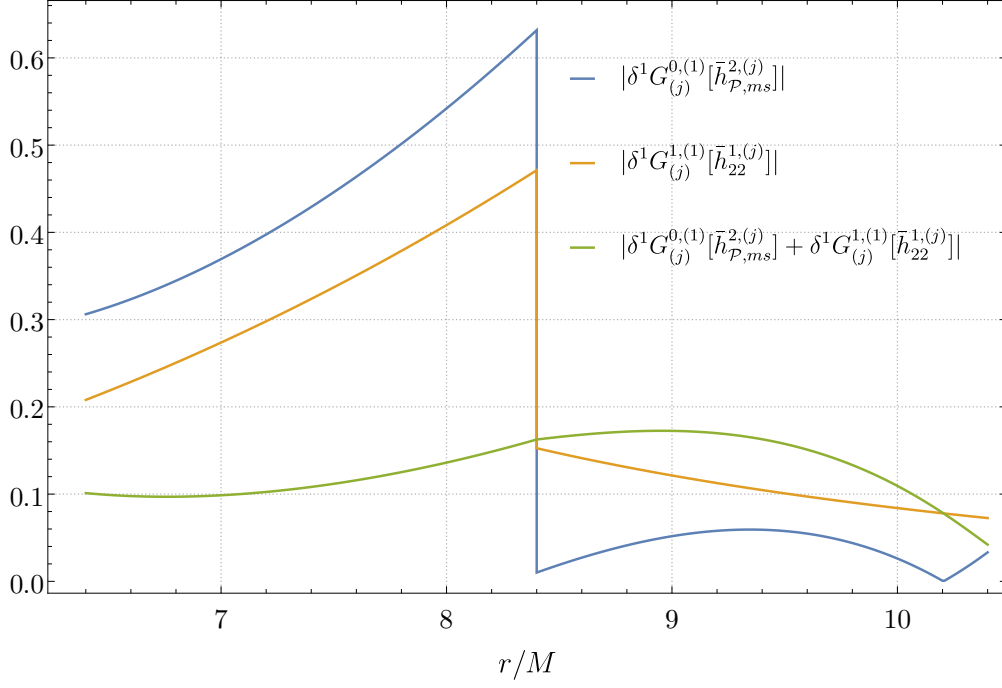
Figure 6.7: Plot of $\delta^1 G^{0,(i)}_{(j)}\left[\bar{h}^{2,(j)}_{\mathcal{P},\mathrm{ms}}\right]$, $\delta^1 G^{1,(i)}_{(j)}\left[\bar{h}^{1,(j)}_{lm}\right]$ when summed over j from 1 to 10, with $i = 1$. In each case, the desired C^0 differentiability of the sum of the terms is achieved [2, 4].
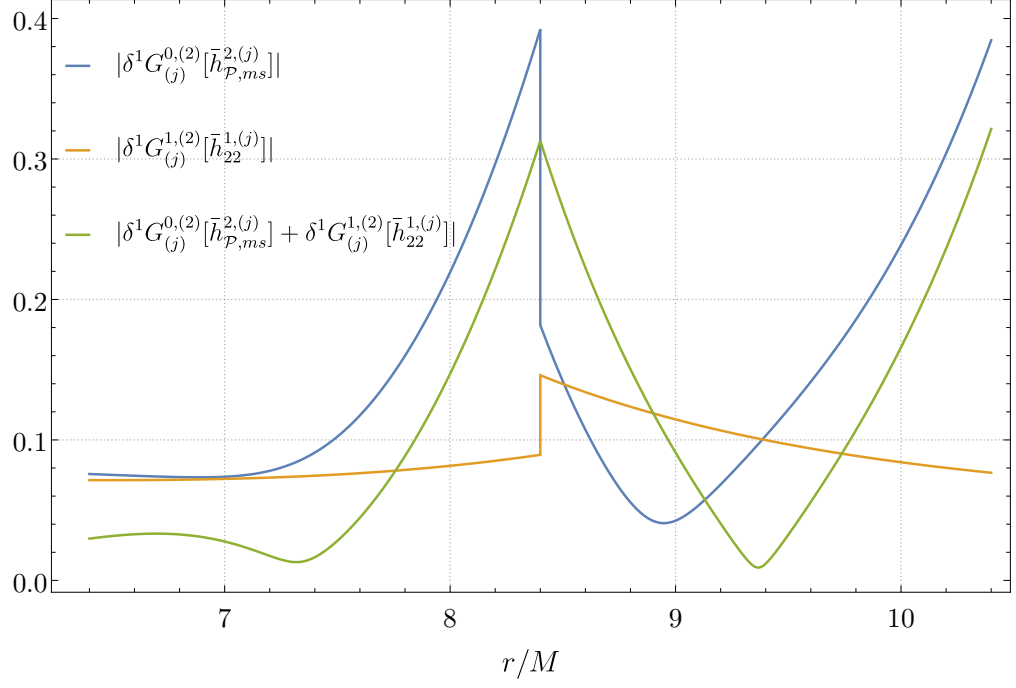
Figure 6.8: Same as Fig. (6.7) except for $i = 2$.
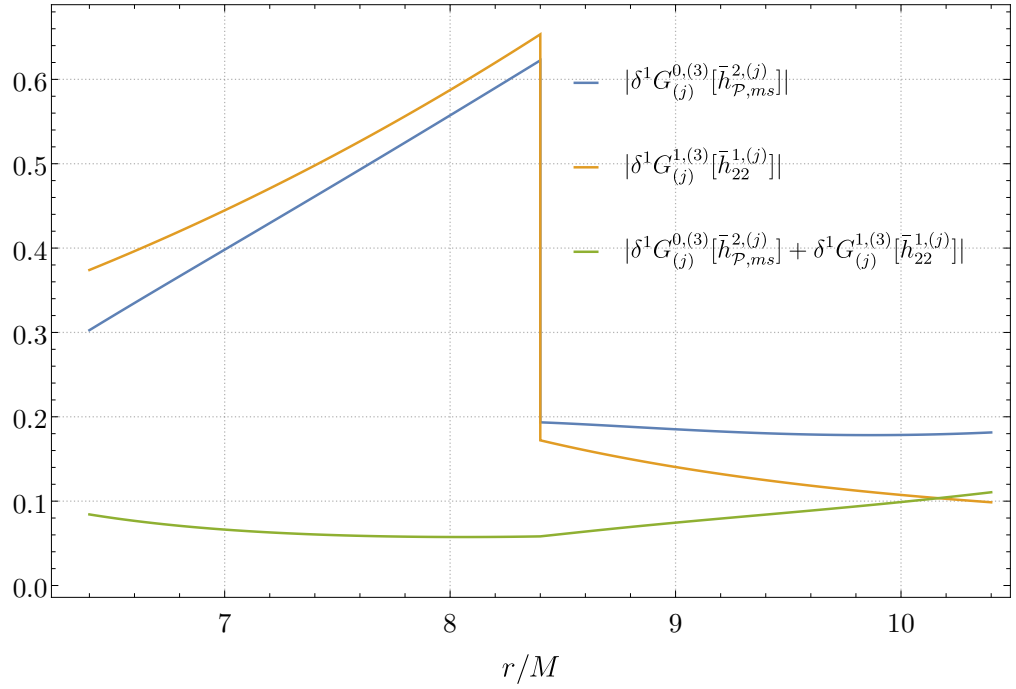
Figure 6.9: Same as Fig. (6.7) except for $i = 3$.

99
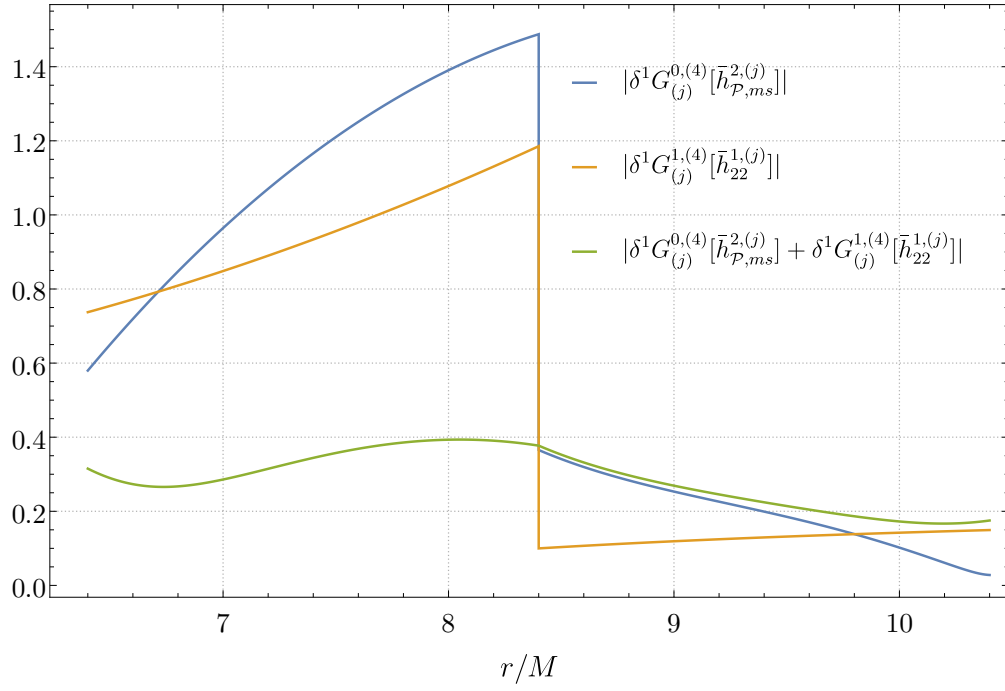
Figure 6.10: Same as Fig. (6.7) except for $i = 4$.
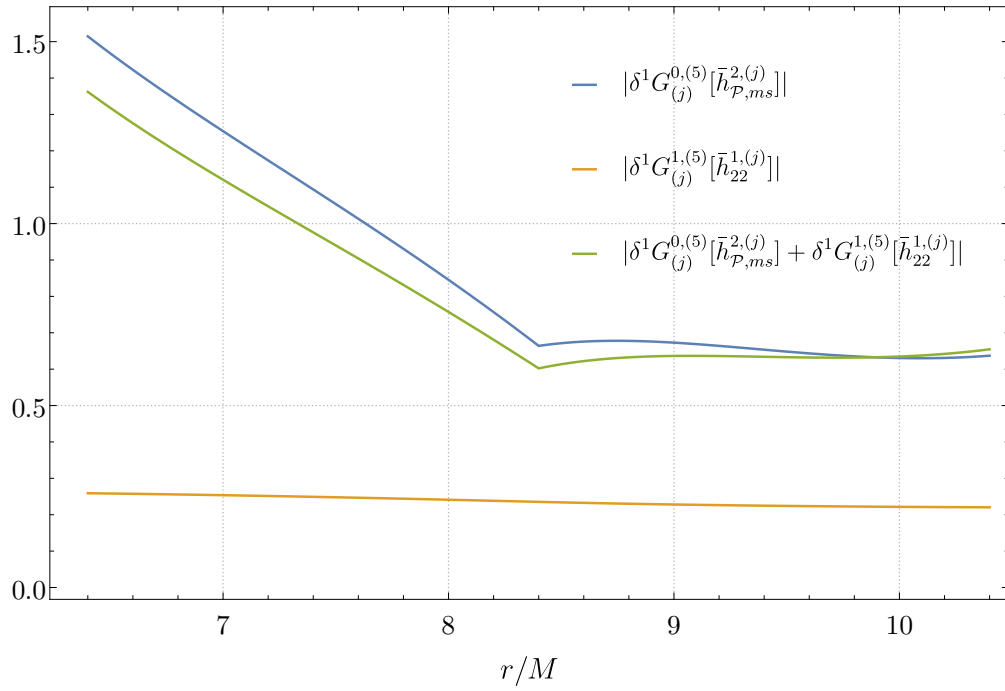
Figure 6.11: Same as Fig. (6.7) except for $i = 5$.
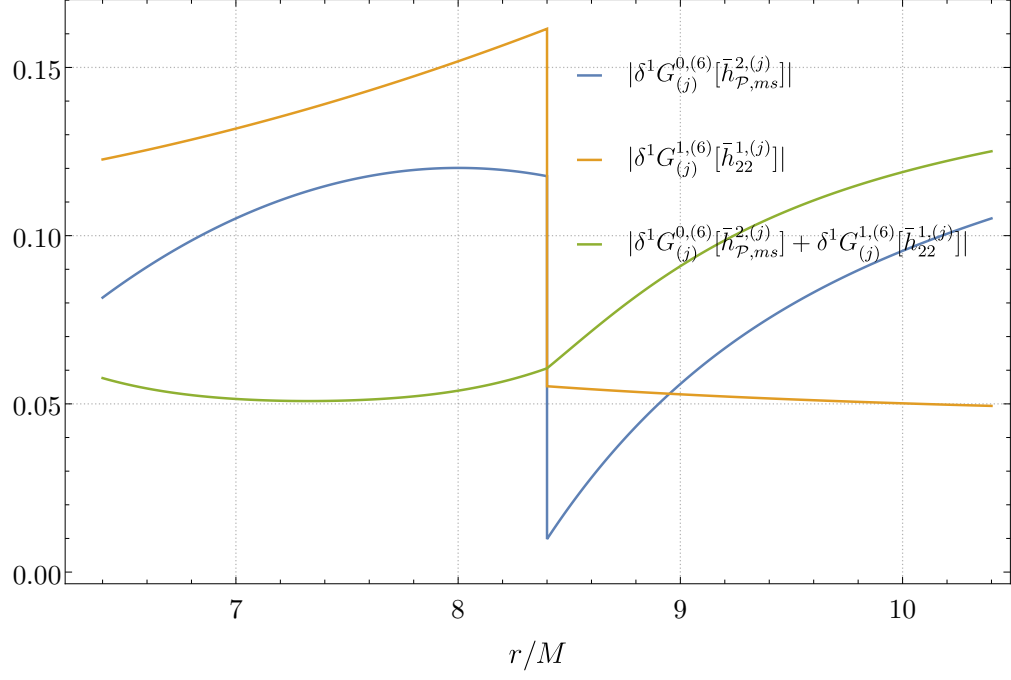
Figure 6.12: Same as Fig. (6.7) except for $i = 6$.
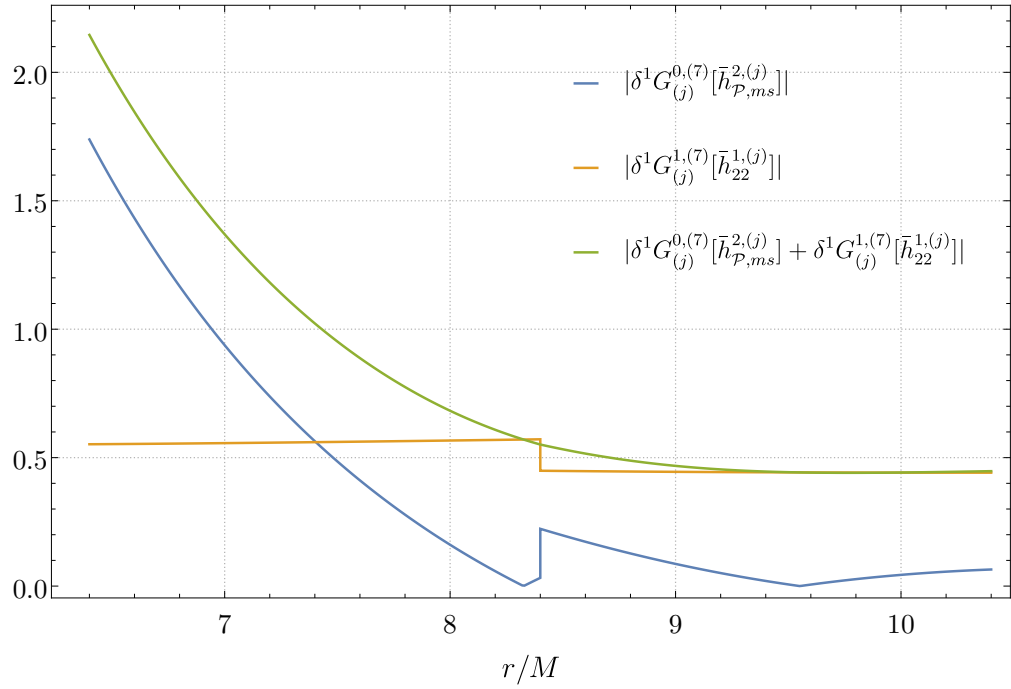
Figure 6.13: Same as Fig. (6.7) except for $i = 7$.

The odd-sector components are then shown for the $(l, m) = (2, 1)$ mode
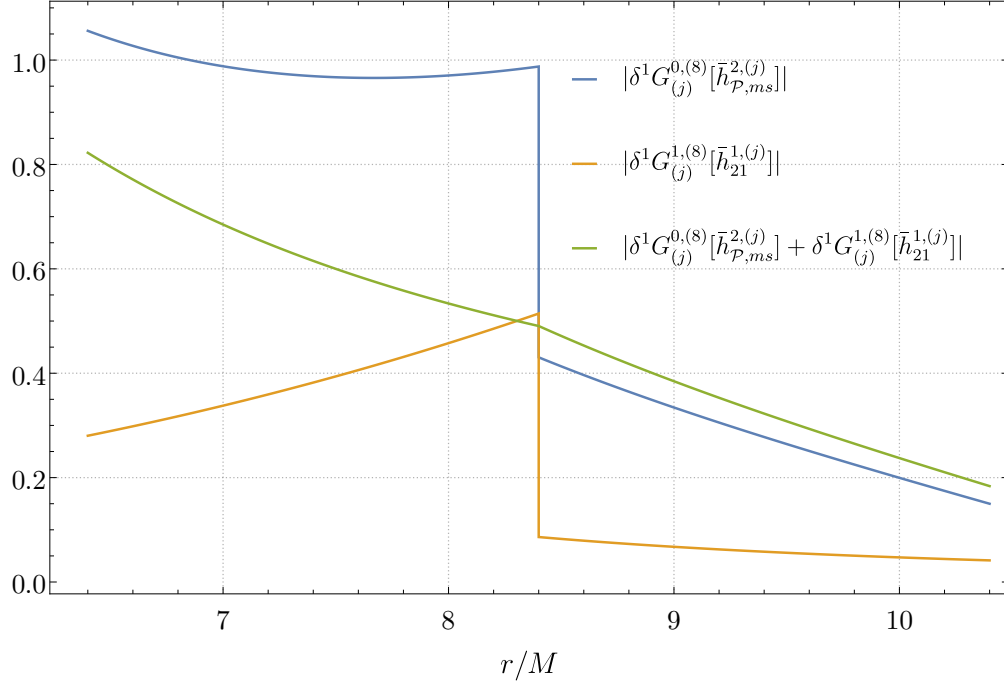
Figure 6.14: Same as Fig. (6.7) except for $i = 8$.
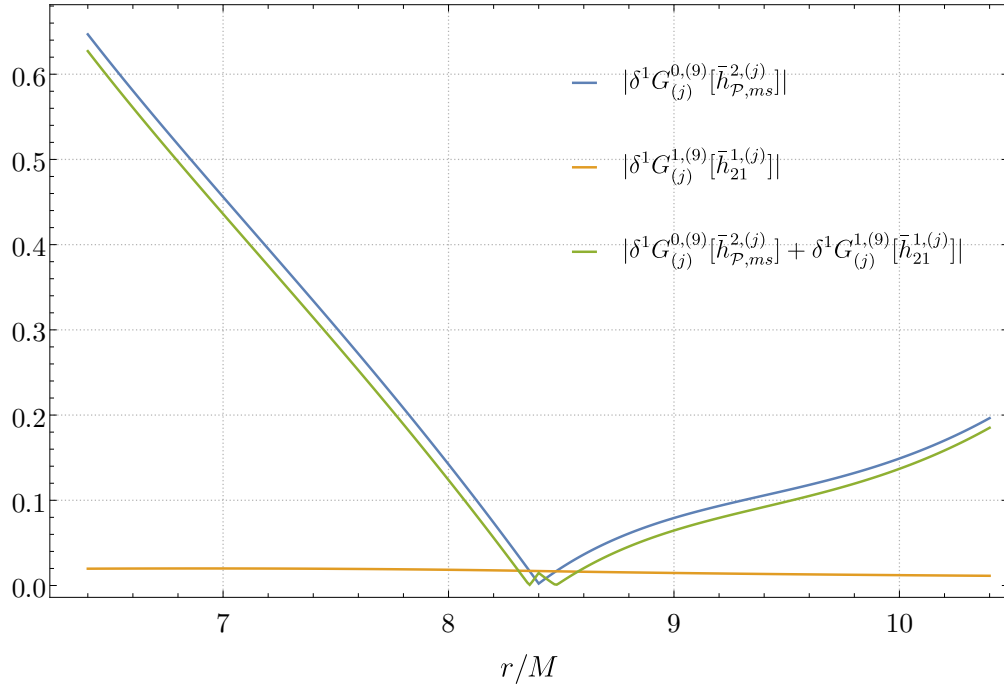
Figure 6.15: Same as Fig. (6.7) except for $i = 9$.
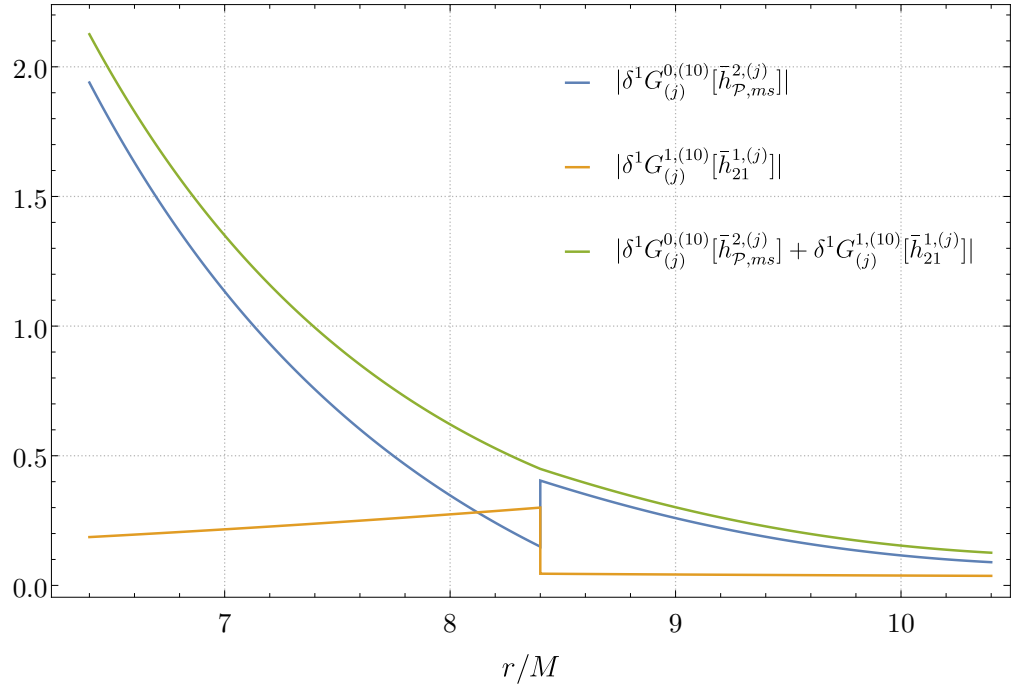
Figure 6.16: Same as Fig. (6.7) except for $i = 10$.

Chapter 7

Transition to Plunge

Throughout this thesis so far, only the inspiral part of the waveform has been considered. To generate the full waveform, the transition to plunge, merger and ring-down of the binary must also be considered [48]. This chapter will focus on modelling the transition to plunge of the binary, in particular on calculating the amplitude and phase of GWs produced by EMRIs. In fact, the results in this chapter are also found to be applicable to intermediate mass ratio inspirals (IMRIs), as will be shown in Chapter 8. For IMRIs, where $\varepsilon \sim 0.1$ can still be considered 'small', are modelled very well using the GSF approach [3, 4]. The transition to plunge is much more important for modelling IMRIs however, where the overall signal length is much shorter than for an EMRI. We are now beginning to detect IMRIs from ground based detectors, for example GW191219_163120 [7] and need improved models for accurate parameter estimation of these signals. This provides the primary motivation for the research in this chapter, which was done in collaboration with Küchler, Geoffrey Compère and Pound, continuing to use a spacetime foliation of hypersurfaces defined by constant t.

To model the transition to plunge, a new time scale must be introduced. In Chapter 4 and Chapter 6 we have seen that the orbital radius shrinks due to GW emission over a timescale of $\tilde{t} = \varepsilon t$, the slow-time, during inspiral. Recall some of the physical quantities of the inspiral as expanded in the small mass ratio, which were introduced in Chapter 4

$$\frac{d\Omega}{dt} = \varepsilon \sum_{n=0}^{\infty} \varepsilon^n F_n^\Omega(\Omega), \tag{7.1}$$

$$r_{\rm p} = \sum_{n=0}^{\infty} \varepsilon^n r_n(\Omega), \tag{7.2}$$

$$f^\mu(\Omega) = \varepsilon \sum_{n=0}^{\infty} \varepsilon^n f_n^\mu(\Omega), \tag{7.3}$$

$$\bar{h}_{lm}^{(i)} = \sum_{n=1}^{\infty} \varepsilon^n \bar{h}_{lm}^{n,(i)}(r, \Omega, \phi_{\rm p}) = \sum_{n=1}^{\infty} \varepsilon^n \bar{h}_{lm}^{n,(i)}(r, \Omega) e^{-im\phi_{\rm p}}, \tag{7.4}$$

$$S_{lm}^{(i)} = \sum_{n=1}^{\infty} \varepsilon^n S_{lm}^{n,(i)}(r, r_{\rm p}, \dot{r}_{\rm p}, \Omega, \phi_{\rm p}), \tag{7.5}$$

where an overdot denotes differentiation with respect to t and the tilde on the SF and metric perturbation of Chapter 4 are dropped henceforth, with all quantities assumed to be expanded using the two-timescale approximation. The explicit dependence on variables in Eq. (7.5) will be made clear later in Section 7.3. Note that in the inspiral, we may wish to write the dependence on Ω of some quantity equivalently as dependence on r_p, as $\Omega = \Omega(r_p)$. One must take care however as explicit dependence on both r_p and Ω may appear, as will be seen in Eq. (7.76). Regardless, in both the inspiral and the transition regimes, ϕ_p is not a slowly evolving quantity, and while it is a functional of Ω, it depends only on t and not on $\tilde{t}$.

During the transition, the binary evolves more quickly than in the inspiral. The entire transition to plunge occurs over a much shorter time compared to the full inspiral of an EMRI, and is expected to contribute very little to the overall waveform, lasting for a proper time of [48, 60, 93]

$$\Delta\tau \sim \varepsilon^{-1/5}, \tag{7.6}$$

which corresponds to a radial width of

$$\Delta r \sim \varepsilon^{2/5}, \tag{7.7}$$

and a change in frequency of

$$\Delta\Omega \sim \varepsilon^{2/5}. \tag{7.8}$$

A more concrete estimate of the width of the transition from inspiral to plunge is given in Ref. [93]. Therefore, in the transition regime, we introduce the 'slightly faster' slow-time [48]

$$\tilde{t} = \lambda t, \quad \text{where} \quad \lambda = \varepsilon^{\frac{1}{5}}. \tag{7.9}$$

The metric perturbation and frequency can be determined during the transition by using the new timescale and setting $\varepsilon \to \lambda^5$. To calculate the metric perturbation to second-order in the small mass ratio, terms in the expansion must be included up to λ^{10} therefore. The two-timescale approximation of the inspiral starts to break down near the ISCO [14, 4]. As such, quantities such as the orbital radius and frequency during the transition are expanded near the ISCO. Physical quantities of interest for modelling GWs during the transition are then given instead by [125, 126, 62]

$$\Omega = \Omega_I + \lambda^2 \Delta\Omega, \tag{7.10}$$

$$\frac{d\Omega}{dt} = \lambda^2 \frac{d\Delta\Omega}{dt} = \lambda^3 \sum_{n=0}^{\infty} \lambda^n F_n^{\Delta\Omega}(\Delta\Omega), \tag{7.11}$$

$$r_p = r_I + \lambda^2 \sum_{n=0}^{\infty} \lambda^n R_n(\Delta\Omega), \tag{7.12}$$

$$f^\mu(\Omega) = \lambda^5 \sum_{n=0}^{\infty} \lambda^n F_n^\mu(\Omega), \tag{7.13}$$

106

and

$$\bar{h}_{lm}^{(i)} = \sum_{n=5}^{\infty} \lambda^n j_{lm}^{n,(i)}(r, \Delta\Omega, \phi_{\mathrm{p}}), \tag{7.14}$$

$$S_{lm}^{(i)} = \sum_{n=5}^{\infty} \lambda^n s_{lm}^{n,(i)}(r, r_{\mathrm{p}}, \dot{r}_{\mathrm{p}}, \Omega, \phi_{\mathrm{p}}), \tag{7.15}$$

where

$$r_{\mathrm{I}} = 6M, \tag{7.16}$$

$$\Omega_{\mathrm{I}} = \frac{1}{M}\sqrt{\frac{1}{6^3}}. \tag{7.17}$$

Note that, for $r_{\mathrm{p}} > r_{\mathrm{I}}$, $\Delta\Omega < 0$ and for $r_{\mathrm{p}} < r_{\mathrm{I}}$, $\Delta\Omega > 0$. Unlike the inspiral, there is no longer a direct relationship between Ω and r_{p}during the transition to plunge. To model GWs in the transition therefore, one can solve for the transition quantities above by two different means. The first method involves re-deriving the linearised Einstein field equations and equations of motion in the new timescale and solving directly for transition quantities. The second method involves re-expanding the inspiral solutions in the new timescale, taking the limit of late times in the inspiral, and matching to transition quantities in the limit of early times in the transition. Both methods must of course yield identical solutions, and hence exploring both avenues provides a useful check on one's results. In this chapter, the second method shall be used, as this will allow transition quantities to be written in terms of inspiral quantities, most of which have already been solved in references [14, 119, 3, 4, 2], and some of which are solved earlier in this thesis, leaving fewer unknowns to be determined. Using the equations of motion from Chapter 4 and expanding about the ISCO we can determine the evolution of the frequency during the transition in terms of inspiral quantities as an expansion in powers of λ.

7.1 Revisiting the equations of motion

In this section we will determine the terms in the expansions for $r_{\rm p}$ and $\frac{d\Omega}{dt}$ in both the inspiral and transition, that is r_n, R_n, F_n^{Ω} and $F_n^{\Delta\Omega}$. The late time limit for inspiral quantities and the early time limit for transition quantities will be examined as each of these limits correspond to the limit near the ISCO, where both inspiral and transition solutions should match. The quantities derived in this section will prove useful in determining the phase and amplitudes of GWs during the transition.

7.1.1 Inspiral

Specifying $\Omega = \Omega_0$ as in methods 2 and 3 outlined in Section 4.8, the equations of motion from Eq. (4.24) establish that the coefficients of the powers of ε in $r_{\rm p}$ from Eq. (7.2) are given by [62, 126, 125]

$$r_0 = \frac{M}{(M\Omega)^{2/3}}, \tag{7.18}$$

$$r_1 = -\frac{f_1^r}{3\Omega^2 U_0^2 f_0}, \tag{7.19}$$

$$r_2 = -\frac{1}{3\Omega^2 U_0^2 f_0} f_2^r + \frac{2(4 - 45(M\Omega)^{2/3} + 114(M\Omega)^{4/3} - 72(M\Omega)^2)}{3\Omega^3 (M\Omega) U_0^6 D^3} \left(f_1^t\right)^2 + \tag{7.20}$$

$$+ \frac{(1 - 4(M\Omega)^{2/3})}{9\Omega^3 (M\Omega)^{1/3} U_0^4 f_0^3} \left(f_1^r\right)^2 + \frac{2f_0}{\Omega^2 (M\Omega) U_0^8 D^2} f_1^t \partial_\Omega f_1^t,$$

with

$$U_0 = \frac{1}{(1 - 3(M\Omega)^{2/3})^{1/2}}, \tag{7.21}$$

$$D = \left(1 - 6(M\Omega)^{2/3}\right), \tag{7.22}$$

$$f_0 = 1 - \frac{2M}{r_0} = 1 - 2(M\Omega)^{2/3}. \tag{7.23}$$

Recall from Eq. (4.105) that we also have

$$F_0^{\Omega} = -\frac{3f_0\Omega}{(M\Omega)^{2/3} U_0^4 D} f_1^t. \tag{7.24}$$

and from Eq. (4.107) that the next-to-leading order forcing term is given by

$$F_1^{\Omega} = \frac{3\Omega U_0^2 f_0 \left(2f_1^t(\Omega) \left(\frac{1}{U_0^4}\right)^4 \partial_\Omega f_1^r(\Omega) - f_2^t(\Omega)(M\Omega)^{1/3} D f_0\right) - 4f_1^r(\Omega) f_1^t(\Omega) \left(12(M\Omega)^{4/3} + D\right)}{M\Omega D^2 U_0^6 f_0}. \tag{7.25}$$

The frequency Ω will be determined from its evolution, $\frac{d\Omega}{dt}$, after initially solving for F_n^{Ω} from Eq. (7.1), following method 3 from Section 4.8. It is worth noting here one of the crucial differences

between the work here and that of OT, discussed in the introduction. While OT strictly imposes quasi-circularity such that $f^r = 0$ [48], Eq. (7.19) and Eq. (7.20) capture the deviation from quasi-circularity during the transition from inspiral to plunge, following the self-consistent approach of Compère and Küchler [62].

7.1.2   Inspiral at late times

At late times in the inspiral we set $\Omega \to \Omega_I + \lambda^2 \Delta\Omega$, with $\Delta\Omega < 0$ [48]. Taking the limit of r_0, r_1, r_2, F_0^Ω and F_1^Ω from Eqs. (7.18)-(7.20) and Eq. (7.24) near the ISCO, by setting $\Omega \to \Omega_I + \lambda^2 \Delta\Omega$ and re-expanding in terms of powers of $\lambda^2 \Delta\Omega$ determines that [125] This establishes that at late times in the inspiral, corrections to the orbital radius and forcing terms take the form [125, 126]

$$r_0^\Omega = 6M + r^{(2,1)}\lambda^2\Delta\Omega + r^{(4,2)}\lambda^4\Delta\Omega^2 + r^{(6,3)}\lambda^6\Delta\Omega^3 + \mathcal{O}(\lambda^8) \tag{7.26}$$

$$r_1^\Omega = \lambda^5\left[r^{(5,0)} + r^{(7,1)}\lambda^2\Delta\Omega + \mathcal{O}(\lambda^4)\right], \tag{7.27}$$

$$F_0^\Omega = \frac{F_\Omega^{(3,-1)}}{\lambda^2\Delta\Omega} + F_\Omega^{(5,0)} + F_\Omega^{(7,1)}\lambda^2\Delta\Omega + F_\Omega^{(9,2)}\lambda^4\Delta\Omega^2 + \mathcal{O}(\lambda^6), \tag{7.28}$$

$$F_1^\Omega = \frac{F_\Omega^{(6,-2)}}{\lambda^4\Delta\Omega^2} + \frac{F_\Omega^{(8,-1)}}{\lambda^2\Delta\Omega} + F_\Omega^{(10,0)} + \mathcal{O}(\lambda^2). \tag{7.29}$$

where the notation of the superscripts will be explained momentarily, and the constant coefficients are given by [125, 126]

$$r^{(2,1)} = -24\sqrt{6}M^2, \tag{7.30a}$$

$$r^{(4,2)} = 720M^3, \tag{7.30b}$$

$$r^{(6,3)} = -3840\sqrt{6}M^4, \tag{7.30c}$$

$$r^{(5,0)} = -108M^2 f_r^1(\Omega_I), \tag{7.30d}$$

$$r^{(7,1)} = 108M^2(10\sqrt{6}M f_r^1(\Omega_I) - 20\sqrt{6}M\partial_\Omega f_r^1(\Omega_I)), \tag{7.30e}$$

and [125, 126]

$$F_\Omega^{(3,-1)} = \frac{f_1^t(\Omega_I)}{24M^2}, \tag{7.31a}$$

$$F_\Omega^{(5,0)} = \frac{-3\sqrt{6}M f_1^t(\Omega_I) + \partial_\Omega f_1^t(\Omega_I)}{24M^2}, \tag{7.31b}$$

$$F_\Omega^{(7,1)} = \frac{-92M^2 f_1^t(\Omega_I) - 6\sqrt{6}M\partial_\Omega f_1^t(\Omega_I) + \partial_\Omega^2 f_1^t(\Omega_I)}{48M^2}, \tag{7.31c}$$

$$F_\Omega^{(9,2)} = \frac{1548\sqrt{6}M^3 f_1^t(\Omega_I) - 276M^2\partial_\Omega f_1^t(\Omega_I) - 9\sqrt{6}M\partial_\Omega^2 f_1^t(\Omega_I) + \partial_\Omega^3 f_1^t(\Omega_I)}{144M^2}, \tag{7.31d}$$

which are the 0PA contributions to the GSF. For the purposes of the calculations in this chapter, the other coefficients will not be listed.

Using the equations of motion, the first-order SF can be written in terms of the first-order energy flux in the following way [127]

$$f_1^t(\Omega) = -\frac{1}{f_0 U_0^2} \mathcal{F}^1(r_0(\Omega)), \tag{7.32}$$

$$\partial_\Omega f_1^t(\Omega) = 3\sqrt{6}M(-\mathcal{F}^1(6M) + 12M\partial_{r_0}\mathcal{F}^1(6M)), \tag{7.33}$$

where $\mathcal{F}^1$ is the sum of the first order energy fluxes through infinity and the horizon, defined in Section 4.6. The values of the first-order total flux and its derivative with respect to r_0, when evaluated at the ISCO, are given below in Table (7.1)

$\left(\frac{M}{\mu}\right)^2 \mathcal{F}^1(6M)$	$\frac{M^3}{\mu^2}\partial_{r_0}\mathcal{F}^1(6M)$
0.0009403393563150952	-0.0008920288801933012

Table 7.1: Numerical results for first-order total energy flux and its r_0 derivative evaluated at the ISCO for quasicircular equatorial orbits. The value for $\mathcal{F}^1(6M)$ can be calculated using the BHPToolkit [1], and $\partial_{r_0}\mathcal{F}^1(6M)$ is determined using the method outline in Section 6.4. Note the difference with Table (6.1), which includes only the first-order energy flux radiated to infinity.

Therefore, as the particle approaches the ISCO, $\frac{d\Omega}{dt}$ and $r_{\rm p}$ can be written in the following form [125]

$$\frac{d\Omega}{dt} = \lambda^5 \left[\frac{F_\Omega^{(3,-1)}}{\lambda^2 \Delta\Omega} + F_\Omega^{(5,0)} + F_\Omega^{(7,1)}\lambda^2\Delta\Omega + F_\Omega^{(9,2)}\lambda^4\Delta\Omega^2 + \mathcal{O}(\lambda^6) \right] \tag{7.34}$$

$$+ \lambda^{10} \left[\frac{F_\Omega^{(6,-2)}}{\lambda^4\Delta\Omega^2} + \frac{F_\Omega^{(8,-1)}}{\lambda^2\Delta\Omega} + F_\Omega^{(10,0)} + \mathcal{O}(\lambda^2) \right] + \mathcal{O}(\lambda^{15}),$$

$$r_{\rm p} = 6M + r^{(2,1)}\lambda^2\Delta\Omega + r^{(4,2)}\lambda^4\Delta\Omega^2 + r^{(6,3)}\lambda^6\Delta\Omega^3 + \mathcal{O}(\lambda^8) \tag{7.35}$$

$$+ \lambda^5 \left[r^{(5,0)} + r^{(7,1)}\lambda^2\Delta\Omega + \mathcal{O}(\lambda^4) \right] + \mathcal{O}(\lambda^{10}).$$

It is from Eqs.(7.34) and (7.35) where the choice of notation becomes clear. In the expansion of $d\Omega/dt$ and $r_{\rm p}$, the first superscript on the constant coefficients is chosen to represent the power of λ and the second superscript denotes the power of $\Delta\Omega$.

7.1.3 Transition

By choosing $r_{\rm p}$ and f^μ to be the transition expansions from Eq. (7.12) and Eq. (7.13) respectively, the t component of the equations of motion from Eq. (4.24) determines that, at $\mathcal{O}(\lambda^5)$ [125]

$$-24M^2 F_0^{\Delta\Omega}(\Delta\Omega) \left[-\Delta\Omega + 9\sqrt{6}M \left(\partial_{\Delta\Omega} F_0^{\Delta\Omega}(\Delta\Omega) \right)^2 + 9\sqrt{6}M F_0^{\Delta\Omega}(\Delta\Omega)\partial_{\Delta\Omega}^2 F_0^{\Delta\Omega}(\Delta\Omega) \right] = f_1^t(\Omega_{\rm I}), \tag{7.36}$$

110

and at $\mathcal{O}(\lambda^{10})$[1]

$$F_1^{\Delta\Omega}(\Delta\Omega) = 0. \tag{7.37}$$

At $\mathcal{O}(\lambda^{15})$, $F_2^{\Delta\Omega}$ couples to $F_0^{\Delta\Omega}$ in the following way

$$24\sqrt{6}M^3 F_0^{\Delta\Omega}(\Delta\Omega)\left(18\partial_{\Delta\Omega}F_0^{\Delta\Omega}(\Delta\Omega)\partial_{\Delta\Omega}F_2^{\Delta\Omega}(\Delta\Omega) - 11\Delta\Omega^2\right) + \Delta\Omega\left(8\sqrt{6}f_1^t(\Omega_I)M + \partial_\Omega f_1^t(\Omega_I)\right) =$$
$$F_2^{\Delta\Omega}(\Delta\Omega)\left(\frac{2f_1^t(\Omega_I)}{F_0^{\Delta\Omega}(\Delta\Omega)} + 24M^2\left(9\sqrt{6}M\left(\partial_{\Delta\Omega}F_0^{\Delta\Omega}(\Delta\Omega)\right)^2 - \Delta\Omega\right)\right)$$
$$+216M^3 F_0^{\Delta\Omega}(\Delta\Omega)^2\left(156M\partial_{\Delta\Omega}F_0^{\Delta\Omega}(\Delta\Omega) - \sqrt{6}\partial_{\Delta\Omega}^2 F_2^{\Delta\Omega}(\Delta\Omega)\right), \tag{7.38}$$

where terms involving $\partial_{\Delta\Omega}^2 F_0^{\Delta\Omega}$ have been reduced to a combination of $F_0^{\Delta\Omega}$ and $\partial_{\Delta\Omega}F_0^{\Delta\Omega}$ using Eq. (7.36). The coupled equations Eq. (7.36) and Eq. (7.38) can then be solved numerically in the following way. The coupled equations are difficult to solve directly, and are made easier to solve by making the following replacements, which were first observed by Compère [126]

$$\Delta\Omega = \alpha^{2/5}\beta^{3/5}t, \tag{7.39}$$
$$F_0^{\Delta\Omega}(\Delta\Omega) = \alpha^{3/5}\beta^{-2/5}X_0(\alpha^{-2/5}\beta^{3/5}\Delta\Omega), \tag{7.40}$$
$$F_2^{\Delta\Omega}(\Delta\Omega) = \alpha^{3/5}\beta^{-2/5}X_2(\alpha^{-2/5}\beta^{3/5}\Delta\Omega), \tag{7.41}$$

where [104]

$$\alpha = -\frac{f_1^t(\Omega_I)}{432\sqrt{6}M^3}, \tag{7.42}$$
$$\beta = \frac{1}{9\sqrt{6}M}, \tag{7.43}$$

so that Eq. (7.36) and Eq. (7.38) become [126]

$$X_0(t)\left(X_0'(t)^2 - t\right) + X_0(t)^2 X_0''(t) - 1 = 0, \tag{7.44}$$

$$-\frac{3^{1/10}\partial_\Omega f_t^1(\Omega_I)}{2\sqrt{2}(Mf_t^1(\Omega_I))^{3/5}}t - 3^{3/5}(-Mf_t^1(\Omega_I))^{2/5}\left[2t + \frac{11}{2}X_0(t)t^2 + 13X_0(t)^2 X_0'(t)\right] \tag{7.45}$$
$$- X_2(t)X_0'(t)^2 + X_0(t)^2 X_0''(t) + 2X_0(t)X_0'(t)X_2'(t) + \frac{2X_2(t)}{X_0(t)} + tX_2(t) = 0.$$

Using *Mathematica's* `NDSolveValue` function with `Method` $\rightarrow$ 'ImplicitRungeKutta' and `AccuracyGoal` $\rightarrow \infty$, the simplified coupled ODEs can be solved numerically, and the results can be seen in Fig. (7.1) [126]. The initial conditions are given by rearranging Eq. (7.40) and Eq. (7.41) for X_0 and X_2, and replacing $F_0^{\Delta\Omega}$ and $F_2^{\Delta\Omega}$ with their respective early time expansions, given in the next subsection by Eq. (7.53) and Eq. (7.54) respectively. However, to obtain stable numerical

---

[1]Note that $F_1^{\Delta\Omega}$ is non-zero on hyperboloidal slicing, which is key in matching to the plunge [126].

solutions we must include higher order contributions. Converting to the variable X_0 and X_2, the initial conditions are then given by [126]

$$X_0(t_0) = -\frac{1}{t} - \frac{3}{t^6} - \frac{177}{t^{11}} - \frac{29349}{t^{16}} - \frac{9346005}{t^{21}} - \frac{4846966614}{t^{26}} - \frac{3722335794387}{t^{31}} \tag{7.46}$$
$$-\frac{3972772364116824}{t^{36}} - \frac{5628415395384607293}{t^{41}} - \frac{10223331600760441482825}{t^{46}}$$
$$-\frac{2316735550293679598 6195010}{t^{51}},$$

$$X_2(t_0) = -1.2433885691468331826294563 0044 - \frac{5.727061224928909527219737 9651}{t^5} \tag{7.47}$$
$$-\frac{538.1466995336574265734193 7005}{t^{10}} - \frac{123573.89804232118327623597 8732}{t^{15}},$$

which are evaluated at some sufficiently negative early time t_0.
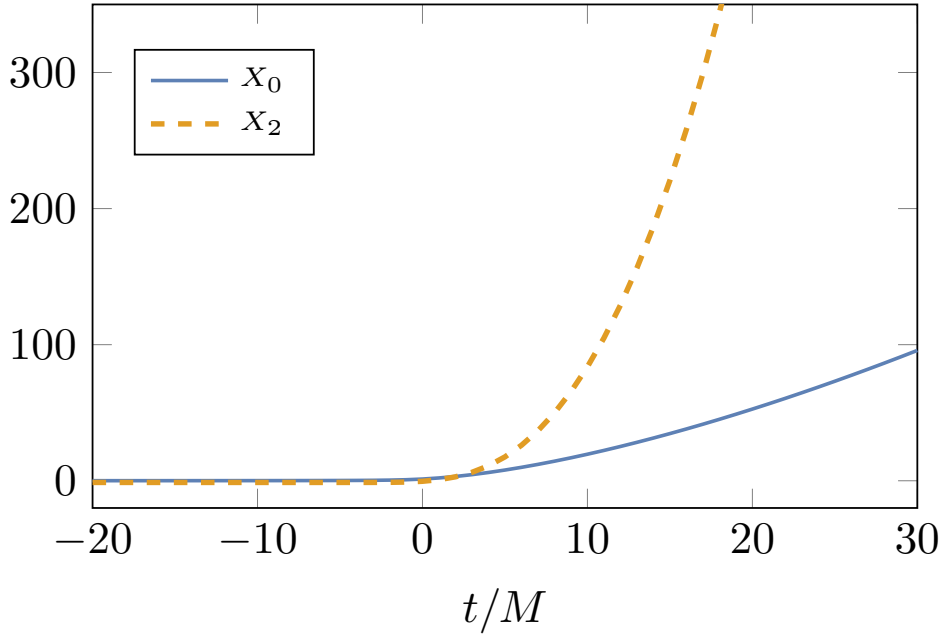
Figure 7.1: Leading order and next-to-leading order terms in the evolution of the frequency during the transition. The quantities X_0 and X_2 are defined in Eq. (7.40) and Eq. (7.41) respectively. The initial time is chosen to be $t_0 = -20M$, which lies deep in the inspiral.

The r component of the equations of motion Eq. (4.24) at $\mathcal{O}(\lambda^2)$, $\mathcal{O}(\lambda^3)$ and $\mathcal{O}(\lambda^4)$ then determine respectively that [126]

$$R_0 = -24\sqrt{6}M^2\Delta\Omega, \tag{7.48}$$
$$R_1 = 0, \tag{7.49}$$
$$R_2 = -144\left[-5M^3\Delta\Omega^2 + 18\sqrt{6}M^4 F_0^{\Delta\Omega}(\Delta\Omega)\partial_{\Delta\Omega}F_0^{\Delta\Omega}(\Delta\Omega)\right]. \tag{7.50}$$

7.1.4 Transition at early times

The near ISCO limit for $F_1^{\Delta\Omega}$, R_0 and R_1 are trivial, and given immediately by Eq. (7.37), Eq. (7.48) and Eq. (7.49) respectively. As the particle approaches the ISCO, $\frac{d\Omega}{dt}$ and $r_{\rm p}$ are expected to take the following form in terms of powers of λ and $\Delta\Omega$ [125]

$$\frac{d\Omega}{dt} = \lambda^2 \frac{d\Delta\Omega}{dt} = \lambda^2 \left\{ \lambda \left[\frac{F_\Omega^{(3,-1)}}{\Delta\Omega} + \frac{F_\Omega^{(3,-6)}}{\Delta\Omega^6} + \frac{F_\Omega^{(3,-11)}}{\Delta\Omega^{11}} + \mathcal{O}(\Delta\Omega^{-16}) \right] + \lambda^2(0) + \lambda^3 \left[F_\Omega^{(5,0)} + \mathcal{O}(\Delta\Omega^{-5}) \right] \right. \tag{7.51}$$

$$+ \lambda^4 \left[F_\Omega^{(6,-2)} \Delta\Omega^{-2} + \mathcal{O}(\Delta\Omega^{-7}) \right] + \lambda^5 \left[F_\Omega^{(7,-1)} \Delta\Omega + \mathcal{O}(\Delta\Omega^{-4}) \right]$$
$$+ \lambda^6 \left[F_\Omega^{(8,-1)} \Delta\Omega^{-1} + \mathcal{O}(\Delta\Omega^{-6}) \right] + \lambda^7 \left[F_\Omega^{(9,2)} \Delta\Omega^2 + \mathcal{O}(\Delta\Omega^{-3}) \right]$$
$$\left. + \lambda^8 \left[F_\Omega^{(10,0)} + \mathcal{O}(\Delta\Omega^{-5}) \right] + \mathcal{O}(\lambda^9) \right\},$$

$$r_{\rm p} = 6M + r^{(2,1)}\lambda^2 \Delta\Omega + \lambda^3(0) + \lambda^4 \left[r^{(4,2)} \Delta\Omega^2 + \mathcal{O}(\Delta\Omega^{-3}) \right] + \lambda^5 r^{(5,0)} \tag{7.52}$$
$$+ \lambda^6 \left[r^{(6,3)} \Delta\Omega^3 + \mathcal{O}(\Delta\Omega^{-2}) \right] + \lambda^7 \left[r^{(7,1)} \Delta\Omega + \mathcal{O}(\Delta\Omega^{-4}) \right] + \mathcal{O}(\lambda^8),$$

where the first superscripts have the same meanings as in the inspiral regime. The above expansions establish that the transition quantities at early times then take the following form

$$F_0^{\Delta\Omega} = \frac{f_1^t(\Omega_{\rm I})}{24M^2 \Delta\Omega} + \sqrt{\frac{3}{2}} \frac{f_1^t(\Omega_{\rm I})^3}{256M^5 \Delta\Omega^6} + \frac{177 f_1^t(\Omega_{\rm I})^5}{16384 M^8 \Delta\Omega^{11}} + \mathcal{O}\left(\Delta\Omega^{-16}\right), \tag{7.53}$$

$$F_2^{\Delta\Omega} = \frac{-3\sqrt{6}M f_1^t(\Omega_{\rm I}) + \partial_\Omega f_1^t(\Omega_{\rm I})}{24M^2} + \frac{-132M f_1^t(\Omega_{\rm I})^3 + 5\sqrt{6} f_1^t(\Omega_{\rm I})^2 \partial_\Omega f_1^t(\Omega_{\rm I})}{1536 M^5 \Delta\Omega^5} \tag{7.54}$$
$$+ \frac{-3213\sqrt{6}M f_1^t(\Omega_{\rm I})^5 + 525 f_1^t(\Omega_{\rm I})^4 \partial_\Omega f_1^t(\Omega_{\rm I})}{16384 M^8 \Delta\Omega^{10}} + \mathcal{O}\left(\Delta\Omega^{-15}\right),$$

and

$$R_2 = 720M^3 \Delta\Omega^2 + \frac{9\sqrt{\frac{3}{2}} f_1^t(\Omega_{\rm I})^2}{\Delta\Omega^3} + \frac{567 f_1^t(\Omega_{\rm I})^4}{64M^3 \Delta\Omega^8}. \tag{7.55}$$

$$\tag{7.56}$$

Note that $F_0^{\Delta\Omega}$ at early times and F_0^{Ω} at late times are equivalent. Note also that for a spacetime foliation of hyperboloidal slicing, $F_1^{\Delta\Omega}$ is no longer zero, which becomes important when matching to the plunge [104]. This is beyond the scope of this thesis however and is currently being implemented by collaborators.

7.2 Composite solution for the phase at 0PA order

We must now find a way to combine the inspiral and transition solutions so that they match in the near ISCO limit. This is done using a composite expansion. At 0PA order, that is to first-order in ε, in terms of Ω and ε, the frequency evolves as

$$\frac{d\Omega}{dt} = \begin{cases} \varepsilon F_0^\Omega(\Omega) + \varepsilon^{\frac{3}{5}}\left[F_0^{\Delta\Omega}\left(\frac{\Omega-\Omega_I}{\varepsilon^{\frac{2}{5}}}\right) + \varepsilon^{\frac{2}{5}}F_2^{\Delta\Omega}\left(\frac{\Omega-\Omega_I}{\varepsilon^{\frac{2}{5}}}\right)\right] - \varepsilon\left[\frac{F_\Omega^{(3,-1)}}{\Omega-\Omega_I} + F_\Omega^{(5,0)}\right], & r > 6M \\ \varepsilon^{\frac{3}{5}}\left[F_0^{\Delta\Omega}\left(\frac{\Omega-\Omega_I}{\varepsilon^{\frac{2}{5}}}\right) + \varepsilon^{\frac{2}{5}}F_2^{\Delta\Omega}\left(\frac{\Omega-\Omega_I}{\varepsilon^{\frac{2}{5}}}\right)\right], & r < 6M, \end{cases} \tag{7.57}$$

which includes only dissipative effects of the GSF, f_1^t discussed in Section 4.4. The first term describes the inspiral and all remaining terms describe the transition, except the final term for when $r > 6M$, which is required to cancel the inspiral term at late times, as will be demonstrated momentarily. In the near ISCO limit, and using Eq. (7.28) to replace the F_0^Ω term, the evolution of the frequency for $r > 6M$ becomes

$$\frac{d\Omega}{dt} \approx \varepsilon\left[\frac{F_\Omega^{(3,-1)}}{(\Omega-\Omega_I)} + F_\Omega^{(5,0)} + F_\Omega^{(7,1)}(\Omega-\Omega_I) + F_\Omega^{(9,2)}(\Omega-\Omega_I)^2\right] \tag{7.58}$$

$$+ \varepsilon^{\frac{3}{5}}\left[F_0^{\Delta\Omega}\left(\frac{\Omega-\Omega_I}{\varepsilon^{\frac{2}{5}}}\right) + \varepsilon^{\frac{2}{5}}F_2^{\Delta\Omega}\left(\frac{\Omega-\Omega_I}{\varepsilon^{\frac{2}{5}}}\right)\right] - \varepsilon\left[\frac{F_\Omega^{(3,-1)}}{\Omega-\Omega_I} + F_\Omega^{(5,0)}\right],$$

$$= \varepsilon\left[F_\Omega^{(7,1)}(\Omega-\Omega_I) + F_\Omega^{(9,2)}(\Omega-\Omega_I)^2\right] + \varepsilon^{\frac{3}{5}}\left[F_0^{\Delta\Omega}\left(\frac{\Omega-\Omega_I}{\varepsilon^{\frac{2}{5}}}\right) + \varepsilon^{\frac{2}{5}}F_2^{\Delta\Omega}\left(\frac{\Omega-\Omega_I}{\varepsilon^{\frac{2}{5}}}\right)\right], \tag{7.59}$$

so that in the limit $\Omega \to \Omega_I$, where $\Delta\Omega \to 0$, the divergent terms involving $F^{(3,-1)}/(\Omega-\Omega_I)$ cancel analytically, in addition to terms involving $F_\Omega^{(5,0)}$ and the solutions either side of the ISCO match at $r = 6M$.

To demonstrate how the frequency and phase change when the transition is included, it is instructive to compare the numerical solutions of the frequency and phase from the composite expansion, which contains information about both the inspiral and transition, with the solutions obtained when one considers the inspiral only. With an initial orbital radius of $r_p = 9M$, initial phase $\phi_p = 0$ and using *Mathematica's* `NDSolveValue` function with the precision and accuracy goals both set to 13, the frequency and phase were obtained numerically by solving a set of coupled differential equations. The parameters $M + \mu = 1.00001$ and $\nu = 0.084279$ were chosen, corresponding to the SXS catalogue NR simulation SXS:BBH:1108 [128]. NR simulations were used to set the parameters M and ν to compare GSF waveforms with those from NR later on in Chapter 8. This particular simulation was chosen because it was one of the few available in the IMRI regime at the time of writing, as most SXS simulations are for near comparable masses. For the inspiral-only solution, denoted by the label 0PA the following set of equations were integrated up to $r_p \leq 6.0001M$

$$\frac{d\Omega_{0PA}}{dt} = \nu F_0^\Omega(\Omega_{0PA}), \quad \frac{d\phi_p^{0PA}}{dt} = \Omega_{0PA}(t), \tag{7.60}$$

with the initial conditions

$$\Omega_{0\mathrm{PA}}(t) = \sqrt{\frac{M+\mu}{r_\mathrm{p}(t)^3}}, \quad r_\mathrm{p}\left(t_{\min}^{0\mathrm{PA}}\right) = 9(M+\mu), \quad \phi_\mathrm{p}\left(t_{\min}^{0\mathrm{PA}}\right) = 0. \tag{7.61}$$

The numerical solver then determines the beginning and end times of the integration, $t_{\min}^{0\mathrm{PA}} = 0$ and $t_{\max}^{0\mathrm{PA}}$. Two different versions of the composite expansions were then integrated. The first, which shall be referred to as Composite0, denoted by the label $C0$, as it includes only F_0^Ω and $F_0^{\Delta\Omega}$ and not $F_2^{\Delta\Omega}$ and hence only a part of the 0PA solution, involves solving the following set of equations over different intervals. The first set of equations

$$\frac{d\Omega_{\mathrm{C0}}^\mathrm{L}}{dt} = \nu F_0^\Omega(\Omega_{\mathrm{C0}}^\mathrm{L}) + \nu^{\frac{3}{5}} F_0^{\Delta\Omega}\left(\frac{\Omega_{\mathrm{C0}}^\mathrm{L} - \Omega_\mathrm{I}}{\nu^{\frac{2}{5}}}\right) - \frac{F_\Omega^{(3,-1)}}{\Omega_{\mathrm{C0}}^\mathrm{L} - \Omega_\mathrm{I}}\nu, \quad \frac{d\phi_\mathrm{p}^{\mathrm{C0,L}}}{dt} = \Omega_{\mathrm{C0}}^\mathrm{L}(t), \tag{7.62}$$

are integrated up to $\Omega_{\mathrm{C0}}^\mathrm{L}(t) \geq \Omega_\mathrm{I} - 0.001$, with initial conditions

$$\Omega_{\mathrm{C0}}^\mathrm{L}\left(t_{\min}^{\mathrm{C0,L}}\right) = \sqrt{\frac{M}{(9M)^3}}, \quad \phi_\mathrm{p}^{\mathrm{C0,L}}\left(t_{\min}^{\mathrm{C0,L}}\right) = 0, \tag{7.63}$$

where the label L denotes the solution 'left' of, or for times before the ISCO. The integration of the above equations will stop at some end time $t_{\max}^{\mathrm{C0,L}}$, with $t_{\min}^{\mathrm{C0,L}} = 0$. Then, the set of equations

$$\frac{d\Omega_{\mathrm{NI}}}{dt} = \nu\left[F_\Omega^{(5,0)} + F_\Omega^{(7,1)}(\Omega_{\mathrm{NI}} - \Omega_\mathrm{I}) + F_\Omega^{(9,2)}(\Omega_{\mathrm{NI}} - \Omega_\mathrm{I})^2\right] + \nu^{\frac{3}{5}} F_0^{\Delta\Omega}\left(\frac{\Omega_\mathrm{L} - \Omega_\mathrm{I}}{\nu^{\frac{2}{5}}}\right), \quad \frac{d\phi_\mathrm{p}^{\mathrm{NI}}}{dt} = \Omega_{\mathrm{NI}}(t), \tag{7.64}$$

and initial conditions

$$\Omega_{\mathrm{C0}}^{\mathrm{NI}}\left(t_{\min}^{\mathrm{C0,NI}}\right) = \Omega_{\mathrm{C0}}^\mathrm{L}\left(t_{\max}^{\mathrm{C0,L}}\right), \quad \phi_\mathrm{p}^{\mathrm{NI}}\left(t_{\min}^{\mathrm{C0,NI}}\right) = \phi_\mathrm{p}^{\mathrm{C0,L}}\left(t_{\max}^{\mathrm{C0,L}}\right), \tag{7.65}$$

were integrated from $t_{\min}^{\mathrm{C0,NI}} = t_{\max}^{\mathrm{C0,L}}$ to where $\Omega_{\mathrm{C0}}^{\mathrm{NI}}(t) = \Omega_\mathrm{I}$, which occurs at some time $t = t_\mathrm{I}^{\mathrm{C0}}$. The label NI refers to the near ISCO solution, and I the time at which the ISCO is reached. Finally, the equations

$$\frac{d\Omega_{\mathrm{C0}}^\mathrm{R}}{dt} = \nu^{\frac{3}{5}} F_0^{\Delta\Omega}\left(\frac{\Omega_{\mathrm{C0}}^\mathrm{R} - \Omega_\mathrm{I}}{\nu^{\frac{2}{5}}}\right), \quad \frac{d\phi_\mathrm{p}^{\mathrm{C0,R}}}{dt} = \Omega_{\mathrm{C0}}^\mathrm{R}(t), \tag{7.66}$$

with initial conditions

$$\Omega_{\mathrm{C0}}^\mathrm{R}\left(t_{\min}^{\mathrm{C0,R}}\right) = \Omega_{\mathrm{NI}}\left(t_\mathrm{I}^{\mathrm{C0}}\right), \quad \phi_\mathrm{p}^{\mathrm{C0,R}}\left(t_{\min}^{\mathrm{C0,R}}\right) = \phi_\mathrm{p}^{\mathrm{NI}}\left(t_\mathrm{I}^{\mathrm{C0}}\right), \tag{7.67}$$

will be solved by integrating from $t_{\min}^{\mathrm{C0,R}} = t_\mathrm{I}\mathrm{C0}$ to when $\Omega_{\mathrm{C0}}^\mathrm{R}(t) \geq \sqrt{\frac{M}{(3M)^3}}$, which occurs at some time $t = t_{\max}^{\mathrm{C0,R}}$, where the label R refers to a solution that is to the 'right' of, or for times after the ISCO. The choice of cut-off is rather arbitrary, so long as the orbital radius is far enough from the

horizon of the primary. The total frequency is then determined by

$$\Omega_{C0}(t) = \begin{cases} \Omega_{C0}^{L}, & \text{for} \quad 0 \leq t \leq t_{\max}^{C0,L}, \\ \Omega_{C0}^{NI}, & \text{for} \quad t_{\max}^{C0,L} \leq t \leq t_I C0, \\ \Omega_{C0}^{R}, & \text{for} \quad t_I C0 \leq t \leq t_{\max}^{C0,R}, \end{cases} \tag{7.68}$$

and similarly for the phase. The second composite expansion, referred to as Composite2, denoted by the label $C2$, is the same as for the $C0$ solution except for that now we include $F_2^{\Delta\Omega}$ to the right of the ISCO, and an additional term of $-\nu F_\Omega^{(5,0)}$ to the left such that

$$\frac{d\Omega_{C2}^{L}}{dt} = \nu F_0^\Omega(\Omega_{C2}^{L}) + \nu^{\frac{3}{5}}\left[F_0^{\Delta\Omega}\left(\frac{\Omega_{C2}^{L} - \Omega_I}{\nu^{\frac{2}{5}}}\right) + \nu^{\frac{2}{5}}F_2^{\Delta\Omega}\left(\frac{\Omega_{C2}^{L} - \Omega_I}{\nu^{\frac{2}{5}}}\right)\right] - \left(\frac{F_\Omega^{(3,-1)}}{\Omega_{C2}^{L} - \Omega_I} + F_\Omega^{(5,0)}\right)\nu, \tag{7.69}$$

$$\frac{d\Omega_{C2}^{NI}}{dt} = \nu\left[F_\Omega^{(7,1)}(\Omega_{C2}^{NI} - \Omega_I) + F_\Omega^{(9,2)}(\Omega_{C2}^{NI} - \Omega_I)^2\right] + \nu^{\frac{3}{5}}F_0^{\Delta\Omega}\left(\frac{\Omega_{C2}^{NI} - \Omega_I}{\nu^{\frac{2}{5}}}\right) \tag{7.70}$$

$$+ \nu F_2^{\Delta\Omega}\left(\frac{\Omega_{C2}^{NI} - \Omega_I}{\nu^{\frac{2}{5}}}\right),$$

$$\frac{d\Omega_{C2}^{R}}{dt} = \nu^{\frac{3}{5}}F_0^{\Delta\Omega}\left(\frac{\Omega_{C2}^{R} - \Omega_I}{\nu^{\frac{2}{5}}}\right) + \nu F_2^{\Delta\Omega}\left(\frac{\Omega_{C2}^{R} - \Omega_I}{\nu^{\frac{2}{5}}}\right). \tag{7.71}$$

The initial conditions, equations governing the phase and the times at which the left, near ISCO and right solutions are used are the same as before except that the label $C0$ is replaced with $C2$. The numerical results for the frequency and the phase are given below in Fig. (7.2) and Fig. (7.3) respectively, using values for $f_1^t(\Omega_I)$ and $\partial_\Omega f_1^t(\Omega_I)$ from Table (7.1).
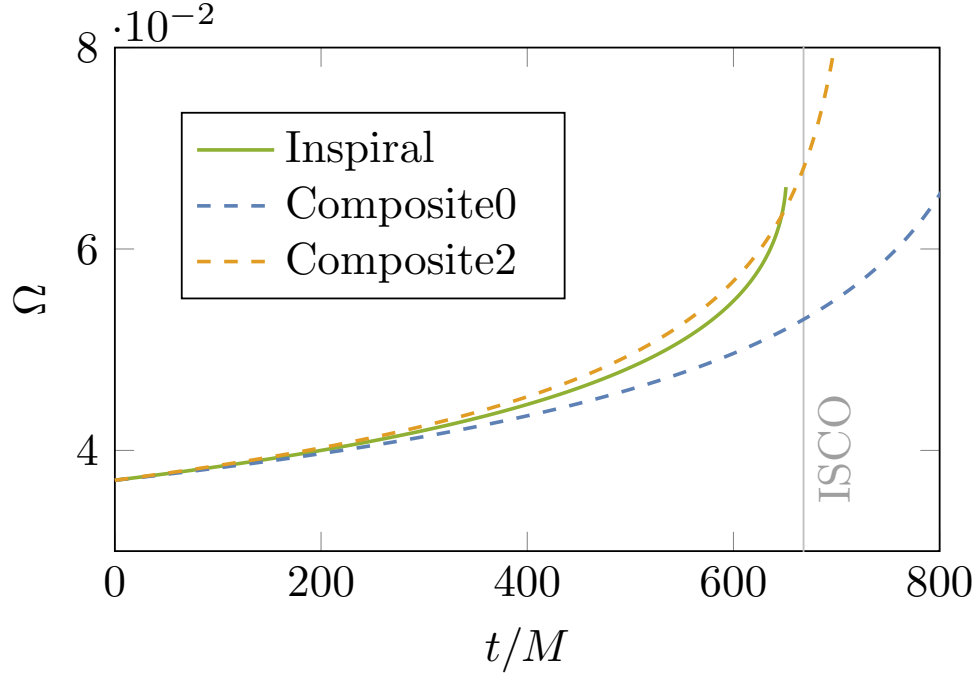
Figure 7.2: The difference between computing the frequency using only the inspiral compared to using the composite solutions Composite0 and Composite2. For the parameters $M + \mu = 1.00001$ and $\nu = 0.084279$ and initial conditions $r_\mathrm{p} = 9M$ and $\phi_\mathrm{p} = 0$ at $t = 0$, the ISCO is reached at $t_\mathrm{I} = 667.983M$, shown by the grey vertical line. For the inspiral-only results, the phase blows up near the ISCO and its integration is cut off at $r_\mathrm{p} \leq 6.0001M$. The Composite0 and Composite2 solutions show how the calculation of the phase can be smoothly extended through the ISCO. Composite2 improves on the results of Composite0 by taking into account more terms in the 0PA composite solution.
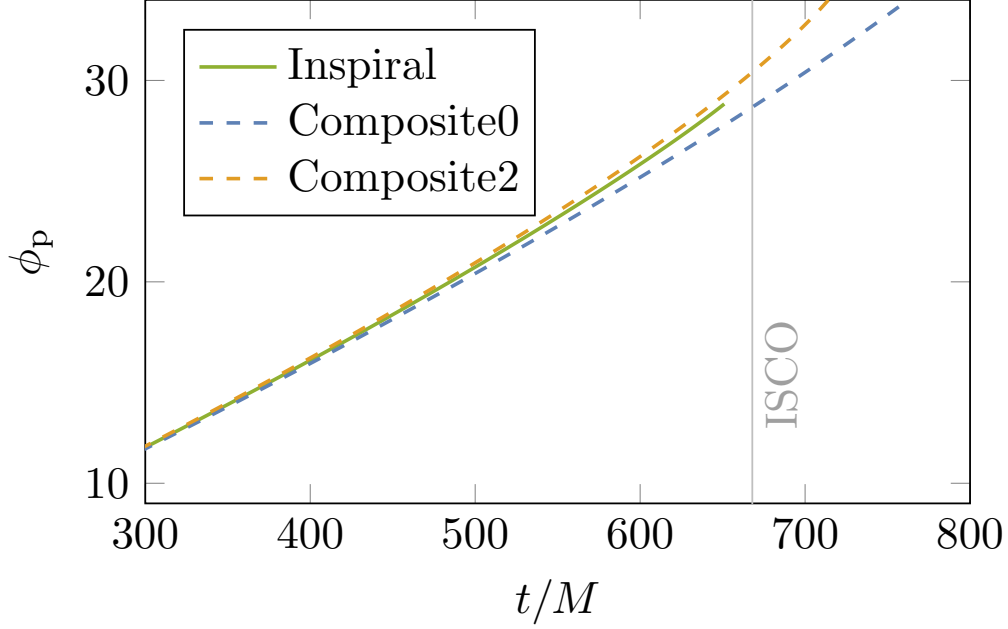
Figure 7.3: The same as Fig. (7.2) except for the orbital phase. It is vital to capture even a small change in the phase during the transition for parameter estimation of IMRIs signals measured by ground based detectors.

To obtain the evolution of the frequency and hence the orbital phase to 1PA order, we must first calculate the retarded metric perturbation and SET to second-order in the small mass ratio, now in the transition regime. The remainder of this chapter is dedicated to doing just that, leaving the 1PA phase calculation to future research, which is currently being implemented by collaborators (Küchler and Compère) at the time of writing.

7.3 The stress-energy tensor

Recall the self-consistent expansion of the SET from Eq. (2.14), Eq. (2.78) and Eq. (2.79)

$$T_{\mu\nu}^{lm}(x^\alpha; z^\alpha) = \sum_{n=1}^{\infty} \varepsilon^n T_{\mu\nu}^{n,lm}(x^\alpha; z^\alpha), \tag{7.72}$$

$$T_{lm}^{(i)}(t,r) = \sum_{n=1}^{\infty} \varepsilon^n T_{lm}^{n,(i)}(t,r), \tag{7.73}$$

$$S_{lm}^{(i)}(t,r) = \sum_{n=1}^{\infty} \varepsilon^n S_{lm}^{n,(i)}(t,r), \tag{7.74}$$

where there is a suppressed dependence on z^α, which will be made explicit momentarily. Recall from Eq. (2.41) and Eq. (2.75) that for equatorial orbits

$$T_{lm}^{1,(i)}(r, r_{\rm p}, \dot{r}_{\rm p}, \Omega, \phi_{\rm p}) = -\frac{1}{\kappa_{(i)}} \oint d\Omega \; \eta^{\alpha\mu}\eta^{\beta\nu} \frac{u_\alpha u_\beta}{u^t r_{\rm p}^2} \bar{Y}_{\mu\nu}^{(i),lm}(r_{\rm p}, \theta, \phi)\delta(r-r_{\rm p})\delta(\theta-\pi/2)\delta(\phi-\phi_{\rm p})$$

$$= -\frac{1}{\kappa_{(i)}(r_{\rm p})} \frac{u_\alpha(r_{\rm p})u_\beta(r_{\rm p})}{u^t(r_{\rm p})r_{\rm p}^2} \eta^{\alpha\mu}(r_{\rm p})\eta^{\beta\nu}(r_{\rm p})\bar{Y}_{\mu\nu}^{(i),lm}(r_{\rm p}, \pi/2, \phi_{\rm p})\delta(r-r_{\rm p}) \quad (7.75)$$

$$S_{lm}^{1,(i)}(r, r_{\rm p}, \dot{r}_{\rm p}, \Omega, \phi_{\rm p}) = -\frac{\pi f(r_{\rm p})}{4a_l^{(i)}\kappa_{(i)}(r_{\rm p})} \frac{u_\alpha(r_{\rm p})u_\beta(r_{\rm p})}{u^t(r_{\rm p})r_{\rm p}} \eta^{\alpha\mu}(r_{\rm p})\eta^{\beta\nu}(r_{\rm p})\bar{Y}_{\mu\nu}^{(i),lm}(r_{\rm p}, \pi/2, \phi_{\rm p})\delta(r-r_{\rm p}),$$

$$\tag{7.76}$$

where in the two-timescale approximation, $\phi_{\rm p} = \phi_{\rm p}(t)$, $r_{\rm p} = r_{\rm p}(\tilde{t})$ and $\Omega = \Omega(\tilde{t})$. The explicit dependence on $\dot{r}_{\rm p}$ and Ω, in addition to $r_{\rm p}$ appear in the components of u_α for quasicircular, equatorial orbits. The explicit dependence on t is absorbed by the dependence on $\phi_{\rm p}$. At second-order in ε we have [14]

$$T_{\mu\nu}^2 = -\frac{\mu}{2} \int u_\mu u_\nu \left(g^{\rho\sigma} - u^\rho u^\sigma\right) h_{\rho\sigma}^{1\mathcal{R}} \frac{\delta^4\left(x^\alpha - z^\alpha(\tau)\right)}{\sqrt{-g}} d\tau, \tag{7.77}$$

where $h_{\mu\nu}^{1\mathcal{R}}$ is the residual field introduced in Section 4.4.

During the inspiral, for quasicircular equatorial orbits, expanding $S_{lm}^{(i)}$ gives

$$S_{lm}^{(i)}(r, r_{\rm p}, \dot{r}_{\rm p}, \Omega, \phi_{\rm p}) = \tag{7.78}$$

$$\varepsilon S_{lm}^{1,(i)}(r, r_0(\Omega), 0, \Omega, \phi_{\rm p})\delta(r - r_0(\Omega))$$

$$+ \varepsilon^2 \bigg\{ S_{lm}^{2,(i)}(r, r_0(\Omega), 0, \Omega, \phi_{\rm p})\delta(r - r_0(\Omega)) - S_{lm}^{1,(i)}(r, r_0(\Omega), 0, \Omega, \phi_{\rm p})r_1(\Omega)\delta'(r - r_0(\Omega))$$

$$+ \bigg[F_0^\Omega \partial_{\dot{r}_0} S_{lm}^{1,(i)}(r, r_0(\Omega), 0, \Omega, \phi_{\rm p}) \, (\partial_\Omega r_0(\Omega))$$

$$+ \partial_{r_0} S_{lm}^{1,(i)}(r, r_0(\Omega), 0, \Omega, \phi_{\rm p})r_1(\Omega) \bigg] \delta(r - r_0(\Omega)) \bigg\}$$

$$+ \varepsilon^3 \bigg\{ S_{lm}^{3,(i)}(r, r_0(\Omega), 0, \Omega, \phi_{\rm p})\delta\left(r - r_0(\Omega)\right) - S_{lm}^{2,(i)}(r, r_0(\Omega), 0, \Omega, \phi_{\rm p})r_1(\Omega)\delta'\left(r - r_0(\Omega)\right)$$

$$+ S_{lm}^{1,(i)}(r, r_0(\Omega), 0, \Omega, \phi_{\rm p})\bigg[\frac{1}{2}r_1(\Omega)^2\delta''\left(r - r_0(\Omega)\right) - r_2(\Omega)\delta'\left(r - r_0(\Omega)\right) \bigg]$$

$$+ F_0^\Omega(\Omega)\bigg(\partial_{\dot{r}_0} S_{lm}^{2,(i)}(r, r_0(\Omega), 0, \Omega, \phi_{\rm p}) \, (\partial_\Omega r_0(\Omega))\, \delta\left(r - r_0(\Omega)\right)$$

$$- \partial_{\dot{r}_0} S_{lm}^{1,(i)}(r, r_0(\Omega), 0, \Omega, \phi_{\rm p}) \, (\partial_\Omega r_0(\Omega))\, r_1(\Omega)\delta'\left(r - r_0(\Omega)\right) \bigg)$$

$$- \partial_{r_0} S_{lm}^{1,(i)}(r, r_0(\Omega), 0, \Omega, \phi_{\rm p})r_1(\Omega)^2\delta'\left(r - r_0(\Omega)\right)$$

$$+ \partial_{r_0} S_{lm}^{2,(i)}(r, r_0(\Omega), 0, \Omega, \phi_{\rm p})r_1(\Omega)\delta\left(r - r_0(\Omega)\right)$$

$$+ \bigg(\big[F_1^\Omega(\Omega)\,(\partial_\Omega r_0(\Omega)) + F_0^\Omega(\Omega)\,(\partial_\Omega r_1(\Omega)) \big] \partial_{\dot{r}_0} S_{lm}^{1,(i)}(r, r_0(\Omega), 0, \Omega, \phi_{\rm p})$$

$$+ \frac{1}{2}\left(F_0^\Omega(\Omega) \right)^2 \partial_{\dot{r}_0}^2 S_{lm}^{1,(i)}(r, r_0(\Omega), 0, \Omega, \phi_{\rm p}) \, (\partial_\Omega r_0(\Omega))^2$$

$$+ \partial_{r_{\rm p}} S_{lm}^{1,(i)}(r, r_0(\Omega), 0, \Omega, \phi_{\rm p})r_2(\Omega)$$

$$+ F_0^\Omega(\Omega)\partial_{r_0}\partial_{\dot{r}_0} S_{lm}^{1,(i)}(r, r_0(\Omega), 0, \Omega, \phi_{\rm p})r_1(\Omega) \, (\partial_\Omega r_0(\Omega))$$

$$+ \frac{1}{2}\partial_{r_0}^2 S_{lm}^{1,(i)}(r, r_0(\Omega), 0, \Omega, \phi_{\rm p})r_1(\Omega)^2 \bigg) \delta\left(r - r_0(\Omega)\right) \bigg\}$$

$$+ \mathcal{O}(\varepsilon^4),$$

where δ' refers to differentiation with respect to r and the chain rule has been applied

$$\frac{dr_{\rm p}}{dt} = \frac{dr_{\rm p}}{d\Omega}\frac{d\Omega}{dt}, \quad \frac{dr_0}{dt} = \frac{dr_0}{d\Omega}\frac{d\Omega}{dt}.$$

To obtain the source for the transition, we must re-expand around Ω_I. Setting $\Omega \to \Omega_I + \lambda^2 \Delta\Omega$, terms such as $S_{lm}^{1,(i)}(r, r_0(\Omega), 0, \Omega, \phi_p)$ become

$$S_{lm}^{1,(i)}(r, r_0(\Omega), 0, \Omega, \phi_p) \to S_{lm}^{1,(i)}(r, r_0(\Omega_I), 0, \Omega_I, \phi_p) \tag{7.79}$$
$$+ \lambda^2 \Delta\Omega \partial_\Omega r_0(\Omega_I) \partial_{r_0} S_{lm}^{1,(i)}(r, r_0(\Omega_I), 0, \Omega_I, \phi_p)$$
$$+ \lambda^2 \partial_\Omega S_{lm}^{1,(i)}(r, r_0(\Omega_I), 0, \Omega_I, \phi_p).$$

where $r_0(\Omega_I) = 6M$, and $\partial_\Omega r_0(\Omega_I) = r^{(2,1)}$ by Eq. (7.26). It turns out that the only term appearing at $\mathcal{O}(\varepsilon^3)$ in the inspiral source, that contributes to $\mathcal{O}(\varepsilon^2)$ or lower in the transition, is that involving r_2, in particular the last term in the expression for r_2 from Eq. (7.20). Rewriting this term by replacing f_1^t in terms of F_0^Ω using Eq. (7.24) yields

$$\frac{2f_0}{\Omega^2(M\Omega)U_0^8 D^2} f_1^t \partial_\Omega f_1^t = \frac{1}{9\Omega^6 r_0^2 (r_0 - 2M)^2 \left(r_0^2 - 9Mr_0 + 18M^2\right)} \tag{7.80}$$
$$\times \left\{ 2MF_0^\Omega \left(-\Omega F_0^\Omega \left(r_0^3 - 9Mr_0^2 + 36M^3\right) \partial_\Omega r_0 \right. \right.$$
$$\left. \left. - r_0 \left(F_0^\Omega - \Omega \partial_\Omega F_0^\Omega\right)(r_0 - 6M)(r_0 - 3M)(r_0 - 2M) \right) \right\},$$

Replacing the forcing term F_0^Ω and r_0 in Eq. (7.80) with their respective late time expansions from Eq. (7.29) and Eq. (7.26), the leading term of the resulting expression for r_2 is

$$r_2 = -\frac{\left(F_\Omega^{(3,-1)}\right)^2}{108\Delta\Omega^3 \Omega_I^5 \lambda^6} + \mathcal{O}(\Delta\Omega^2 \lambda^{-4}). \tag{7.81}$$

Therefore we expect to see a contribution of the term involving r_2 to the source at $\mathcal{O}(\lambda^9)$ during the transition. All other terms that contribute to the source at $\mathcal{O}(\varepsilon^3)$ during the inspiral will not be reduced in order significantly enough to appear at $\mathcal{O}(\lambda^{10})$ or lower. Thankfully this means we do not need to compute the third-order SF, as only contributions from f_1^t appear!

In the transition regime, the source from Eq. (7.78) then becomes

$$S_{lm}^{(i)}(r, r_{\mathrm{p}}, \dot{r}_{\mathrm{p}}, \Omega, \phi_{\mathrm{p}}) = \tag{7.82}$$

$$\left\{ \lambda^5 S_{lm}^{1,(i)}(r, 6M, 0, \Omega_{\mathrm{I}}, \phi_{\mathrm{p}}) \delta(r - 6M) \right.$$

$$+ \lambda^7 \Delta\Omega \left\{ -S_{lm}^{1,(i)}(r, 6M, 0, \Omega_{\mathrm{I}}, \phi_{\mathrm{p}}) r^{(2,1)} \delta'(r - 6M) + \left[\partial_{r_0} S_{lm}^{1,(i)}(r, 6M, 0, \Omega_{\mathrm{I}}, \phi_{\mathrm{p}}) r^{(2,1)} \right. \right.$$

$$\left. \left. + \partial_\Omega S_{lm}^{1,(i)}(r, 6M, 0, \Omega_{\mathrm{I}}, \phi_{\mathrm{p}}) \right] \delta(r - 6M) \right\}$$

$$+ \lambda^8 \frac{F_\Omega^{(3,-1)} r^{(2,1)}}{\Delta\Omega} \partial_{\dot{r}_0} S_{lm}^{1,(i)}(r, 6M, 0, \Omega_{\mathrm{I}}, \phi_{\mathrm{p}}) \delta(r - 6M)$$

$$+ \lambda^9 \frac{\Delta\Omega^2}{2} \left\{ S_{lm}^{1,(i)}(r, 6M, 0, \Omega_{\mathrm{I}}, \phi_{\mathrm{p}}) \left[\left(r^{(2,1)} \right)^2 \delta''(r - 6M) - 2r^{(4,2)} \delta'(r - 6M) \right] \right.$$

$$+ 2 \left[\partial_\Omega S_{lm}^{1,(i)}(r, 6M, 0, \Omega_{\mathrm{I}}, \phi_{\mathrm{p}}) + \partial_{r_0} S_{lm}^{1,(i)}(r, 6M, 0, \Omega_{\mathrm{I}}, \phi_{\mathrm{p}}) r^{(2,1)} \right] \left(r^{(2,1)} \right) \delta'(r - 6M)$$

$$+ \left[\partial_{r_0}^2 S_{lm}^{1,(i)}(r, 6M, 0, \Omega_{\mathrm{I}}, \phi_{\mathrm{p}}) \left(r^{(2,1)} \right)^2 + 2\partial_{r_0} S_{lm}^{1,(i)}(r, 6M, 0, \Omega_{\mathrm{I}}, \phi_{\mathrm{p}}) r^{(4,2)} \right.$$

$$\left. + \partial_\Omega^2 S_{lm}^{1,(i)}(r, 6M, 0, \Omega_{\mathrm{I}}, \phi_{\mathrm{p}}) + \partial_{r_0} \partial_\Omega 2 S_{lm}^{1,(i)}(r, 6M, 0, \Omega_{\mathrm{I}}, \phi_{\mathrm{p}}) r^{(2,1)} \right] \delta(r - 6M)$$

$$+ \frac{\left(F_\Omega^{(3,-1)} \right)^2}{108 M \Delta\Omega^3 \Omega_{\mathrm{I}}^5} \left[S_{lm}^{1,(i)}(r, 6M, 0, \Omega_{\mathrm{I}}, \phi_{\mathrm{p}}) \delta'(r - 6M) \right.$$

$$\left. \left. - \partial_{r_0} S_{lm}^{1,(i)}(r, 6M, 0, \Omega_{\mathrm{I}}, \phi_{\mathrm{p}}) \delta(r - 6M) \right] \right\}$$

$$+ \lambda^{10} \left\{ S_{lm}^{2,(i)}(r, 6M, 0, \Omega_{\mathrm{I}}, \phi_{\mathrm{p}}) \delta(r - 6M) - S_{lm}^{1,(i)}(r, 6M, 0, \Omega_{\mathrm{I}}, \phi_{\mathrm{p}}) r^{(5,0)} \delta'(r - 6M) \right.$$

$$- F_\Omega^{(3,-1)} \partial_{\dot{r}_0} S_{lm}^{1,(i)}(r, 6M, 0, \Omega_{\mathrm{I}}, \phi_{\mathrm{p}}) \left(r^{(2,1)} \right)^2 \delta'(r - 6M)$$

$$+ \partial_{\dot{r}_0} S_{lm}^{1,(i)}(r, 6M, 0, \Omega_{\mathrm{I}}, \phi_{\mathrm{p}}) \left(F_\Omega^{(5,0)} r^{(2,1)} + 2F_\Omega^{(3,-1)} r^{(4,2)} \right) \delta(r - 6M)$$

$$+ \left[\partial_{r_0} S_{lm}^{1,(i)}(r, 6M, 0, \Omega_{\mathrm{I}}, \phi_{\mathrm{p}}) r^{(5,0)} + F_\Omega^{(3,-1)} \partial_{\dot{r}_0} \partial_{r_0} S_{lm}^{1,(i)}(r, 6M, 0, \Omega_{\mathrm{I}}, \phi_{\mathrm{p}}) \left(r^{(2,1)} \right)^2 \right] \delta(r - 6M)$$

$$+ F_\Omega^{(3,-1)} \left[\partial_{r_0} \partial_\Omega S_{lm}^{1,(i)}(r, 6M, 0, \Omega_{\mathrm{I}}, \phi_{\mathrm{p}}) \left(r^{(2,1)} \right)^2 \right] \delta(r - 6M) \right\}$$

$$\left. + \mathcal{O}(\lambda^{11}) \right\}.$$

7.4 The metric perturbation and field equations

We have now determined the phase during both the inspiral and the transition. What remains to generate a waveform is to calculate the metric perturbation amplitudes. The inspiral amplitudes were calculated in Chapter 5, and we must now calculate the amplitudes during the transition. To do so, we will examine the structure of the metric perturbation in the inspiral, re-expanded in the near ISCO limit. Naïvely expanding the inspiral metric perturbation about the ISCO yields

$$
\begin{aligned}
\bar{h}_{lm}^{(i)}(r, \Omega, \phi_{\mathrm{p}}) &= \lambda^5 \bar{h}_{lm}^{1,(i)}(r, \lambda^2 \Delta\Omega + \Omega_{\mathrm{I}}, \phi_{\mathrm{p}}) + \lambda^{10} \bar{h}_{lm}^{2,(i)}(r, \lambda^2 \Delta\Omega + \Omega_{\mathrm{I}}, \phi_{\mathrm{p}}) + \mathcal{O}(\lambda^{15}) \\
&= \lambda^5 \bar{h}_{lm}^{1,(i)}(r, \Omega_{\mathrm{I}}, \phi_{\mathrm{p}}) + \lambda^7 \Delta\Omega \partial_\Omega \bar{h}^1(r, \Omega_{\mathrm{I}}, \phi_{\mathrm{p}}) + \lambda^9 \frac{(\Delta\Omega)^2}{2} \partial_\Omega^2 \bar{h}^1(r, \Omega_{\mathrm{I}}, \phi_{\mathrm{p}}) \\
&\quad + \lambda^{10} \bar{h}_{lm}^{2,(i)}(r, \Omega_{\mathrm{I}}, \phi_{\mathrm{p}}).
\end{aligned}
\tag{7.83}
$$

We will discover however that this naive Taylor expansion is not the full story, and that there are missing contributions to the metric perturbation in the transition. To rectify this, we must return to the field equations in search of this missing information.

7.4.1 Slowly evolving time derivative operators during inspiral

To obtain the transition amplitudes, we must examine the linearised Einstein field equations in the transition regime, in particularly, how time derivatives behave on the transition timescale. Recall the operator $\delta G_{(j)}^{(i)}$ from Eq. (2.82) in the self-consistent expansion. The operator contains terms involving ∂_t and ∂_t^2, which for quasicircular, equatorial orbits, can be written as

$$
\partial_t = \Omega \partial_{\phi_{\mathrm{p}}} + \dot{\Omega} \partial_\Omega,
\tag{7.84}
$$

$$
\begin{aligned}
\partial_t^2 &= (\Omega \partial_{\phi_{\mathrm{p}}} + \dot{\Omega} \partial_\Omega)(\Omega \partial_{\phi_{\mathrm{p}}} + \dot{\Omega} \partial_\Omega), \\
&= \Omega^2 \partial_{\phi_{\mathrm{p}}}^2 + 2\Omega\dot{\Omega}\partial_\Omega\partial_{\phi_{\mathrm{p}}} + \dot{\Omega}\partial_{\phi_{\mathrm{p}}} + \dot{\Omega}(\partial_\Omega\dot{\Omega})\partial_\Omega + \dot{\Omega}^2 \partial_\Omega^2,
\end{aligned}
\tag{7.85}
$$

where an overdot here denotes a full derivative with respect to t. The time derivative operator can be expanded in the inspiral regime by defining

$$
\partial_t = \sum_{n=0}^{\infty} \varepsilon^n \partial_t^{(n)},
\tag{7.86}
$$

$$
\partial_t^2 = \sum_{n=0}^{\infty} \varepsilon^n \Box_t^{(n)},
\tag{7.87}
$$

such that

$$
\partial_t^{(0)} = \Omega \partial_{\phi_{\mathrm{p}}}, \quad \partial_t^{(1)} = F_0^\Omega \partial_\Omega, \quad \partial_t^{(2)} = F_1^\Omega \partial_\Omega, \quad \partial_t^{(3)} = F_2^\Omega \partial_\Omega,
\tag{7.88}
$$

123

and

$$\Box_t^{(0)} = \Omega^2 \partial_{\phi_\mathrm{p}}^2, \tag{7.89}$$

$$\Box_t^{(1)} = F_0^\Omega (2\Omega \partial_\Omega \partial_{\phi_\mathrm{p}} + \partial_{\phi_\mathrm{p}}), \tag{7.90}$$

$$\Box_t^{(2)} = F_0^\Omega \left(\partial_\Omega F_0^\Omega\right) \partial_\Omega + \left(F_0^\Omega\right)^2 \partial_\Omega^2 + F_1^\Omega (2\Omega \partial_\Omega \partial_{\phi_\mathrm{p}} + \partial_{\phi_\mathrm{p}},) \tag{7.91}$$

$$\Box_t^{(3)} = \left(F_1^\Omega \partial_\Omega F_0^\Omega + F_0^\Omega \partial_\Omega F_1^\Omega\right) \partial_\Omega + 2F_0^\Omega F_1^\Omega \partial_\Omega^2 + F_2^\Omega (2\Omega \partial_\Omega \partial_{\phi_\mathrm{p}} + \partial_{\phi_\mathrm{p}}). \tag{7.92}$$

The time derivative operators from the inspiral can then be determined in the near ISCO limit, using, Eq. (7.28) and Eq. (7.29) to obtain time derivatives, and hence the linearised Einstein operators for the transition regime.

7.4.2 Inspiral metric perturbation at late times

Recall the self-consistent expansion of Eq. (4.63) from Chapter 4

$$\delta^1 G_{(j)}^{(i)} \left(\varepsilon \bar{h}_{lm}^{1,(i)}(r, \Omega, \phi_\mathrm{p}) + \varepsilon^2 \bar{h}_{lm}^{2,(i)}(r, \Omega, \phi_\mathrm{p}) + \cdots \right) \tag{7.93}$$
$$+ \delta^2 G_{(j)(k)}^{(i)} \left(\varepsilon \bar{h}_{lm}^{1,(i)}(r, \Omega, \phi_\mathrm{p}) + \varepsilon^2 \bar{h}_{lm}^{2,(i)}(r, \Omega, \phi_\mathrm{p}) + \cdots \right) \left(\varepsilon \bar{h}_{lm}^{1,(k)}(r, \Omega, \phi_\mathrm{p}) + \varepsilon^2 \bar{h}_{lm}^{2,(k)}(r, \Omega, \phi_\mathrm{p}) + \cdots \right) + \cdots$$
$$= \varepsilon S_{lm}^{1,(i)}(r, r_\mathrm{p}, \dot{r}_\mathrm{p}, \Omega, \phi_\mathrm{p}) + \varepsilon^2 S_{lm}^{2,(i)}(r, r_\mathrm{p}, \dot{r}_\mathrm{p}, \Omega, \phi_\mathrm{p}) + \cdots .$$

In the two-timescale expansion, recall from Eq. (4.65) that $\delta^1 G_{(j)}^{(i)}$ becomes

$$\delta^1 G_{(j)}^{(i)} = \sum_{n=0}^\infty \varepsilon^n \delta^1 G_{(j)}^{n,(i)}, \tag{7.94}$$

where, after dropping the l subscripts on $\mathcal{M}_\Omega$ and $\mathcal{M}_r$ for convenience and making use of the slowly evolving time derivative operators during the inspiral

$$\delta^1 G_{(j)}^{0,(i)} = \delta_{(j)}^{(i)} \left(\frac{1}{4}(\Box_t^{(0)} - \partial_{r_*}^2) + V_l(r) \right) + \mathcal{M}_{\Omega(j)}^{(i)} \partial_t^{(0)} + \mathcal{M}_{r(j)}^{(i)}, \tag{7.95a}$$

$$\delta^1 G_{(j)}^{1,(i)} = \frac{1}{4}\delta_{(j)}^{(i)} \Box_t^{(1)} + \mathcal{M}_{\Omega(j)}^{(i)} \partial_t^{(1)}, \tag{7.95b}$$

$$\delta^1 G_{(j)}^{2,(i)} = \frac{1}{4}\delta_{(j)}^{(i)} \Box_t^{(2)} + \mathcal{M}_{\Omega(j)}^{(i)} \partial_t^{(2)}. \tag{7.95c}$$

At first-order in ε, the Lorenz gauge field equations in the two-timescale approximation during inspiral are

$$\delta^1 G_{(j)}^{0,(i)} \left[\bar{h}_{lm}^{1,(j)}(r, \Omega, \phi_\mathrm{p}) \right] = S_{lm}^{1,(i)}(r, r_0(\Omega), 0, \Omega, \phi_\mathrm{p}) \delta(r - r_0(\Omega)), \tag{7.96}$$

as we have seen before in Eq. (4.67). In the limit near the ISCO, this becomes simply

$$\delta^1 G_{(j)}^{0,(i)} \left[\bar{h}_{lm}^{1,(j)}(r, \Omega_\mathrm{I}, \phi_\mathrm{p}) \right] = S_{lm}^{1,(i)}(r, 6M, 0, \Omega_\mathrm{I}, \phi_\mathrm{p}) \delta(r - 6M). \tag{7.97}$$

At second-order in ε, the Lorenz gauge field equations in the two-timescale approximation during inspiral are

$$\delta^1 G_{(j)}^{0,(i)}\left[\bar{h}_{lm}^{2,(j)}(r,\Omega,\phi_{\rm p})\right] = \tilde{S}_{lm}^{2,(i)}(r,r_0(\Omega),0,\Omega,\phi_{\rm p}) - 2\delta^2 G_{(j)(k)}^{0,(i)}\left[\bar{h}_{lm}^{1,(j)},\bar{h}_{lm}^{1,(k)}\right] - \delta^1 G_{(j)}^{1,(i)}\left[\bar{h}_{lm}^{1,(i)}\right]$$
$$+ F_0^\Omega(\Omega)\partial_{\dot{r}_0}S_{lm}^{1,(i)}(r,r_0(\Omega),0,\Omega,\phi_{\rm p})\partial_\Omega r_0(\Omega)\delta(r-r_0(\Omega)), \quad (7.98)$$

with

$$\tilde{S}_{lm}^{2,(i)}(r,r_0(\Omega),0,\Omega,\phi_{\rm p}) = - S_{lm}^{1,(i)}(r,r_0(\Omega),0,\Omega,\phi_{\rm p})r_1^\Omega(\Omega)\delta'(r-r_0(\Omega)) \quad (7.99)$$
$$+ \Big[S_{lm}^{2,(i)}(r,r_0(\Omega),0,\Omega,\phi_{\rm p})$$
$$+ r_1^\Omega(\Omega)\partial_{r_0}S_{lm}^{1,(i)}(r,r_0(\Omega),0,\Omega,\phi_{\rm p})\Big]\delta(r-r_0(\Omega)),$$

where the source terms can be read from the coefficient of ε^2 in Eq. (7.78) and $\tilde{S}_{lm}^{2,(i)}$ should not be confused with that from Chapter 4. We shall let

$$\bar{h}_{lm}^{2,(i)}(r,\Omega,\phi_{\rm p}) = \bar{h}_{\mathcal{P}}^{2,(i)}(r,\Omega,\phi_{\rm p}) + \bar{h}_{\rm R1}^{2,(i)}(r,\Omega,\phi_{\rm p}) + \bar{h}_{\rm R2}^{2,(i)}(r,\Omega,\phi_{\rm p}), \quad (7.100)$$

for a given l,m mode, such that

$$\delta^1 G_{(j)}^{0,(i)}\left[\bar{h}_{\mathcal{P}}^{2,(j)}\right] = \tilde{S}_{lm}^{2,(i)}, \quad (7.101)$$

$$\delta^1 G_{(j)}^{0,(i)}\left[\bar{h}_{\rm R1}^{2,(j)}\right] = - 2\delta^2 G_{(j)(k)}^{0,(i)}\left[\bar{h}_{lm}^{1,(j)},\bar{h}_{lm}^{1,(k)}\right], \quad (7.102)$$

$$\delta^1 G_{(j)}^{0,(i)}\left[\bar{h}_{\rm R2}^{2,(i)}\right] = - \delta^1 G_{(j)}^{1,(i)}\left[\bar{h}_{lm}^{1,(j)}\right] + F_0^\Omega \tilde{S}_{lm}^{1,(i)}, \quad (7.103)$$

where

$$\tilde{S}_{lm}^{1,(i)}(r,r_0(\Omega),0,\Omega,\phi_{\rm p}) = \partial_{\dot{r}_0}S^{1,(i)}(r,r_0(\Omega),0,\Omega,\phi_{\rm p})\left(\partial_\Omega r_0(\Omega)\right)\delta(r-r_0(\Omega)). \quad (7.104)$$

Equation (7.103) can then be written as

$$\delta^1 G_{(j)}^{0,(i)}\left[\bar{h}_{\rm R2}^{2,(j)}\right] = - \delta^1 G_{(j)}^{1,(i)}\left[\bar{h}_{lm}^{1,(j)}\right] + F_0^\Omega \tilde{S}_{lm}^{1,(i)}, \quad (7.105)$$
$$= - \left(\frac{1}{4}\delta_{(j)}^{(i)}\Box_t^{(1)} + \mathcal{M}_{\Omega(j)}^{(i)}\partial_t^{(1)}\right)\bar{h}_{lm}^{1,(j)} + F_0^\Omega \tilde{S}_{lm}^{1,(i)},$$
$$= - \left(\frac{1}{4}\delta_{(j)}^{(i)}F_0^\Omega(2\Omega\partial_\Omega\partial_{\phi_{\rm p}} + \partial_{\phi_{\rm p}}) + \mathcal{M}_{\Omega(j)}^{(i)}F_0^\Omega\partial_\Omega\right)\bar{h}_{lm}^{1,(j)} + F_0^\Omega \tilde{S}_{lm}^{1,(i)},$$
$$= - F_0^\Omega\left(\frac{1}{4}\delta_{(j)}^{(i)}(2\Omega\partial_\Omega\partial_{\phi_{\rm p}} + \partial_{\phi_{\rm p}}) + \mathcal{M}_{\Omega(j)}^{(i)}\partial_\Omega\right)\bar{h}_{lm}^{1,(j)} + F_0^\Omega \tilde{S}_{lm}^{1,(i)}.$$

Therefore, we can rewrite $\bar{h}_{lm}^{2,(i)}$ as

$$\bar{h}_{lm}^{2,(i)}(r,\Omega,\phi_{\rm p}) = \bar{h}_{\mathcal{P}}^{2,(i)}(r,\Omega,\phi_{\rm p}) + \bar{h}_{\rm R1}^{2,(i)}(r,\Omega,\phi_{\rm p}) + F_0^\Omega(\Omega)\hat{h}_{\rm R2}^{2,(i)}(r,\Omega,\phi_{\rm p}), \quad (7.106)$$

such that

$$\delta^1 G^{0,(i)}_{(j)} \left[\hat{h}^2_{\text{R2}} \right] = -\left(\frac{1}{4} \delta^{(i)}_{(j)} (2\Omega \partial_\Omega \partial_{\phi_\text{p}} + \partial_{\phi_\text{p}}) + \mathcal{M}^{(i)}_{\Omega(j)} \partial_\Omega \right) \bar{h}^{1,(j)}_{lm} + \tilde{S}^{1,(i)}_{lm}. \qquad (7.107)$$

We can factor out F^Ω_0 because the operator $\delta^1 G^{0,(i)}_{(j)}$ does not contain any Ω derivatives and hence leaves functions of Ω unchanged. The expansion of the metric perturbation in the inspiral near the ISCO then becomes

$$\bar{h}^{(i)}_{lm}(r, \Delta\Omega, \phi_\text{p}) = \lambda^5 \bar{h}^{1,(i)}_{lm}(r, \Omega_\text{I}, \phi_\text{p}) + \lambda^7 \Delta\Omega \partial_\Omega \bar{h}^{1,(i)}_{lm}(r, \Omega_\text{I}, \phi_\text{p}) + \lambda^8 \frac{F^{(3,-1)}_\Omega}{\Delta\Omega} \hat{h}^{2,(i)}_{\text{R2}}(r, \Omega_\text{I}, \phi_\text{p}) \qquad (7.108)$$

$$+ \lambda^9 \frac{(\Delta\Omega)^2}{2} \partial^2_\Omega \bar{h}^{1,(i)}_{lm}(r, \Omega_\text{I}, \phi_\text{p}) + \lambda^{10} \bar{h}^{2,(i)}_{\mathcal{P}}(r, \Omega_\text{I}, \phi_\text{p}) + \lambda^{10} \bar{h}^{2,(i)}_{\text{R1}}(r, \Omega_\text{I}, \phi_\text{p})$$

$$+ \lambda^{10} F^{(5,0)}_\Omega \hat{h}^{2,(i)}_{\text{R2}}(r, \Omega_\text{I}, \phi_\text{p}) + \lambda^{10} F^{(3,-1)}_\Omega \partial_\Omega \hat{h}^{2,(i)}_{\text{R2}}(r, \Omega_\text{I}, \phi_\text{p}).$$

The term $\hat{h}^{2,(i)}_{\text{R2}}$ appears in the inspiral at $\mathcal{O}(\varepsilon^2)$, but in the limit near the ISCO has a contribution to both $\mathcal{O}(\lambda^8)$ and $\mathcal{O}(\lambda^{10})$. Hence we have recovered additional information in the transition that was previously unaccounted for. We will repeat the same procedure for higher order terms in the inspiral metric perturbation to ensure we are not neglecting any contributions that may appear at lower orders in the transition.

At third-order in ε, the field equations are

$$\delta^1 G^{0,(i)}_{(j)} \left[\bar{h}^{3,(j)}_{lm} \right] = -\delta^1 G^{1,(i)}_{(j)} \left[\bar{h}^{2,(j)}_{lm} \right] - \delta^1 G^{2,(i)}_{(j)(k)} \left[\bar{h}^{1,(j)}_{lm} \right] - \delta^3 G^{0,(i)}_{(j)(k)(t)} \left[\bar{h}^{1,(j)}_{lm}, \bar{h}^{1,(k)}_{lm}, \bar{h}^{1,(t)}_{lm} \right] \qquad (7.109)$$

$$- \delta^2 G^{1,(i)}_{(j)(k)} \left[\bar{h}^{1,(j)}_{lm}, \bar{h}^{1,(k)}_{lm} \right] - \delta^2 G^{0,(i)}_{(j)(k)} \left[\bar{h}^{1,(j)}_{lm}, \bar{h}^{2,(k)}_{lm} \right],$$

where the source terms can be read from the coefficient of ε^3 in Eq. (7.78), but are not given explicitly here due to the length of expressions. The sources will be reinstated later on in Section 7.4.3 as they are too long to express here. After some investigation it was found that all terms on the right-hand side of the third-order equation other than the first two would not be reduced by $\mathcal{O}(\lambda^5)$ or more. Therefore, considering only the first two terms on the right-hand side, we let

$$\bar{h}^{3,(i)}_{lm}(r, \Omega, \phi_\text{p}) = \bar{h}^{3,(i)}_\text{A}(r, \Omega, \phi_\text{p}) + \bar{h}^{3,(i)}_\text{B}(r, \Omega, \phi_\text{p}), \qquad (7.110)$$

for a given l, m mode, such that

$$\delta^1 G^{0,(i)}_{(j)} \left[\bar{h}^{3,(j)}_\text{A} \right] = -\delta^1 G^{1,(i)}_{(j)} \left[\bar{h}^{2,(j)}_{lm} \right], \qquad (7.111)$$

$$\delta^1 G^{0,(i)}_{(j)} \left[\bar{h}^{3,(j)}_\text{B} \right] = -\delta^1 G^{2,(i)}_{(j)} \left[\bar{h}^{1,(j)}_{lm} \right]. \qquad (7.112)$$

Considering first Eq. (7.111)

$$\delta^1 G^{0,(i)}_{(j)}\left[\bar{h}^{3,(j)}_{\mathrm{A}}\right] = -\,\delta^1 G^{1,(i)}_{(j)}\left[\bar{h}^{2,(j)}_{lm}\right],\tag{7.113}$$

$$= -\,\delta^1 G^{1,(i)}_{(j)}\left[\bar{h}^{2,(j)}_{\mathcal{P}} + \bar{h}^{2,(j)}_{\mathrm{R1}} + F^{\Omega}_0 \hat{h}^{2,(j)}_{\mathrm{R2}}\right],$$

$$= -\,F^{\Omega}_0\left(\frac{1}{4}\delta^{(i)}_{(j)}(2\Omega\partial_\Omega\partial_{\phi_{\mathrm{P}}} + \partial_{\phi_{\mathrm{P}}}) + \mathcal{M}^{(i)}_{\Omega(j)}\partial_\Omega\right)\left(\bar{h}^{2,(j)}_{\mathrm{R1}} + F^{\Omega}_0 \hat{h}^{2,(j)}_{\mathrm{R2}}\right),$$

$$= -\,F^{\Omega}_0\left(\frac{1}{4}\delta^{(i)}_{(j)}(2\Omega\partial_\Omega\partial_{\phi_{\mathrm{P}}} + \partial_{\phi_{\mathrm{P}}}) + \mathcal{M}^{(i)}_{\Omega(j)}\partial_\Omega\right)\bar{h}^{2,(j)}_{\mathrm{R1}}$$

$$- \left(F^{\Omega}_0\right)^2\left(\frac{1}{4}\delta^{(i)}_{(j)}(2\Omega\partial_\Omega\partial_{\phi_{\mathrm{P}}} + \partial_{\phi_{\mathrm{P}}}) + \mathcal{M}^{(i)}_{\Omega(j)}\partial_\Omega\right)\hat{h}^{2,(j)}_{\mathrm{R2}}$$

$$- F^{\Omega}_0\left(\frac{1}{4}\delta^{(i)}_{(j)}2\Omega\left(\partial_\Omega F^{\Omega}_0\right)\partial_{\phi_{\mathrm{P}}}\hat{h}^{2,(j)}_{\mathrm{R2}} + \mathcal{M}^{(i)}_{\Omega(j)}\left(\partial_\Omega F^{\Omega}_0\right)\hat{h}^{2,(j)}_{\mathrm{R2}}\right),$$

where higher-order terms are ignored and the puncture terms have been discarded, to be reinstated later on. In the limit near the ISCO

$$\delta^1 G^{0,(i)}_{(j)}\left[\bar{h}^{3,(j)}_{\mathrm{A}}\right] = -\frac{F^{(3,-1)}_\Omega}{\lambda^2\Delta\Omega}\left(\frac{1}{4}\delta^{(i)}_{(j)}(2\Omega\partial_\Omega\partial_{\phi_{\mathrm{P}}} + \partial_{\phi_{\mathrm{P}}}) + \mathcal{M}^{(i)}_{\Omega(j)}\partial_\Omega\right)\bar{h}^{2,(j)}_{\mathrm{R1}}\tag{7.114}$$

$$- \left(\frac{F^{(3,-1)}_\Omega}{\lambda^2\Delta\Omega}\right)^2\left(\frac{1}{4}\delta^{(i)}_{(j)}(2\Omega\partial_\Omega\partial_{\phi_{\mathrm{P}}} + \partial_{\phi_{\mathrm{P}}}) + \mathcal{M}^{(i)}_{\Omega(j)}\partial_\Omega\right)\hat{h}^{2,(j)}_{\mathrm{R2}}$$

$$- \frac{F^{(3,-1)}_\Omega}{\lambda^2\Delta\Omega}\left\{\frac{1}{4}\delta^{(i)}_{(j)}2\Omega\left(\partial_\Omega\frac{F^{(3,-1)}_\Omega}{\lambda^2\Delta\Omega}\right)\right\}\partial_{\phi_{\mathrm{P}}}\hat{h}^{2,(j)}_{\mathrm{R2}} - \mathcal{M}^{(i)}_{\Omega(j)}\left(\partial_\Omega\frac{F^{(3,-1)}_\Omega}{\lambda^2\Delta\Omega}\right)\hat{h}^{2,(j)}_{\mathrm{R2}},$$

$$= \delta^{(i)}_{(j)}\frac{\Omega}{2}\frac{\left(F^{(3,-1)}_\Omega\right)^2}{\lambda^6\Delta\Omega^3}\partial_{\phi_{\mathrm{P}}}\hat{h}^{2,(j)}_{\mathrm{R2}},$$

where only terms contributing to $\mathcal{O}(\lambda^{10})$ or lower are considered, that is, in the limit near the ISCO, $\mathcal{O}(\varepsilon^3)$ contributions from the inspiral must be lowered by at least λ^5. All higher order terms are neglected. Next, considering Eq. (7.112)

$$\delta^1 G^{0,(i)}_{(j)}\left[\bar{h}^{3,(j)}_{\mathrm{B}}\right] = -\,\delta^1 G^{2,(i)}_{(j)}\left[\bar{h}^{1,(j)}_{lm}\right],\tag{7.115}$$

$$= -\left(\frac{1}{4}\delta^{(i)}_{(j)}\Box^{(2)}_t + \mathcal{M}^{(i)}_{\Omega(j)}\partial^{(2)}_t\right)\bar{h}^{1,(j)}_{lm},$$

$$= -\left\{\frac{1}{4}\delta^{(i)}_{(j)}\left(F^{\Omega}_0(\partial_\Omega F^{\Omega}_0)\partial_\Omega + (F^{\Omega}_0)^2\partial^2_\Omega + F^{\Omega}_1(2\Omega\partial_\Omega\partial_{\phi_{\mathrm{P}}} + \partial_{\phi_{\mathrm{P}}})\right) + \mathcal{M}^{(i)}_{\Omega(j)}\left(F^{\Omega}_1\partial_\Omega\right)\right\}\bar{h}^{1,(j)}_{lm},$$

which in the near ISCO limit becomes

$$\delta^1 G_{(j)}^{0,(i)} \left[\bar{h}_{\mathrm{B}}^{3,(j)} \right] = \delta_{(j)}^{(i)} \frac{\left(F_\Omega^{(3,-1)} \right)^2}{4\lambda^6 \Delta\Omega^3} \partial_\Omega \bar{h}_{lm}^{1,(j)}. \tag{7.116}$$

Therefore we can rewrite $\bar{h}_{lm}^{3,(j)}$ as

$$\bar{h}_{lm}^{3,(j)}(r,\Omega,\phi_{\mathrm{p}}) = F_0^\Omega(\Omega) \left(\partial_\Omega F_0^\Omega(\Omega) \right) \hat{h}_{\mathrm{A}}^3(r,\Omega,\phi_{\mathrm{p}}) + F_0^\Omega(\Omega) \left(\partial_\Omega F_0^\Omega(\Omega) \right) \hat{h}_{\mathrm{B}}^3(r,\Omega,\phi_{\mathrm{p}}), \tag{7.117}$$

where, ignoring higher order terms,

$$\delta^1 G_{(j)}^{0,(i)} \left[\hat{h}_{\mathrm{A}}^{3,(j)} \right] = \delta_{(j)}^{(i)} \frac{\Omega}{2} \partial_{\phi_{\mathrm{p}}} \hat{h}_{\mathrm{R2}}^{2,(j)}, \tag{7.118}$$

$$\delta^1 G_{(j)}^{0,(i)} \left[\hat{h}_{\mathrm{B}}^{3,(j)} \right] = \frac{1}{4} \delta_{(j)}^{(i)} \partial_\Omega \bar{h}_{lm}^{1,(j)}. \tag{7.119}$$

Seeing as both terms in Eq. (7.117) have the same structure, we can write

$$\hat{h}_{lm}^{3,(i)} = \hat{h}_{\mathrm{A}}^{3,(i)} + \hat{h}_{\mathrm{B}}^{3,(i)}, \tag{7.120}$$

$$\bar{h}_{lm}^{3,(i)} = F_0^\Omega \left(\partial_\Omega F_0^\Omega \right) \hat{h}^3, \tag{7.121}$$

$$\delta^1 G_{(j)}^{0,(i)} \left[\hat{h}_{lm}^{3,(j)} \right] = \delta_{(j)}^{(i)} \frac{\Omega}{2} \partial_{\phi_{\mathrm{p}}} \hat{h}_{\mathrm{R2}}^{2,(j)} + \frac{1}{4} \delta_{(j)}^{(i)} \partial_\Omega \bar{h}_{lm}^{1,(j)}. \tag{7.122}$$

Finally, at fourth-order in ε, the field equations are

$$\delta^1 G_{(j)}^{0,(i)} \left[\bar{h}_{lm}^{4,(j)} \right] = -\delta^1 G_{(j)}^{1,(i)} \left[\bar{h}_{lm}^{3,(j)} \right] - \delta^1 G_{(j)}^{2,(i)} \left[\bar{h}_{lm}^{2,(j)} \right] - \delta^1 G_{(j)}^{3,(i)} \left[\bar{h}_{lm}^{1,(j)} \right], \tag{7.123}$$

where the source terms are neglected here due to the length of expressions, and it will turn out they will not be needed anyway as we will see later that all fourth-order contributions vanish. Terms involving $\delta^2 G, \delta^3 G$ and $\delta^4 G$ are also neglected here as they do not reduce the order of the metric perturbation significantly enough. We shall let

$$\bar{h}_{lm}^{4,(i)}(r,\Omega,\phi_{\mathrm{p}}) = \bar{h}_{\mathrm{A}}^{4,(i)}(r,\Omega,\phi_{\mathrm{p}}) + \bar{h}_{\mathrm{B}}^{4,(i)}(r,\Omega,\phi_{\mathrm{p}}) + \bar{h}_{\mathrm{C}}^{4,(i)}(r,\Omega,\phi_{\mathrm{p}}), \tag{7.124}$$

such that

$$\delta^1 G_{(j)}^{0,(i)} \left[\bar{h}_{\mathrm{A}}^{4,(i)} \right] = -\delta^1 G_{(j)}^{1,(i)} \left[\bar{h}_{lm}^{3,(j)} \right], \tag{7.125}$$

$$\delta^1 G_{(j)}^{0,(i)} \left[\bar{h}_{\mathrm{B}}^{4,(i)} \right] = -\delta^1 G_{(j)}^{2,(i)} \left[\bar{h}_{lm}^{2,(j)} \right], \tag{7.126}$$

$$\delta^1 G_{(j)}^{0,(i)} \left[\bar{h}_{\mathrm{C}}^{4,(i)} \right] = -\delta^1 G_{(j)}^{3,(i)} \left[\bar{h}_{lm}^{1,(j)} \right]. \tag{7.127}$$

Considering first Eq. (7.125), we shall only keep terms that lower the $\mathcal{O}(\varepsilon^4)$ terms in the inspiral by λ^{10} or more in the near ISCO limit

$$\delta^1 G^{0,(i)}_{(j)}\left[\bar{h}^{4,(i)}_{\mathrm{A}}\right] = -\,\delta^1 G^1\left[\bar{h}^{3,(j)}_{lm}\right],\tag{7.128}$$

$$= -\,F^{\Omega}_0\left(\frac{1}{4}\delta^{(i)}_{(j)}(2\Omega\partial_{\Omega}\partial_{\phi_{\mathrm{p}}} + \partial_{\phi_{\mathrm{p}}}) + \mathcal{M}^{(i)}_{\Omega(j)}\partial_{\Omega}\right)\left(F^{\Omega}_0\left(\partial_{\Omega}F^{\Omega}_0\right)\hat{h}^{3,(j)}_{lm}\right),$$

$$= -\left(F^{\Omega}_0\right)^2\left(\partial_{\Omega}F^{\Omega}_0\right)\left(\frac{1}{4}\delta^{(i)}_{(j)}(2\Omega\partial_{\Omega}\partial_{\phi_{\mathrm{p}}} + \partial_{\phi_{\mathrm{p}}}) + \mathcal{M}^{(i)}_{\Omega(j)}\partial_{\Omega}\right)\hat{h}^{3,(j)}_{lm}$$
$$-\,F^{\Omega}_0\left(\frac{1}{4}\delta^{(i)}_{(j)}2\Omega\left(\partial_{\Omega}F^{\Omega}_0\right)^2\partial_{\phi_{\mathrm{p}}}\hat{h}^{3,(j)}_{\tilde{\mathrm{A}}} + \mathcal{M}^{(i)}_{\Omega(j)}\left(\partial_{\Omega}F^{\Omega}_0\right)^2\hat{h}^{3,(j)}_{lm}\right)$$
$$-\left(F^{\Omega}_0\right)^2\left(\frac{1}{4}\delta^{(i)}_{(j)}2\Omega\left(\partial^2_{\Omega}F^{\Omega}_0\right)\partial_{\phi_{\mathrm{p}}}\hat{h}^{3,(j)}_{\tilde{\mathrm{A}}} + \mathcal{M}^{(i)}_{\Omega(j)}\left(\partial^2_{\Omega}F^{\Omega}_0\right)\hat{h}^{3,(j)}_{lm}\right),$$

$$= -\left(F^{\Omega}_0\left(\partial_{\Omega}F^{\Omega}_0\right)^2 + \left(F^{\Omega}_0\right)^2\left(\partial^2_{\Omega}F^{\Omega}_0\right)\right)\left(\delta^{(i)}_{(j)}\frac{\Omega}{2}\partial_{\phi_{\mathrm{p}}} + \mathcal{M}^{(i)}_{\Omega(j)}\right)\hat{h}^{3,(j)}_{lm},$$

which in the near ISCO limit become

$$\delta^1 G^{0,(i)}_{(j)}\left[\bar{h}^{4,(i)}_{\mathrm{A}}\right] = -\,2\frac{\left(F^{(3,-1)}_{\Omega}\right)^3}{\lambda^{10}\Delta\Omega^5}\left(\delta^{(i)}_{(j)}\frac{\Omega}{2}\partial_{\phi_{\mathrm{p}}} + \mathcal{M}^{(i)}_{\Omega(j)}\right)\hat{h}^{3,(j)}_{lm}.$$

Next, considering Eq. (7.126)

$$\delta^1 G^{0,(i)}_{(j)}\left[\bar{h}^{4,(i)}_{\mathrm{B}}\right] = -\,\delta^1 G^2\left[\bar{h}^{2,(j)}_{lm}\right],\tag{7.129}$$
$$= \left\{\frac{1}{4}\delta^{(i)}_{(j)}\left[F^{\Omega}_0(\partial_{\Omega}F^{\Omega}_0)\partial_{\Omega} + (F^{\Omega}_0)^2\partial^2_{\Omega} + F^{\Omega}_1(2\Omega\partial_{\Omega}\partial_{\phi_{\mathrm{p}}} + \partial_{\phi_{\mathrm{p}}})\right] + \mathcal{M}^{(i)}_{\Omega(j)}\left(F^{\Omega}_1\partial_{\Omega}\right)\right\}\left(F^{\Omega}_0\hat{h}^{2,(j)}_{\mathrm{R2}}\right),$$
$$= \left\{\frac{1}{4}\delta^{(i)}_{(j)}\left[F^{\Omega}_0(\partial_{\Omega}F^{\Omega}_0)\partial_{\Omega} + (F^{\Omega}_0)^2\partial^2_{\Omega}\right]\right\}\left(F^{\Omega}_0\hat{h}^{2,(j)}_{\mathrm{R2}}\right),$$
$$= \frac{1}{4}\delta^{(i)}_{(j)}\left[F^{\Omega}_0(\partial_{\Omega}F^{\Omega}_0)^2 + (F^{\Omega}_0)^2\left(\partial^2_{\Omega}F^{\Omega}_0\right)\right]\hat{h}^{2,(j)}_{\mathrm{R2}},$$

which in the near ISCO limit becomes

$$\delta^1 G^{0,(i)}_{(j)}\left[\bar{h}^{4,(i)}_{\mathrm{B}}\right] = \frac{3}{4}\delta^{(i)}_{(j)}\frac{\left(F^{(3,-1)}_{\Omega}\right)^3}{\lambda^{10}\Delta\Omega^5}\hat{h}^{2,(j)}_{\mathrm{R2}}$$

129

Finally, considering Eq. (7.127)

$$\delta^1 G^0 \left[\bar{h}_{\rm C}^4 \right] = - \delta^1 G^3 \left[\bar{h}_{lm}^1 \right], \tag{7.130}$$

$$= \left(\frac{1}{4} \delta_{(j)}^{(i)} \Box_t^{(3)} + \mathcal{M}_{\Omega(j)}^{(i)} \partial_t^{(3)} \right) \bar{h}_{lm}^{1,(j)},$$

$$= \left\{ \frac{1}{4} \delta_{(j)}^{(i)} \left[\left(F_1^\Omega \partial_\Omega F_0^\Omega + F_0^\Omega \partial_\Omega F_1^\Omega \right) \partial_\Omega + 2 F_0^\Omega F_1^\Omega \partial_\Omega^2 + F_2^\Omega (2\Omega \partial_\Omega \partial_{\phi_{\rm P}} + \partial_{\phi_{\rm P}}) \right] \tag{7.131}$$

$$+ \mathcal{M}_{\Omega(j)}^{(i)} \left(F_2^\Omega \partial_\Omega \right) \right\} \bar{h}_{lm}^{1,(j)},$$

which in the near ISCO limit becomes

$$\delta^1 G^0 \left[\bar{h}_{\rm C}^4 \right] = \frac{1}{4} \delta_{(j)}^{(i)} \left[\left(\frac{F_\Omega^{(6,-2)}}{\lambda^4 \Delta\Omega^2} \left(-\frac{F_\Omega^{(3,-1)}}{\lambda^4 \Delta\Omega^2} \right) + \frac{F_\Omega^{(3,-1)}}{\lambda^2 \Delta\Omega} \left(-2\frac{F_\Omega^{(6,-2)}}{\lambda^6 \Delta\Omega^3} - \right) \right) \partial_\Omega \tag{7.132}$$

$$+ 2\frac{F_\Omega^{(3,-1)}}{\lambda^2 \Delta\Omega} \frac{F_\Omega^{(6,-2)}}{\lambda^4 \Delta\Omega^2} \partial_\Omega^2 \right] \bar{h}_{lm}^{1,(j)},$$

$$> \mathcal{O}(\lambda^{10}).$$

Putting this altogether we have

$$\bar{h}_{lm}^{4,(i)} = \left[F_0^\Omega (\partial_\Omega F_0^\Omega)^2 + (F_0^\Omega)^2 \left(\partial_\Omega^2 F_0^\Omega \right) \right] \hat{h}_{\rm A}^{4,(i)} + \left[F_0^\Omega (\partial_\Omega F_0^\Omega)^2 + (F_0^\Omega)^2 \left(\partial_\Omega^2 F_0^\Omega \right) \right] \hat{h}_{\rm B}^{4,(i)}, \tag{7.133}$$

where, ignoring higher order terms

$$\delta^1 G_{(j)}^{0,(i)} \left[\hat{h}_{\rm A}^{4,(j)} \right] = \left(\delta_{(j)}^{(i)} \frac{\Omega}{2} \partial_{\phi_{\rm P}} + \mathcal{M}_{\Omega(j)}^{(i)} \right) \hat{h}_{lm}^{3,(j)}, \tag{7.134}$$

$$\delta^1 G_{(j)}^{0,(i)} \left[\hat{h}_{\rm B}^{4,(j)} \right] = \frac{1}{4} \delta_{(j)}^{(i)} \hat{h}_{\rm R2}^{2,(j)}. \tag{7.135}$$

$$\tag{7.136}$$

As both terms in Eq. (7.133) have the same structure, similarly to our approach at third-order in ε, we can write

$$\hat{h}_{lm}^{4,(i)} = \hat{h}_{\rm A}^{4,(i)} + \hat{h}_{\rm B}^{4,(i)}, \tag{7.137}$$

$$\bar{h}_{lm}^{4,(i)} = \left[F_0^\Omega (\partial_\Omega F_0^\Omega)^2 + (F_0^\Omega)^2 \left(\partial_\Omega^2 F_0^\Omega \right) \right] \hat{h}_{lm}^{4,(i)}, \tag{7.138}$$

$$\delta^1 G_{(j)}^{0,(i)} \left[\hat{h}_{lm}^{4,(j)} \right] = \left(\delta_{(j)}^{(i)} \frac{\Omega}{2} \partial_{\phi_{\rm P}} + \mathcal{M}_{\Omega(j)}^{(i)} \right) \hat{h}_{\tilde{\rm A}}^{3,(j)} + \frac{1}{4} \delta_{(j)}^{(i)} \hat{h}_{\rm R2}^{2,(j)}. \tag{7.139}$$

This concludes all of the inspiral metric perturbation contributions at $\mathcal{O}(\lambda^{10})$ or lower that appear in the limit near the ISCO, and hence are valid during the transition. The full metric perturbation,

valid in both the inspiral and transition can therefore be written in terms of inspiral quantities as

$$\bar{h}_{lm}^{(i)}(r,\Omega,\phi_{\rm p}) = \lambda^5 \bar{h}_{lm}^{1,(i)}(r,\Omega_{\rm I},\phi_{\rm p}) + \lambda^7 \Delta\Omega\partial_\Omega\bar{h}_{lm}^{1,(i)}(r,\Omega_{\rm I},\phi_{\rm p}) + \lambda^9 \frac{(\Delta\Omega)^2}{2}\partial_\Omega^2\bar{h}_{lm}^1(r,\Omega_{\rm I},\phi_{\rm p}) \qquad (7.140)$$

$$+ \lambda^{10}\left\{\bar{h}_\mathcal{P}^{2,(i)}(r,\Omega_{\rm I},\phi_{\rm p}) + \bar{h}_{\rm R1}^{2,(i)}(r,\Omega_{\rm I},\phi_{\rm p})\right\} + \lambda^{10}F_0^\Omega\hat{h}_{\rm R2}^{2,(i)}(r,\Omega,\phi_{\rm p})$$

$$+ \lambda^{15}F_0^\Omega\left(\partial_\Omega F_0^\Omega\right)\hat{h}_{lm}^{3,(i)}(r,\Omega_{\rm I},\phi_{\rm p}) + \lambda^{20}\left\{F_0^\Omega\left(\partial_\Omega F_0^\Omega\right)^2 + \left(F_0^\Omega\right)^2\left(\partial_\Omega^2 F_0^\Omega\right)\right\}\hat{h}_{lm}^{4,(i)}(r,\Omega_{\rm I},\phi_{\rm p})$$

$$+ \mathcal{O}(\lambda^{25}).$$

Noting the dependence on Ω and not $\Omega_{\rm I}$ of $\hat{h}_{\rm R2}^2$. The term involving $\partial_\Omega^2 F_0^\Omega$ can be replaced using Eq. (7.36), using the fact that F_0^Ω and $F_0^{\Delta\Omega}$ match in the transition regime. In the limit near the ISCO, Eq. (7.140) then becomes

$$\bar{h}_{lm}^{(i)}(r,\Delta\Omega,\phi_{\rm p}) = \lambda^5 \bar{h}_{lm}^{1,(i)}(r,\Omega_{\rm I},\phi_{\rm p}) + \lambda^7 \Delta\Omega\partial_\Omega\bar{h}_{lm}^{1,(i)}(r,\Omega_{\rm I},\phi_{\rm p}) + \lambda^8 \frac{F_\Omega^{(3,-1)}}{\Delta\Omega}\hat{h}_{\rm R2}^{2,(i)}(r,\Omega_{\rm I},\phi_{\rm p}) \quad (7.141)$$

$$+ \lambda^9 \frac{(\Delta\Omega)^2}{2}\partial_\Omega^2\bar{h}_{lm}^{1,(i)}(r,\Omega_{\rm I},\phi_{\rm p}) - \lambda^9 \frac{\left(F_\Omega^{(3,-1)}\right)^2}{\Delta\Omega^3}\hat{h}_{lm}^{3,(i)}(r,\Omega_{\rm I},\phi_{\rm p})$$

$$+ \lambda^{10}\left[\bar{h}_\mathcal{P}^{2,(i)}(r,\Omega_{\rm I},\phi_{\rm p}) + \bar{h}_{\rm R1}^{2,(i)}(r,\Omega_{\rm I},\phi_{\rm p})\right]$$

$$+ \lambda^{10}F_\Omega^{(5,0)}\hat{h}_{\rm R2}^{2,(i)}(r,\Omega_{\rm I},\phi_{\rm p}) + \lambda^{10}F_\Omega^{(3,-1)}\partial_\Omega\hat{h}_{\rm R2}^{2,(i)}(r,\Omega_{\rm I},\phi_{\rm p}) + \mathcal{O}(\lambda^{11}),$$

where any contribution from $\bar{h}_{lm}^{4,(i)}$ has been eliminated using the second-order ODE for F_0^Ω. In Chapter 5 we calculate $\bar{h}_{lm}^{1,(i)}$, and in $\partial_{r_0}\bar{h}_{lm}^{1,(i)}$, from which we can easily obtain $\partial_\Omega\bar{h}_{lm}^{1,(i)}$ by the chain rule. The terms $\bar{h}_\mathcal{P}^{2,(i)}, \bar{h}_{\rm R1}^{2,(i)}, \hat{h}_{\rm R2}^{2,(i)}$ have also already been calculated by Warburton $et\ al$ [118, 4, 3]. What remains to be calculated are: $\partial_\Omega^2\bar{h}_{lm}^{1,(i)}$ and $\hat{h}_{lm}^{3,(i)}$. Most of the work involved in calculating the GW amplitudes is already done therefore. The above derivation demonstrates that we need not solve directly for the transition amplitudes $j_{\mu\nu}^{n,(i)}$ therefore, which would require re-deriving the Einstein field equations in the transition and solving a completely new set of equations.

7.4.3 Inspiral field equations at late times

Reinstating the source terms, the full set of field equations in the transition regime that we need to solve are listed as follows

$$
\mathcal{O}(\lambda^5): \quad \delta^1 G^{0,(i)}_{(j)}\left[\bar{h}^{1,(j)}_{lm}(r,\Omega_{\rm I},\phi_{\rm p})\right] = S^{1,(i)}_{lm}(r,6M,0,\Omega_{\rm I},\phi_{\rm p})\delta(r-6M), \tag{7.142}
$$

$$
\mathcal{O}(\lambda^7): \quad \delta^1 G^{0,(i)}_{(j)}\left[\partial_\Omega \bar{h}^{1,(j)}_{lm}(r,\Omega_{\rm I},\phi_{\rm p})\right] = r^{(2,1)}\big[-S^{1,(i)}_{lm}(r,6M,0,\Omega_{\rm I},\phi_{\rm p})\delta'(r-6M) \tag{7.143}
$$
$$
+\left(\partial_{r_0}+\partial_\Omega\right)S^{1,(i)}_{lm}(r,6M,0,\Omega_{\rm I},\phi_{\rm p})\delta(r-6M)\big],
$$

$$
\mathcal{O}(\lambda^8): \quad \delta^1 G^{0,(i)}_{(j)}\left[\hat{h}^{2,(j)}_{\rm R2}(r,\Omega_{\rm I},\phi_{\rm p})\right] = -\left(\frac{1}{4}\delta^{(i)}_{(j)}(2\Omega\partial_\Omega\partial_{\phi_{\rm p}}+\partial_{\phi_{\rm p}})+\mathcal{M}^{(i)}_{r(j)}\partial_\Omega\right)\bar{h}^{1,(j)}_{lm}(r,\Omega_{\rm I},\phi_{\rm p})
$$
$$
+\partial_{\dot{r}_0}S^{1,(i)}_{lm}(r,6M,0,\Omega_{\rm I},\phi_{\rm p})r^{(2,1)}\delta(r-6M), \tag{7.144}
$$

$$
\mathcal{O}(\lambda^9): \quad \delta^1 G^{0,(i)}_{(j)}\left[\partial^2_\Omega \bar{h}^{1,(j)}_{lm}(r,\Omega_{\rm I},\phi_{\rm p})\right] = S^{1,(i)}_{lm}(r,6M,0,\Omega_{\rm I},\phi_{\rm p}) \tag{7.145}
$$
$$
\times\left[\left(r^{(2,1)}\right)^2\delta''(r-6M)-2r^{(4,2)}\delta'(r-6M)\right]
$$
$$
+2\left(r^{(2,1)}\partial_{r_0}+\partial_\Omega\right)S^{1,(i)}_{lm}(r,6M,0,\Omega_{\rm I},\phi_{\rm p})r^{(2,1)}\delta'(r-6M)
$$
$$
+\left[\partial^2_{r_0}S^{1,(i)}_{lm}(r,6M,0,\Omega_{\rm I},\phi_{\rm p})\left(r^{(2,1)}\right)^2\right.
$$
$$
+2\partial_{r_0}S^{1,(i)}_{lm}(r,6M,0,\Omega_{\rm I},\phi_{\rm p})r^{(4,2)}
$$
$$
+\partial^2_\Omega S^{1,(i)}_{lm}(r,6M,0,\Omega_{\rm I},\phi_{\rm p})
$$
$$
\left.+\partial_{r_0}\partial_\Omega S^{1,(i)}_{lm}(r,6M,0,\Omega_{\rm I},\phi_{\rm p})r^{(2,1)}\right]\delta(r-6M),
$$

$$
\delta^1 G^{0,(i)}_{(j)}\left[\hat{h}^{3,(j)}_{lm}(r,\Omega_{\rm I},\phi_{\rm p})\right] = \delta^{(i)}_{(j)}\left(\frac{\Omega}{2}\partial_{\phi_{\rm p}}\hat{h}^{2,(j)}_{\rm R2}(r,\Omega_{\rm I},\phi_{\rm p})+\frac{1}{4}\partial_\Omega\bar{h}^{1,(j)}_{lm}(r,\Omega_{\rm I},\phi_{\rm p})\right) \tag{7.146}
$$
$$
+\frac{1}{108M\Omega^5_{\rm p}}\left[\partial_{r_0}S^{1,(i)}_{lm}(r,6M,0,\Omega_{\rm I},\phi_{\rm p})\delta(r-6M)\right.
$$
$$
\left.-S^{1,(i)}_{lm}(r,6M,0,\Omega_{\rm I},\phi_{\rm p})\delta'(r-6M)\right],
$$

$$\mathcal{O}(\lambda^{10}): \quad \delta^1 G_{(j)}^{0,(i)}\left[\bar{h}_{\mathcal{P}}^{2,(j)}(r,\Omega_{\mathrm{I}},\phi_{\mathrm{p}})\right] = S_{lm}^{2,(i)}(r,6M,0,\Omega_{\mathrm{I}},\phi_{\mathrm{p}})\delta(r-6M) \tag{7.147}$$

$$- S_{lm}^{1,(i)}(r,6M,0,\Omega_{\mathrm{I}},\phi_{\mathrm{p}})r^{(5,0)}\delta'(r-6M)$$

$$+ \partial_{r_{\mathrm{p}}}S_{lm}^{1,(i)}(r,6M,0,\Omega_{\mathrm{I}},\phi_{\mathrm{p}})r^{(5,0)}\delta(r-6M),$$

$$\delta^1 G_{(j)}^{0,(i)}\left[\bar{h}_{\mathrm{R1}}^{2,(j)}(r,\Omega_{\mathrm{I}},\phi_{\mathrm{p}})\right] = -2\delta^2 G_{(j)(k)}^{0,(i)}\left[\bar{h}_{lm}^{1,(j)}(r,\Omega_{\mathrm{I}},\phi_{\mathrm{p}}),\bar{h}_{lm}^{1,(k)}(r,\Omega_{\mathrm{I}},\phi_{\mathrm{p}})\right], \tag{7.148}$$

$$\delta^1 G_{(j)}^{0,(i)}\left[F_\Omega^{(5,0)}\hat{h}_{\mathrm{R2}}^{2,(j)}(r,\Omega_{\mathrm{I}},\phi_{\mathrm{p}})\right] = F_\Omega^{(5,0)}\left(\frac{1}{4}\delta_{(j)}^{(i)}(2\Omega\partial_\Omega\partial_{\phi_{\mathrm{p}}}+\partial_{\phi_{\mathrm{p}}})+\mathcal{M}_{r(j)}^{(i)}\partial_\Omega\right)\bar{h}_{lm}^{1,(j)}(r,\Omega_{\mathrm{I}},\phi_{\mathrm{p}})$$

$$- F_\Omega^{(3,-1)}\left(\frac{1}{4}\delta_{(j)}^{(i)}(2\Omega\partial_\Omega\partial_{\phi_{\mathrm{p}}}+\partial_{\phi_{\mathrm{p}}})+\mathcal{M}_{r(j)}^{(i)}\partial_\Omega\right)\partial_\Omega\bar{h}_{lm}^{1,(j)}(r,\Omega_{\mathrm{I}},\phi_{\mathrm{p}})$$

$$+ \partial_{\dot{r}_0}S_{lm}^{1,(i)}(r,6M,0,\Omega_{\mathrm{I}},\phi_{\mathrm{p}})\left[-F_\Omega^{(3,-1)}\left(r^{(2,1)}\right)^2\delta'(r-6M)\right.$$

$$\left.+ \left(F_\Omega^{(5,0)}r^{(2,1)}+2F_\Omega^{(3,-1)}r^{(4,2)}\right)\delta(r-6M)\right], \tag{7.149}$$

$$\delta^1 G_{(j)}^{0,(i)}\left[\partial_\Omega\hat{h}_{\mathrm{R2}}^{2,(j)}(r,\Omega_{\mathrm{I}},\phi_{\mathrm{p}})\right] = \partial_{\dot{r}_0}\left(\partial_{r_0}+\partial_\Omega\right)S_{lm}^{1,(i)}(r,6M,0,\Omega_{\mathrm{I}},\phi_{\mathrm{p}})\left(r^{(2,1)}\right)^2\delta(r-6M). \tag{7.150}$$

Notice how the terms involving $F_\Omega^{(3,-1)}$ in Eq. (7.149) cancel, recovering the same equation as Eq. (7.144), due to the fact that the second term on the right-hand side of Eq. (7.103) becomes

$$\delta^1 G_{(j)}^{1,(i)}[\bar{h}_{lm}^{1,(j)}] = \left(\frac{1}{4}\delta_{(j)}^{(i)}\Box_t^{(1)}+\mathcal{M}_{\Omega(j)}^{(i)}\partial_t^{(1)}\right)\bar{h}^{1,(j)}(r,\Omega,\phi_{\mathrm{p}}) \tag{7.151}$$

$$= F_0^\Omega\left(\frac{1}{4}\delta_{(j)}^{(i)}(2\Omega\partial_\Omega\partial_{\phi_{\mathrm{p}}}+\partial_{\phi_{\mathrm{p}}})+\mathcal{M}_{\Omega(j)}^{(i)}\partial_\Omega\right)\left(\bar{h}^{1,(j)}(r,\Omega_{\mathrm{I}},\phi_{\mathrm{p}})+\lambda^2\Delta\Omega\partial_\Omega\bar{h}^{1,(j)}(r,\Omega_{\mathrm{I}},\phi_{\mathrm{p}})\right)$$

$$= \frac{F_\Omega^{(3,-1)}}{\lambda^2\Delta\Omega}\left(\frac{1}{4}\delta_{(j)}^{(i)}(2\Omega\partial_\Omega\partial_{\phi_{\mathrm{p}}}+\partial_{\phi_{\mathrm{p}}})+\mathcal{M}_{\Omega(j)}^{(i)}\partial_\Omega\right)\bar{h}^{1,(j)}(r,\Omega_{\mathrm{I}},\phi_{\mathrm{p}})$$

$$+ F_\Omega^{(5,0)}\left(\frac{1}{4}\delta_{(j)}^{(i)}(2\Omega\partial_\Omega\partial_{\phi_{\mathrm{p}}}+\partial_{\phi_{\mathrm{p}}})+\mathcal{M}_{\Omega(j)}^{(i)}\partial_\Omega\right)\bar{h}^{1,(j)}(r,\Omega_{\mathrm{I}},\phi_{\mathrm{p}})$$

$$+ F_\Omega^{(3,-1)}\left(\frac{1}{4}\delta_{(j)}^{(i)}(2\Omega\partial_\Omega\partial_{\phi_{\mathrm{p}}}+\partial_{\phi_{\mathrm{p}}})+\mathcal{M}_{\Omega(j)}^{(i)}\partial_\Omega\right)\partial_\Omega\bar{h}^{1,(j)}(r,\Omega_{\mathrm{I}},\phi_{\mathrm{p}}),$$

where the third term is sourced in the following way

$$\left(\frac{1}{4}\delta_{(j)}^{(i)}(2\Omega\partial_\Omega\partial_{\phi_{\mathrm{p}}}+\partial_{\phi_{\mathrm{p}}})+\mathcal{M}_{\Omega(j)}^{(i)}\partial_\Omega\right)\partial_\Omega\bar{h}^{1,(j)} = \partial_{\dot{r}_0}S_{lm}^{1,(i)}\left[\left(\partial_\Omega^2 r_0\right)\delta(r-6M)-(\partial_\Omega r_0)^2\delta'(r-6M)\right]. \tag{7.152}$$

133

Replacing the term

$$F_\Omega^{(3,-1)} \left(\frac{1}{4} \delta_{(j)}^{(i)} (2\Omega \partial_\Omega \partial_{\phi_{\rm p}} + \partial_{\phi_{\rm p}}) + \mathcal{M}_{\Omega(j)}^{(i)} \partial_\Omega \right) \partial_\Omega \bar{h}_{lm}^{1,(j)}(r, \Omega_{\rm I}, \phi_{\rm p}),$$

in Eq. (7.149) with the right-hand side of Eq. (7.152), all terms involving $F_\Omega^{(3,-1)}$ cancel, then dividing across by $F_\Omega^{(5,0)}$ recovers the Eq. (7.144).

The quantity $\partial_\Omega^2 \bar{h}_{lm}^{1,(i)}$ can be determined from $\partial_{r_0}^2 \bar{h}_{lm}^{1,(i)}$ by numerically differentiating $\partial_{r_0} \bar{h}_{lm}^{1,(i)}$ from Chapter 6. While a numerical derivative will be less accurate than directly solving Eq. (7.145), it will surely save many hours of work if we can avoid solving Eq. (7.145), or alternatively, implementing a partial annihilators scheme for second r_0 derivatives. Both of these methods would involve deriving new boundary conditions and jump conditions. As we only need to evaluate the second Ω derivative of the first-order metric perturbation for when $\Omega = \Omega_{\rm I}$, it makes more sense therefore to proceed with numerical integration. We must also find a way to solve for $\hat{h}_{lm}^{3,(i)}$ to complete the 0PA waveform in the transition. We know all of the source terms in Eq. (7.146) already, but we shall leave solving this equation to future research.

7.4.4 Matching to the transition metric perturbation at early times

We have saved a lot of time by avoiding solving the field equations directly in the transition regime. However, it remains instructive to examine the structure of the metric perturbation in the transition to ensure we have captured all of the information when re-expanding the inspiral quantities in the near ISCO limit. During the transition, the time derivative operator is now

$$\partial_t = \sum_{n=0}^\infty \lambda^n \partial_t^{(n)} \tag{7.153}$$

where

$$\partial_t^{(0)} = \Omega \partial_{\phi_{\rm p}}, \quad \partial_t^{(1)} = \partial_t^{(2)} = 0, \quad \partial_t^{(3)} = F_0^{\Delta\Omega} \partial_\Omega, \quad \partial_t^{(4)} = 0, \quad \partial_t^{(5)} = F_2^{\Delta\Omega} \partial_\Omega. \tag{7.154}$$

Writing the metric perturbation and linearised Einstein field equations in the BSL basis and using the two-timescale expansion tells us that the structure of the metric perturbation in the transition is [125, 126, 104]

$$\mathcal{O}(\lambda^5): \quad j_{lm}^{5,(i)}(r,\Omega,\phi_p) = \hat{j}_{lm}^{5,(i)}(r,\Omega_I,\phi_p), \tag{7.155a}$$

$$\mathcal{O}(\lambda^6): \quad j_{lm}^{6,(i)}(r,\Omega,\phi_p) = 0, \tag{7.155b}$$

$$\mathcal{O}(\lambda^7): \quad j_{lm}^{7,(i)}(r,\Omega,\phi_p) = \Delta\Omega \hat{j}_{lm}^{7,(i)}(r,\Omega_I,\phi_p), \tag{7.155c}$$

$$\mathcal{O}(\lambda^8): \quad j_{lm}^{8,(i)}(r,\Omega,\phi_p) = F_0^{\Delta\Omega} \hat{j}_{lm}^{8,(i)}(r,\Omega_I,\phi_p), \tag{7.155d}$$

$$\mathcal{O}(\lambda^9): \quad j_{lm}^{9,(i)}(r,\Omega,\phi_p) = F_0^{\Delta\Omega}\left(\partial_{\Delta\Omega}F_0^{\Delta\Omega}\right)\hat{j}_A^{9,(i)}(r,\Omega_I,\phi_p) + \Delta\Omega^2\hat{j}_B^{9,(i)}(r,\Omega_I,\phi_p), \tag{7.155e}$$

$$\mathcal{O}(\lambda^{10}): \quad j_{lm}^{10,(i)}(r,\Omega,\phi_p) = \hat{j}_A^{10,(i)}(r,\Omega_I,\phi_p) + F_2^{\Delta\Omega}\hat{j}_B^{10,(i)}(r,\Omega_I,\phi_p) \tag{7.155f}$$
$$+ F_0^{\Delta\Omega}\left(\partial_{\Delta\Omega}F_0^{\Delta\Omega}\right)^2\hat{j}_C^{10,(i)}(r,\Omega_I,\phi_p)$$
$$+ \left(F_0^{\Delta\Omega}\right)^2\left(\partial_{\Delta\Omega}^2F_0^{\Delta\Omega}\right)\hat{j}_D^{10,(i)}(r,\Omega_I,\phi_p) + \Delta\Omega F_0^{\Delta\Omega}\hat{j}_E^{10,(i)}(r,\Omega_I,\phi_p).$$

Matching the transition to the inspiral in the near ISCO limit gives

$$\mathcal{O}(\lambda^5): \quad \hat{j}_{lm}^{5,(i)}(r,\Omega_I,\phi_p) = \bar{h}_{lm}^{1,(i)}(r,\Omega_I,\phi_p), \tag{7.156a}$$

$$\mathcal{O}(\lambda^6): \quad \hat{j}_{lm}^{6,(i)} = 0, \tag{7.156b}$$

$$\mathcal{O}(\lambda^7): \quad \hat{j}_{lm}^{7,(i)}(r,\Omega_I,\phi_p) = \partial_\Omega\bar{h}_{lm}^{1,(i)}(r,\Omega_I,\phi_p), \tag{7.156c}$$

$$\mathcal{O}(\lambda^8): \quad \hat{j}_{lm}^{8,(i)}(r,\Omega_I,\phi_p) = \hat{h}_{R2}^{2,(i)}(r,\Omega_I,\phi_p), \tag{7.156d}$$

$$\mathcal{O}(\lambda^9): \quad \hat{j}_A^{9,(i)}(r,\Omega_I,\phi_p) = \hat{h}_{lm}^{3,(i)}(r,\Omega_I,\phi_p), \quad \hat{j}_B^{9,(i)}(r,\Omega_I,\phi_p) = \frac{1}{2}\partial_\Omega^2\bar{h}_{lm}^{1,(i)}(r,\Omega_I,\phi_p), \tag{7.156e}$$

$$\mathcal{O}(\lambda^{10}): \quad \hat{j}_A^{10,(i)}(r,\Omega_I,\phi_p) = \bar{h}_{R1}^{2,(i)}(r,\Omega_I,\phi_p) + \bar{h}_{\mathcal{P}}^{2,(i)}(r,\Omega_I,\phi_p), \tag{7.156f}$$
$$\hat{j}_B^{10,(i)}(r,\Omega_I,\phi_p) = \hat{h}_{R2}^{2,(i)}(r,\Omega_I,\phi_p),$$
$$\hat{j}_C^{10,(i)}(r,\Omega_I,\phi_p) = \hat{j}_D^{10,(i)}(r,\Omega_I,\phi_p) = \hat{h}_{lm}^{4,(i)}(r,\Omega_I,\phi_p),$$
$$\hat{j}_E^{10,(i)}(r,\Omega_I,\phi_p) = \partial_\Omega\hat{h}_{R2}^{2,(i)}(r,\Omega_I,\phi_p).$$

Rearranging the equation of motion for $F_0^{\Delta\Omega}$, Eq. (7.36) so that

$$F_0^{\Delta\Omega}\left(\partial_\Omega F_0^{\Delta\Omega}\right)^2 + \left(F_0^{\Delta\Omega}\right)^2\partial_\Omega^2 F_0^{\Delta\Omega} = \frac{1}{9\sqrt{6}M}\left(\frac{3\mathcal{F}_1(6M)}{96M^2} - \Delta\Omega\right), \tag{7.157}$$

where we have used Eq. (7.33) to make the replacement in Eq. (7.157) [14]

$$f_1^t(\Omega_I) = -\frac{3}{4}\mathcal{F}_1(r_I), \tag{7.158}$$

and using the fact that $\hat{j}_C^{10,(i)} = \hat{j}_D^{10,(i)}$, we can simplify the behaviour at $\mathcal{O}(\lambda^{10})$ to

$$\mathcal{O}(\lambda^{10}): \quad j_{lm}^{10} = \hat{j}_A^{10,(i)} + \frac{\mathcal{F}_1(6M)}{288\sqrt{6}M^3}\hat{j}_C^{10,(i)} + F_2^{\Delta\Omega}\hat{j}_B^{10,(i)} + \Delta\Omega F_0^{\Delta\Omega}\left(\hat{j}_E^{5,(i)} - \frac{1}{9\sqrt{6}M}\hat{j}_C^{5,(i)}\right), \tag{7.159}$$

when evaluated at $\Omega = \Omega_{\mathrm{I}}$.

Setting

$$\hat{\jmath}_{\mathrm{A}}^{10,(i)} + \frac{\mathcal{F}_1(6M)}{288\sqrt{6}M^3}\hat{\jmath}_{\mathrm{C}}^{10,(i)} \rightarrow \hat{\jmath}_{\mathrm{A}}^{10,(i)}, \quad \hat{\jmath}_{\mathrm{E}}^{10,(i)} - \frac{1}{9\sqrt{6}M}\hat{\jmath}_{\mathrm{C}}^{10,(i)} \rightarrow \hat{\jmath}_{\mathrm{C}}^{10,(i)}, \tag{7.160}$$

we have

$$\mathcal{O}(\lambda^{10}): \quad j_{lm}^{10} = \left. \left\{ \hat{\jmath}_{\mathrm{A}}^{10,(i)} + F_2^{\Delta\Omega}\hat{\jmath}_{\mathrm{B}}^{10,(i)} + \Delta\Omega F_0^{\Delta\Omega}\hat{\jmath}_{\mathrm{C}}^{10,(i)} \right\} \right|_{\Omega=\Omega_{\mathrm{I}}}. \tag{7.161}$$

Finally, for the matching we have

$$\mathcal{O}(\lambda^{10}): \quad \hat{\jmath}_{\mathrm{A}}^{10,(i)}(r,\Omega_{\mathrm{I}},\phi_{\mathrm{p}}) = \bar{h}_{\mathrm{R1}}^{2,(i)}(r,\Omega_{\mathrm{I}},\phi_{\mathrm{p}}) + \bar{h}_{\mathcal{P}}^{2,(i)}(r,\Omega_{\mathrm{I}},\phi_{\mathrm{p}}), \tag{7.162}$$

$$\hat{\jmath}_{\mathrm{B}}^{10,(i)}(r,\Omega_{\mathrm{I}},\phi_{\mathrm{p}}) = \hat{h}_{\mathrm{R2}}^{2,(i)}(r,\Omega_{\mathrm{I}},\phi_{\mathrm{p}}),$$

$$\hat{\jmath}_{\mathrm{C}}^{10,(i)}(r,\Omega_{\mathrm{I}},\phi_{\mathrm{p}}) = \partial_\Omega \hat{h}_{\mathrm{R2}}^{2,(i)}(r,\Omega_{\mathrm{I}},\phi_{\mathrm{p}}).$$

This simplification has the benefit that we are no longer required to solve for a part of the metric perturbation at fourth-order in the inspiral so that

$$\mathcal{O}(\lambda^5): \quad \hat{\jmath}_{lm}^{5,(i)}(r,\Omega_{\mathrm{I}},\phi_{\mathrm{p}}) = \bar{h}_{lm}^{1,(i)}(r,\Omega_{\mathrm{I}},\phi_{\mathrm{p}}), \tag{7.163a}$$

$$\mathcal{O}(\lambda^6): \quad \hat{\jmath}_{lm}^{6,(i)}(r,\Omega_{\mathrm{I}},\phi_{\mathrm{p}}) = 0, \tag{7.163b}$$

$$\mathcal{O}(\lambda^7): \quad \hat{\jmath}_{lm}^{7,(i)}(r,\Omega_{\mathrm{I}},\phi_{\mathrm{p}}) = \partial_\Omega h^1(r,\Omega_{\mathrm{I}},\phi_{\mathrm{p}}), \tag{7.163c}$$

$$\mathcal{O}(\lambda^8): \quad \hat{\jmath}_{lm}^{8,(i)}(r,\Omega_{\mathrm{I}},\phi_{\mathrm{p}}) = \hat{h}_{\mathrm{R2}}^2(r,\Omega_{\mathrm{I}},\phi_{\mathrm{p}}), \tag{7.163d}$$

$$\mathcal{O}(\lambda^9): \quad \hat{\jmath}_{\mathrm{A}}^{9,(i)}(r,\Omega_{\mathrm{I}},\phi_{\mathrm{p}}) = \hat{h}_{lm}^{3,(i)}(r,\Omega_{\mathrm{I}},\phi_{\mathrm{p}}), \quad \hat{\jmath}_{\mathrm{B}}^{9,(i)}(r,\Omega_{\mathrm{I}},\phi_{\mathrm{p}}) = \frac{1}{2}\partial_\Omega^2 h^1(r,\Omega_{\mathrm{I}},\phi_{\mathrm{p}}), \tag{7.163e}$$

$$\mathcal{O}(\lambda^{10}): \quad \hat{\jmath}_{\mathrm{A}}^{10,(i)}(r,\Omega_{\mathrm{I}},\phi_{\mathrm{p}}) = \bar{h}_{\mathrm{R1}}^{2,(i)}(r,\Omega_{\mathrm{I}},\phi_{\mathrm{p}}) + \bar{h}_{\mathcal{P}}^{2,(i)}(r,\Omega_{\mathrm{I}},\phi_{\mathrm{p}}), \tag{7.163f}$$

$$\hat{\jmath}_{\mathrm{B}}^{10,(i)}(r,\Omega_{\mathrm{I}},\phi_{\mathrm{p}}) = \hat{h}_{\mathrm{R2}}^{2,(i)}(r,\Omega_{\mathrm{I}},\phi_{\mathrm{p}}), \quad \hat{\jmath}_{\mathrm{C}}^{10,(i)}(r,\Omega_{\mathrm{I}},\phi_{\mathrm{p}}) = \partial_\Omega \hat{h}_{\mathrm{R2}}^{2,(i)}(r,\Omega_{\mathrm{I}},\phi_{\mathrm{p}}).$$

Chapter 8

Second-Order Waveforms and Energy Flux

The results presented in this chapter build on over a decade of progress of the 2GSF program. In this chapter, numerical results for the total energy flux through second-order will be presented, in addition to gravitational waveforms generated using method 2 which was outlined in Section 4.4. In Section 8.1, results for the flux will be presented, in Section 8.2 the 1PA inspiral waveform, and in Section 8.3, the 0PA waveform during the transition regime. Results from the first two sections were obtained in collaboration with Pound, Wardell, Warburton, Miller and in the latter case, Le Tiec. The final section was done in collaboration with Pound, Küchler and Compère, using codes written by the previous group of collaborators. All results will be compared with NR simulations, for the dominant $(l, m) = (2, 2)$ mode. The flux and inspiral waveforms shown here include data for the slow-time derivative of the metric perturbation components in the Lorenz gauge, calculated in Chapter 6. This data has also been used recently to make comparisons between waveforms generated using GSF theory and EOB theory, the results of which can be found in references [93, 94].

8.1 Comparing GSF energy flux with NR during inspiral

Recall from Eq. (4.95) that the total energy flux can be expanded in powers of ν as [3, 4]

$$\mathcal{F}(x) = \nu^2 \mathcal{F}_\nu^1(x) + \nu^3 \mathcal{F}_\nu^2(x) + \mathcal{O}(\nu^4), \tag{8.1}$$

where

$$x = [(\mu + M)\,\Omega]^{2/3}. \tag{8.2}$$

The variable x is used in order to make comparisons with NR and expansions in ε are re-summed in terms of ν to restore the inherent symmetry of the full perturbed solution, which also yields the most accurate waveforms in comparison with NR [3]. We shall consider only the energy flux radiated to infinity up to $\mathcal{O}(\nu^3)$, and through the horizon at leading order, and discard the flux radiated through

the horizon at $\mathcal{O}(\nu^3)$, as this is expected to be small and has not yet been calculated [93, 94, 4]. For a given l, m mode, the total energy flux we shall calculate is

$$\mathcal{F}_{lm}(x) = \nu^2 \left[\dot{E}_{\nu,lm}^{1,\infty}(x) + \dot{E}_{\nu,lm}^{1,\mathcal{H}}(x) \right] + \nu^3 \dot{E}_{\nu,lm}^{2,\infty}(x) + \mathcal{O}(\nu^4). \tag{8.3}$$

Recall that the quantities $\dot{E}_{\nu,lm}^{1,\infty}$, $\dot{E}_{\nu,lm}^{1,\mathcal{H}}$ and $\dot{E}_{\nu,lm}^{2,\infty}$ are obtained by expanding in powers of ν the expressions [117, 4, 3]

$$\dot{E}_{lm}^{\infty} = \frac{1}{16\pi} \left| \dot{\tilde{h}}_{lm}^{\infty} \right|^2, \tag{8.4}$$

$$\dot{E}_{lm}^{\mathcal{H}} = \frac{1}{16\pi} \left| \dot{\tilde{h}}_{lm}^{\mathcal{H}} \right|^2, \tag{8.5}$$

which were introduced earlier in Section 4.6. Note that the leading-order energy flux is the same when expanded in powers of either ε or ν. Again to assist with the comparison to NR, the quantity that will be plotted is the Newtonian normalised flux [4]

$$\hat{\mathcal{F}}_{lm} = \frac{\mathcal{F}_{lm}}{\mathcal{F}_{lm}^{\mathrm{N}}}, \tag{8.6}$$

where $\mathcal{F}_{lm}^{\mathrm{N}}$ is the leading-order term in the PN series for a given l, m mode. For example [4, 129]

$$\mathcal{F}_{22}^{\mathrm{N}} = \frac{32}{5} x^5 \nu^2. \tag{8.7}$$

Finally, rather than x, we use $\bar{x}$, which is given by

$$\bar{x} = [(M + \mu)\varpi]^{2/3}, \tag{8.8}$$

where

$$\varpi = \dot{\Phi}_{22}/2. \tag{8.9}$$

In the weak field and for small mass ratios is [3]

$$\varpi = \Omega_0 + \mathcal{O}(\varepsilon). \tag{8.10}$$

A comparison between the energy flux radiated to infinity calculated using the GSF approach and NR for the dominant $(l, m) = (2, 2)$ mode is shown in Fig. (8.1) and Fig. (8.2) for $q = 10$ and $q = 1$ respectively, where

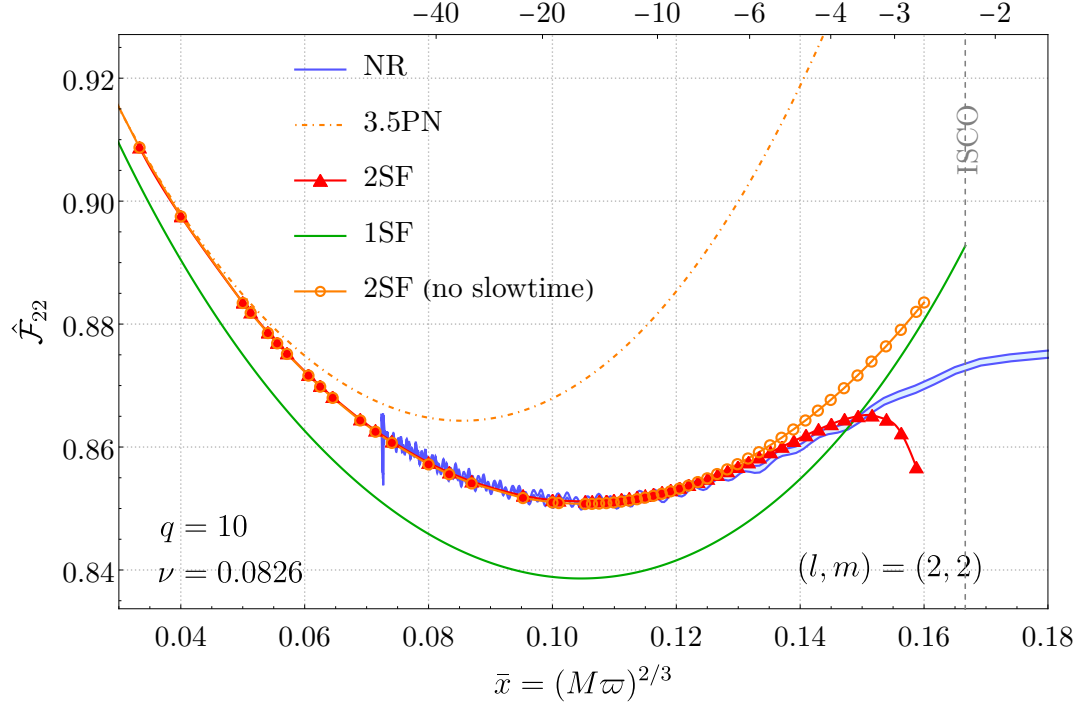$$q = M/\mu = \varepsilon^{-1}. \tag{8.11}$$

Figure 8.1: Total Newtonian normalised GW energy flux for the dominant $(l, m) = (2, 2)$ mode and a mass ratio of 1:10 [4]. The numbers on the top horizontal axis denote the number of GW cycles before merger. The green line shows the results for the flux calculated when considering only 0PA effects, that is when only ν^2 terms are included. The orange dashed line shows results from the PN series at 3.5PN order. In blue are the results from the NR simulation SXS:BBH:1107 [128], where the blue window shows the uncertainty in these results, given by the difference between extrapolation from third and fourth-order polynomial fits in the NR simulations. The red triangles are the data points obtained when including the full second-order GSF energy flux calculation using Eq. (8.3). The orange circles denote the second-order GSF results obtained if the multi-timescale piece of the puncture, which contains the slow-time derivatives of the metric perturbation, are not included. The horizontal dashed line delineates the location of the ISCO.
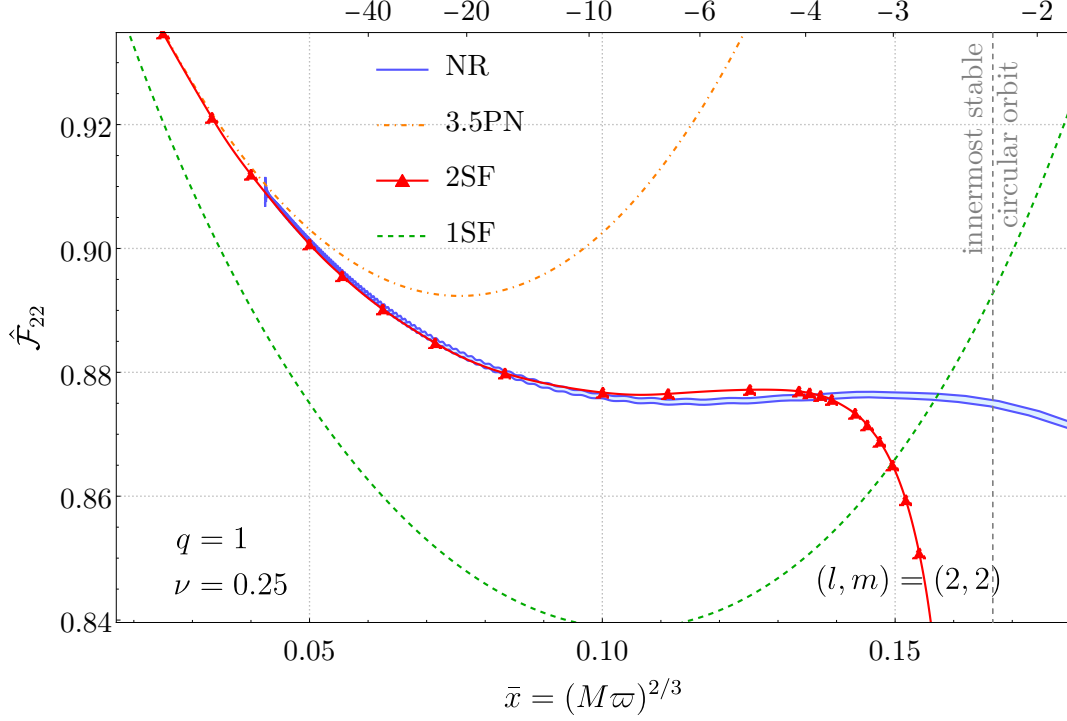
Figure 8.2: The same as Fig. (8.1), with $q = 1$. For this equal mass ratio binary, the NR simulation SXS:BBH:1132 was used [128] [4].

In both Fig. (8.1) and Fig. (8.2), there is very good agreement with the 2GSF calculation of the total energy flux compared to NR simulations. For an IMRI with a mass ratio of 1:10, the flux calculation using the 2GSF approach lies within the blue NR window up until around 8 GW cycles before merger, and remains close to NR results up to about 3.5 cycles before merger. For an equal mass ratio binary, the 2GSF results remain within the blue NR window up to around 10 cycles before merger. These results demonstrate the power of the 2GSF approach to accurately model much more than the EMRI parameter space. In both the $q = 10$ and $q = 1$ cases, we see the 2GSF flux calculation breaks down as the secondary approaches the ISCO, and the 2GSF data diverges from the NR results. This is unsurprising. Recall from Eq. (4.69) that any terms in the source for the inhomogeneous second-order metric perturbation that contain slow-time derivatives of the first order metric perturbation will behave like

$$\frac{d\bar{h}^1_{\mu\nu}}{d\tilde{t}} = \frac{dr_0}{d\tilde{t}} \frac{d\bar{h}^1_{\mu\nu}}{dr_0}, \tag{8.12}$$

during the inspiral, and from Eq. (4.36) we saw that $\frac{dr_0}{dt}$ blows up near the ISCO. As discussed in Chapter 7, a new timescale must be used once the binary enters the transition to plunge regime as the secondary nears the ISCO. The calculation of the second-order flux is particularly important for EMRIs due to their long signal lengths and any error in the phase accumulates over long timescales.

Modelling the GSF energy flux calculations though second-order in the small mass ratio during the transition is ongoing research, based on the work of Chapter 7.

8.2   Comparing GSF waveforms with NR during inspiral

Following method 2 outlined in Section 4.8, waveforms using the 2GSF program can be generated and compared to NR simulations. The 1PA GW phase, re-summed in terms of ν, is calculated by solving the following coupled set of equations

$$\frac{d\Omega}{dt} = \frac{3\left(1 - \frac{3M}{r_0(t)}\right)^{3/2}\sqrt{\frac{M}{r_0(t)}}}{M^2\left(1 - \frac{6M}{r_0(t)}\right)}\mathcal{F}_\nu^1(r_0(t))\nu \tag{8.13}$$

$$+ \frac{3\left(1 - \frac{3M}{r_0(t)}\right)^{3/2}\sqrt{\frac{M}{r_0(t)}}}{M^2\left(1 - \frac{6M}{r_0(t)}\right)}\left\{2\frac{\left(1 - \frac{3M}{r_0(t)}\right)^{3/2}}{\left(1 - \frac{6M}{r_0(t)}\right)}\mathcal{F}_\nu^1(r_0(t))\partial_x E_{\mathrm{bind}}^{\mathrm{1^{st}law}}(x) + \mathcal{F}_\nu^2(r_0(t))\right\}\nu^2,$$

$$\frac{d\phi_{\mathrm{p}}}{dt} = \Omega(t), \tag{8.14}$$

$$\Omega(t) = \sqrt{\frac{M}{r_0^3(t)}}, \tag{8.15}$$

with initial conditions

$$r_0(0) = 25M, \quad \phi_{\mathrm{p}}(0) = 0. \tag{8.16}$$

For the numerical calculations, M is set to 1. An initial orbital radius of $r_0 = 25M$ is chosen because the NR simulations are relatively short. The 0PA GW can be determined similarly by discarding the ν^2 term in the frequency evolution. Rather than using the binding energy in Eq. (4.96), we use the binding energy that comes from the first law of black hole mechanics [130, 118]

$$E_{\mathrm{bind}}^{\mathrm{1^{st}law}}(x) = -\frac{1}{3}xz'(x) + \frac{z(x)}{2} + \frac{(7-24x)x}{6(1-3x)^{3/2}} + \sqrt{1-3x} - 1, \tag{8.17}$$

where z is the first-order Detweiler red-shift [130, 118]. In Ref. [118] it is shown that the first law binding energy is comparable to that from GSF results [1]. Additionally, in order to make a meaningful comparison with between the NR waveform and the composite waveform during the transition, we must find a time t_{match} where the NR phase matches that of our 1PA inspiral solution, occurring at

---

[1]The reason for using the first-law binding energy for generating waveforms rather than that defined in Eq. (4.96) is purely logistical. Currently there is more data for $E_{\mathrm{bind}}^{\mathrm{1^{st}law}}$ than E_{bind}, and the former is easier to calculate as we don't need to determine $\hat{E}_{\mathrm{SF}}$. The binding energy also depends on the choice of spacetime foliation, and the calculation of E_{bind} has currently not been optimised for the best choice of slicing.

some choice of initial radius r_0^{init}. Integrating the following equation over the entire NR waveform

$$\frac{d\Phi_{22}^{\text{NR}}}{dt} = -2\sqrt{\frac{M}{(r_0^{\text{init}})^3}}, \tag{8.18}$$

and solving for t will determine when $t = t_{\text{match}}$. The time frame integrated over will depend on whether we are matching to the 0PA or 1PA solutions. Therefore, there will be different matching times for both the 0PA and 1PA waveforms, corresponding to $t_{\text{match}}^{\text{0PA}}$ and $t_{\text{match}}^{\text{1PA}}$ respectively. The GW amplitudes are then determined from

$$h_{lm}^{\text{0PA}}(\Omega(t)) = \frac{2Z_{lm}^{1,\infty}\left([(M+\mu)\Omega(t)]^{-2/3}\right)}{(imM(M+\mu)^2\Omega(t))^2}, \tag{8.19}$$

$$h_{lm}^{\text{1PA}}(\Omega(t)) = -\frac{2Z_{lm}^{2,\infty}\left([(M+\mu)\Omega(t)]^{-2/3}\right)}{(imM(M+\mu)^2\Omega(t))^2}, \tag{8.20}$$

where $Z_{lm}^{1,\infty}$ and $Z_{lm}^{2,\infty}$ are the first- and second-order radially perturbed Weyl scalars evaluated at infinity, which can be determined by the BHPToolkit [1]. The quantity $Z_{lm}^{1,\infty}$ is related to the leading order of Eq. (2.132). The quantities $Z_{lm}^{1,\infty}$ and $Z_{lm}^{2,\infty}$ can be written respectively in terms of the first- and second-order contributions to the metric perturbation components $\bar{h}_{lm}^{(7)}$ and $\bar{h}_{lm}^{(10)}$ in the two-timescale approximation. This can be seen using the fact that in the limit as $r \to \infty$ we have

$$\Psi_4^{\text{P}} = \frac{1}{2}\frac{\partial^2}{\partial t^2}\left(h_+ - ih_\times\right), \tag{8.21}$$

$$= -\frac{\omega^2}{2}\left(h_+ - ih_\times\right). \tag{8.22}$$

The second equality holds in the frequency domain, or equivalently for quasicircular orbits in the two-timescale approximation. Research is currently being done to construct the GW amplitudes directly from the first and second-order perturbed Weyl scalars, where the latter remains to be solved [43, 5, 75]. Recall from Chapter 4 that the full GW is then constructed using Eq. (4.20)

$$\tilde{h}_{lm}^{\infty}(\tilde{t}, \phi_{\text{p}}(t,\varepsilon), r, \varepsilon) = \left(h_+ - ih_\times\right), \tag{8.23}$$

$$= \lim_{r\to\infty} a_l\left(\tilde{\bar{h}}_{lm}^{(7)} + i\tilde{\bar{h}}_{lm}^{(10)}\right)e^{-im\phi_{\text{p}}(t,\varepsilon)}, \tag{8.24}$$

$$= \tilde{A}_{lm}^{\infty}(\tilde{t}, r, \varepsilon)e^{i\Phi_{lm}(t,\varepsilon)}. \tag{8.25}$$

The GW amplitude is expanded in powers of ν using the two-timescale approximation to 1PA order as

$$\tilde{A}_{lm}^{\nu\infty} = \nu\tilde{A}_{lm}^{1\nu,\infty} + \nu^2\tilde{A}_{lm}^{2\nu,\infty}. \tag{8.26}$$

For the 0PA waveform in the even-sector we have

$$\tilde{A}_{lm}^{1\nu,\infty} = h_{lm}^{\text{0PA}}(\Omega_{\text{0PA}}(t)), \tag{8.27}$$

where Ω_{0PA} is the solution to Ω in Eq. (8.13) when only the leading order term in ν is included. For the full 1PA waveform in the even-sector we then have

$$\tilde{A}_{lm}^{1\nu,\infty} = h_{lm}^{\text{0PA}}(\Omega_{\text{1PA}}(t)), \tag{8.28}$$

$$\tilde{A}_{lm}^{2\nu,\infty} = h_{lm}^{\text{0PA}}(\Omega_{\text{1PA}}(t)) + h_{lm}^{\text{1PA}}(\Omega_{\text{1PA}}(t)) + \frac{2r_0}{3M}\left(1 - \frac{M}{r_0(t)}\frac{1}{\sqrt{1 - \frac{3M}{r_0(t)}}}\right)\frac{d\Omega}{dr_0}\partial_\Omega h_{lm}^{\text{0PA}}(\Omega_{\text{1PA}}(t)). \tag{8.29}$$

and Ω_{1PA} is the solution to Eq. (8.13) when terms up to ν^2 are included. For comparison with NR, the 0PA and 1PA GSF GWs are then generated in the following way

$$\tilde{h}_{lm}^{\infty,\text{0PA}}(t) = \text{Re}\left[\nu\tilde{A}_{lm}^{1\nu,\infty}(t - t_0 + t_{\text{match}}^{\text{0PA}})e^{-im(\phi_{\text{p}}^{\text{0PA}}(t - t_0 + t_{\text{match}}^{\text{0PA}}) - \Delta\phi_{\text{p}}^{\text{0PA}})}\right], \tag{8.30}$$

$$\tilde{h}_{lm}^{\infty,\text{1PA}}(t) = \text{Re}\left[\left(\nu\tilde{A}_{lm}^{1\nu,\infty}(t - t_0 + t_{\text{match}}^{\text{1PA}}) + \nu^2\tilde{A}_{lm}^{2\nu,\infty}(t - t_0 + t_{\text{match}}^{\text{1PA}})\right)^{-im(\phi_{\text{p}}^{\text{1PA}}(t - t_0 + t_{\text{match}}^{\text{1PA}}) - \Delta\phi_{\text{p}}^{\text{1PA}})}\right], \tag{8.31}$$

where

$$\Delta\phi_{\text{p}}^{\text{0PA}} = \frac{\Phi_{22}^{\text{NR}}(t_0)}{2} - \phi_{\text{p}}^{\text{0PA}}(t_{\text{match}}^{\text{0PA}}), \tag{8.32}$$

$$\Delta\phi_{\text{p}}^{\text{1PA}} = \frac{\Phi_{22}^{\text{NR}}(t_0)}{2} - \phi_{\text{p}}^{\text{1PA}}(t_{\text{match}}^{\text{1PA}}), \tag{8.33}$$

and t_0 is the start time of a given NR simulation. Note that the definition of $A_{lm}^{1\nu,\infty}$ is different depending on whether we are generating the 0PA waveform, or the full 1PA waveform, and we should use either Eq. (8.27) or Eq. (8.28) respectively. Results for both the 0PA and 1PA waveforms generated via the GSF approach are shown in Fig. (8.3) and Fig. (8.4) for two different mass ratios, and are compared with NR simulations SXS:BBH:1107 and SXS:BBH:1132 [128] respectively, which take the form

$$\tilde{h}_{lm}^{\infty,\text{NR}}(t) = \text{Re}\left[\tilde{A}_{lm}^{\text{NR},\infty}(t)e^{i2\Phi_{22}^{\text{NR}}(t)}\right], \tag{8.34}$$

and the choice of NR simulation determines the choice of mass ratio, which is then also used in the GSF waveform parameters for a meaningful comparison.
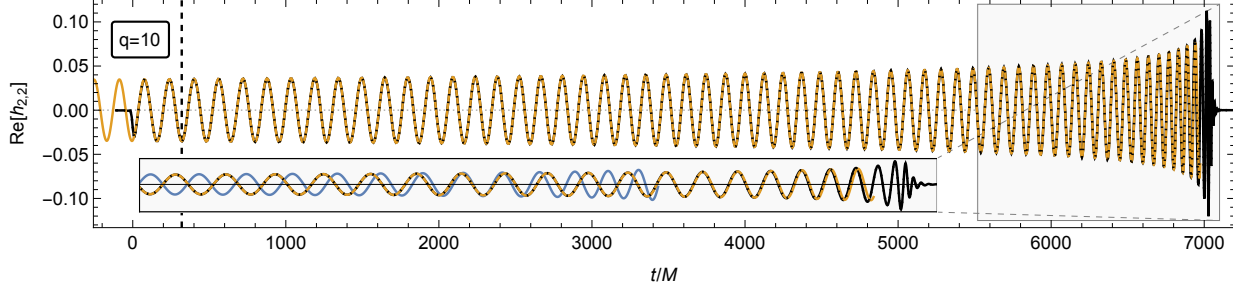
Figure 8.3: Waveform of the dominant $(l, m) = (2, 2)$ mode for a mass ratio of $\nu = 0.0826458$, corresponding to $\varepsilon = 0.100002$, with $M + \mu = 0.999995$ and $r_0^{\text{init}} = 13.828M$. In black is the NR waveform generated by the SXS:BBH:1107 simulation [128] and in yellow is the 1PA GSF waveform. In the inset, the blue line is the 0PA GSF waveform. The 1PA signals were matched at $t_{\text{match}}^{1\text{PA}} = 81172M$ [3]. The vertical dashed black line denotes the initial time of the SXS simulation.
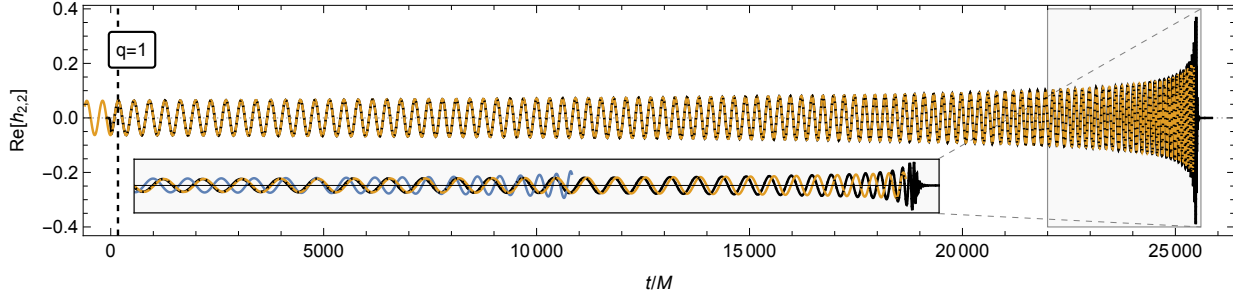

Figure 8.4: The same as Fig. (8.3) except using the NR simulation SXS:BBH:1132 [128], which determines that $\nu = 0.25$, corresponding to $\varepsilon = 1$, $M + \mu = 1$ and $r_0^{\text{init}} = 23.935M$. The 1PA signals were matched at $t_{\text{match}}^{1\text{PA}} = 4869M$. The vertical dashed black line denotes the initial time of the SXS simulation.

As in Section 8.2, Fig. (8.3) and Fig. (8.4) show that there is good agreement between the GSF and NR waveforms, even for intermediate and equal mass ratios. The 1PA signals begin to de-phase close to the ISCO and end before the two-timescale approximation of the inspiral breaks down. The next section extends these waveforms further into the transition regime. It is worth noting that even the 0PA waveforms agree very well with the NR simulations at early times, which is demonstrated by Fig. (8.5) and Fig. (8.6). However, this is because the GSF waveforms being compared with NR signals are for comparable mass ratios, with relatively short signals and there is less accumulated error in the phase than we would see from 0PA results for longer signals. An additional point of discussion is that the de-phasing seen between the GSF waveforms and NR results is worse for $q = 1$ than for $q = 10$ as expected. This is consistent with a larger accumulated error in the phase from the greater number of oscillations that can be seen in Fig. (8.4) compared to Fig. (8.3).

Figure 8.5: The same as Fig. (8.3) except now we are including the full 0PA signal to demonstrate where the 0PA de-phasing occurs compared to NR. The black dashed lines corresponds to that Fig. (8.3) and the solid vertical line denotes the time at which the inset from Fig. (8.3) begins.

Re[$h_{2,2}$]

0.4

0.2

0.0

-0.2

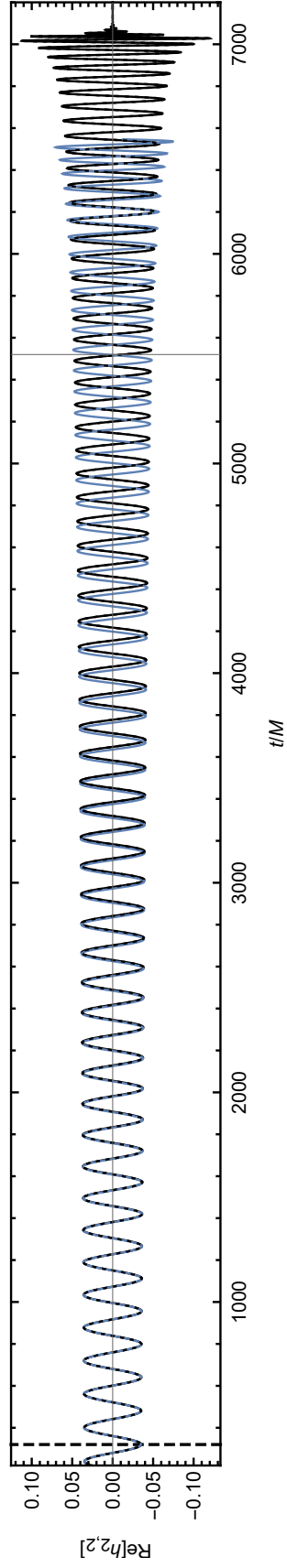-0.4

5000

10000

15000

20000

25000

t/M

Figure 8.6: The same as Fig. (8.4) except now we are including the full 0PA signal to demonstrate where the 0PA de-phasing occurs compared to NR. The black dashed lines corresponds to that Fig. (8.4) and the solid vertical line denotes the time at which the inset from Fig. (8.4) begins.
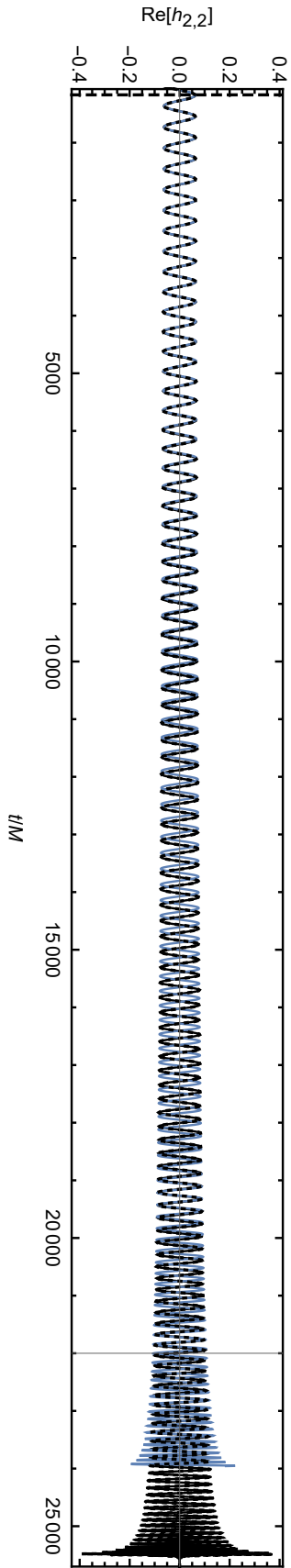
146

8.3   Comparing GSF waveforms with NR during transition

We will now generate the GSF waveform during the transition, using the results from Chapter 7, for the $(l, m) = (2, 2)$ mode, to 0PA order only. The results in this section were obtained in collaboration with Küchler, Compère and Pound. For comparison, the NR phase Φ_{lm}^{NR} and amplitude $\tilde{A}_{lm}^{\mathrm{NR},\infty}$ are imported from the SXS catalogue, using the NR simulation: SXS:BBH:1108 [128], where $\nu = 0.0884279$, corresponding to $\varepsilon = 0.108696$ and $M + \mu = 1.00001$. In order to make a meaningful comparison with between the NR waveform and the composite waveform during the transition, once again we must find a time t_{match} where the NR phase matches that of our composite solution. To determine t_{match} for the C0 model from Section 7.2, this can be achieved by integrating the following equation from the beginning to end times of the NR waveform

$$\frac{d\Phi_{22}^{\mathrm{NR}}}{dt} = -2\Omega_{\mathrm{C0}}(0), \tag{8.35}$$

and solving for t, which will give the solution $t_{\mathrm{match}}^{\mathrm{C0}}$. It turns out that the solution is the same regardless of the choice of either Ω_{C0} or Ω_{C2}, hence there will be no label to distinguish the C0 or C2 solution to t_{match}. Note how in the transition, $\Omega \neq \sqrt{M/r_0^3}$ and the frequency is solved following the method outlined in Section 7.2. For the mode and NR simulation used here, $t_{\mathrm{match}} = 5887.61M$. We would first like to compare the NR simulation with the $0PA$ solution when considering the inspiral only. As in previous chapters, to generate the GSF waveform, all numerical calculations will be done by setting $M = 1$. Recall that the composite solutions C0 and C2, and inspiral-only solutions for Ω and ϕ from Section 7.2 were solved to 0PA order with the initial conditions that $r_{\mathrm{p}} = 9(M + \mu)$. Starting the integration reasonably close to the ISCO ensures not only that the composite solution will be valid during the transition, but also minimises the de-phasing with the NR simulated waveform, especially given that we are only consider the 0PA order. The 0PA inspiral-only waveform is then given by

$$\tilde{h}_{lm}^{\mathrm{GW},0\mathrm{PA}}(t) = \mathrm{Re}\left[\nu\tilde{A}_{lm}^{1\nu,\infty}(t - t_{\mathrm{match}}^{0\mathrm{PA}})e^{-im(\phi_{\mathrm{p}}^{0\mathrm{PA}}(t - t_{\mathrm{match}}^{0\mathrm{PA}}) - \Delta\phi_{\mathrm{p}}^{0\mathrm{PA}})}\right], \tag{8.36}$$

where

$$\Delta\phi_{\mathrm{p}}^{0\mathrm{PA}} = \frac{\Phi_{22}^{\mathrm{NR}}(t_{\mathrm{match}}^{0\mathrm{PA}})}{2} - \phi_{\mathrm{p}}^{0\mathrm{PA}}(t_{\mathrm{min}}^{0\mathrm{PA}}). \tag{8.37}$$

Notice how the times are switched compared to Eq. (8.32) and Eq. (8.33). The quantities $t_0 = t_{\mathrm{min}}^{0\mathrm{PA}}$ and $t_{\mathrm{match}}^{0\mathrm{PA}}$ are determined similarly to the previous section, except that the latter is determined by integrating the equation

$$\frac{d\Phi_{22}^{\mathrm{NR}}}{dt} = -m\Omega_0 = -2\sqrt{\frac{M+\mu}{(M+\mu)^3 9^3}} = -\frac{2}{27(M+\mu)}, \tag{8.38}$$

following from the initial conditions of the 0PA frequency in Section 7.2. We see from Fig. (8.7) that the 0PA inspiral-only solution quickly de-phases compared to NR results and does not capture the
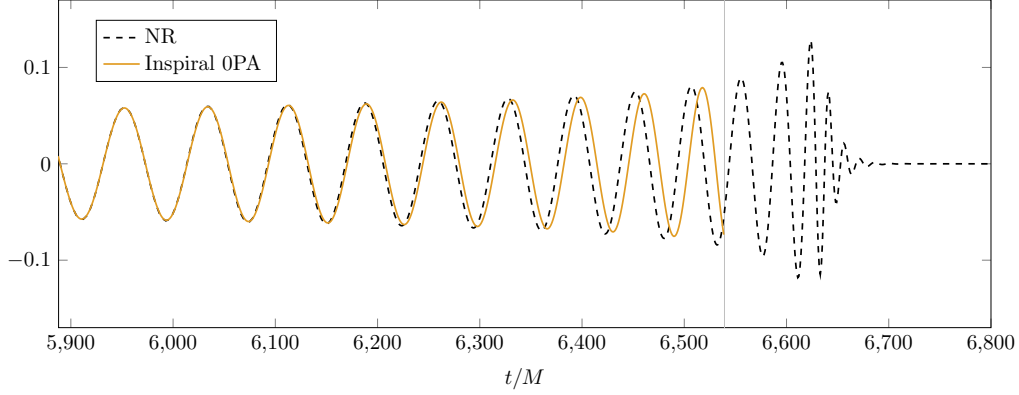
transition very well, as was to be expected.

Figure 8.7: Comparison between the 0PA GSF waveform and NR simulation SXS:BBH:1108 [128] during the transition for the $(l, m) = (2, 2)$ mode. The GSF waveform is generated using inspiral quantities only. The ISCO is delineated by the grey line and occurs at $t_{\text{max}}^{\text{0PA}} = 6539.34M$.

To improve on the results of Fig. (8.7), we shall implement the Composite0 solution, for which the waveform will look like

$$\tilde{h}_{lm}^{\text{GW,C0}}(t) = \begin{cases} \text{Re} \left[\nu \tilde{A}_{lm}^{1\nu,\infty}(t - t_{\text{match}}^{\text{C0}}) e^{-im(\phi_{\text{p}}^{\text{C0}}(t - t_{\text{match}}^{\text{C0}}) - \Delta\phi_{\text{p}}^{\text{0PA}})} \right], & \left\{ 0, t_{\text{max}}^{\text{C0,L}} \right\}, \\ \text{Re} \big[\{ \nu \tilde{A}_{lm}^{1\nu,\infty} \left(t_{\text{I}} - t_{\text{match}}^{\text{C0}} \right) + (\Omega_{\text{C0}} \left(t - t_{\text{match}}^{\text{C0}} \right) - \Omega_{\text{I}}) \\ \quad \times \partial_{\Omega} \tilde{A}_{lm}^{1\nu,\infty} \left(t_{\text{I}} - t_{\text{match}}^{\text{C0}} \right) \} e^{-im(\phi_{\text{p}}^{\text{C0}}(t - t_{\text{match}}^{\text{C0}}) + \Delta\phi_{\text{p}}^{\text{C0}})} \big], & \left\{ t_{\text{max}}^{\text{C0,L}}, t_{\text{max}}^{\text{C0,R}} \right\}, \end{cases} \quad (8.39)$$

which recovers the $\mathcal{O}(\lambda^5)$ and $\mathcal{O}(\lambda^7)$ portion of Eq. (7.83), with

$$\Delta\phi_{\text{p}}^{\text{C0}} = \frac{\Phi_{22}^{\text{NR}}(t_{\text{match}}^{\text{C0}})}{2} - \phi_{\text{p}}^{\text{C0}}(0). \quad (8.40)$$

The new and improved comparison between the NR simulation and Composite0 solution can be seen in Fig. (8.8).
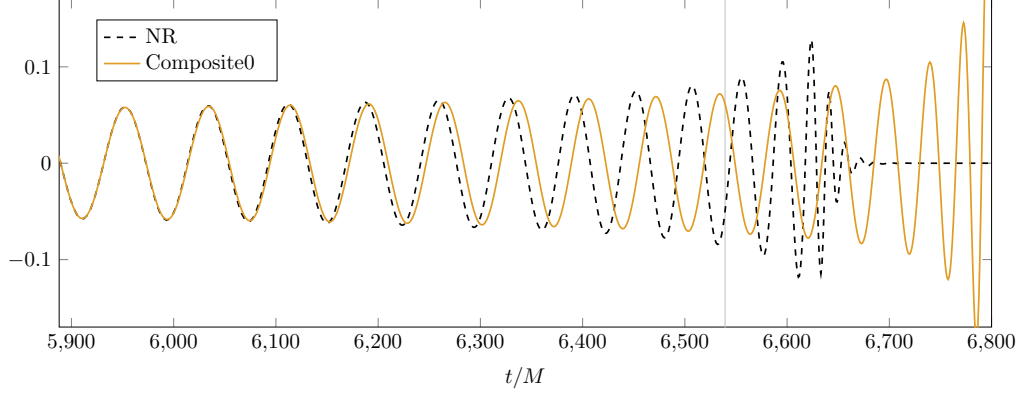
Figure 8.8: The same as Fig. (8.7), except that the 0PA GSF waveform is now generated using the Composite0 solution. Recall that this does not include all 0PA corrections.

The 0PA GSF waveform now extends through the transition, though there are still issues with de-phasing in comparison to the NR results. In fact the de-phasing gets worse before it gets better, and the $C0$ waveform is worse than the inspiral only solution. The $C0$ amplitude during the transition is also obviously incorrect. These results can be improved further by replacing $C0$ in Eq. (8.39) with $C2$ to obtain Fig. (8.9).
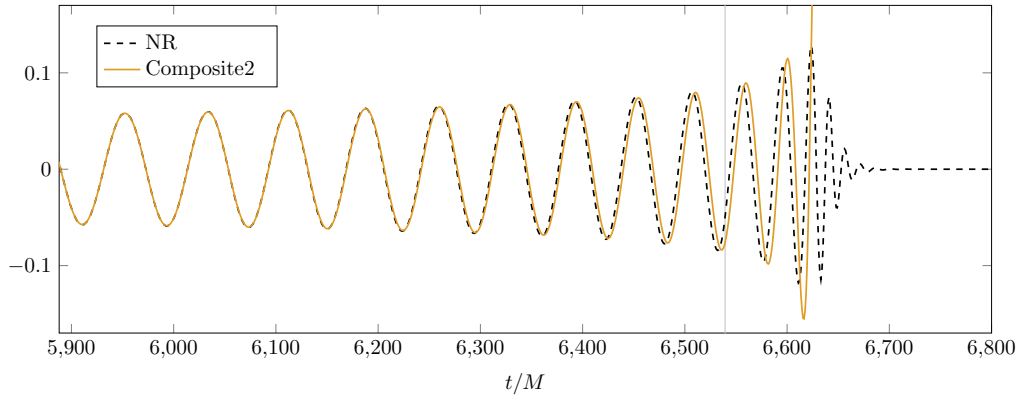
Figure 8.9: The same as Fig. (8.8), except that the 0PA GSF waveform is now generated using the Composite2 solutions. This contains all 0PA corrections.

Figure (8.9) demonstrates the comparison between the full 0PA composite GSF waveform during the transition and the NR simulation SXS:BBH:1108. There is less de-phasing compared to the Composite0 results, and the amplitude is greatly improved. Implementing the 1PA results using the methods outlined in Chapter 7 will only improve the agreement further. The agreement between NR and GSF results can be improved further by attaching the plunge to the waveform. These extensions shall be left to future research however, and are currently being implemented by collaborators. The

1PA results will also make further use of the slowly evolving metric perturbation calculation from Chapter 6. A final point worth noting is how to chose the best method to stitch the full waveform together. The time $t_{\max}^{\text{C0,L}}$ is determined by stopping the integration at $r_{\text{p}} \leq 6.0001M$. This could be made more precise by allowing the cut-off radius to be determined by the width of the transition for a given mass ratio, recalling from Eq. (7.7) that the radial width of the transition is given by

$$\Delta r \sim \varepsilon^{2/5}. \tag{8.41}$$

Calculating this cut off radius for every possible mass ratio would not be efficient however if the goal is to produce waveforms quickly. Alternatively, one could use the composite solution throughout the entire waveform. However, another issue arises with this approach. Recall from Eq. (7.57) that from $r > 6M$, the composite frequency evolves as

$$\frac{d\Omega}{dt} = \varepsilon F_0^\Omega(\Omega) + \varepsilon^{3/5} \left[F_0^{\Delta\Omega} \left(\frac{\Omega - \Omega_{\text{I}}}{\varepsilon^{2/5}} \right) + \varepsilon^{2/5} F_2^{\Delta\Omega} \left(\frac{\Omega - \Omega_{\text{I}}}{\varepsilon^{2/5}} \right) \right] - \varepsilon \left[\frac{F_\Omega^{(3,-1)}}{\Omega - \Omega_{\text{I}}} + F_\Omega^{(5,0)} \right], \tag{8.42}$$

which, so far we have only been concerned with at late times in the inspiral. Recalling the early time expansion, if extended to early inspiral times, the frequency now evolves as

$$\frac{d\Omega}{dt} = \varepsilon F_0^\Omega(\Omega) + \varepsilon^{3/5} \left[\frac{F_\Omega^{(3,-1)} \varepsilon^{2/5}}{(\Omega - \Omega_{\text{I}})} + \frac{F_\Omega^{(3,-6)} \varepsilon^{12/5}}{(\Omega - \Omega_{\text{I}})^6} + \frac{F_\Omega^{(3,-11)} \varepsilon^{22/5}}{(\Omega - \Omega_{\text{I}})^{11}} + \mathcal{O}(\Delta\Omega^{-16}) \right] \tag{8.43}$$
$$+ \varepsilon^{2/5} \left[F_2^{\Delta\Omega} \left(\frac{\Omega - \Omega_{\text{I}}}{\varepsilon^{2/5}} \right) \right] - \varepsilon \left[\frac{F_\Omega^{(3,-1)}}{\Omega - \Omega_{\text{I}}} + F_\Omega^{(5,0)} \right],$$
$$= \varepsilon F_0^\Omega(\Omega) + \left[\varepsilon \frac{F_\Omega^{(3,-1)}}{(\Omega - \Omega_{\text{I}})} + \varepsilon^2 \frac{F_\Omega^{(3,-6)}}{(\Omega - \Omega_{\text{I}})^6} + \varepsilon^5 \frac{F_\Omega^{(3,-11)}}{(\Omega - \Omega_{\text{I}})^{11}} + \mathcal{O}(\Delta\Omega^{-16}) \right] \tag{8.44}$$
$$+ \varepsilon^{2/5} \left[F_2^{\Delta\Omega} \left(\frac{\Omega - \Omega_{\text{I}}}{\varepsilon^{2/5}} \right) \right] - \varepsilon \left[\frac{F_\Omega^{(3,-1)}}{\Omega - \Omega_{\text{I}}} + F_\Omega^{(5,0)} \right],$$

where only the term $F_0^{\Delta\Omega}$ has been expanded at early times, as there is no need to expand inspiral quantities during the early inspiral. We see a number of divergent terms appearing. While at early times Ω should be much smaller than Ω_{I}, and of course so is ε^3, the quantity $\Omega - \Omega_{\text{I}}$, that appears in the denominator, is not as numerically large as we would like compared to the coefficient $F_\Omega^{(3,-6)}$, meaning that $F_0^{\Delta\Omega}$ is more dominant at early times than it should be. We see that the divergent terms in Eq. (8.44) involving $F_\Omega^{(3,-1)}$ cancel, however there are still additional divergent terms appearing at early times. We would need to include additional terms in the composite solution to cancel divergences at early times. We must also check whether higher order terms compete with their corresponding coefficients. Research is ongoing to determine the best approach for generating full waveforms, through all of the inspiral, transition and plunge, and indeed how many additional divergent terms need to be included, if this number is at all finite.

Chapter 9

Lorenz Gauge Perturbations to Kerr Spacetime

In general, physical BHs are expected to be rotating. A review of the observational constraints on black hole spin is given in Ref. [18]. As such, modelling EMRIs on a fully generic Kerr background will allow us to explore a larger portion of the GW parameter space, allowing future tests of GR by space-bourne detectors. Introducing rotation deeply complicates calculations in BHPT. While separable solutions to the first-order metric perturbation of a Schwarzschild background can be determined by solving the linearised Einstein field equations in the Lorenz gauge and by using a mode-sum decomposition in conjunction with either Berndtson's or the BSL basis, the same cannot be done in Kerr. Separable solutions are instead found curvature perturbations on a Kerr background, when projecting onto a set of null tetrads, usually in either the NP or GHP formalism [37, 68, 105, 106]. It is the existence of a particular tetrad which allows for this separability.

Progress in calculating perturbations of a Kerr background was discussed in the introduction, as well as at the end of Section 2.7, which in particular addressed issues with using the radiation gauge. Current state of the art SF calculations are those of Van de Meent, who uses the no-string radiation gauge reconstruction to implement the first-order SF calculation for a fully generic, inclined and eccentric bound orbits in the frequency domain [72]. This calculation is however, in its current implementation, is too slow to generate enough waveforms that are also long enough on time to perform matched filtering with LISA's future data stream. Another means to obtain the SF through second-order is presented in the work of Toomani *et al.* [43], who combine the corrector-tensor method of GHZ [75] with the no-string radiation gauge, proposing a more regular Teukolsky puncture scheme.

Another possible avenue is to construct the Kerr metric perturbation in the Lorenz gauge, where the regularisation of the SF is well understood. At present, there are no known solutions for metric perturbations sourced by a small compact object orbiting a Kerr black hole in the Lorenz gauge and the frequency domain, though Dolan does this for quasicircular orbits in the time domain [76, 77, 78, 79]. We saw in Chapter 2, 5 and 6 how Berndtson constructs the Lorenz gauge metric perturbation

to a Schwarzschild background in terms of RW gauge perturbations and a gauge transformation [46]. Berndtson's method is however not general enough to easily extend to Kerr or to second-order in the small mass ratio as all of the calculations in [46] are specific to a Schwarzschild background at first-order. The primary objective of this chapter is to progress in constructing a regular Lorenz gauge metric perturbation at first-order in the small mass ratio on a Kerr background as a sum of modes, in the frequency domain.

In this chapter, source-free metric perturbations will be constructed explicitly from a spin-weight $s = 1$ gauge vector on a Kerr background in the Lorenz gauge using the method of Dolan, Kavanagh and Wardell from Ref. [5]. While pure gauge contributions to the metric perturbation are unphysical, they are necessary to determine the SF, which is gauge dependent quantity. The $s = 0, 1$ perturbations will also be derived in the Schwarzschild limit and are shown to recover Berndtson's homogeneous expressions [46]. This provides insight to the meaning of M_{2af} and to the form of sourced Lorenz gauge metric perturbation expressions in the Kerr case, using Berndtson's inhomogeneous expressions. We will first introduce the concept of constructing the metric perturbation using a Hertz potential via Wald's method of adjoints [108] and use yet another of Wald's results [69] to understand the contribution of either the RWZ fields and M_{2af} or the perturbed Weyl scalars to the metric in Schwarzschild and Kerr respectively. We will introduce the GHP like formalism of Ref. [5] in the Kinnersley tetrad, which will provide the machinery from which we derive our main results in this chapter. All of the research presented in this chapter was done in collaboration with Dolan.

9.1 Radiative and non-radiative multipoles of the metric perturbation

For the mode-sum decomposition of Eq. (2.68), the $l = 0$ mode contributes to only scalar perturbations, the $l = 1$ mode contributes to scalar and vector perturbations, and $l \geq 2$ modes contribute scalar, vector and tensor perturbations to the metric. Only the $l \geq 2$ modes of the metric perturbation are responsible for gravitational radiation in both Schwarzschild and Kerr background spacetimes. In [69], Wald proves that for a Kerr background, either of the perturbed Weyl scalars Ψ_0^P or Ψ_4^P, related to $R_{\pm 2}^{lm}$ by Eqs. (2.131)-(2.133, fully determine the radiative part of the metric (the part responsible for gravitational radiation), or what is referred to as the 'non-trivial' part of the metric perturbation by Wald in Ref. [69]. However, there are perturbations on which neither Ψ_0^P nor Ψ_4^P contain information. The non-radiative contributions to the metric, often referred to as the completion parts of the metric or as the 'trivial' parts of the metric perturbation in [69], are the perturbations to the mass M and angular momentum a of the Kerr metric, given by δM and δa respectively, in addition to perturbations that are 'pure gauge', which are unphysical [69]. Any other perturbations such as those toward the Kerr-NUT and 'C metric' solutions, are considered physically unacceptable [69] and will be ignored here. We shall however concern ourselves with the non-physical contribution to the metric that a gauge choice provides, as this will still contribute

to the GSF, which is gauge independent [83]. We can then consider the metric perturbation to be comprised in the following way

$$h_{\mu\nu} \sim \text{curvature purturbations} + \delta a + \delta M + \text{gauge.} \tag{9.1}$$

Hence GWs encode information on δM and δa as well as the perturbed Weyl scalars, through the phase evolution due to the GSF. In the Schwarzschild case for example, the $l = 0$ and $l = 1$ modes correspond exactly to the mass (scalar) and angular momentum (vector) perturbations to the spacetime respectively, and any scalar or vector-like perturbations from the $l \geq 2$ modes contribute to a gauge piece.

From Wald's result we can determine whether the various RWZ fields and M_{2af} contribute to the radiative or completion parts of the metric perturbation by examining how these fields contribute to the perturbed Weyl scalars. It is not immediately obvious how the RWZ fields and M_{2af} will contribute to the metric perturbation as they all appear in Berndtson's expressions for the metric perturbation for the $l \geq 2$ modes [46], and hence may either contribute to the radiative modes or pure gauge completion piece. For type D spacetimes, the tetrad is chosen so that the only non-zero perturbed Weyl scalars are those that are gauge invariant [46, 37, 68], which are given by

$$\Psi_0^{\text{P}} = -\delta R_{\alpha\beta\gamma\delta} l^\alpha m^\beta l^\gamma m^\delta, \tag{9.2}$$

$$\Psi_4^{\text{P}} = -\delta R_{\alpha\beta\gamma\delta} n^\alpha \bar{m}^\beta n^\gamma \bar{m}^\delta, \tag{9.3}$$

where $\delta R_{\alpha\beta\gamma\delta}$ is the perturbed Riemann tensor and the tetrad legs are defined explicitly in Eq. (2.114) for the Kinnersley tetrad. Berndtson shows that only the RWZ field ψ_2 contributes to either of the perturbed Weyl scalars in the odd- or even-sector [46]. This result was independently corroborated by Wardell and Durkan, by projecting Berndtson's metric components from Eqs. (2.106a)-(2.106c) and Eqs. (2.108a)-(2.108f) onto the Kinnersley tetrad, given in Eqs. (9.21a)-(9.21j) and substituting into the perturbed Weyl scalars expressed in terms of the perturbed metric tetrad components, provided in [68, 37]. The expressions recovered, which relates Teukolsky variables to RWZ variables, are in fact identically the Chandrasekhar transformations. It is not trivial to expect this result however. It is not necessarily the case that only ψ_2 should contribute to the perturbed Weyl scalars, which have spin weight ± 2 as differential operators can raise or lower the spin weight of a scalar [68, 37].

This result allows us to defer solving for M_{2af} in order to obtain the radiative part of the Lorenz gauge metric perturbation. Then the radiative modes of $h_{\mu\nu}^L$ can de fully determined using the semi-analytical MST method. Even though M_{2af}, in addition to ψ_s for $s \in \{0, 0b, 1\}$ do not contribute to the radiative part of the metric, caution should be taken not to disregard them entirely. Detweiler and Poisson show that the $l = 0$ and $l = 1$ modes of the metric perturbation have a significant contribution to the SF [83]. The gauge completion parts are also important in calculating the SF, which is gauge dependent, though can be ignored when calculating gauge invariants such as the flux.

9.2   Useful identities

The following identities of the spin coefficients in the Kinnersley tetrad will come into use in Section 9.4 and Section 9.5 and are given here for reference [107]

$$l_\pm^\nu \nabla_\nu l_\pm^\mu = 0, \tag{9.4a}$$

$$m_\pm^\nu \nabla_\nu m_\pm^\mu = \cot\theta\, m_\pm^\mu, \tag{9.4b}$$

$$l_+^\nu \nabla_\nu m_+^\mu = m_+^\nu \nabla_\nu l_+^\mu = \frac{\rho_{,\theta}}{\rho} l_+^\mu + \frac{\rho_{,r}}{\rho} m_+^\mu, \tag{9.4c}$$

$$l_-^\nu \nabla_\nu m_+^\mu = m_+^\nu \nabla_\nu l_-^\mu = \frac{\bar\rho_{,\theta}}{\bar\rho} l_-^\mu + \frac{\bar\rho_{,r}}{\bar\rho} m_+^\mu, \tag{9.4d}$$

$$l_+^\nu \nabla_\nu l_-^\mu + l_-^\nu \nabla_\nu l_+^\mu = \left(\frac{\Sigma_{,r}}{\Sigma} - \frac{\Delta_{,r}}{\Delta} \right) \left(l_+^\mu + l_-^\mu \right) - \frac{1}{\Delta} \frac{\Sigma_{,\theta}}{\Sigma} \left(m_+^\mu + m_-^\mu \right), \tag{9.4e}$$

$$m_+^\nu \nabla_\nu m_-^\mu + m_-^\nu \nabla_\nu m_+^\mu = -\frac{\Delta \Sigma_{,r}}{\Sigma} \left(l_+^\mu + l_-^\mu \right) + \left(\frac{\Sigma_{,\theta}}{\Sigma} - \cot\theta \right) \left(m_+^\mu + m_-^\mu \right), \tag{9.4f}$$

where $,r$ and $,\theta$ on Σ and Δ denote differentiation with respect to r and θ respectively. The tetrad legs are defined explicitly in Eq. (2.115). The following identities of the differential operators will also prove useful later in this chapter [107]

$$\mathcal{D}_n = \mathcal{D} + n\frac{\Delta_{,r}}{\Delta}, \tag{9.5a}$$

$$\mathcal{D}_n^\dagger = \mathcal{D}^\dagger + n\frac{\Delta_{,r}}{\Delta}, \tag{9.5b}$$

$$\mathcal{L}_n = \mathcal{L} + n\cot\theta, \tag{9.5c}$$

$$\mathcal{L}_n^\dagger = \mathcal{L}^\dagger + n\cot\theta, \tag{9.5d}$$

where $n \in \mathbb{Z}$ and the operators $\mathcal{D}, \mathcal{D}^\dagger, \mathcal{L}, \mathcal{L}^\dagger$ are defined earlier in Eq. (2.124). It is then easy to show that [107]

$$\mathcal{D}^\dagger \left(\frac{\varphi}{\Delta} \right) = \frac{1}{\Delta} \mathcal{D}_{-1}^\dagger \varphi, \tag{9.6a}$$

$$\mathcal{D}^\dagger \left(\Delta\varphi \right) = \Delta \mathcal{D}_1^\dagger \varphi, \tag{9.6b}$$

$$\mathcal{D} \left(\frac{\varphi}{\Delta} \right) = \frac{1}{\Delta} \mathcal{D}_{-1} \varphi, \tag{9.6c}$$

$$\mathcal{D} \left(\Delta\varphi \right) = \Delta \mathcal{D}_1 \varphi, \tag{9.6d}$$

where φ is an arbitrary scalar field which is a function of r.

In the Schwarzschild limit, the derivatives along the $m_\pm^\mu$ tetrad legs act as spin raising and lowering operators on the spin-weighted spherical harmonics $_sY_{lm}(\theta,\phi)$ and provide some further useful identities. Suppressing the explicit dependence on θ and ϕ of $_sY_{lm}$ henceforth, unless it is instructive to include, we have [107]

$$\mathcal{L}\left(Y_{lm}\right) = \lambda_1\left(_{-1}Y_{lm}\right), \qquad (9.7\text{a})$$

$$\mathcal{L}^\dagger\left(Y_{lm}\right) = -\lambda_1\left(_{-1}Y_{lm}\right), \qquad (9.7\text{b})$$

$$\mathcal{L}_{-1}\left(_{-1}Y_{lm}\right) = \lambda_2\left(_{-2}Y_{lm}\right), \qquad (9.7\text{c})$$

$$\mathcal{L}_{-1}^\dagger\left(_1Y_{lm}\right) = -\lambda_2\left(_2Y_{lm}\right), \qquad (9.7\text{d})$$

$$\mathcal{L}_{-1}\mathcal{L}\left(Y_{lm}\right) = \Lambda\left(_{-2}Y_{lm}\right), \qquad (9.7\text{e})$$

$$\mathcal{L}_{-1}^\dagger\mathcal{L}^\dagger\left(Y_{lm}\right) = \Lambda\left(_2Y_{lm}\right), \qquad (9.7\text{f})$$

$$\mathcal{L}_1^\dagger\left(_{-1}Y_{lm}\right) = -\lambda_1\left(Y_{lm}\right), \qquad (9.7\text{g})$$

$$\mathcal{L}_1\left(_1Y_{lm}\right) = \lambda_1\left(Y_{lm}\right), \qquad (9.7\text{h})$$

$$\mathcal{L}_2^\dagger\left(_{-2}Y_{lm}\right) = -\lambda_2\left(_{-1}Y_{lm}\right), \qquad (9.7\text{i})$$

$$\mathcal{L}_2\left(_2Y_{lm}\right) = \lambda_2\left(_1Y_{lm}\right), \qquad (9.7\text{j})$$

$$\mathcal{L}_1^\dagger\mathcal{L}_2^\dagger\left(_{-2}Y_{lm}\right) = \Lambda\left(Y_{lm}\right), \qquad (9.7\text{k})$$

$$\mathcal{L}_1\mathcal{L}_2\left(_2Y_{lm}\right) = \Lambda\left(Y_{lm}\right), \qquad (9.7\text{l})$$

where Y_{lm} has spin weight $s = 0$, with normalisation defined in Eq. (2.24) and the eigenvalues are defined as [107]

$$\lambda_1 = \sqrt{2(\lambda+1)} = \sqrt{l(l+1)}, \qquad (9.8)$$

$$\lambda_2 = \sqrt{2\lambda} = \sqrt{(l-1)(l+2)}, \qquad (9.9)$$

$$\Lambda = \lambda_1\lambda_2, \qquad (9.10)$$

where λ is defined earlier in Eq. (2.107). By comparing Berndtson's definitions of W and X from Eq. (2.31) and Eq. (2.32) to the directional derivatives from Eqs. (2.124d)-(2.124c) and Eqs. (9.5c)-(9.5d) it can also be determined that

$$W + iX = \mathcal{L}_{-1}^\dagger\mathcal{L}^\dagger Y_{lm}, \qquad (9.11)$$

$$W - iX = \mathcal{L}_{-1}\mathcal{L} Y_{lm}. \qquad (9.12)$$

9.3 Constructing pure gauge metric perturbations

We must now generate the pieces of the metric perturbation that are missing from a radiation gauge construction. Contributions to the metric perturbation that are not captured by the radiation gauge solution will either be 'pure gauge', or contribute to mass and angular momentum perturbations to the background spacetime. In this chapter we shall only consider perturbations that are pure gauge. We would also like to transform from the radiation gauge to the Lorenz gauge, so that the metric perturbation is in a suitable gauge for SF calculations. Therefore, any pure gauge contributions we consider in this chapter shall also be chosen to satisfy the Lorenz gauge. We shall also consider only source free perturbations. For convenience the superscript indicating the order of the metric perturbation will be dropped, as only the first-order metric perturbation will be considered. A

generic vector potential can be written in the follow way [107]

$$\xi^\mu = \frac{1}{\Sigma}\left(\alpha_+ l_+^\mu + \alpha_- l_-^\mu + \beta_+ m_+^\mu + \beta_- m_-^\mu\right) \tag{9.13}$$

A homogeneous metric perturbation that is pure gauge, for a given spin-weight s can be generated by a gauge vector ξ_s^μ as follows

$$h_{\mu\nu} = -2\xi_{(\mu;\nu)}^s. \tag{9.14}$$

The metric perturbation will satisfy the Lorenz gauge condition of Eq. (2.65) provided that the gauge vector satisfies

$$\Box\xi_s^\mu = 0, \tag{9.15}$$

$$\nabla_\mu \xi_s^\mu = \frac{1}{2}h, \tag{9.16}$$

which are true for both homogeneous and inhomogeneous perturbations. In the following sections we will chose a gauge vector that satisfies these properties in order to generate spin-weight $s = 0, 1$ perturbations. It will also be useful to determine the metric perturbation as projected onto a tetrad, as perturbations in Kerr become more tractable in this formalism. The metric perturbation can then be written as

$$h_{ab} = h_{\mu\nu}e_a^\mu e_b^\nu. \tag{9.17}$$

where $\{a,b\} \in \{1,2,3,4\}$ and $e_a = \{l_+, l_-, m_+, m_-\}$. Putting Eq. (9.14) together with Eq. (9.17) we obtain

$$h_{ab}^{(\xi_s)} = e_a^\mu \left(e_b^\nu \xi_\nu^s\right)_{,\mu} + e_b^\mu \left(e_a^\nu \xi_\nu^s\right)_{,\mu} - \left(e_a^\mu \nabla_\mu e_b^\nu + e_b^\mu \nabla_\mu e_a^\nu\right)\xi_\nu^s. \tag{9.18}$$

For example, the metric perturbation as projected along the l_+^μ, l_+^μ direction is given by

$$\begin{aligned}
h_{l_+ l_+} &= h_{\mu\nu} l_+^\mu l_+^\nu, \tag{9.19}\\
&= \left(\nabla_\mu \xi_\nu^1 + \nabla_\nu \xi_\mu^1\right) l_+^\mu l_+^\nu,\\
&= l_+^\mu \nabla_\mu \left(l_+^\nu \xi_\nu^1\right) + l_+^\nu \nabla_\nu \left(l_+^\mu \xi_\mu^1\right) - l_+^\mu \left(\nabla_\mu l_+^\nu\right)\xi_\nu^1 - l_+^\nu \left(\nabla_\nu l_+^\mu\right)\xi_\mu^1,\\
&= 2l_+^\mu \partial_\mu \left(l_+^\nu \xi_\nu^1\right) - \left(l_+^\mu \nabla_\mu l_+^\nu + l_+^\mu \nabla_\mu l_+^\nu\right)\xi_\nu^1,\\
&= 2\mathcal{D}\left(\xi^1 \cdot l_+\right),
\end{aligned}$$

where we have used identities from Eqs. (2.120)-(2.123) and Eqs. (9.4a) - (9.4f).

The remaining metric perturbation components as projected onto the Kinnersley tetrad can also be determined from the gauge vector as follows [107]

$$h_{l_+ l_+} = 2\mathcal{D}\left(\xi_s \cdot l_+\right), \tag{9.20a}$$

$$h_{l_- l_-} = 2\mathcal{D}^\dagger\left(\xi_s \cdot l_-\right), \tag{9.20b}$$

$$h_{l_+ l_-} = \left(\mathcal{D} + \frac{f'}{f}\right)\left(\xi_s \cdot l_-\right) + \left(\mathcal{D}^\dagger + \frac{f'}{f}\right)\left(\xi_s \cdot l_+\right), \tag{9.20c}$$

$$h_{l_+ m_+} = \left(\mathcal{D} - \frac{2}{r}\right)\left(\xi_s \cdot m_+\right) + \mathcal{L}^\dagger\left(\xi_s \cdot l_+\right), \tag{9.20d}$$

$$h_{l_+ m_-} = \left(\mathcal{D} - \frac{2}{r}\right)\left(\xi_s \cdot m_-\right) + \mathcal{L}\left(\xi_s \cdot l_+\right), \tag{9.20e}$$

$$h_{l_- m_+} = \left(\mathcal{D}^\dagger - \frac{2}{r}\right)\left(\xi_s \cdot m_+\right) + \mathcal{L}^\dagger\left(\xi_s \cdot l_-\right), \tag{9.20f}$$

$$h_{l_- m_-} = \left(\mathcal{D}^\dagger - \frac{2}{r}\right)\left(\xi_s \cdot m_-\right) + \mathcal{L}\left(\xi_s \cdot l_-\right), \tag{9.20g}$$

$$h_{m_+ m_+} = 2\mathcal{L}^\dagger_{-1}\left(\xi_s \cdot m_+\right), \tag{9.20h}$$

$$h_{m_- m_-} = 2\mathcal{L}_{-1}\left(\xi_s \cdot m_-\right), \tag{9.20i}$$

$$h_{m_+ m_-} = \mathcal{L}^\dagger_1\left(\xi_s \cdot m_-\right) + \mathcal{L}_1\left(\xi_s \cdot m_+\right) + 2rf\left(\xi_s \cdot l_+ + \xi_s \cdot l_-\right). \tag{9.20j}$$

It will be useful to compare equations from Eq. (9.20) in the Schwarzschild limit with Berndtson's expressions for the first-order metric perturbation in the Lorenz gauge [46]. Using the identities for W and X from Eq. (9.11) and Eq. (9.11) then projecting the odd and even-sector metric perturbations in terms of Berndtson's variables from Eq. (2.30) and Eq. (2.33) onto the Kinnersley tetrad yields the following expressions

$$h_{l_+l_+} = \frac{1}{f}\left(H_0 + 2H_1 + H_2\right)Y_{lm}, \tag{9.21a}$$

$$h_{l_-l_-} = \frac{1}{f}\left(H_0 - 2H_1 + H_2\right)Y_{lm}, \tag{9.21b}$$

$$h_{l_+l_-} = -\frac{1}{f}\left(H_0 - H_2\right)Y_{lm}, \tag{9.21c}$$

$$h_{m_+m_-} = 2r^2 K Y_{lm}, \tag{9.21d}$$

$$h_{m_+m_+} = 2\left(ih_2^o + r^2 G\right)\mathcal{L}_{-1}^\dagger \mathcal{L}^\dagger Y_{lm} = 2\Lambda\left(ih_2^o + r^2 G\right){}_2 Y_{lm}, \tag{9.21e}$$

$$h_{m_-m_-} = 2\left(-ih_2^o + r^2 G\right)\mathcal{L}_{-1}\mathcal{L}Y_{lm} = 2\Lambda\left(-ih_2^o + r^2 G\right){}_{-2} Y_{lm}, \tag{9.21f}$$

$$h_{l_+m_+} = -\frac{\lambda_1}{f}\left[\left(-ih_0^o + h_0^e\right) + f\left(-ih_1^o + h_1^e\right)\right]{}_1 Y_{lm}, \tag{9.21g}$$

$$h_{l_+m_-} = \frac{\lambda_1}{f}\left[\left(ih_0^o + h_0^e\right) + f\left(ih_1^o + h_1^e\right)\right]{}_{-1} Y_{lm}, \tag{9.21h}$$

$$h_{l_-m_+} = -\frac{\lambda_1}{f}\left[\left(ih_0^o - h_0^e\right) - f\left(ih_1^o - h_1^e\right)\right]{}_1 Y_{lm}, \tag{9.21i}$$

$$h_{l_-m_-} = i\frac{\lambda_1}{f}\left[\left(ih_0^o + h_0^e\right) - f\left(ih_1^o + h_1^e\right)\right]{}_{-1} Y_{lm}, \tag{9.21j}$$

which are also multiplied by an additional factor of $e^{-im\phi_{\mathrm{p}}(t)}$ on the right-hand side and the superscripts o and e are used to differentiate between odd- and even-sector perturbations with the same labels. We can interpret these equations as either having a sum over modes on the right-hand side, or a suppressed l, m label on the right. The dependence of the various functions on the radial coordinate r has also been suppressed. Note that Eq. (9.21) is true only in cases where $l \geq 2$ and $\omega \neq 0$.

9.4 Constructing $s = 0$ perturbations

As discussed in Section 2.7.3, the radiation gauges are defined such that that the metric perturbation is trace free. However, considering only trace free solutions leads to missing contributions from the non-radiative sector, which have been shown to contribute to the SF [83]. In this section, we shall construct a gauge vector that generates a trace of the metric perturbation, left out by the radiation gauges by definition. We will start by taking the trace for the first-order linearised Einstein field equations Eq. (2.67), which tells us that the trace of the homogeneous metric perturbation must satisfy

$$\Box h = 0, \tag{9.22}$$

where

$$\Box \equiv \frac{1}{\sqrt{-g}} \nabla_\mu \left(\sqrt{-g} \nabla^\mu \right), \tag{9.23}$$

when acting on a scalar field, with $g = \det(g_{\mu\nu})$. For a Schwarzschild background and using the mode-sum decomposition of Eq. (9.28), Eq. (9.22) becomes

$$\left[f(r)\partial_r^2 + \left(\frac{2f(r)}{r} + f'(r) \right) \partial_r - \frac{l(l+1)}{r^2} + \frac{\omega^2}{f(r)} \right] h_{lm} = 0. \tag{9.24}$$

An example of a spin-weight $s = 0$ gauge vector that satisfies gauges Eq. (9.15) and Eq. (9.16), but is non-unique was determined in Ref. [5], and can be written as

$$\xi_0^\mu = -\frac{1}{2i\omega} \mathcal{K}^{\mu\nu} \nabla_\nu h + 2\nabla^\mu \kappa, \tag{9.25}$$

where $\mathcal{K}^{\mu\nu}$ is the conformal Killing-Yano tensor, given by [5]

$$\begin{aligned} \mathcal{K}^{\mu\nu} &= (\rho + \bar{\rho})n^{[\mu}l^{\nu]} + (\bar{\rho} - \rho)m^{[\mu}\bar{m}^{\nu]}, \\ &= \frac{r\Delta}{\Sigma} l_+^{[\mu}l_-^{\nu]} - \frac{ia\cos\theta}{\Sigma} m_+^{[\mu}m_-^{\nu]}, \end{aligned} \tag{9.26}$$

and κ describes the scalar, trace-free perturbations, satisfying [5]

$$\Box \kappa = \frac{1}{2}h, \tag{9.27}$$

which is also true in the presence of sources. In the Schwarzschild limit, the scalars h and κ can be written as a mode-sum decomposition [5]

$$\begin{aligned} h &= \sum_{l=0}^{\infty} \sum_{m=-l}^{l} h_{lm}(r)Y_{lm}(\theta,\phi)e^{-im\phi_{\mathrm{p}}(t)}, \quad m \neq \{0, \pm 1\}, \\ \kappa &= \sum_{l=0}^{\infty} \sum_{m=-l}^{l} \kappa_{lm}(r)Y_{lm}(\theta,\phi)e^{-im\phi_{\mathrm{p}}(t)}, \quad m \neq \{0, \pm 1\}, \end{aligned} \tag{9.28}$$

where $h_{lm}(r)$ here should not be confused with that from Section 4.4.

The explicit form of the scalar homogeneous metric perturbation components, generated by a gauge vector with spin-weight $s = 0$, as projected onto the Kinnersley tetrad are not provided in Ref. [5] and were derived independently by Dolan and Durkan, whose results were corroborated and are given here, in the Schwarzschild limit

$$h_{l_+l_+} = -\left(\frac{1}{i\omega}\mathcal{D}r\mathcal{D}h_{lm} + 4\mathcal{D}\mathcal{D}\kappa_{lm}\right)Y_{lm}, \tag{9.29a}$$

$$h_{l_-l_-} = -\left(-\frac{1}{i\omega}\mathcal{D}^\dagger r\mathcal{D}^\dagger h_{lm} + 4\mathcal{D}^\dagger\mathcal{D}^\dagger\kappa_{lm}\right)Y_{lm}, \tag{9.29b}$$

$$h_{l_+l_-} = -\frac{2}{f}\left[-\frac{1}{2}h_{lm} + \frac{1}{r^2}\left(\left(\mathcal{D}r^2f\mathcal{D}^\dagger + \mathcal{D}^\dagger r^2f\mathcal{D}\right)\kappa_{lm} - 4rf\kappa_{lm,r}\right)\right]Y_{lm}, \tag{9.29c}$$

$$h_{m_+m_-} = 2r^2\left[h_{lm} + \frac{2}{r^2}\left(l(l+1)\kappa_{lm} - 2rf\kappa_{lm,r}\right)\right]Y_{lm}, \tag{9.29d}$$

$$h_{m_+m_+} = -4\Lambda\kappa_{lm+2}Y_{lm}, \tag{9.29e}$$

$$h_{m_-m_-} = -4\Lambda\kappa_{lm-2}Y_{lm}, \tag{9.29f}$$

$$h_{l_+m_+} = l(l+1)\left[\frac{r}{2i\omega}\mathcal{D}h_{lm} + 4\mathcal{D}\kappa_{lm} - \frac{4}{r}\kappa_{lm}\right]_{+1}Y_{lm}, \tag{9.29g}$$

$$h_{l_+m_-} = -l(l+1)\left[\frac{r}{2i\omega}\mathcal{D}h_{lm} + 4\mathcal{D}\kappa_{lm} - \frac{4}{r}\kappa_{lm}\right]_{-1}Y_{lm}, \tag{9.29h}$$

$$h_{l_-m_+} = l(l+1)\left[-\frac{r}{2i\omega}\mathcal{D}^\dagger h_{lm} + 4\mathcal{D}^\dagger\kappa_{lm} - \frac{4}{r}\kappa_{lm}\right]_{+1}Y_{lm}, \tag{9.29i}$$

$$h_{l_-m_-} = -l(l+1)\left[-\frac{r}{2i\omega}\mathcal{D}^\dagger h_{lm} + 4\mathcal{D}^\dagger\kappa_{lm} - \frac{4}{r}\kappa_{lm}\right]_{-1}Y_{lm}, \tag{9.29j}$$

where the right-hand sides of the above equations are multiplied by an additional factor of $e^{-im\phi_\mathrm{P}(t)}$.

The next question to answer is: how are these results related to those of Berndtson in Eqs. (2.108a)-(2.108f)? Noting that there is no $s = 0$ contribution in the odd-sector, by taking the trace of the even-sector metric perturbation from Eq. (2.33) respectively, we immediately find that

$$\mathrm{Tr}\left(h_{\mu\nu}^e\right) = \sum_{l=0}^{\infty}\sum_{m=-l}^{l}\frac{\psi_0^{lm}}{r}Y_{lm}(\theta, \phi)e^{-im\phi_\mathrm{P}(t)}, \tag{9.30}$$

$$\implies h_{lm} = \frac{\psi_0^{lm}}{r}, \quad \text{for} \quad l + m = \text{even}, \tag{9.31}$$

which is a well known result. Note that we have reinstated the l, m labels on ψ_0. By substituting Berndtson's homogeneous even-sector expressions for $H_0, H_1, H_2, h_0, h_1, K$ and G from Eqs. 2.108a)-(2.108f) in terms of RWZ variables and M_{2af} into Eqs. (9.21a)-(9.21j), turning off all odd-sector perturbations and the RWZ fields in the even-sector with $s = \{0b, 1, 2\}$, then comparing with Eqs.

(9.29j)-(9.29j), determines that

$$M_{2af} = 2r\kappa, \tag{9.32}$$

$$\psi_0 = rh, \tag{9.33}$$

which also hold separately for each l, m mode. Note that in the homogeneous case, $\psi_{0b} = \psi_0$, and turning off the field ψ_{0b} is equivalent to setting $M_{2af} = 2r\kappa - \psi_{0b}$. While Eq. (9.33) is just a rearrangement of Eq. (9.31), the new result in Eq. (9.32) relates M_{2af} to κ from Ref. [5] in the Schwarzschild limit. It turns out that Eq. (9.27) is exactly the same as Eq. (5.17) for homogeneous ψ_0 and we have the following equivalences for the Schwarzschild limit

$$\Box h = \ 0 \quad \leftrightarrow \quad \mathcal{L}_0 \psi_0 = 0, \tag{9.34}$$

$$\Box \kappa = \ \frac{1}{2}h \quad \leftrightarrow \quad \mathcal{L}_0 M_{2af} = f\psi_0. \tag{9.35}$$

While M_{2af} comes from the gauge transformation from the RW to Lorenz gauge, it is difficult to understand the exact meaning of M_{2af} from Berndtson's derivation. The result in Eq. (9.32) elucidates that M_{2af} contributes to the metric perturbation as a pure gauge quantity, and is the piece of the $s = 0$ gauge vector that generates the scalar, trace-free perturbation to the metric, at least in the homogeneous case and in the Schwarzschild limit.

9.5 Constructing $s = \pm 1$ perturbations

As the trace of the metric perturbation is entirely generated by a gauge vector with spin-weight $s = 0$, we need only consider $s = 1$ perturbations that are trace free [5]. Chrzanowski showed that one can construct metric perturbations in the IRG from a vector potential ξ^μ_{IRG} with spin-weight $s = 1$ in the following way[63]

$$\xi^\mu_{\text{IRG}} = -l^\mu(\delta + 2\beta + \tau)\Psi_1 + m^\mu(\mathcal{D} + \rho)\Psi_1, \tag{9.36}$$

$$= \frac{\bar{\rho}^2}{\sqrt{2}\Sigma} \left(-l^\mu_+ \mathcal{L}^\dagger_1 + m^\mu_+ \mathcal{D} \right) \frac{\Psi_1}{\bar{\rho}}, \tag{9.37}$$

where Ψ_1 is the $s = 1$ Hertz potential. The Hertz potential for the IRG can be written in the separable form, in the mode-sum decomposition

$$\Psi_1 = \sum_{l=0}^{\infty} \sum_{m=-l}^{l} P^{lm}_{-1}(r) S^{lm}_{-1}(\theta, \phi) e^{-im\phi_{\text{p}}(t)}, \quad m \neq 0, \tag{9.38}$$

where

$$P^{lm}_{-1} = R^{lm}_{-1}, \tag{9.39}$$

$$P^{lm}_{+1} = \Delta R^{lm}_{+1}, \tag{9.40}$$

161

and $S_s^{lm}(\theta, \phi) = S_s^{lm}(\theta, 0)e^{im\phi}$ are the spin-weighted spheroidal harmonics with normalisation defined in Eq. (2.135), not to be confused with the sources of the RWZ equations, and $R_{\pm 1}^{lm}$ is the solution to the homogeneous Teukolsky equation for spin-weight $s = \pm 1$ from Eq. (2.133). In the Schwarzschild limit $S_s^{lm}(\theta, \phi)$ become the spin-weighted spherical harmonics, $_sY_{lm}(\theta, \phi)$, which for $s = 0$ are just Y_{lm}. In the Lorenz gauge, the $s = 1$ vector potential should satisfy Eqs. (9.15)-(9.16). We can then transform from the IRG to the Lorenz gauge in the following way

$$\xi_{\mathrm{L}}^{\mu} = \xi_{\mathrm{IRG}}^{\mu} - \nabla^{\mu}\chi, \tag{9.41}$$

where subscript L denotes the Lorenz gauge, and IRG denotes the ingoing radiation gauge. The Lorenz gauge is preserved if [107]

$$\Box\chi = \nabla_{\mu}\xi_{\mathrm{IRG}}^{\mu}. \tag{9.42}$$

Solving for χ gives [107]

$$\chi = -\frac{\sqrt{2}}{2i\omega}\mathcal{D}\mathcal{L}_1^{\dagger}\Psi_1. \tag{9.43}$$

Therefore, Lorenz gauge metric perturbations can be generated by the $s = 1$ vector [107]

$$\xi_1^{\mu} = \frac{\bar{\rho}^2}{\sqrt{2}\Sigma}\left(-l_+^{\mu}\mathcal{L}_1^{\dagger} + m_+^{\mu}\mathcal{D}\right)\frac{\Psi_1}{\bar{\rho}} - \nabla^{\mu}\frac{\sqrt{2}}{2i\omega}\mathcal{D}\mathcal{L}_1^{\dagger}\Psi_1. \tag{9.44}$$

We can check that ξ_1^{μ} satisfies the condition that the metric perturbation is trace free, with $h = g^{\mu\nu}h_{\mu\nu}$, and $\nabla_{\mu}\xi_1^{\mu} = 0$ and Eq. (9.15) are automatically satisfied by construction. These are recognisable as the electromagnetic field equations in the Lorenz gauge, though ξ_1^{μ} is not necessarily an electromagnetic field. In our case, ξ_1^{μ} generates gravitational perturbations. Unlike in the $s = 0$ case, constructing a metric perturbation from the vector Eq. (9.44) will generate a metric perturbation with contributions that come from the IRG, and that are pure gauge. For this reason we shall not refer to ξ_1^{μ} as a gauge vector, but as a vector potential.

The tetrad components of the first-order, trace-free, Lorenz gauge metric perturbation to a Kerr background that are generated purely by an $s = 1$ vector in the absence of sources can be obtained by substituting Eq. (9.44) into Eq. (9.20). The resulting components are given by

$$h_{l_+ l_+} = \frac{\sqrt{2}}{i\omega} \mathcal{D}\mathcal{D}\mathcal{D}\mathcal{L}_1^\dagger \Psi_1, \tag{9.45a}$$

$$h_{l_- l_-} = -\frac{4}{\sqrt{2}} \mathcal{D}^\dagger \left(\frac{\bar\rho \mathcal{L}_1^\dagger \Psi_1}{\Delta} \right) + \frac{\sqrt{2}}{i\omega} \mathcal{D}^\dagger \mathcal{D}^\dagger \mathcal{D}\mathcal{L}_1^\dagger \Psi_1, \tag{9.45b}$$

$$h_{l_+ l_-} = -2\mathcal{D}^\dagger \left(\frac{\bar\rho \mathcal{L}_1^\dagger \Psi_1}{\Delta} \right) + \frac{1}{\sqrt{2}i\omega} \mathcal{D}^\dagger \mathcal{D}^\dagger \mathcal{D}\mathcal{L}_1^\dagger \Psi_1 + \frac{1}{\sqrt{2}i\omega} \mathcal{D}^\dagger \mathcal{D}\mathcal{D}\mathcal{L}_1^\dagger \Psi_1 \tag{9.45c}$$
$$- \left(\frac{\Sigma_{,r}}{\Sigma} - \frac{\Delta'}{\Delta} \right) \left[\frac{1}{\sqrt{2}i\omega} \mathcal{D}\mathcal{D}\mathcal{L}_1^\dagger \Psi_1 - \frac{2\bar\rho}{\Delta} \mathcal{L}_1^\dagger \Psi_1 + \frac{1}{\sqrt{2}i\omega} \mathcal{D}^\dagger \mathcal{D}\mathcal{L}_1^\dagger \Psi_1 \right]$$
$$+ \frac{1}{\Delta} \frac{\Sigma_{,\theta}}{\Sigma} \left[\frac{1}{\sqrt{2}i\omega} \mathcal{L}^\dagger \mathcal{D}\mathcal{L}_1^\dagger \Psi_1 + \sqrt{2}\bar\rho^2 \mathcal{D}\left(\frac{\Psi_1}{\bar\rho} \right) + \frac{1}{\sqrt{2}i\omega} \mathcal{L}\mathcal{D}\mathcal{L}_1^\dagger \Psi_1 \right],$$

$$h_{l_+ m_+} = \frac{1}{\sqrt{2}i\omega} \left(\mathcal{L}^\dagger - 2\frac{\rho_{,\theta}}{\rho} \right) \mathcal{D}\mathcal{D}\mathcal{L}_1^\dagger \Psi_1 + \frac{1}{\sqrt{2}i\omega} \left(\mathcal{D} - 2\frac{\rho_{,r}}{\rho} \right) \mathcal{L}^\dagger \mathcal{D}\mathcal{L}_1^\dagger \Psi_1, \tag{9.45d}$$

$$h_{l_+ m_-} = \frac{1}{\sqrt{2}i\omega} \left(\mathcal{L} - 2\frac{\bar\rho_{,\theta}}{\bar\rho} \right) \mathcal{D}\mathcal{D}\mathcal{L}_1^\dagger \Psi_1 + \frac{1}{\sqrt{2}i\omega} \left(\mathcal{D} - 2\frac{\bar\rho_{,r}}{\bar\rho} \right) \mathcal{L}\mathcal{D}\mathcal{L}_1^\dagger \Psi_1 \tag{9.45e}$$
$$+ \mathcal{D}\left[\sqrt{2}\bar\rho^2 \mathcal{D}\left(\frac{\Psi_1}{\bar\rho} \right) \right] - 2\sqrt{2}\bar\rho\bar\rho_{,r} \mathcal{D}\left(\frac{\Psi_1}{\bar\rho} \right),$$

$$h_{l_- m_+} = \frac{1}{\sqrt{2}i\omega} \left(\mathcal{D}^\dagger - 2\frac{\bar\rho_{,r}}{\bar\rho} \right) \mathcal{L}^\dagger \mathcal{D}\mathcal{L}_1^\dagger \Psi_1 + \frac{1}{\sqrt{2}i\omega} \left(\mathcal{L}^\dagger - 2\frac{\bar\rho_{,\theta}}{\bar\rho} \right) \mathcal{D}^\dagger \mathcal{D}\mathcal{L}_1^\dagger \Psi_1 \tag{9.45f}$$
$$- \sqrt{2}\frac{\bar\rho}{\Delta} \left(\mathcal{L}^\dagger - 2\frac{\bar\rho_{,\theta}}{\bar\rho} \right) \mathcal{L}_1^\dagger \Psi_1,$$

$$h_{l_- m_-} = \left(\mathcal{D}^\dagger - 2\frac{\rho_{,r}}{\rho} \right) \left[\sqrt{2}\bar\rho^2 \mathcal{D}\left(\frac{\Psi_1}{\bar\rho} \right) \right] - \sqrt{2}\frac{\bar\rho}{\Delta} \left(\mathcal{L} - 2\frac{\rho_{,\theta}}{\rho} \right) \mathcal{L}_1^\dagger \Psi_1 \tag{9.45g}$$
$$+ \frac{\sqrt{2}}{i\omega} \mathcal{D}^\dagger \mathcal{D}\mathcal{L}\mathcal{L}_1^\dagger \Psi_1 - \frac{\sqrt{2}}{i\omega} \left(\frac{\rho_{,\theta}}{\rho} \mathcal{D}^\dagger \mathcal{D}\mathcal{L}_1^\dagger \psi + \frac{\rho_{,r}}{\rho} \mathcal{L}\mathcal{D}\mathcal{L}_1^\dagger \Psi_1 \right),$$

$$h_{m_+ m_+} = \frac{\sqrt{2}}{i\omega} \mathcal{L}_{-1}^\dagger \mathcal{L}^\dagger \mathcal{D}\mathcal{L}_1^\dagger \Psi_1, \tag{9.45h}$$

$$h_{m_- m_-} = 2\sqrt{2}\bar\rho^2 \mathcal{L}_{-1} \mathcal{D}\left(\frac{\Psi_1}{\bar\rho} \right) + \frac{\sqrt{2}}{i\omega} \mathcal{L}_{-1} \mathcal{L}\mathcal{D}\mathcal{L}_1^\dagger \Psi_1, \tag{9.45i}$$

$$h_{m_+ m_-} = \sqrt{2}\bar\rho^2 \mathcal{D}\mathcal{L}^\dagger \left(\frac{\Psi_1}{\bar\rho} \right) + \frac{\sqrt{2}}{i\omega} \mathcal{D}\mathcal{L}^\dagger \mathcal{L}\mathcal{L}_1^\dagger \Psi_1 + \frac{\sqrt{2}}{i\omega} \mathcal{D}\mathcal{L}\mathcal{L}^\dagger \mathcal{L}_1^\dagger \Psi_1 \tag{9.45j}$$
$$- \sqrt{2}\bar\rho \frac{\Sigma_{,r}}{\Sigma} \mathcal{L}_1^\dagger \Psi_1 + \frac{\Delta}{\sqrt{2}i\omega} \frac{\Sigma_{,r}}{\Sigma} \left(\mathcal{D} + \mathcal{D}^\dagger \right) \mathcal{D}\mathcal{L}_1^\dagger \Psi_1$$
$$- \left(\frac{\Sigma_{,\theta}}{\Sigma} - \cot\theta \right) \left[\sqrt{2}\bar\rho^2 \mathcal{D}\left(\frac{\Psi_1}{\bar\rho} \right) + \frac{1}{\sqrt{2}i\omega} \left(\mathcal{L}^\dagger + \mathcal{L} \right) \mathcal{D}\mathcal{L}_1^\dagger \Psi_1 \right].$$

These results are not given in [5] and are given here for the first time. When the Hertz potential Ψ_1 is written in its separable form and in a mode sum decomposition we quickly find that the metric perturbation components from Eq. (9.45) mix together spin-weighted spheroidal harmonics

of different spin weights. The above expressions can be simplified using the vacuum Teukolsky Equations for $s = \pm 1$, which are given by [37, 107]

$$\left(\Delta \mathcal{D}^\dagger \mathcal{D} - 2i\omega r\right) P_{-1}^{lm} = l(l+1) P_{-1}^{lm}, \tag{9.46a}$$

$$\left(\Delta \mathcal{D} \mathcal{D}^\dagger + 2i\omega r\right) P_{+1}^{lm} = l(l+1) P_{+1}^{lm}, \tag{9.46b}$$

$$\left(\mathcal{L}_0 \mathcal{L}_1^\dagger + 2a\omega \cos\theta\right) S_{-1}^{lm} = -l(l+1) S_{-1}^{lm}, \tag{9.46c}$$

$$\left(\mathcal{L}_0^\dagger \mathcal{L}_1 - 2a\omega \cos\theta\right) S_{+1}^{lm} = -l(l+1) S_{+1}^{lm}, \tag{9.46d}$$

and the vacuum Teukolsky-Starobinsky identities for the $s = \pm 1$ case, given by [107]

$$\Delta \mathcal{D} \mathcal{D} P_{-1}^{lm} = \mathcal{B} P_{+1}^{lm}, \tag{9.47a}$$

$$\Delta \mathcal{D}^\dagger \mathcal{D}^\dagger P_{+1}^{lm} = \mathcal{B} P_{-1}^{lm} \tag{9.47b}$$

$$\mathcal{L}_0^\dagger \mathcal{L}_1^\dagger S_{-1}^{lm} = \mathcal{B} S_{+1}^{lm}, \tag{9.47c}$$

$$\mathcal{L}_0 \mathcal{L}_1 S_{+1}^{lm} = \mathcal{B} S_{-1}^{lm}, \tag{9.47d}$$

where [107]

$$\mathcal{B} \equiv \sqrt{\lambda_1^4 + 4am\omega - 4a^2\omega^2}. \tag{9.48}$$

In the Schwarzschild limit we choose a slightly different gauge vector, which better exploits the symmetry of the problem, from which a piece of the first-order metric perturbation can be constructed [107]

$$\xi_1^\mu = \sum_{l=1}^\infty \sum_{m=-l}^l \frac{\alpha}{2r^2} \left[l(l+1) \left(P_{-1}^{lm} l_+^\mu + P_{+1}^{lm} l_-^\mu \right) Y_{lm} + \mathcal{D}^\dagger P_{+1}^{lm} \mathcal{L} Y_{lm} m_+^\mu + \mathcal{D} P_{-1}^{lm} \mathcal{L}^\dagger Y_{lm} m_-^\mu \right] e^{-im\phi_{\mathrm{p}}(t)}, \tag{9.49}$$

with $m \neq 0$ and where

$$\alpha \equiv -\frac{\sqrt{l(l+1)}}{\sqrt{2}i\omega}. \tag{9.50}$$

We can check that ξ_1^μ from Eq. (9.49) satisfies the condition that $\nabla_\mu \xi_1^\mu = 0$ and that it generates a metric perturbation which is trace free, such that $h = g^{\mu\nu} h_{\mu\nu}$.

Applying the spin coefficient identities, the spin-weighted spherical harmonics identities from Eq. (9.2), the $s = 1$ vacuum Teukolsky equations from Eq. (9.46d), the $s = 1$ vacuum Teukolsky-Starobinsky identities from Eqs. (9.5) and the identities from Eq. (9.6) to the individual components of h_{ab}^1 yields

$$h_{l_+l_+} = \left[\frac{2\alpha\lambda_1^2}{r^2 f} \mathcal{D}_{-1} P_{+1}^{lm} \right] Y_{lm}, \tag{9.51a}$$

$$h_{l_-l_-} = \left[\frac{2\alpha\lambda_1^2}{r^2 f} \mathcal{D}_{-1}^\dagger P_{-1}^{lm} \right] Y_{lm}, \tag{9.51b}$$

$$h_{l_+l_-} = \frac{\alpha\lambda_1^2}{r^2 f} \left[\left(\mathcal{D} - \frac{2}{r} \right) P_{-1}^{lm} + \left(\mathcal{D}^\dagger - \frac{2}{r} \right) P_{+1}^{lm} \right] Y_{lm}, \tag{9.51c}$$

$$h_{l_+m_+} = -\frac{2\alpha\lambda_1}{r^2 f} \left[\lambda_1^2 P_{+1}^{lm} - rf\mathcal{D} P_{-1}^{lm} \right]{}_{+1}Y_{lm}, \tag{9.51d}$$

$$h_{l_+m_-} = \frac{2\alpha\lambda_1}{r^2 f} \left[(\lambda_1^2 - i\omega r) P_{+1}^{lm} - rf\mathcal{D}^\dagger P_{+1}^{lm} \right]{}_{-1}Y_{lm}, \tag{9.51e}$$

$$h_{l_-m_+} = -\frac{2\alpha\lambda_1}{r^2 f} \left[(\lambda_1^2 + i\omega r) P_{-1}^{lm} - rf\mathcal{D} P_{-1}^{lm} \right]{}_{+1}Y_{lm}, \tag{9.51f}$$

$$h_{l_-m_-} = \frac{2\alpha\lambda_1}{r^2 f} \left[\lambda_1^2 P_{-1}^{lm} - rf\mathcal{D}^\dagger P_{+1}^{lm} \right]{}_{-1}Y_{lm}, \tag{9.51g}$$

$$h_{m_+m_+} = 2\alpha\Lambda \left(\mathcal{D} P_{-1}^{lm} \right){}_{+2}Y_{lm}, \tag{9.51h}$$

$$h_{m_-m_-} = 2\alpha\Lambda \left(\mathcal{D} P_{+1}^{lm} \right){}_{-2}Y_{lm}, \tag{9.51i}$$

$$h_{m_+m_-} = -\alpha\lambda_1^2 \left[\left(\mathcal{D}^\dagger - \frac{2}{r} \right) P_{+1}^{lm} + \left(\mathcal{D} - \frac{2}{r} \right) P_{-1}^{lm} \right] Y_{lm}, \tag{9.51j}$$

where the right-hand side of the above equations are also multiplied by an additional factor of $e^{-im\phi_{\rm P}(t)}$ and summed over l and m modes, as in Eq. (9.38). These expressions are also true for an individual l, m mode. Recall from Section 2.7, one could also have used the Carter tetrad. While the Carter tetrad provides more symmetric solutions, which is useful if one is considering contributions from both $\Psi_0^{\rm P}$ and $\Psi_4^{\rm P}$, it carries an additional factor that depends on the NP spin coefficients. This factor is zero in the Kinnersley tetrad. The Kinnersley tetrad provides slightly more concise results therefore, particularly if one only wishes to consider contributions from one of $\Psi_0^{\rm P}$ or $\Psi_4^{\rm P}$. Much of literature is also based on the Kinnersley tetrad, meaning that many useful identities used throughout this chapter are more readily available and do not need to be derived from scratch.

As shown in Section 9.4, comparing the metric perturbation components in the Schwarzschild limit with Berndtson's expressions provide a useful check of results in Kerr. In order to compare Eq. (9.51) with Berndtson's source-free metric components as projected onto a tetrad from Eq. (9.21) however, we must first convert $P_{\pm 1}^{lm}$ into RW fields. The Chandrasekhar transformations, given earlier in Section 3.1, relate the homogeneous solutions to the Teukolsky and Regge-Wheeler equations in the Schwarzschild limit. Dropping the l, m labels for now, for the $s = 1$ case, these relations are given by [86, 107]

$$\psi_1 = c_- \left(r\mathcal{D}P_{-1} - P_{-1} \right) = c_- r^2 \mathcal{D}\frac{P_{-1}}{r} \tag{9.52}$$

$$\psi_1 = c_+ \left(r\mathcal{D}^\dagger P_{+1} - P_+ \right) = c_+ r^2 \mathcal{D}^\dagger \frac{P_{+1}}{r}. \tag{9.53}$$

Inversely [86, 107]

$$P_{-1} = \frac{rf}{c_- \lambda_1^2} \mathcal{D}^\dagger \psi_1, \tag{9.54}$$

$$P_{+1} = \frac{rf}{c_+ \lambda_1^2} \mathcal{D}\psi_1. \tag{9.55}$$

From the $s = 1$ vacuum Teukolsky-Starobinsky identities in Eq. (9.5) we find that the constants c_- and c_+ must be equal, so we will chose $c_\pm = 1$ [86, 107]. From Eq. (9.51) we see that we must convert various combinations of the operators $\mathcal{D}_n$ and $\mathcal{D}_n^\dagger$ acting on $P_{\pm 1}$ into expressions written in terms of RW fields. Using Eqs. (9.52)-(9.55) it is straightforward to show that [107]

$$\mathcal{D}P_{-1} = \frac{1}{r}\left(\psi_1 + \frac{rf}{\lambda_1^2}\mathcal{D}^\dagger \psi_1 \right), \tag{9.56}$$

$$\mathcal{D}^\dagger P_{+1} = \frac{1}{r}\left(\psi_1 + \frac{rf}{\lambda_1^2}\mathcal{D}\psi_1 \right). \tag{9.57}$$

Some further rearranging yields [107]

$$\mathcal{D}^\dagger P_{-1} = \frac{1}{\lambda_1^2}(f + 2i\omega r)\mathcal{D}^\dagger \psi_1 + \frac{\psi_1}{r},$$
$$\mathcal{D}P_{+1} = \frac{1}{\lambda_1^2}(f - 2i\omega r)\mathcal{D}\psi_1 + \frac{\psi_1}{r}. \tag{9.58}$$

Finally, we can also show that [107]

$$\mathcal{D}_{-1}P_{+1} = -\frac{1}{\lambda_1^2}(1 + 2i\omega r)\mathcal{D}\psi_1 + \frac{\psi_1}{r},$$
$$\mathcal{D}_{-1}^\dagger P_{-1} = -\frac{1}{\lambda_1^2}(1 - 2i\omega r)\mathcal{D}^\dagger \psi_1 + \frac{\psi_1}{r}. \tag{9.59}$$

Note that the above expressions relating ψ_1 to $P_{\pm 1}$ hold for a given l, m mode.

The metric perturbations of Eq. (9.51) then become

$$h_{l_+l_+} = \frac{2\alpha}{r^2 f}\left(\frac{\lambda_1^2}{r}\psi_1 - (1+2i\omega r)\mathcal{D}\psi_1\right)Y_{lm}, \tag{9.60a}$$

$$h_{l_-l_-} = \frac{2\alpha}{r^2 f}\left(\frac{\lambda_1^2}{r}\psi_1 - (1-2i\omega r)\mathcal{D}^\dagger\psi_1\right)Y_{lm}, \tag{9.60b}$$

$$h_{l_+l_-} = \frac{\alpha}{r^2}\left[\frac{2\lambda_1^2}{rf}\psi_1 - \left(\mathcal{D}^\dagger + \mathcal{D}\right)\psi_1\right]Y_{lm}, \tag{9.60c}$$

$$h_{m_+m_-} = \alpha\left[-\frac{2\lambda_1^2}{r}\psi_1 + f\left(\mathcal{D}^\dagger + \mathcal{D}\right)\psi_1\right]Y_{lm}, \tag{9.60d}$$

$$h_{m_+m_+} = 2\alpha\Lambda\left(\frac{\psi_1}{r} + \frac{rf}{\lambda_1^2}\mathcal{D}^\dagger\psi_1\right){}_{+2}Y_{lm}, \tag{9.60e}$$

$$h_{m_-m_-} = 2\alpha\Lambda\left(\frac{\psi_1}{r} + \frac{f}{\lambda_1^2}\mathcal{D}\psi_1\right){}_{-2}Y_{lm}, \tag{9.60f}$$

$$h_{l_+m_+} = 2\alpha\lambda\left(-\frac{1}{r}\mathcal{D} + \frac{f}{r\lambda_1^2}\mathcal{D}^\dagger + \frac{1}{r^2}\right)\psi_{1\,+1}Y_{lm}, \tag{9.60g}$$

$$h_{l_+m_-} = 2\alpha\lambda\left(\frac{1}{r}\mathcal{D} - \frac{f}{r\lambda_1^2}\mathcal{D}^\dagger + \frac{i\omega}{\lambda_1^2} - \frac{1}{r^2}\right)\psi_{1\,-1}Y_{lm}, \tag{9.60h}$$

$$h_{l_-m_+} = 2\alpha\lambda\left[\left(-\frac{1}{r} + \frac{f}{r\lambda_1^2} - \frac{i\omega}{\lambda_1^2}\right)\mathcal{D}^\dagger + \frac{1}{r^2}\right]\psi_{1\,+1}Y_{lm}, \tag{9.60i}$$

$$h_{l_-m_-} = 2\alpha\lambda\left(\frac{1}{r}\mathcal{D}^\dagger - \frac{f}{r\lambda_1^2}\mathcal{D} - \frac{1}{r^2}\right)\psi_{1\,-1}Y_{lm}, \tag{9.60j}$$

where the right hand side of the above equations are multiplied by an additional factor of $e^{-im\phi_{\mathrm{p}}(t)}$. As before, the above expressions are applicable as expressions for individual modes or as a sum of modes.

Notice how the radial Hertz potentials $P_{\pm1}^{lm}$ collapse to the $s=1$ RW field in Eq. (9.52) and Eq. (9.53), where no distinction is made between $s=\pm1$ due to s^2 term in the RW equation, Eq. (2.49). Unlike in the $s=0$ case, where only the even-sector components are non-zero, there is no way to tell from Eq. (9.60) when ψ_1 is that of the odd-sector or that of the even-sector. How then can we compare with Berndtson's tetrad components of the metric perturbation from Eq. (9.21)? There are two facts we must consider. The first is that thus far, we have only considered a single polarisation in the mode sum decomposition of either the Hertz potential or the metric perturbation, described by $e^{-im\phi}$. This is exactly what we did when modelling GWs in Section 4.2 and Chapter 8. Defining

$$\hat{\phi}(t,\phi) = \phi - \phi_{\mathrm{p}}(t), \tag{9.61}$$

and recalling Eq. (9.38), the Hertz potential can be rewritten in the following way

$$\Psi_1 = \sum_{l=1}^\infty \sum_{m=1}^l \left(\beta_1 P_{\pm1}^{lm}\hat{Y}_{\pm1}^{lm}e^{im\hat{\phi}} + \beta_2 P_{\pm1}^{l,-m}\hat{Y}_{\pm1}^{l,-m}e^{-im\hat{\phi}}\right), \tag{9.62}$$

167

capturing both ingoing and outgoing radiation, where β_1 and β_2 are complex constants to be determined and $\hat{Y}_s^{lm}(\theta) = {}_sY_{lm}(\theta,0)$ and $\hat{Y}_{lm}(\theta) = Y_{lm}(\theta,0)$. The gauge potential generated by the Hertz potential then takes the form

$$\xi_\mu(t,r,\theta,\phi) = \sum_{l=0}^{\infty}\sum_{m=0}^{l}\left(\beta_1\hat{\xi}_\mu^{lm}(r,\theta)e^{im\hat{\phi}(t,\phi)} + \beta_2\hat{\xi}_\mu^{l,-m}(r,\theta)e^{-im\hat{\phi}(t,\phi)}\right). \tag{9.63}$$

The second fact we must consider is that the full physical metric is real valued and should be written as

$$\mathrm{Re}[h_{\mu\nu}] = h_{\mu\nu} + h_{\mu\nu}^*, \tag{9.64}$$

where $*$ denotes complex conjugation, which we have previously ignored in earlier chapters. Using these two facts, the metric perturbation can be rewritten in the form

$$\mathrm{Re}[h_{\mu\nu}] = \sum_{l=0}^{\infty}\sum_{m=0}^{l}2\left(\beta_1\hat{\xi}_{(\mu;\nu)}^{lm}e^{im\hat{\phi}}\right) + 2\left(\beta_2\hat{\xi}_{(\mu;\nu)}^{l,-m}e^{-im\hat{\phi}}\right) + \mathrm{c.c} \tag{9.65}$$

$$= \sum_{l=0}^{\infty}\sum_{m=0}^{l}2\left(\beta_1\hat{\xi}_{(\mu;\nu)}^{lm}e^{im\hat{\phi}}\right) + 2\left(\beta_2\hat{\xi}_{(\mu;\nu)}^{l,-m}e^{-im\hat{\phi}}\right)^* + \mathrm{c.c} \tag{9.66}$$

$$= \sum_{l=0}^{\infty}\sum_{m=0}^{l}2\left[\beta_1\hat{\xi}_{(\mu;\nu)}^{lm} + \left(\beta_2\hat{\xi}_{(\mu;\nu)}^{l,-m}\right)^*\right]e^{im\hat{\phi}} + \mathrm{c.c.}, \tag{9.67}$$

$$\tag{9.68}$$

where 'c.c' denotes complex conjugate terms. Projected onto tetrad components yields

$$\mathrm{Re}[h_{\mu\nu}]e_a^\mu e_b^\nu = \mathrm{Re}[h_{ab}] = \sum_{l=0}^{\infty}\sum_{m=0}^{l}\left[\beta_1\hat{h}_{\mu\nu}^{lm} + \left(\beta_2\hat{h}_{\mu\nu}^{l,-m}\right)^*\right]e_a^\mu e_b^\mu e^{im\hat{\phi}} + \mathrm{c.c} \tag{9.69}$$

$$= \sum_{l=0}^{\infty}\sum_{m=0}^{l}\left[\beta_1\hat{h}_{ab}^{lm} + \left(\beta_2\hat{h}_{\bar{e}_a\bar{e}_b}^{l,-m}\right)^*\right]e^{im\hat{\phi}} + \mathrm{c.c.} \tag{9.70}$$

The term in the square brackets now captures everything required to extract the odd and even parity contributions. Therefore the complex conjugate terms can once again be ignored for the purposes of the remainder of the calculation in this section. Consider the coefficient of $e^{im\hat{\phi}}$ of the metric perturbation tetrad components for a given l, m mode

$$h_{ab}^{lm} = \left[\beta_1\hat{h}_{ab}^{lm} + \left(\beta_2\hat{h}_{e_a^*e_b^*}^{l,-m}\right)^*\right]e^{im\hat{\phi}}. \tag{9.71}$$

The quantity $\hat{h}_{ab}^{lm}$ can be written in the separable form

$$\hat{h}_{ab}^{lm} = \mathfrak{h}_{ab}^{lm}(r)\,{}_sY_{lm}^{ab}(\theta)e^{-im\hat{\phi}}, \tag{9.72}$$

where the superscript a, b on ${}_sY^{ab}_{lm}$ is a label, not an index.

For example, for $(a, b) = (1, 1)$, Eq. (9.51a) sets

$$\mathfrak{h}^{lm}_{l_+l_+} = \frac{2\alpha\lambda_1^2}{r^2 f}\mathcal{D}_{-1}P^{lm}_{+1}(r), \tag{9.73}$$

$${}_sY^{l_+l_+}_{lm} = \hat{Y}_{lm}(\theta), \quad s = 0. \tag{9.74}$$

The remaining quantities $\hat{h}^{lm}_{ab}$ can be determined from Eq. (9.51). However, the quantities $\left(\hat{h}^{l,-m}_{e^*_a e^*_b}\right)^*$ still need to be determined. The following identities will prove useful in determining these. Under the operation $X_{lm} \to X^*_{l,-m}$, for some quantity X, the radial and spherical parts of the Hertz potential transform as [97, 37, 107]

$$P^{lm}_{\pm 1}(r) \to (-1)^m P^{lm}_{\pm 1}(r), \tag{9.75}$$

$$\hat{S}^{lm}_s(\theta) \to (-1)^{s-m}\hat{S}^{lm}_{-s}(\theta), \tag{9.76}$$

$$\hat{Y}^{lm}_s(\theta) \to (-1)^{s-m}\ \hat{Y}^{lm}_{-s}(\theta), \tag{9.77}$$

$$\hat{Y}_{lm}(\theta) \to (-1)^{-m}\ \hat{Y}_{lm}(\theta), \tag{9.78}$$

where we have defined

$$\hat{S}^{lm}_s(\theta) = S^{lm}_s(\theta, 0). \tag{9.79}$$

The quantities ω, α, K and Q and the directional derivatives then transform as [107]

$$\omega \to -\omega, \tag{9.80a} \qquad\qquad \mathcal{D} \to \mathcal{D}, \tag{9.80e}$$

$$\alpha \to \alpha, \tag{9.80b} \qquad\qquad \mathcal{D}^\dagger \to \mathcal{D}^\dagger, \tag{9.80f}$$

$$K \to -K, \tag{9.80c} \qquad\qquad \mathcal{L} \to \mathcal{L}^\dagger, \tag{9.80g}$$

$$Q \to -Q, \tag{9.80d} \qquad\qquad \mathcal{L}^\dagger \to \mathcal{L}, \tag{9.80h}$$

and under complex conjugation the tetrad basis vectors are

$$\bar{l}^\mu_+ = l^\mu_+, \quad \bar{l}^\mu_- = l^\mu_-, \quad \bar{m}^\mu_+ = m^\mu_-, \quad \bar{m}^\mu_- = m^\mu_+, \tag{9.81}$$

where an over bar on $l^\mu_\pm$ or $m^\mu_\pm$ denotes complex conjugation. The quantities $\left(\hat{h}^{l,-m}_{e^*_a e^*_b}\right)^*$ can now be determined. For example

$$\left(\mathfrak{h}^{l,-m}_{\bar{l}_+\bar{l}_+}\right)^* = \left(\mathfrak{h}^{l,-m}_{l_+l_+}\right)^* = (-1)^m\frac{2\alpha\lambda_1^2}{r^2 f}\mathcal{D}_{-1}P^{lm}_{+1}(r) = (-1)^m\mathfrak{h}^{lm}_{l_+l_+} \tag{9.82}$$

$$\left(Y^{\bar{l}_+\bar{l}_+}_{l,-m}\right)^* = \left(Y^{l_+l_+}_{l,-m}\right)^* = (-1)^m\ \hat{Y}_{lm}(\theta). \tag{9.83}$$

Therefore

$$\left(\hat{h}^{l,-m}_{\bar{l}_+\bar{l}_+}\right)^* = \hat{h}^{lm}_{l_+l_+}, \tag{9.84}$$

and

$$h_{l_+ l_+}^{lm} = (\beta_1 + \beta_2^*)\hat{h}_{l_+ l_+}^{lm} e^{im\hat{\phi}}. \tag{9.85}$$

In general it can be shown that

$$\left(\mathfrak{h}_{\bar{a}\bar{b}}^{l,-m}\right)^* {}_s Y_{l,-m}^{ab} = (-1)^s \mathfrak{h}_{ab}^{lm} {}_{-s} Y_{lm}^{ab}. \tag{9.86}$$

Finally we have

$$h_{l_+ l_+}^{lm} = \left[\beta_1 \hat{h}_{l_+ l_+}^{lm} + \left(\beta_2 \hat{h}_{l_+ l_+}^{l,-m}\right)^*\right] = (\beta_1 + \beta_2^*)\mathfrak{h}_{l_+ l_+}^{lm} Y_{lm}, \tag{9.87a}$$

$$h_{l_- l_-}^{lm} = \left[\beta_1 \hat{h}_{l_- l_-}^{lm} + \left(\beta_2 \hat{h}_{l_- l_-}^{l,-m}\right)^*\right] = (\beta_1 + \beta_2^*)\mathfrak{h}_{l_- l_-}^{lm} Y_{lm}, \tag{9.87b}$$

$$h_{l_+ l_-}^{lm} = \left[\beta_1 \hat{h}_{l_+ l_-}^{lm} + \left(\beta_2 \hat{h}_{l_+ l_-}^{l,-m}\right)^*\right] = (\beta_1 + \beta_2^*)\mathfrak{h}_{l_+ l_-}^{lm} Y_{lm}, \tag{9.87c}$$

$$h_{m_+ m_-}^{lm} = \left[\beta_1 \hat{h}_{m_+ m_-}^{lm} + \left(\beta_2 \hat{h}_{m_- m_+}^{l,-m}\right)^*\right] = (\beta_1 + \beta_2^*)\mathfrak{h}_{m_+ m_-}^{lm} Y_{lm}, \tag{9.87d}$$

$$h_{m_+ m_+}^{lm} = \left[\beta_1 \hat{h}_{m_+ m_+}^{lm} + \left(\beta_2 \hat{h}_{m_- m_-}^{l,-m}\right)^*\right] = \left(\beta_1 \mathfrak{h}_{m_+ m_+}^{lm} + \beta_2^* \mathfrak{h}_{m_- m_-}^{lm}\right) {}_2 Y_{lm}, \tag{9.87e}$$

$$h_{m_- m_-}^{lm} = \left[\beta_1 \hat{h}_{m_- m_-}^{lm} + \left(\beta_2 \hat{h}_{m_+ m_+}^{l,-m}\right)^*\right] = \left(\beta_1 \mathfrak{h}_{m_- m_-}^{lm} + \beta_2^* \mathfrak{h}_{m_+ m_+}^{lm}\right) {}_{-2} Y_{lm}, \tag{9.87f}$$

$$h_{l_+ m_+}^{lm} = \left[\beta_1 \hat{h}_{l_+ m_+}^{lm} + \left(\beta_2 \hat{h}_{l_+ m_-}^{l,-m}\right)^*\right] = \left(\beta_1 \mathfrak{h}_{l_+ m_+}^{lm} - \beta_2^* \mathfrak{h}_{l_+ m_-}^{lm}\right) {}_1 Y_{lm}, \tag{9.87g}$$

$$h_{l_+ m_-}^{lm} = \left[\beta_1 \hat{h}_{l_+ m_-}^{lm} + \left(\beta_2 \hat{h}_{l_+ m_+}^{l,-m}\right)^*\right] = \left(\beta_1 \mathfrak{h}_{l_+ m_-}^{lm} - \beta_2^* \mathfrak{h}_{l_+ m_+}^{lm}\right) {}_{-1} Y_{lm}, \tag{9.87h}$$

$$h_{l_- m_+}^{lm} = \left[\beta_1 \hat{h}_{l_- m_+}^{lm} + \left(\beta_2 \hat{h}_{l_- m_-}^{l,-m}\right)^*\right] = \left(\beta_1 \mathfrak{h}_{l_- m_+}^{lm} - \beta_2^* \mathfrak{h}_{l_- m_-}^{lm}\right) {}_1 Y_{lm}, \tag{9.87i}$$

$$h_{l_- m_-}^{lm} = \left[\beta_1 \hat{h}_{l_- m_-}^{lm} + \left(\beta_2 \hat{h}_{l_- m_+}^{l,-m}\right)^*\right] = \left(\beta_1 \mathfrak{h}_{l_- m_-}^{lm} - \beta_2^* \mathfrak{h}_{l_- m_+}^{lm}\right) {}_{-1} Y_{lm}, \tag{9.87j}$$

where the central part and right hand side of the above equations are also multiplied by an additional factor of $e^{-im\phi_{\mathrm{P}}(t)}$. We can now begin to extract the odd- and even-parity contributions. Equating right-hand sides of Eq. (9.87) with the right-hand sides of Eq. (9.21) respectively and solving for

Berndtson's variables in terms of $\mathfrak{h}^{lm}_{ab}$ yields

$$H^{lm}_0 = \frac{f}{4}\left(\mathfrak{h}^{lm}_{l_+l_+} - 2\mathfrak{h}^{lm}_{l_+l_-} + \mathfrak{h}^{lm}_{l_+l_+} + \mathfrak{h}^{lm}_{l_-l_-}\right)(\beta_1 + \beta_2^*),\tag{9.88a}$$

$$H^{lm}_1 = \frac{f}{4}\left(\mathfrak{h}^{lm}_{l_+l_+} - \mathfrak{h}^{lm}_{l_-l_-}\right)(\beta_1 + \beta_2^*),\tag{9.88b}$$

$$H^{lm}_2 = \frac{f}{4}\left(\mathfrak{h}^{lm}_{l_+l_+} + 2\mathfrak{h}^{lm}_{l_+l_-} + \mathfrak{h}^{lm}_{l_+l_+} + \mathfrak{h}^{lm}_{l_-l_-}\right)(\beta_1 + \beta_2^*),\tag{9.88c}$$

$$K^{lm} = \frac{1}{2R^2}\mathfrak{h}^{lm}_{m_+m_-}(\beta_1 + \beta_2^*),\tag{9.88d}$$

$$G^{lm} = \frac{1}{4r^2\Lambda}\left(\mathfrak{h}^{lm}_{m_-m_-} + \mathfrak{h}^{lm}_{m_+m_+}\right)(\beta_1 + \beta_2^*),\tag{9.88e}$$

$$h^{lm}_0 = \frac{f}{4\lambda_1}\left(-\mathfrak{h}^{lm}_{l_+m_+} + \mathfrak{h}^{lm}_{l_+m_-} + \mathfrak{h}^{lm}_{l_-m_+} - \mathfrak{h}^{lm}_{l_-m_-}\right)(\beta_1 + \beta_2^*),\tag{9.88f}$$

$$h^{lm}_1 = \frac{1}{4\lambda_1}\left(-\mathfrak{h}^{lm}_{l_+m_+} + \mathfrak{h}^{lm}_{l_+m_-} - \mathfrak{h}^{lm}_{l_-m_+} + \mathfrak{h}^{lm}_{l_-m_-}\right)(\beta_1 + \beta_2^*),\tag{9.88g}$$

in the even-sector, where there is always a factor of $\beta_1 + \beta_2^*$ and

$$h^{lm}_0 = \frac{f}{4i\lambda_1}\left(\mathfrak{h}^{lm}_{l_+m_+} + \mathfrak{h}^{lm}_{l_+m_-} - \mathfrak{h}^{lm}_{l_-m_+} - \mathfrak{h}^{lm}_{l_-m_-}\right)(\beta_1 - \beta_2^*),\tag{9.89a}$$

$$h^{lm}_1 = \frac{1}{4\lambda_1}\left(\mathfrak{h}^{lm}_{l_+m_+} + \mathfrak{h}^{lm}_{l_+m_-} + \mathfrak{h}^{lm}_{l_-m_+} + \mathfrak{h}^{lm}_{l_-m_-}\right)(\beta_1 - \beta_2^*),\tag{9.89b}$$

$$h^{lm}_2 = \frac{i}{4\Lambda}\left(\mathfrak{h}^{lm}_{m_-m_-} - \mathfrak{h}^{lm}_{m_+m_+}\right)(\beta_1 - \beta_2^*),\tag{9.89c}$$

in the odd-sector, where there is always a factor of $\beta_1 - \beta_2^*$. By considering the two polarization degrees of freedom we have been able to extract the odd- and even-sector components, which are given by the imaginary and real parts of Eq. (9.21) respectively. This parity extraction only makes sense in the Schwarzschild limit however. This result is similar to that of Lousto and Whiting, who also made use of the parity decomposition to reconstruct the metric perturbation from a Hertz potential for a Schwarzschild background in the time domain [66]. Substituting in for $\mathfrak{h}^{lm}_{ab}$ to the equations above gives

$$
\begin{aligned}
H_0 &= \frac{\alpha\lambda}{2r^2}\left(\mathcal{D}_{-1}P_{+1} + \mathcal{D}^\dagger_{-1}P_{+1} - \left(\mathcal{D} - \frac{2}{r}\right)P_{-1} - \left(\mathcal{D}^\dagger - \frac{2}{r}\right)P_{+1}\right)(\beta_1 + \beta_2^*),\\
H_2 &= \frac{\alpha\lambda}{2r^2}\left(\mathcal{D}_{-1}P_{+1} + \mathcal{D}^\dagger_{-1}P_{+1} + \left(\mathcal{D} - \frac{2}{r}\right)P_{-1} + \left(\mathcal{D}^\dagger - \frac{2}{r}\right)P_{+1}\right)(\beta_1 + \beta_2^*),\\
H_1 &= \frac{\alpha\lambda}{2r^2}\left(\mathcal{D}_{-1}P_{+1} - \mathcal{D}^\dagger_{-1}P_{-1}\right)(\beta_1 + \beta_2^*),\\
h_0 &= \frac{\alpha}{2r^2}\left(2\lambda_1^2\left(P_{+1} - P_{-1}\right) - i\omega r\left(P_{+1} + P_{-1}\right)\right)(\beta_1 + \beta_2^*),\\
h_1 &= \frac{\alpha}{2r^2f}\left(2\lambda_1^2\left(P_{+1} + P_{-1}\right) - 2rf\left(\mathcal{D}P_{-1} + \mathcal{D}^\dagger P_{+1}\right) - i\omega r\left(P_{+1} - P_{-1}\right)\right)(\beta_1 + \beta_2^*),\\
K &= -\frac{\alpha\lambda}{2r^2}\left[\mathcal{D}^\dagger P_{+1} + \mathcal{D}P_{-1} - \frac{2}{r}\left(P_{+1} + P_{-1}\right)\right](\beta_1 + \beta_2^*),\\
G &= \frac{\alpha}{2r^2}\left(\mathcal{D}P_{-1} + \mathcal{D}^\dagger P_{+1}\right)(\beta_1 + \beta_2^*),
\end{aligned}
\tag{9.90}
$$

in the even-sector and

$$h_0 = \frac{\alpha\omega}{2r}\left(P_{-1} - P_{+1}\right)\left(\beta_1 - \beta_2^*\right),$$
$$h_1 = \frac{\alpha}{2ir}\left(2\left(\mathcal{D}P_{-1} - \mathcal{D}^\dagger P_{+1}\right) - \frac{i\omega}{f}\left(P_{+1} + P_{-1}\right)\right)\left(\beta_1 - \beta_2^*\right), \quad (9.91)$$
$$h_2 = \frac{\alpha}{2i}\left(\mathcal{D}P_{-1} - \mathcal{D}^\dagger P_{+1}\right)\left(\beta_1 - \beta_2^*\right),$$

in the odd-sector, for a given l, m mode.

Making use of the relations from Eqs. (9.52) - (9.59) which converts $P_{\pm 1}$ and its directional derivatives to ψ_1, we can recover Berndtson's source-free gauge transformation for the $s = 1$ contributions [46]

$$H_0 = -\frac{\alpha}{r^2}\left((1-f)\partial_r + \frac{2\omega^2 r}{f}\right)\left(\beta_1 + \beta_2^*\right)\psi_1,$$
$$H_2 = -\frac{\alpha}{r^2}\left((1+f)\partial_r + \frac{2\omega^2 r}{f} - \frac{2\lambda_1^2}{r}\right)\left(\beta_1 + \beta_2^*\right)\psi_1,$$
$$H_1 = -\frac{i\alpha\omega}{rf}\left(2f\partial_r - \frac{1}{r}\right)\left(\beta_1 + \beta_2^*\right)\psi_1,$$
$$h_0 = -\frac{i\alpha\omega}{\lambda}\left(f\partial_r + \frac{2\lambda_1^2}{r}\right)\left(\beta_1 + \beta_2^*\right)\psi_1, \quad (9.92)$$
$$h_1 = \frac{2\alpha}{\lambda_1^2}\left(\frac{(\lambda_1^2 - f)}{r}\partial_r - \frac{\omega^2}{2f} - \frac{\lambda_1^2}{r^2}\right)\left(\beta_1 + \beta_2^*\right)\psi_1,$$
$$K = \frac{\alpha}{r^2}\left(f\partial_r - \frac{\lambda_1^2}{r}\right)\left(\beta_1 + \beta_2^*\right)\psi_1,$$
$$G = \frac{\alpha}{\lambda_1^2 r^2}\left(f\partial_r + \frac{\lambda_1^2}{r}\right)\left(\beta_1 + \beta_2^*\right)\psi_1,$$

and

$$h_0 = \frac{i\alpha\omega^2}{\lambda_1^2}\left(\beta_1 - \beta_2^*\right)\psi_1,$$
$$h_1 = -\frac{\alpha\omega}{\lambda_1^2}\left(\partial_r - \frac{2}{r}\right)\left(\beta_1 - \beta_2^*\right)\psi_1, \quad (9.93)$$
$$h_2 = \frac{\alpha\omega}{\lambda_1^2}\left(\beta_1 - \beta_2^*\right)\psi_1.$$

in the odd-sector, again for a given l, m mode. Comparing with Eq. (2.106) and Eq. (2.108) determines that [107]

$$\beta_1 + \beta_2^* = -\sqrt{2}\sqrt{l(l+1)}, \quad (9.94)$$

and

$$\beta_1 - \beta_2^* = \frac{\sqrt{2}\sqrt{l(l+1)}}{\omega^2}i. \quad (9.95)$$

Therefore

$$\beta_1 = \frac{\sqrt{l(l+1)}}{\sqrt{2}} \left(\frac{i}{\omega^2} - 1 \right),$$ (9.96)

$$\beta_2 = \frac{\sqrt{l(l+1)}}{\sqrt{2}} \left(\frac{i}{\omega^2} + 1 \right).$$ (9.97)

Here we have shown for the first time that Berndtson's gauge transformation and metric reconstruction can be recovered in the Schwarzschild limit of the perturbation to a Kerr background as constructed by a spin-weight $s = \pm 1$ vector, when projected onto the Kinnersley tetrad in the absence of sources. The odd- and even-sector split, previously unknown, was also recovered. This result, in conjunction with the fact that Berndtson provides expressions for the metric perturbation to a Schwarzschild background in the sourced case bodes well for determining a sourced Lorenz gauge metric perturbation for a Kerr background.

9.6   Adding sources

Before attempting to add sources to the Lorenz gauge metric perturbation of a Kerr background, we should aim to recover Berndtson's sourced expressions from Ref. [46] with a Hertz potential and gauge transformation. This shall be left to future work, but we shall summarise how to begin. In the $s = 0$ case it is straightforward to show that the source S_0 from Eq. (A.5) can be derived from the trace of the even-sector SET in Eq. (2.37)

$$S_0^{lm} = -16\pi r f T^{e,lm}, \quad \text{where} \quad T^{e,lm} = g^{\mu\nu} T^{e,lm}_{\mu\nu}.$$ (9.98)

From the trace of the sourced Einstein field equations Eq. (2.67) we find that

$$\Box h_{lm} = -16\pi T_{lm},$$ (9.99)

which is equivalent to

$$\mathcal{L}_0 \psi_0 = S_0,$$ (9.100)

where the l, m labels have once again been dropped, as in Chapter 5. In the presence of sources, there is no immediate change to the $s = 0$ metric perturbation expressions given in Eq. (9.29) other than h_{lm} is now inhomogeneous and κ_{lm} is also sourced by the retarded solution to h_{lm}. Notice how any terms in Eq. (9.29) containing two directional derivatives along $l^\mu_\pm$ will introduce terms involving T_{lm}, which for the point-like particles that we are considering, contain Dirac-delta functions. We can use the fact that in the Lorenz gauge, the first-order metric perturbation components are C^0 differentiable. This is true in both Boyer-Lindquist/Schwarzschild coordinates and in the Kinnersley tetrad [90]. Therefore, additional terms must be added to the metric components to exactly cancel any distributional terms that are introduced in the sourced case to ensure C^0 differential behaviour. This idea can be applied to contributions to the metric perturbation from all spin weights.

When comparing the results to Berndtson's inhomogeneous even-sector expressions, a number of things remain unclear however. It is difficult to see from Berndtson's expressions which components of the SET are introduced by which fields. This is due to a number of factors. Components of the SET and their radial derivatives can be replaced by using the condition that the SET is divergence free. We have also seen that spin weights can be raised and lowered by directional derivatives. Berndtson's expressions also combine fields of different spin weights. Furthermore, it remains unclear how to introduce the field ψ_{0b}, which only differentiates itself from ψ_0 in the sourced case. Noticing that ψ_{0b} always appears together with M_{2af} in the even-sector expressions for $H_0, H1, H_2, h_0, h_1, K$ and G from Eqs. (2.108a)-(2.108f), one approach would be to combine the $s = 0$ equations in the following way

$$\Box \left(\kappa + \kappa_{0b} \right) = \frac{1}{2} h + \frac{S_{0b}}{2rf}, \tag{9.101}$$

which is equivalent to

$$\mathcal{L}_0 \left(M_{2af} + \psi_{0b} \right) = f\psi_0 + S_{0b}, \tag{9.102}$$

where we have introduced the field κ_{0b} such that

$$\Box \kappa_{0b} = \frac{S_{0b}}{2rf}. \tag{9.103}$$

Unlike S_0^{lm}, S_{0b}^{lm} contains a term proportional to the radial derivative of the Dirac delta function. This means that any terms in the metric perturbation components in Eq. (9.29) that include a single radial derivative of κ will give rise to a distributional term which must also be cancelled to achieve C^0 differentiability, required of the Lorenz gauge metric perturbation.

Chapter 10

Conclusion

In this chapter a comprehensive summary of all results presented in this thesis will be discussed, followed by an exposition of possible directions for future research, that build on this work.

10.1   Summary of results

In Chapter 3, the MST package was implemented to the BHPToolkit [1], in particularly the novel feature for calculating MST solutions to the homogeneous Teukolsky equation. The implementation relied on the derivation provided in this thesis of contiguous Hypergeometric functions for the Teukolsky MST parameters. Later in Chapter 6, the calculation for the r_0 derivative of the radiative modes of the first-order metric perturbation in the Lorenz gauge was presented, on a Schwarzschild background, for circular orbits in the frequency domain, based on the work in Ref. [2]. Using the gauge transformation first derived in Ref. [46], solutions to $h^{1L}_{\mu\nu}$ were obtained in terms of RWZ master functions and the gauge field M_{2af}, in addition to their radial derivatives. The quantity $h^{1L}_{\mu\nu,r_0}$ was determined in terms of Regge-Wheeler-Zerilli (RWZ) master functions, M_{2af}, their derivatives with respect to r_0, in addition the radial derivatives of the listed fields. The field equations for the r_0 derivative of the RWZ master functions and M_{2af} have sources which with unbounded support which is challenging for the standard variation of parameters method to tackle. To overcome this, the method of partial annihilators was used [102, 122, 95] which gives us higher-order differential equations but with distributional sources. While this work was being prepared for publication, a similar procedure for computing the RWZ master functions was sketched in Appendix C of Ref. ([122]). In Figs. 6.2, 6.4 and 6.6, the numerical results presented show agreement with results obtained by taking a numerical derivative of the relevant field. The results of this work are already being used to compute slow-time derivatives of the metric perturbation that feed into the source for second-order in the mass ratio calculations in order to determine the GW phase to 1PA order [14], forming part of the recent calculations of the second-order energy flux at infinity [4] and waveforms through second-order [3], as shown in Chapter 8, in addition to comparisons with EOB theory [93, 94].

In Chapter 7, the transition to plunge was discussed, and the structure of the phase and metric perturbation, in addition to the perturbed Einstein field equations were determined to 1PA order.

Transition waveforms were then implemented using the GSF approach in Chapter 8 for the first time. These waveforms were generated for quasicircular, equatorial orbits on a Schwarzschild background to 0PA order, for mass ratios of $\sim 1 : 10$ and $1 : 1$. Finally, in Chapter 9, contributions to the first-order Lorenz gauge metric perturbation to a Kerr black hole were generated from a spin-weighted $s = 1$ gauge vector in the absence of sources, and were shown to recover Berndtson's gauge transformation in the Schwarzschild limit.

10.2   Future work

There is a variety of natural extensions to the work in this thesis. Firstly, with the numerical results from Chapter 5 and Chapter 6, one could immediately construct the first-order metric perturbation and its r_0 derivative in the RW gauge. It is also worth noting that whilst this work was being prepared, a new numerical approach to frequency-domain calculations of perturbations of black hole spacetimes was developed [95]. That work showed, using a scalar-field toy model for a Schwarzschild background, that using hyperboloidal compactified coordinates with a pseudo-spectral numerical scheme allows the r_0 derivative of the scalar field to be calculated efficiently. It would be interesting future work to compare the pros and cons of the partial annihilator method used in this work with the hyperboloidal approach.

Secondly, the partial annihilator approach can also be applied to the Teukolsky formalism [105]. This would allow for the slow-time derivative of the metric perturbation of a particle moving on either circular or spherical orbits around a Kerr black hole to be calculated in either a radiation gauge [131, 132, 133, 43] or, following recent work, the Lorenz gauge, as presented in Chapter 9 and Ref. [5]. However, it seems unlikely that the method of partial annihilators will be applicable to second-order perturbations, due to the form of the second-order equations. Recent work by Green et al. [75] and Toomani et al. [43] instead present schemes on how to implement the second-order Teukolsky equation in Kerr. Thirdly, recall that up to M_{2af}, $h_{\mu\nu}^{1\mathrm{L}}$ can be written in terms of semi-analytic MST expansions [85]. The gauge field M_{2af} currently has no known MST-type expansion however, excluding analytic high-order PN calculations of $h_{\mu\nu}^{1\mathrm{L}}$ similar to those in, e.g., [134, 87, 135, 136]. Research is currently being done to find a PN solution for M_{2af} [88], which would allow one to obtain a PN series solutions of the complete Lorenz gauge metric perturbation.

A further extension to the work of Chapter 5 and Chapter 6 would be to include eccentric orbits, which are more challenging to implement than circular orbits. The same partial annihilator method can be applied to eccentric orbit equations, arriving at sources which only have support within the radial libration region [102]. For highly eccentric orbits it is likely that a time-domain approach would be preferable. In this approach, the derivative with respect to eccentricity or, e.g., the semi-major axis would only act on the source, leaving the time-domain operator unchanged. This suggests that already existing time-domain codes, e.g., [137, 138, 139], could be quickly modified to calculate the slow-time derivatives for these orbits. After the application of the method of partial annihilators, the r_0 derivative of the eccentric source for the resulting fourth-order ODE of the spin-weight $s = 2$

RW master function in the odd-sector was calculated by Durkan. The weighting coefficients for the retarded ψ_0 field were also calculated, following the method of variation of parameters and extended homogeneous solutions [103, 140], making use of integration by parts and regularising the integrand, removing singularities introduced in the eccentric case [89]. The retarded field recovered the correct numerical solution in the limit of circular orbits. However, the calculation for eccentric orbits currently fails to converge, and for this reason these results were omitted from this thesis. Fourier theory tells us that if the retarded field is continuously differentiable, its Fourier series will converge exponentially. If the retarded field is C^0 differentiable, the Fourier series will converge as $1/n^2$, where n is the number of terms in the Fourier series. It is expected that the solution to $\partial_{r_0}\psi_0$ should converge, and further research is required to understand the error in the current implementation.

Work from Chapter 7 on the transition regime is only the beginning of a long research program, as waveforms will need to be implemented to 1PA order for generic orbits on a Kerr background and must be extended to include the plunge, merger and ring-down. Currently research is being done by collaborators to calculate the amplitude and phase to next-to-leading-order in the small mass ratio within the two-timescale approximation, for quasicircular, equatorial orbits on a Schwarzschild background, in addition to extending the waveform through to plunge. To complete the 1PA transition calculation, recall from Chapter 7 that only $\partial_{r_0}^2 h_{lm}^{1,(i)}$ and $\hat{h}_{lm}^{3,(i)}$ need be determined, evaluated at Ω_{I}. The majority of work from Chapter 7 should be easily extendible to Kerr, as derivations were primarily concerned with the structure of solutions. Of course quantities such as Ω_0, and the equations of motion will differ in the Kerr case, however the principles remain the same. The main hurdle therefore remains the calculation of the second-order metric perturbation on a Kerr background. Solving the perturbed field equations for eccentric orbits shall also be left to future research.

Finally, possible extensions to the work from Chapter 9 are detailed as follows. The $s = 2$ contribution to the Lorenz gauge metric perturbation of a Kerr black hole in the absence of sources are presented in [5]. It would be insightful to check that Berndtson's transformation is recovered in the $s = 2$ case, in the absence of sources. The next logical step would then be to implement the metric perturbations of Dolan et. al [5] and Chapter 9 for circular orbits. As discussed in earlier chapters, for a point-like particle we can solve the retarded Lorenz gauge metric perturbation components everywhere in spacetime, even in the absence of sources. Away from the world-line, distributional terms go to zero, and on the world-line, distributional terms cancel, ensuring C^0 differentiability of Lorenz gauge solutions. Therefore, we can already begin to implement the retarded first-order metric perturbation to a Kerr background in the Lorenz gauge without needing to add sources to either the work of Dolan et al. [5] or work from Chapter 9. To do this, one need only update the current algorithm for calculating $h_{\mu\nu}^{1\mathrm{L}}$ and $h_{\mu\nu,r_0}^{1\mathrm{L}}$ in terms of Teukolsky variables and any gauge fields, which can be done in a similar way to the RWZ and M_{2af} fields. Ultimately, sources will need to be added however, and again these should recover Berndtson's transformation in the sourced case, providing an insightful check on results in Kerr. Current research by Wardell, Kavanagh and Dolan will provide source Lorenz gauge perturbations to Kerr in the electromagnetic case. For the

sourced gravitational case, one possible path would be to first determine sources for circular orbits. One could determine the distributional pieces of the retarded Teukolsky and gauge fields, and in principle subtract the same term from the overall expression for the metric perturbation components to recover C^0 differentiability. This may provide insight as to how to add source terms to the metric perturbation for generic orbits in the gravitational case, which remains an open problem.

Appendix A

Sources for Regge-Wheeler and Zerilli master functions

Here we provide expressions for the sources to the RWZ master functions from Eq. (2.49) in terms of the components of $T^1_{\mu\nu}$. All of the expressions in this section are provided by reference [46]. The components of $T^1_{\mu\nu}$ are given explicitly by Eq. (2.48). The following expressions are the sources for the odd-sector RW master functions [46]:

$$
\begin{aligned}
S_1^{lm}(r) = \ & \frac{32\pi(\lambda+3)(r-2M)^2}{3r^3}So_{12}^{lm}(r) + \frac{32\pi\lambda(r-2M)}{3r^3}So_{22}^{lm}(r) \\
& + \frac{16\pi(r-2M)^3}{r^3}\partial_r So_{12}^{lm}(r) + \frac{32\pi\lambda(r-2M)^2}{3r^3}\partial_r So_{22}^{lm}(r),
\end{aligned}
\tag{A.1}
$$

$$
S_2^{lm}(r) = \ -\frac{16\pi f(r)^2}{r}So_{12}^{lm}(r) + \frac{32\pi\left(6M^2 - 5Mr + r^2\right)}{r^4}So_{22}^{lm}(r) - \frac{16\pi f(r)^2}{r}\partial_r So_{22}^{lm}(r).
\tag{A.2}
$$

The following expressions are the sources for the even-sector RWZ master functions. Here S_2^{lm} refers to the source for the Zerilli master function [46]:

$$S_2^{lm}(r) = \frac{16\pi M(2M-r)(3M-(\lambda+3)r)}{i\omega r(3M+\lambda r)^2}Se_{01}^{lm}(r) + \frac{8\pi(r-2M)^2}{3M+\lambda r}Se_{11}^{lm}(r) \tag{A.3}$$
$$+ \frac{16\pi(2M-r)\left(6M^2+(\lambda-3)Mr+\lambda(\lambda+1)r^2\right)}{i\omega r^2(3M+\lambda r)^2}Se_{02}^{lm}(r)$$
$$+ \frac{16\pi(r-2M)^2}{r(3M+\lambda r)}Se_{12}^{lm}(r) + \frac{32\pi(2M-r)}{r^2}Se_{22}^{lm}(r) + \frac{8\pi(r-2M)^2}{i\omega(3M+\lambda r)}\partial_r Se_{01}^{lm}(r)$$
$$+ \frac{16\pi(r-2M)^2}{i\omega r(3M+\lambda r)}\partial_r Se_{02}^{lm}(r),$$

$$S_1^{lm}(r) = \frac{16\pi r}{3i\omega}Se_{00}^{lm}(r) + \frac{32\pi(r-2M)^2}{3(i\omega)^2 r^2}Se_{01}^{lm}(r) + \frac{64\pi M(2M-r)}{3(i\omega)^2 r^3}Se_{02}^{lm}(r) \tag{A.4}$$
$$- \frac{16\pi(r-2M)^2}{3i\omega r}Se_{11}^{lm}(r) + \frac{16\pi(r-2M)^2}{3i\omega r^2}Se_{12}^{lm}(r) + \frac{32\pi\lambda(2M-r)}{3i\omega r^2}Se_{22}^{lm}(r)$$
$$+ \frac{16\pi(2M-r)}{i\omega r^2}Ue_{22}^{lm}(r) - \frac{32\pi(r-2M)^2}{3(i\omega)^2 r^2}\partial_r Se_{02}^{lm}(r),$$

$$S_0^{lm}(r) = -16\pi r Se_{00}^{lm}(r) + \frac{16\pi(r-2M)^2}{r}Se_{11}^{lm}(r) + \frac{32\pi(r-2M)}{r^2}Ue_{22}^{lm}(r), \tag{A.5}$$

$$S_{0b}^{lm}(r) = \frac{4\pi r\left((-6\lambda-5)M + r\left(3\lambda+2(i\omega)^2 r^2+2\right)\right)}{(i\omega)^2(2M-r)}Se_{00}^{lm}(r) \tag{A.6}$$
$$- \frac{8\pi\left(M\left(-2\lambda+8(i\omega)^2 r^2-3\right)-2(i\omega)^2 r^3+\lambda r+r\right)}{(i\omega)^3 r}Se_{01}^{lm}(r)$$
$$- \frac{16\pi(\lambda+1)\left(M-2(i\omega)^2 r^3\right)}{(i\omega)^3 r^2}Se_{02}^{lm}(r)$$
$$+ \frac{4\pi(2M-r)\left((14\lambda+17)M-r\left(7\lambda+2(i\omega)^2 r^2+8\right)\right)}{(i\omega)^2 r}Se_{11}^{lm}(r)$$
$$- \frac{8\pi(\lambda+1)(2M-r)}{(i\omega)^2 r}Se_{12}^{lm}(r) + \frac{16\pi\lambda(\lambda+1)(2M-r)}{(i\omega)^2 r^2}Se_{22}^{lm}(r)$$
$$- \frac{8\pi(6\lambda+7)(2M-r)}{(i\omega)^2 r^2}Ue_{22}^{lm}(r) - \frac{8\pi(\lambda+1)(2M-r)}{(i\omega)^3 r}\partial_r Se_{02}^{lm}(r).$$

Appendix B

Coupling matrices for linearised Einstein field equations in the Lorenz gauge

The matrices $\mathcal{M}_{\Omega,l(j)}^{(i)}$ and $\mathcal{M}_{r,l(j)}^{(i)}$ are given here explicitly for constant t slicing [90, 89, 104]:

$$\mathcal{M}_{\Omega(1)}^{(2)} = -\mathcal{M}_{\Omega(2)}^{(2)} = -\frac{f'}{2}, \tag{B.1}$$

$$\mathcal{M}_{\Omega(3)}^{(2)} = -\frac{f'f}{2}, \tag{B.2}$$

$$\mathcal{M}_{\Omega(4)}^{(4)} = -\mathcal{M}_{\Omega(5)}^{(4)} = \mathcal{M}_{\Omega(8)}^{(8)} = -\mathcal{M}_{\Omega(9)}^{(8)} = \frac{f'}{4}, \tag{B.3}$$

$$\mathcal{M}_{r(1)}^{(1)} = -\mathcal{M}_{r(5)}^{(1)} = \mathcal{M}_{r(3)}^{(3)} = \mathcal{M}_{r(6)}^{(3)} = \mathcal{M}_{r(3)}^{(6)} = \mathcal{M}_{r(6)}^{(6)} = \frac{f}{2r^2}\left(1 - \frac{4M}{r}\right), \tag{B.4}$$

$$\mathcal{M}_{r(3)}^{(1)} = \frac{1}{2}(f'f^2)\partial_r - \frac{f^2}{2r^2}\left(1 - \frac{4M}{r}\right), \tag{B.5}$$

$$\mathcal{M}_{r(6)}^{(1)} = -\frac{f^2}{2r^2}\left(1 - \frac{6M}{r}\right), \tag{B.6}$$

$$\mathcal{M}_{r(1)}^{(2)} = -\frac{1}{2}(f'f)\partial_r - \frac{f'f}{2r}, \tag{B.7}$$

$$\mathcal{M}_{r(3)}^{(2)} = \frac{1}{2}(f'f^2)\partial_r + \frac{f'f^2}{2r}, \tag{B.8}$$

$$\mathcal{M}_{r(4)}^{(2)} = -\frac{f^2}{2r^2}, \tag{B.9}$$

$$\mathcal{M}_{r(5)}^{(2)} = 2\mathcal{M}_{r(7)}^{(4)} = 2\mathcal{M}_{r(10)}^{(8)} = \frac{f'f}{2r}, \tag{B.10}$$

$$\mathcal{M}_{r(6)}^{(2)} = \frac{f'f^2}{r}, \tag{B.11}$$

$$\mathcal{M}_{r(1)}^{(3)} = -\mathcal{M}_{r(5)}^{(3)} = \mathcal{M}_{r(1)}^{(6)} = -\mathcal{M}_{r(5)}^{(6)} = \mathcal{M}_{r(7)}^{(7)} = \mathcal{M}_{r(10)}^{(10)} = -\frac{f}{2r^2}, \tag{B.12}$$

$$\mathcal{M}_{r(2)}^{(4)} = \mathcal{M}_{r(1)}^{(5)} = -\mathcal{M}_{r(3)}^{(5)} = -\frac{l(l+1)f}{2r^2}, \tag{B.13}$$

$$\mathcal{M}_{r(4)}^{(4)} = \mathcal{M}_{r(8)}^{(8)} = \frac{1}{4}(f'f)\partial_r - \frac{3f'f}{4r}, \tag{B.14}$$

$$\mathcal{M}_{r(5)}^{(4)} = -\frac{1}{4}(f'f)\partial_r - \frac{f'f}{2r}, \tag{B.15}$$

$$\mathcal{M}_{r(6)}^{(4)} = -\frac{l(l+1)f'f}{4r}, \tag{B.16}$$

$$\mathcal{M}_{r(3)}^{(5)} = \frac{l(l+1)f^2}{2r^2}, \tag{B.17}$$

$$\mathcal{M}_{r(5)}^{(5)} = \mathcal{M}_{r(9)}^{(9)} = \frac{f}{r^2}\left(1 - \frac{9M}{2r}\right), \tag{B.18}$$

$$\mathcal{M}_{r(6)}^{(5)} = \frac{l(l+1)f}{2r^2}\left(1 - \frac{3M}{r}\right), \tag{B.19}$$

$$\mathcal{M}_{r(7)}^{(5)} = \mathcal{M}_{r(10)}^{(9)} = -\frac{f}{2r^2}\left(1 - \frac{3M}{r}\right), \tag{B.20}$$

$$\mathcal{M}_{r(5)}^{(7)} = -2\mathcal{M}_{r(9)}^{(10)} = -\frac{1}{2}(l-1)(l+2)\frac{f}{r^2}, \tag{B.21}$$

$$\mathcal{M}_{r(9)}^{(8)} = -\frac{1}{4}(f'f)\partial_r - \frac{f'f}{2r}, \tag{B.22}$$

where the l subscripts have been dropped, and prime denotes a derivative with respect to r.

Appendix C

Properties of delta functions and their derivatives

The following properties can be derived by taking repeated derivatives of the first rule, rearranging and applying previous rules [102]:

$$f(x)\delta(x-a) = f(a)\delta(x-a), \tag{C.1}$$

$$f(x)\delta'(x-a) = -f'(a)\delta(x-a) + f(a)\delta'(x-a), \tag{C.2}$$

$$f(x)\delta''(x-a) = f''(a)\delta(x-a) - 2f'(a)\delta'(x-a) + f(a)\delta''(x-a), \tag{C.3}$$

$$f(x)\delta'''(x-a) = -f'''(a)\delta(x-a) - 3f'(a)\delta''(x-a) + 3f''(a)\delta'(x-a) + f(a)\delta'''(x-a), \tag{C.4}$$

$$f(x)\delta^{(4)}(x-a) = f^{(4)}(a)\delta(x-a) - 4f'''(a)\delta'(x-a) + 6f''(a)\delta''(x-a) - 4f'(a)\delta'''(x-a) \tag{C.5}$$
$$+ f(a)\delta^{(4)}(x-a),$$

$$f(x)\delta^{(5)}(x-a) = -f^{(5)}(a)\delta(x-a) + 5f^{(4)}(a)\delta'(x-a) - 10f'''(a)\delta''(x-a) \tag{C.6}$$
$$+ 10f''(a)\delta'''(x-a) - 5f'(a)\delta^{(4)}(x-a) + f(a)\delta^{(5)}(x-a),$$

where prime denotes derivatives with respect to x and a is a constant and f is some scalar field. These identities are particularly useful in determining the coefficients of the Dirac delta function and its radial derivatives in the expression Eq. (6.16). These coefficients can then be found in Appendix D for the case where $s = 2$ in the odd-sector.

Appendix D

Coefficients of Dirac delta functions and the radial derivatives of Dirac delta functions for s = 2 in the odd-sector

The equations below give the coefficients in Eq. (6.16) for the case of $s = 2$ in the odd-sector.

$$
\begin{aligned}
b_0(r_0) = {} & \frac{8imM\pi}{(l+2)(l+1)l(l-1)r_0^{10}} \left(\frac{r_0}{r_0 - 3M} \right)^{3/2} \big\{ 1080(l^2 + l + 1)M^4 - 6(246l(l+1) \\
& - m^2 + 194)M^3 r_0 + (722l(l+1) - m^2 + 412)M^2 r_0^2 - 3(49l(l+1) + 16)M r_0^3 \\
& + 10l(l+1)r_0^4 \big\} \partial_\theta Y_{lm}^*(\pi/2, 0),
\end{aligned}
\tag{D.1}
$$

$$
\begin{aligned}
b_1(r_0) = {} & \frac{8imM\pi(2M - r_0)}{(l+2)(l+1)l(l-1)r_0^{10}} \left(\frac{r_0}{r_0 - 3M} \right)^{3/2} \big\{ 3240M^4 + 6(38l(l+1) + m^2 - 430)M^3 r_0 \\
& + (-248l(l+1) + 11m^2 + 604)M^2 r_0^2 + (87l(l+1) - 4m^2 - 32)M r_0^3 \\
& - 10l(l+1)r_0^4 \big\} \partial_\theta Y_{lm}^*(\pi/2, 0),
\end{aligned}
\tag{D.2}
$$

$$
\begin{aligned}
b_2(r_0) = {} & \frac{8imM\pi(r_0 - 2M)^2}{(l+2)(l+1)l(l-1)r_0^9} \left(\frac{r_0}{r_0 - 3M} \right)^{3/2} \big\{ 996M^3 + 2(6l(l+1) + 3m^2 - 260)M^2 r_0 \\
& - (10l(l+1) + 2m^2 - 49)M r_0^2 + 2(l(l+1) + 3)r_0^3 \big\} \partial_\theta Y_{lm}^*(\pi/2, 0),
\end{aligned}
\tag{D.3}
$$

$$
b_3(r_0) = \frac{8imM\pi(2M - r_0)^3}{(l+2)(l+1)l(l-1)r_0^8} \left(\frac{r_0}{r_0 - 3M} \right)^{3/2} \left(126M^2 - 47M r_0 + 2r_0^2 \right) \partial_\theta Y_{lm}^*(\pi/2, 0),
\tag{D.4}
$$

$$
b_4(r_0) = -\frac{16imM\pi(r_0 - 2M)^4}{(l+2)(l+1)l(l-1)r_0^6} \sqrt{\frac{r_0}{r_0 - 3M}} \, \partial_\theta Y_{lm}^*(\pi/2, 0).
\tag{D.5}
$$

Appendix E

Jump conditions

In this appendix we present the jump conditions required to construct the various fields that go into calculating $h^{1L}_{\mu\nu,r_0}$. The jump conditions for the r_0 derivative of the Zerilli master function are too long to present here so we including them in the supplemental material of Ref. [2].

E.0.1   Jump conditions in ϕ_2 in the odd-sector

For the odd-sector the jump conditions in Eq. (6.18) are for $s = 2$ given by:

$$J_0 = \frac{8i\pi m M(3M - 2r_0)\partial_\theta Y^*_{lm}(\pi/2, 0)}{(l-1)l(l+1)(l+2)r_0^{5/2}(r_0 - 3M)^{3/2}}, \tag{E.1}$$

$$J_1 = \frac{8i\pi m M \partial_\theta Y^*_{lm}(\pi/2, 0)}{(l-1)l(l+1)(l+2)r_0^{7/2}(r_0 - 3M)^{3/2}(r_0 - 2M)^2}\Big\{ -2\left(l^2 + l - 3\right)r_0^3 \tag{E.2}$$
$$- 2M^2 r_0\big(6l(l+1) + 3m^2 - 22\big) + Mr_0^2\big(10l(l+1) + 2m^2 - 31\big) - 12M^3\Big\},$$

$$J_2 = -\frac{8i\pi m M \partial_\theta Y^*_{lm}(\pi/2, 0)}{(l-1)l(l+1)(l+2)r_0^{9/2}(2M - r_0)^3(r_0 - 3M)^{3/2}}\Big\{2M^3 r_0\big(18l(l+1) + 27m^2 + 16\big) \tag{E.3}$$
$$- M^2 r_0^2\big(40l(l+1) + 41m^2 + 4\big) + Mr_0^3\big(15l(l+1) + 8m^2\big) - 2l(l+1)r_0^4 - 48M^4\Big\}$$

,

$$J_3 = \frac{8i\pi m M \partial_\theta Y^*_{lm}(\pi/2, 0)}{(l-1)l(l+1)(l+2)r_0^{11/2}(r_0 - 3M)^{3/2}(r_0 - 2M)^4}\Big\{ -2l(l+1)\left(l^2 + l - 5\right)r_0^5 \tag{E.4}$$
$$- 24M^4 r_0\big(5l(l+1) + 10m^2 - 42\big) + Mr_0^4\big(l(l+1)\big(14l(l+1) + 4m^2 - 61\big)$$
$$- 12\left(m^2 + 4\right)\big) + 2M^3 r_0^2\big((12l(l+1) + 59)m^2 + 2l(l+1)(6l(l+1) + 5) + 3m^4 - 476\big)$$
$$+ M^2 r_0^3\left(-20l(l+1)m^2 - 2l(l+1)(16l(l+1) - 51) - 2m^4 + 21m^2 + 356\right) - 288M^5\Big\}.$$

The coefficient of the Dirac delta function in Eq. (6.9) is given by:

$$c_s^\delta \phi_2^\delta(r_0) = \frac{-8imM\pi}{\lambda l(l+1)r_0\sqrt{r_0(r_0-3M)}}\partial_\theta Y_{lm}^*(\pi/2,0). \tag{E.5}$$

E.0.2 Jump conditions for χ_1

For χ_1 the $\mathbf{J}$ vector in Eq. (6.34) has components $\mathbf{J} = \{0, 0, J_2, J_3, J_4, J_5\}$ where:

$$J_2 = \frac{16\pi\sqrt{r_0(r_0-3M)}}{(r_0-2M)^2}Y_{lm}^*(\pi/2,0), \tag{E.6}$$

$$J_3 = -\frac{8\pi\left(42M^2 - 21Mr_0 + 2r_0^2\right)}{(2M-r_0)^3\sqrt{r_0(r_0-3M)}}Y_{lm}^*(\pi/2,0), \tag{E.7}$$

$$J_4 = \frac{32\pi\left(M^2r_0\left(6l^2+6l+3m^2-2\right) - Mr_0^2\left(5l^2+5l+m^2-4\right) + l(l+1)r_0^3 - 24M^3\right)}{r_0\sqrt{r_0(r_0-3M)}(r_0-2M)^4} \tag{E.8}$$
$$\times Y_{lm}^*(\pi/2,0),$$

$$J_5 = \frac{16\pi}{r_0^2(2M-r_0)^5\sqrt{r_0(r_0-3M)}}\Big\{4M^3r_0\left(21l^2+21l+33m^2-23\right) - 4M^2r_0^2\big(9l^2+9l \tag{E.9}$$
$$+ 15m^2+16\big) - 5Mr_0^3\left(3l^2+3l-m^2-8\right) + 6l(l+1)r_0^4 - 72M^4\Big\}Y_{lm}^*(\pi/2,0).$$

Bibliography

[1] "Black Hole Perturbation Toolkit." `bhptoolkit.org`.

[2] L. Durkan and N. Warburton, "Slow evolution of the metric perturbation due to a quasicircular inspiral into a Schwarzschild black hole," `arXiv:2206.08179 [gr-qc]`, Jun, 2022.

[3] B. Wardell, A. Pound, N. Warburton, J. Miller, L. Durkan, and A. Le Tiec, "Gravitational waveforms for compact binaries from second-order self-force theory," `arXiv:2112.12265 [gr-qc]`, Dec, 2021.

[4] N. Warburton, A. Pound, B. Wardell, J. Miller, and L. Durkan, "Gravitational-Wave Energy Flux for Compact Binaries through Second Order in the Mass Ratio," *Phys. Rev. Lett.* **127** no. 15, (Jul, 2021) 151102, `arXiv:2107.01298 [gr-qc]`, Jul, 2021.

[5] S. R. Dolan, C. Kavanagh, and B. Wardell, "Gravitational perturbations of rotating black holes in Lorenz gauge," `arXiv:2108.06344 [gr-qc]`, Aug, 2021.

[6] **LIGO Scientific Collaboration and Virgo Collaboration** Collaboration, R. Abbott *et al.*, "Observation of Gravitational Waves from a Binary Black Hole Merger," *Phys. Rev. Lett.* **116** (Feb, 2016) 061102, Feb, 2016.

[7] **LIGO Scientific, VIRGO, KAGRA** Collaboration, R. Abbott *et al.*, "GWTC-3: Compact Binary Coalescences Observed by LIGO and Virgo During the Second Part of the Third Observing Run," `arXiv:2111.03606 [gr-qc]`, Nov, 2021.

[8] **LIGO Scientific Collaboration and Virgo Collaboration** Collaboration, R. Abbott *et al.*, "GW170817: Observation of Gravitational Waves from a Binary Neutron Star Inspiral," *Phys. Rev. Lett.* **119** (Oct, 2017) 161101, Oct, 2017.

[9] **LIGO Scientific Collaboration, KAGRA and Virgo Collaboration** Collaboration, R. Abbott *et al.*, "Observation of Gravitational Waves from Two Neutron Star-Black Hole Coalescences," *Astrophys. J. Lett.* **915** no. 1, (2021) L5, `arXiv:2106.15163 [astro-ph.HE]`, 2021.

[10] **LISA** Collaboration, P. Amaro-Seoane *et al.*, "Laser Interferometer Space Antenna," `arXiv:1702.00786 [astro-ph.IM]`, Feb, 2017.

[11] C. P. L. Berry, S. A. Hughes, C. F. Sopuerta, A. J. K. Chua, A. Heffernan, K. Holley-Bockelmann, D. P. Mihaylov, M. C. Miller, and A. Sesana, "The unique potential of extreme mass-ratio inspirals for gravitational-wave astronomy," arXiv:1903.03686 [astro-ph.HE], 3, 2019.

[12] S. Babak, J. Gair, A. Sesana, E. Barausse, C. F. Sopuerta, C. P. L. Berry, E. Berti, P. Amaro-Seoane, A. Petiteau, and A. Klein, "Science with the space-based interferometer LISA. V: Extreme mass-ratio inspirals," *Phys. Rev. D* **95** no. 10, (2017) 103012, arXiv:1703.09722 [gr-qc], 2017.

[13] T. Hinderer and E. E. Flanagan, "Two timescale analysis of extreme mass ratio inspirals in Kerr. I. Orbital Motion," *Phys. Rev. D* **78** (2008) 064028, arXiv:0805.3337 [gr-qc], 2008.

[14] J. Miller and A. Pound, "Two-timescale evolution of extreme-mass-ratio inspirals: waveform generation scheme for quasicircular orbits in Schwarzschild spacetime," *Phys. Rev. D* **103** no. 6, (2021) 064048, arXiv:2006.11263 [gr-qc], 2021.

[15] M. Pitkin, C. Messenger, and L. Wright, "Astrophysical calibration of gravitational-wave detectors," *Phys. Rev. D* **93** no. 6, (2016) 062002, arXiv:1511.02758 [astro-ph.IM], 2016.

[16] L. Barack and A. Pound, "Self-force and radiation reaction in general relativity," *Rept. Prog. Phys.* **82** no. 1, (2019) 016904, arXiv:1805.10385 [gr-qc], 2019.

[17] A. Pound, "Second-order gravitational self-force," *Phys. Rev. Lett.* **109** (2012) 051101, arXiv:1201.5089 [gr-qc], 2012.

[18] C. S. Reynolds, "Observational Constraints on Black Hole Spin," *Ann. Rev. Astron. Astrophys.* **59** (2021) 117–154, arXiv:2011.08948 [astro-ph.HE], 2021.

[19] A. Le Tiec, "The Overlap of Numerical Relativity, Perturbation Theory and Post-Newtonian Theory in the Binary Black Hole Problem," *International Journal of Modern Physics D* **23** (08, 2014) 4, 08, 2014.

[20] T. Damour and A. Nagar, "The Effective One Body description of the Two-Body problem," *Fundam. Theor. Phys.* **162** (2011) 211–252, arXiv:0906.1769 [gr-qc], 2011.

[21] A. Buonanno and T. Damour, "Effective one-body approach to general relativistic two-body dynamics," *Phys. Rev. D* **59** (1999) 084006, arXiv:gr-qc/9811091, 1999.

[22] Y. Pan, A. Buonanno, A. Taracchini, L. E. Kidder, A. H. Mroué, H. P. Pfeiffer, M. A. Scheel, and B. Szilágyi, "Inspiral-merger-ringdown waveforms of spinning, precessing black-hole binaries in the effective-one-body formalism," *Phys. Rev. D* **89** no. 8, (2014) 084006, arXiv:1307.6232 [gr-qc], 2014.

[23] Y. Mino, M. Sasaki, and T. Tanaka, "Gravitational radiation reaction to a particle motion,"
Phys. Rev. D **55** (Mar, 1997) 3457–3476, Mar, 1997.
https://link.aps.org/doi/10.1103/PhysRevD.55.3457.

[24] T. C. Quinn and R. M. Wald, "Axiomatic approach to electromagnetic and gravitational
radiation reaction of particles in curved spacetime," *Phys. Rev. D* **56** (Sep, 1997) 3381–3394,
Sep, 1997.

[25] A. Einstein, L. Infeld, and B. Hoffmann, "The Gravitational Equations and the Problem of
Motion," *Annals of Mathematics* **39** no. 1, (1938) 65–100, 1938.
http://www.jstor.org/stable/1968714.

[26] L. Infeld and A. Schild, "On the Motion of Test Particles in General Relativity," *Rev. Mod.
Phys.* **21** (Jul, 1949) 408–413, Jul, 1949.
https://link.aps.org/doi/10.1103/RevModPhys.21.408.

[27] R. Geroch and J. O. Weatherall, "The Motion of Small Bodies in Space-time," *Commun.
Math. Phys.* **364** no. 2, (2018) 607–634, `arXiv:1707.04222 [gr-qc]`, 2018.

[28] W. G. Dixon, "Dynamics of Extended Bodies in General Relativity. I. Momentum and
Angular Momentum," *Proceedings of the Royal Society of London. Series A, Mathematical
and Physical Sciences* **314** no. 1519, (1970) 499–527, 1970.
http://www.jstor.org/stable/2416466.

[29] M. Mathisson, "New mechanics of material systems," *General Relativity and Gravitation* **42**
(1937, Republicatoin 2010) 1011–1048, 1937, Republicatoin 2010.

[30] A. Papapetrou *Proceedings from the Royal Society* no. A 64, (1952) 248–258, 1952.

[31] K. S. Thorne and J. B. Hartle, "Laws of motion and precession for black holes and other
bodies," *Phys. Rev. D* **31** (Apr, 1985) 1815–1837, Apr, 1985.
https://link.aps.org/doi/10.1103/PhysRevD.31.1815.

[32] P. D. D'Eath, "Dynamics of a small black hole in a background universe," *Phys. Rev. D* **11**
(Mar, 1975) 1387–1403, Mar, 1975.
https://link.aps.org/doi/10.1103/PhysRevD.11.1387.

[33] R. E. Kates, "Underlying structure of singular perturbations on manifolds," *Annals of
Physics* **132** no. 1, (1981) 1–17, 1981.

[34] S. Detweiler and B. F. Whiting, "Self-force via a Green's function decomposition," *Phys. Rev.
D* **67** (Jan, 2003) 024025, Jan, 2003.

[35] S. Detweiler, "Radiation Reaction and the Self-Force for a Point Mass in General Relativity,"
Phys. Rev. Lett. **86** (Mar, 2001) 1931–1934, Mar, 2001.
https://link.aps.org/doi/10.1103/PhysRevLett.86.1931.

[36] L. Barack and A. Ori, "Gravitational self-force and gauge transformations," *Physical Review D* **64** no. 12, (Oct, 2001) , Oct, 2001. https://doi.org/10.1103%2Fphysrevd.64.124003.

[37] A. Pound and B. Wardell, "Black hole perturbation theory and gravitational self-force," arXiv:2101.04592 [gr-qc], Jan, 2021.

[38] E. Hamilton, L. London, J. E. Thompson, E. Fauchon-Jones, M. Hannam, C. Kalaghatgi, S. Khan, F. Pannarale, and A. Vano-Vinuales, "Model of gravitational waves from precessing black-hole binaries through merger and ringdown," *Phys. Rev. D* **104** no. 12, (2021) 124027, arXiv:2107.08876 [gr-qc], 2021.

[39] A. Pound, "Nonlinear gravitational self-force: second-order equation of motion," *Phys. Rev. D* **95** no. 10, (2017) 104056, arXiv:1703.02836 [gr-qc], 2017.

[40] A. Pound and J. Miller, "Practical, covariant puncture for second-order self-force calculations," *Phys. Rev. D* **89** no. 10, (2014) 104020, arXiv:1403.1843 [gr-qc], 2014.

[41] C. Merlin, A. Ori, L. Barack, A. Pound, and M. van de Meent, "Completion of metric reconstruction for a particle orbiting a Kerr black hole," *Phys. Rev. D* **94** no. 10, (2016) 104066, arXiv:1609.01227 [gr-qc], 2016.

[42] J. E. Thompson, B. Wardell, and B. F. Whiting, "Gravitational Self-Force Regularization in the Regge-Wheeler and Easy Gauges," *Phys. Rev. D* **99** no. 12, (2019) 124046, arXiv:1811.04432 [gr-qc], 2019.

[43] V. Toomani, P. Zimmerman, A. Spiers, S. Hollands, A. Pound, and S. R. Green, "New metric reconstruction scheme for gravitational self-force calculations," *Class. Quant. Grav.* **39** no. 1, (2022) 015019, arXiv:2108.04273 [gr-qc], 2022.

[44] A. Heffernan, *The Self-Force Problem: Local Behaviour of the Detweiler-Whiting Singular Field.* PhD thesis, University Coll., Dublin, 2012. arXiv:1403.6177 [gr-qc].

[45] A. Heffernan, A. Ottewill, and B. Wardell, "High-order expansions of the Detweiler-Whiting singular field in Schwarzschild spacetime," *Phys. Rev. D* **86** (2012) 104023, arXiv:1204.0794 [gr-qc], 2012.

[46] M. V. Berndtson, *Harmonic gauge perturbations of the Schwarzschild metric.* PhD thesis. arXiv:0904.0033 [gr-qc].

[47] K.-H. Lai and T. G. F. Li, "Constraining black-hole horizon effects by LIGO-Virgo detections of inspiralling binary black holes," *Phys. Rev. D* **98** no. 8, (2018) 084059, arXiv:1807.01840 [gr-qc], 2018.

[48] A. Ori and K. S. Thorne, "The Transition from inspiral to plunge for a compact body in a circular equatorial orbit around a massive, spinning black hole," *Phys. Rev. D* **62** (2000) 124022, arXiv:gr-qc/0003032, 2000.

[49] E. A. Huerta and J. R. Gair, "Intermediate-mass-ratio-inspirals in the Einstein Telescope: I. Signal-to-noise ratio calculations," *Phys. Rev. D* **83** (2011) 044020, `arXiv:1009.1985 [gr-qc]`, 2011.

[50] E. A. Huerta and J. R. Gair, "Intermediate-mass-ratio-inspirals in the Einstein Telescope. II. Parameter estimation errors," *Phys. Rev. D* **83** (2011) 044021, `arXiv:1011.0421 [gr-qc]`, 2011.

[51] **LIGO Scientific, Virgo** Collaboration, T. D. Abbott *et al.*, "Improved analysis of GW150914 using a fully spin-precessing waveform Model," *Phys. Rev. X* **6** no. 4, (2016) 041014, `arXiv:1606.01210 [gr-qc]`, 2016.

[52] S. Babak, A. Taracchini, and A. Buonanno, "Validating the effective-one-body model of spinning, precessing binary black holes against numerical relativity," *Phys. Rev. D* **95** no. 2, (2017) 024010, `arXiv:1607.05661 [gr-qc]`, 2017.

[53] A. Bohé *et al.*, "Improved effective-one-body model of spinning, nonprecessing binary black holes for the era of gravitational-wave astrophysics with advanced detectors," *Phys. Rev. D* **95** no. 4, (2017) 044028, `arXiv:1611.03703 [gr-qc]`, 2017.

[54] A. Nagar, G. Riemenschneider, and G. Pratten, "Impact of Numerical Relativity information on effective-one-body waveform models," *Phys. Rev. D* **96** no. 8, (2017) 084045, `arXiv:1703.06814 [gr-qc]`, 2017.

[55] V. Varma, S. E. Field, M. A. Scheel, J. Blackman, L. E. Kidder, and H. P. Pfeiffer, "Surrogate model of hybridized numerical relativity binary black hole waveforms," *Phys. Rev. D* **99** no. 6, (2019) 064045, `arXiv:1812.07865 [gr-qc]`, 2019.

[56] N. E. M. Rifat, S. E. Field, G. Khanna, and V. Varma, "Surrogate model for gravitational wave signals from comparable and large-mass-ratio black hole binaries," *Phys. Rev. D* **101** no. 8, (2020) 081502, `arXiv:1910.10473 [gr-qc]`, 2020.

[57] A. Buonanno and T. Damour, "Transition from inspiral to plunge in binary black hole coalescences," *Phys. Rev. D* **62** (2000) 064015, `arXiv:gr-qc/0001013`, 2000.

[58] A. Apte and S. A. Hughes, "Exciting black hole modes via misaligned coalescences: I. Inspiral, transition, and plunge trajectories using a generalized Ori-Thorne procedure," *Phys. Rev. D* **100** no. 8, (2019) 084031, `arXiv:1901.05901 [gr-qc]`, 2019.

[59] H. Lim, G. Khanna, A. Apte, and S. A. Hughes, "Exciting black hole modes via misaligned coalescences: II. The mode content of late-time coalescence waveforms," *Phys. Rev. D* **100** no. 8, (2019) 084032, `arXiv:1901.05902 [gr-qc]`, 2019.

[60] O. Burke, J. R. Gair, and J. Simón, "Transition from Inspiral to Plunge: A Complete Near-Extremal Trajectory and Associated Waveform," *Phys. Rev. D* **101** no. 6, (2020) 064026, `arXiv:1909.12846 [gr-qc]`, 2020.

[61] G. Compère, K. Fransen, and C. Jonas, "Transition from inspiral to plunge into a highly spinning black hole," *Class. Quant. Grav.* **37** no. 9, (2020) 095013, `arXiv:1909.12848 [gr-qc]`, 2020.

[62] G. Compère and L. Küchler, "Self-consistent adiabatic inspiral and transition motion," *Phys. Rev. Lett.* **126** no. 24, (2021) 241106, `arXiv:2102.12747 [gr-qc]`, 2021.

[63] P. L. Chrzanowski, "Vector potential and metric perturbations of a rotating black hole," *Phys. Rev. D* **11** (Apr, 1975) 2042–2062, Apr, 1975. `https://link.aps.org/doi/10.1103/PhysRevD.11.2042`.

[64] J. M. Cohen and L. S. Kegeles, "Electromagnetic fields in curved spaces: A constructive procedure," *Phys. Rev. D* **10** (Aug, 1974) 1070–1084, Aug, 1974. `https://link.aps.org/doi/10.1103/PhysRevD.10.1070`.

[65] L. S. Kegeles and J. M. Cohen, "Constructive procedure for perturbations of spacetimes," *Phys. Rev. D* **19** (Mar, 1979) 1641–1664, Mar, 1979. `https://link.aps.org/doi/10.1103/PhysRevD.19.1641`.

[66] C. O. Lousto and B. F. Whiting, "Reconstruction of black hole metric perturbations from the Weyl curvature," *Phys. Rev. D* **66** (Jul, 2002) 024026, Jul, 2002. `https://link.aps.org/doi/10.1103/PhysRevD.66.024026`.

[67] A. Ori, "Reconstruction of inhomogeneous metric perturbations and electromagnetic four potential in Kerr space-time," *Phys. Rev. D* **67** (2003) 124010, `arXiv:gr-qc/0207045`, 2003.

[68] L. Price, *Developments in the perturbation theory of algebraically special spacetimes.* PhD thesis, University of Florida, Jan, 2007.

[69] R. M. Wald, "On perturbations of a Kerr black hole," *Journal of Mathematical Physics* **14** no. 10, (1973) 1453–1461, 1973.

[70] A. Pound, C. Merlin, and L. Barack, "Gravitational self-force from radiation-gauge metric perturbations," *Phys. Rev. D* **89** no. 2, (2014) 024009, `arXiv:1310.1513 [gr-qc]`, 2014.

[71] M. van De Meent, "The mass and angular momentum of reconstructed metric perturbations," *Class. Quant. Grav.* **34** no. 12, (2017) 124003, `arXiv:1702.00969 [gr-qc]`, 2017.

[72] M. van de Meent, "Gravitational self-force on generic bound geodesics in Kerr spacetime," *Phys. Rev. D* **97** no. 10, (2018) 104033, `arXiv:1711.09607 [gr-qc]`, 2018.

[73] L. Barack and P. Giudice, "Time-domain metric reconstruction for self-force applications," *Phys. Rev. D* **95** no. 10, (2017) 104033, `arXiv:1702.04204 [gr-qc]`, 2017.

[74] O. Long and L. Barack, "Time-domain metric reconstruction for hyperbolic scattering," *Phys. Rev. D* **104** no. 2, (2021) 024014, `arXiv:2105.05630 [gr-qc]`, 2021.

[75] S. R. Green, S. Hollands, and P. Zimmerman, "Teukolsky formalism for nonlinear Kerr perturbations," *Class. Quant. Grav.* **37** no. 7, (2020) 075001, `arXiv:1908.09095 [gr-qc]`, 2020.

[76] S. R. Dolan and L. Barack, "Self force via m-mode regularization and 2+1D evolution: Foundations and a scalar-field implementation on Schwarzschild," *Phys. Rev. D* **83** (2011) 024019, `arXiv:1010.5255 [gr-qc]`, 2011.

[77] S. R. Dolan, L. Barack, and B. Wardell, "Self force via m-mode regularization and 2+1D evolution: II. Scalar-field implementation on Kerr spacetime," *Phys. Rev. D* **84** (2011) 084001, `arXiv:1107.0012 [gr-qc]`, 2011.

[78] S. R. Dolan and L. Barack, "Self-force via m-mode regularization and 2+1D evolution: III. Gravitational field on Schwarzschild spacetime," *Phys. Rev. D* **87** (2013) 084066, `arXiv:1211.4586 [gr-qc]`, 2013.

[79] S. Isoyama, L. Barack, S. R. Dolan, A. Le Tiec, H. Nakano, A. G. Shah, T. Tanaka, and N. Warburton, "Gravitational Self-Force Correction to the Innermost Stable Circular Equatorial Orbit of a Kerr Black Hole," *Phys. Rev. Lett.* **113** no. 16, (2014) 161101, `arXiv:1404.6133 [gr-qc]`, 2014.

[80] T. Osburn and N. Nishimura, "New self-force method via elliptic PDEs for Kerr inspiral models," `arXiv:2206.07031 [gr-qc]`, Jun, 2022.

[81] S. R. Dolan, "Electromagnetic fields on Kerr spacetime, Hertz potentials and Lorenz gauge," *Phys. Rev. D* **100** no. 4, (2019) 044044, `arXiv:1906.04808 [gr-qc]`, 2019.

[82] B. Wardell and C. Kavanagh, "Separable electromagnetic perturbations of rotating black holes," *Phys. Rev. D* **103** no. 10, (2021) 104049, `arXiv:2011.03548 [gr-qc]`, 2021.

[83] S. Detweiler and E. Poisson, "Low multipole contributions to the gravitational self-force," *Phys. Rev. D* **69** (Apr, 2004) 084019, Apr, 2004. `https://link.aps.org/doi/10.1103/PhysRevD.69.084019`.

[84] M. Sasaki and H. Tagoshi, "Analytic black hole perturbation approach to gravitational radiation," *Living Rev. Rel.* **6** (2003) 6, `arXiv:gr-qc/0306120`, 2003.

[85] S. Mano, H. Suzuki, and E. Takasugi, "Analytic solutions of the Teukolsky equation and their low frequency expansions," *Prog. Theor. Phys.* **95** (1996) 1079–1096, `arXiv:gr-qc/9603020`, 1996.

[86] M. Casals and A. C. Ottewill, "High-order tail in Schwarzschild spacetime," *Phys. Rev. D* **92** no. 12, (2015) 124055, `arXiv:1509.04702 [gr-qc]`, 2015.

[87] C. Kavanagh, A. C. Ottewill, and B. Wardell, "Analytical high-order post-Newtonian expansions for extreme mass ratio binaries," *Phys. Rev. D* **92** no. 8, (2015) 084025, arXiv:1503.02334 [gr-qc], 2015.

[88] C. Kavanagh, "Progress in post-Newtonian self-force at second order in the mass-ratio," *The 24th Capra meeting on radiation reaction in general relativity, Perimeter Institute* (2021) , 2021. https://events.perimeterinstitute.ca/event/7/.

[89] L. Barack and N. Sago, "Gravitational self force on a particle in circular orbit around a Schwarzschild black hole," *Phys. Rev. D* **75** (2007) 064021, arXiv:gr-qc/0701069, 2007.

[90] L. Barack and C. O. Lousto, "Perturbations of Schwarzschild black holes in the Lorenz gauge: Formulation and numerical implementation," *Phys. Rev. D* **72** (2005) 104026, arXiv:gr-qc/0510019, 2005.

[91] S. Akcay, N. Warburton, and L. Barack, "Frequency-domain algorithm for the Lorenz-gauge gravitational self-force," *Phys. Rev. D* **88** no. 10, (2013) 104009, arXiv:1308.5223 [gr-qc], 2013.

[92] T. Osburn, E. Forseth, C. R. Evans, and S. Hopper, "Lorenz gauge gravitational self-force calculations of eccentric binaries using a frequency domain procedure," *Phys. Rev. D* **90** no. 10, (2014) 104031, arXiv:1409.4419 [gr-qc], 2014.

[93] A. Albertini, A. Nagar, A. Pound, N. Warburton, B. Wardell, L. Durkan, and J. Miller, "Comparing second-order gravitational self-force, numerical relativity and effective one body waveforms from inspiralling, quasi-circular and nonspinning black hole binaries," arXiv:2208.01049 [gr-qc], Aug, 2022.

[94] A. Albertini, A. Nagar, A. Pound, N. Warburton, B. Wardell, L. Durkan, and J. Miller, "Comparing second-order gravitational self-force and effective one body waveforms from inspiralling, quasi-circular and nonspinning black hole binaries II: the large-mass-ratio case," arXiv:2208.02055 [gr-qc], 8, 2022.

[95] R. Panosso Macedo, B. Leather, N. Warburton, B. Wardell, and A. Zenginoğlu, "Hyperboloidal method for frequency-domain self-force calculations," *Phys. Rev. D* **105** no. 10, (2022) 104033, arXiv:2202.01794 [gr-qc], 2022.

[96] M. Maggiore, *Gravitational Waves: Volume 2: Astrophysics and Cosmology*. Oxford University Press, 2018.

[97] "NIST Digital Library of Mathematical Functions." Http://dlmf.nist.gov/, release 1.1.6 of 2022-06-30. http://dlmf.nist.gov/. F. W. J. Olver, A. B. Olde Daalhuis, D. W. Lozier, B. I. Schneider, R. F. Boisvert, C. W. Clark, B. R. Miller, B. V. Saunders, H. S. Cohl, and M. A. McClain, eds.

[98] A. Pound, "Nonlinear gravitational self-force. I. Field outside a small body," *Phys. Rev. D* **86** (2012) 084019, `arXiv:1206.6538 [gr-qc]`, 2012.

[99] S. E. Gralla, "Second Order Gravitational Self Force," *Phys. Rev. D* **85** (2012) 124011, `arXiv:1203.3189 [gr-qc]`, 2012.

[100] J. Miller, B. Wardell, and A. Pound, "Second-order perturbation theory: the problem of infinite mode coupling," *Phys. Rev. D* **94** no. 10, (2016) 104018, `arXiv:1608.06783 [gr-qc]`, 2016.

[101] T. Regge and J. A. Wheeler, "Stability of a Schwarzschild Singularity," *Phys. Rev.* **108** (Nov, 1957) 1063–1069, Nov, 1957. `https://link.aps.org/doi/10.1103/PhysRev.108.1063`.

[102] S. Hopper and C. R. Evans, "Metric perturbations from eccentric orbits on a Schwarzschild black hole: I. Odd-parity Regge-Wheeler to Lorenz gauge transformation and two new methods to circumvent the Gibbs phenomenon," *Phys. Rev. D* **87** no. 6, (2013) 064008, `arXiv:1210.7969 [gr-qc]`, 2013.

[103] L. Barack and N. Sago, "Gravitational self-force on a particle in eccentric orbit around a Schwarzschild black hole," *Phys. Rev. D* **81** (2010) 084021, `arXiv:1002.2386 [gr-qc]`, 2010.

[104] L. Küchler and G. Compère, "Private notes on Transition to Plunge." 2021.

[105] S. A. Teukolsky, "Perturbations of a rotating black hole. 1. Fundamental equations for gravitational electromagnetic and neutrino field perturbations," *Astrophys. J.* **185** (1973) 635–647, 1973.

[106] E. Newman and R. Penrose, "An Approach to Gravitational Radiation by a Method of Spin Coefficients," *Journal of Mathematical Physics* **3** no. 3, (1962) 566–578, `https://doi.org/10.1063/1.1724257`, 1962. `https://doi.org/10.1063/1.1724257`.

[107] S. Dolan, "Private notes on metric perturbations on Kerr: from radiation gauge to Lorenz gauge." 2021.

[108] R. M. Wald, "Construction of Solutions of Gravitational, Electromagnetic, or Other Perturbation Equations from Solutions of Decoupled Equations," *Phys. Rev. Lett.* **41** (Jul, 1978) 203–206, Jul, 1978.

[109] S. A. Teukolsky and W. H. Press, "Perturbations of a rotating black hole. III. Interaction of the hole with gravitational and electromagnetic radiation.," *Astrophysical Journal* **193** (Oct., 1974) 443–461, Oct., 1974.

[110] E. W. Leaver, "Solutions to a generalized spheroidal wave equation: Teukolsky's equations in general relativity, and the two-center problem in molecular quantum mechanics," *Journal of Mathematical Physics* **27** no. 5, (1986) 1238–1265, `https://doi.org/10.1063/1.527130`, 1986. `https://doi.org/10.1063/1.527130`.

[111] A. Ottewill, "Renormlised angular momentum for the MST method," 2020. `https://astro.cas.cz/bhptoolkit2020/program.html`. Black Hole Perutbation Toolkit Meeting.

[112] S. A. H. Throwe. W, *High precision calculation of generic extreme mass ratio inspirals*. PhD thesis, Massachusetts Institute of Technology, 2010.

[113] Z. Nasipak and C. R. Evans, "Resonant self-force effects in extreme-mass-ratio binaries: A scalar model," *Phys. Rev. D* **104** no. 8, (2021) 084011, `arXiv:2105.15188 [gr-qc]`, 2021.

[114] N. Warburton and B. Wardell, "Applying the effective-source approach to frequency-domain self-force calculations," *Phys. Rev. D* **89** no. 4, (2014) 044046, `arXiv:1311.3104 [gr-qc]`, 2014.

[115] B. Wardell and N. Warburton, "Applying the effective-source approach to frequency-domain self-force calculations: Lorenz-gauge gravitational perturbations," *Phys. Rev. D* **92** no. 8, (2015) 084019, `arXiv:1505.07841 [gr-qc]`, 2015.

[116] S. D. Upton and A. Pound, "Second-order gravitational self-force in a highly regular gauge," *Phys. Rev. D* **103** no. 12, (2021) 124016, `arXiv:2101.11409 [gr-qc]`, 2021.

[117] S. Akcay, "A Fast Frequency-Domain Algorithm for Gravitational Self-Force: I. Circular Orbits in Schwarzschild Spacetime," *Phys. Rev. D* **83** (2011) 124026, `arXiv:1012.5860 [gr-qc]`, 2011.

[118] A. Pound, B. Wardell, N. Warburton, and J. Miller, "Second-Order Self-Force Calculation of Gravitational Binding Energy in Compact Binaries," *Phys. Rev. Lett.* **124** (Jan, 2020) 021101, Jan, 2020. `https://link.aps.org/doi/10.1103/PhysRevLett.124.021101`.

[119] A. Pound, B. Wardell, N. Warburton, and J. Miller, "Second-Order Self-Force Calculation of Gravitational Binding Energy in Compact Binaries," *Phys. Rev. Lett.* **124** no. 2, (2020) 021101, `arXiv:1908.07419 [gr-qc]`, 2020.

[120] E. Poisson and C. M. Will, *Radiative losses and radiation reaction*. Cambridge University Press, 2014.

[121] J. Miller, B. Leather, A. Pound, and N. Warburton, "Frequency-domain methods for first- and second-order self-force calculations in Schwarzschild spacetime," *in preparation* (2021) , 2021.

[122] J. Mathews, A. Pound, and B. Wardell, "Self-Force Calculations with a Spinning Secondary," `arXiv:2112.13069 [gr-qc]`, Dec, 2021.

[123] W. F. Trench, *Book: Elementary Differential Equations with Boundary Value Problems (Trench)*. LibreTexts, 2021.

[124] S. Hopper and C. R. Evans, "Gravitational perturbations and metric reconstruction: Method of extended homogeneous solutions applied to eccentric orbits on a Schwarzschild black hole," *Phys. Rev. D* **82** (Oct, 2010) 084010, Oct, 2010. https://link.aps.org/doi/10.1103/PhysRevD.82.084010.

[125] A. Pound, "Private notes on Transition to Plunge." 2022.

[126] L. Küchler and G. Compère, "Private mathematica notebook: 0PA EMRI Waveforms." 2021.

[127] N. Warburton and L. Barack, "Self force on a scalar charge in Kerr spacetime: circular equatorial orbits," *Phys. Rev. D* **81** (2010) 084039, arXiv:1003.1860 [gr-qc], 2010.

[128] M. Boyle *et al.*, "The SXS Collaboration catalog of binary black hole simulations," *Class. Quant. Grav.* **36** no. 19, (2019) 195006, arXiv:1904.04831 [gr-qc], 2019.

[129] F. Messina, A. Maldarella, and A. Nagar, "Factorization and resummation: A new paradigm to improve gravitational wave amplitudes. II. The higher multipolar modes," *Phys. Rev. D* **97** (Apr, 2018) 084016, Apr, 2018.

[130] A. Le Tiec, L. Blanchet, and B. F. Whiting, "The First Law of Binary Black Hole Mechanics in General Relativity and Post-Newtonian Theory," *Phys. Rev. D* **85** (2012) 064039, arXiv:1111.5378 [gr-qc], 2012.

[131] P. L. Chrzanowski, "Vector Potential and Metric Perturbations of a Rotating Black Hole," *Phys. Rev. D* **11** (1975) 2042–2062, 1975.

[132] L. S. Kegeles and J. M. Cohen, "Consrtuctive procedure for perturbations of space-times," *Phys. Rev. D* **19** (1979) 1641–1664, 1979.

[133] R. M. Wald, "Construction of Solutions of Gravitational, Electromagnetic, Or Other Perturbation Equations from Solutions of Decoupled Equations," *Phys. Rev. Lett.* **41** (1978) 203–206, 1978.

[134] R. Fujita, "Gravitational Waves from a Particle in Circular Orbits around a Schwarzschild Black Hole to the 22nd Post-Newtonian Order," *Prog. Theor. Phys.* **128** (2012) 971–992, arXiv:1211.5535 [gr-qc], 2012.

[135] D. Bini and T. Damour, "Two-body gravitational spin-orbit interaction at linear order in the mass ratio," *Phys. Rev. D* **90** no. 2, (2014) 024039, arXiv:1404.2747 [gr-qc], 2014.

[136] C. Munna and C. R. Evans, "Post-Newtonian expansion of the spin-precession invariant for eccentric-orbit non-spinning extreme-mass-ratio inspirals to 9PN and e^{16}," arXiv:2206.04085 [gr-qc], Jun, 2022.

[137] P. A. Sundararajan, G. Khanna, and S. A. Hughes, "Towards adiabatic waveforms for inspiral into Kerr black holes. I. A New model of the source for the time domain perturbation equation," *Phys. Rev. D* **76** (2007) 104005, arXiv:gr-qc/0703028, 2007.

[138] E. Harms, S. Bernuzzi, A. Nagar, and A. Zenginoglu, "A new gravitational wave generation algorithm for particle perturbations of the Kerr spacetime," *Class. Quant. Grav.* **31** no. 24, (2014) 245004, arXiv:1406.5983 [gr-qc], 2014.

[139] A. Heffernan, A. C. Ottewill, N. Warburton, B. Wardell, and P. Diener, "Accelerated motion and the self-force in Schwarzschild spacetime," *Class. Quant. Grav.* **35** no. 19, (2018) 194001, arXiv:1712.01098 [gr-qc], 2018.

[140] S. Hopper, E. Forseth, T. Osburn, and C. R. Evans, "Fast spectral source integration in black hole perturbation calculations," *Phys. Rev. D* **92** (2015) 044048, arXiv:1506.04742 [gr-qc], 2015.

[141] P. Amaro-Seoane, H. Audley, S. Babak, J. Baker, E. Barausse, P. Bender, E. Berti, P. Binetruy, M. Born, D. Bortoluzzi, J. Camp, C. Caprini, V. Cardoso, M. Colpi, J. Conklin, N. Cornish, C. Cutler, K. Danzmann, R. Dolesi, L. Ferraioli, V. Ferroni, E. Fitzsimons, J. Gair, L. G. Bote, D. Giardini, F. Gibert, C. Grimani, H. Halloin, G. Heinzel, T. Hertog, M. Hewitson, K. Holley-Bockelmann, D. Hollington, M. Hueller, H. Inchauspe, P. Jetzer, N. Karnesis, C. Killow, A. Klein, B. Klipstein, N. Korsakova, S. L. Larson, J. Livas, I. Lloro, N. Man, D. Mance, J. Martino, I. Mateos, K. McKenzie, S. T. McWilliams, C. Miller, G. Mueller, G. Nardini, G. Nelemans, M. Nofrarias, A. Petiteau, P. Pivato, E. Plagnol, E. Porter, J. Reiche, D. Robertson, N. Robertson, E. Rossi, G. Russano, B. Schutz, A. Sesana, D. Shoemaker, J. Slutsky, C. F. Sopuerta, T. Sumner, N. Tamanini, I. Thorpe, M. Troebs, M. Vallisneri, A. Vecchio, D. Vetrugno, S. Vitale, M. Volonteri, G. Wanner, H. Ward, P. Wass, W. Weber, J. Ziemer, and P. Zweifel, "Laser Interferometer Space Antenna," arXiv:1702.00786 [astro-ph.IM], 2017.

[142] **LIGO Scientific Collaboration and Virgo Collaboration** Collaboration, R. Abbott *et al.*, "GW190412: Observation of a Binary-Black-Hole Coalescence with Asymmetric Masses," *Phys. Rev. D* **102** no. 4, (2020) 043015, arXiv:2004.08342 [astro-ph.HE], 2020.

[143] L. Barack, A. Ori, and N. Sago, "Frequency-domain calculation of the self force: The High-frequency problem and its resolution," *Phys. Rev. D* **78** (2008) 084021, arXiv:0808.2315 [gr-qc], 2008.

[144] N. Warburton and L. Barack, "Self force on a scalar charge in Kerr spacetime: eccentric equatorial orbits," *Phys. Rev. D* **83** (2011) 124038, arXiv:1103.0287 [gr-qc], 2011.

[145] C. Munna, C. R. Evans, S. Hopper, and E. Forseth, "Determination of new coefficients in the angular momentum and energy fluxes at infinity to 9PN order for eccentric Schwarzschild extreme-mass-ratio inspirals using mode-by-mode fitting," *Phys. Rev. D* **102** no. 2, (2020) 024047, arXiv:2005.03044 [gr-qc], 2020.

[146] D. Bini and T. Damour, "Analytical determination of the two-body gravitational interaction potential at the fourth post-Newtonian approximation," *Phys. Rev. D* **87** no. 12, (2013) 121501, `arXiv:1305.4884 [gr-qc]`, 2013.

[147] M. Van De Meent and N. Warburton, "Fast Self-forced Inspirals," *Class. Quant. Grav.* **35** no. 14, (2018) 144003, `arXiv:1802.05281 [gr-qc]`, 2018.

[148] J. McCart, T. Osburn, and J. Y. J. Burton, "Highly eccentric extreme-mass-ratio-inspiral waveforms via fast self-forced inspirals," *Phys. Rev. D* **104** no. 8, (2021) 084050, `arXiv:2109.00056 [gr-qc]`, 2021.

[149] P. Lynch, M. van de Meent, and N. Warburton, "Eccentric self-forced inspirals into a rotating black hole," `arXiv:2112.05651 [gr-qc]`, Dec, 2021.

[150] E. Poisson, A. Pound, and I. Vega, "The Motion of point particles in curved spacetime," *Living Rev. Rel.* **14** (2011) 7, `arXiv:1102.0529 [gr-qc]`, 2011.